NOTICE

The quality of this microform is heavily dependent upon the quality of the original thesis submitted for microfilming. Every effort has been made to ensure the highest quality of reproduction possible.

If pages are missing, contact the university which granted the degree.

Some pages may have indistinct print especially if the original pages were typed with a poor typewriter ribbon or if the university sent us an inferior photocopy.

Reproduction in full or in part of this microform is governed by the Canadian Copyright Act, R.S.C. 1970, c. C-30, and subsequent amendments.

AVIS

La qualité de cette microforme dépend grandement de la qualité de la thèse soumise au microfilmage. Nous avons tout fait pour assurer une qualité supérieure de reproduction.

S'il manque des pages, veuillez communiquer avec l'université qui a conféré le grade.

La qualité d'impression de certaines pages peut laisser à désirer, surtout si les pages originales ont été dactylographiées à l'aide d'un ruban usé ou si l'université nous a fait parvenir une photocopie de qualité inférieure.

La reproduction, même partielle, de cette microforme est soumise à la Loi canadienne sur le droit d'auteur, SRC 1970, c. C-30, et ses amendements subséquents.

Canada

Ni-SODALITE CATALYSTS

FOR

HYDROCRACKING

OF

LLOYDMINSTER ATMOSPHERIC RESIDUUM

By

Marie Colette Isabelle Bergeron

Ottawa, Ontario

August 1993

submitted to

The School of Graduate Studies and Research

University of Ottawa

in partial fulfilment of the requirements

for the degree of

Master of Applied Science

Department of Chemical Engineering

ISBN 0-315-89602-7

Canada

UNIVERSITÉ D'OTTAWA
UNIVERSITY OF OTTAWA

ABSTRACT

Colour degradation and heteroatom removal were studied in hydrocracking of Lloydminster atmospheric residue using conventional $CoMo/Al_2O_3$ catalysts containing a Ni-sodalite component. Nickel ion exchange and impregnation were performed on basic sodalite prepared in laboratory which was combined to an aqueous mixture of α-alumina monohydrate, ammonium paramolybdate and cobalt nitrate to form the final catalysts. Each catalysts was evaluated in a high pressure continuous flow reaction system in which hydrogen and Lloydminster atmospheric bottoms were mixed and flowed upward through a fixed bed catalytic reactor. The reaction conditions were 17.3 MPa, 415°C, and $0.59h^{-1}$ or $1.07h^{-1}$ LSV.

Ni-SOD was found to increase the rate at which the maximum colour of the diesel fraction was developed. Sulphur content of the diesel fraction was related to colour formation and a mathematical expression was developed to express colour degradation. Total nitrogen content was found to have no direct effect on colour formation.

The presence of Ni-SOD also improved hydrodemetallation (HDM), hydrodesulphurization (HDS) and microcarbon residue (MCR) removal with maximum conversion for a Ni-SOD content of 10%. HDN was reduced in the total liquid product, but improved in the diesel fraction as the content of Ni-SOD increased.

CONTRIBUTIONS TO KNOWLEDGE

In this study, the following contributions to scientific knowledge were made:

1. New experimental data were obtained using basic sodalite as a zeolite component in residuum hydrocracking catalysts. The method for basic sodalite synthesis and the preparation of new catalysts were described.

2. It was shown for the first time that colour formation in the diesel fraction could be accurately represented by a mathematical equation containing two exponential terms. Colour formation measurements were correlated with sulphur content in the diesel fraction.

3. Hydrodemetalization (HDM), hydrodesulphurization (HDS) hydrodenitrogenation (HDN) and conversion of microcarbon residue (MCR) results were obtained using different concentration of Ni-sodalite as a component in a residuum hydrocracking catalyst. Ni-sodalite in the catalysts was found to increase HDM, HDS and MCR removal, but to decrease HDN.

ACKNOWLEDGMENT

I wish to thank the Natural Sciences and Engineering Research Council as well as the University of Ottawa, for their financial assistance without which this research would not have been possible. My sincere gratitude to the management of CANMET, Energy Mines and Resources for allowing me to study at ERL as well as to every technologist who performed analysis on my samples. They always provided assistance in all ways possible.

Many thanks to scientists and friends who constantly offered sound advise and encouragements, most particularly Dr Jean-Pierre Charland whose stimulating discussions provided the seed for further progress. He never turned down my cry for help.

Finally, my advisor, Dr Marten Ternan deserves the best of my gratitude for his countless challenges, his patience and his enthusiastic approach to science. He believed in my potential and allowed me to extend my limits to new horizons.

Thank you to all of you who were directly or indirectly involved with my work; I would not have made it this far without you.

NOMENCLATURE

A	Maximum ASTM colour achieved in the specified time
A_1, A_2, B_1, B_2	Constants
C	ASTM colour values at time t
CM_N	Carbonaceous molecules containing nitrogen
CM_S	Carbonaceous molecules containing sulphur
$[CM_N]_o$	Initial concentration in diesel fraction of carbonaceous molecules containing nitrogen
HA_P/HA_F	Ratio of the liquid product content of heteroatom A over the feedstock content of heteroatom A.
k	Reaction rate constant
MCR_P/MCR_F	Ratio of micro carbon residue content in the liquid product over the micro carbon residue content in the feedstock
MW	Molecular weight of N_2 , g/gmol
n	Shull statistical monolayer
N	Avogadro's number, 6.023 X 10^{23} atoms/gmol
N_P/N_F	Ratio of nitrogen content in the liquid product over the nitrogen content in the feedstock
Ni_P/Ni_F	Ratio of nickel content in the liquid product over the nickel content in the feedstock

p^o	Saturated vapour pressure of N_2 , mm Hg
p	Partial pressure of N_2 , mm Hg
S_F	Weight percent of sulphur present in the feed, %
S_P	Weight percent of sulphur present in the product, %
S_P/S_F	Ratio of sulphur content in the liquid product over the sulphur content in the feedstock
SA	Surface area of the catalyst, m^2/g cat
SA_{BET}	Surface area of the catalyst determined by the BET method, m^2/g cat
SA_{Hg}	Surface area of the catalyst determined by mercury porosimetry, m^2/g cat
SA_{N2}	Surface area of a N_2 molecule, m^2
$(SA)_t$	Surface area determined by the t-curve method, m^2/g cat
V_P/V_F	Ratio of vanadium content in the liquid product over the vanadium content in the feedstock
V_p	Total pore volume, mL/g of cat
X	Amount of N_2 adsorbed, mL N_2/g cat
X_m	Amount of N_2 adsorbed in the first monolayers, mL N_2/g cat
$(X_m)_t$	Amount of N_2 adsorbed between the statistical monolayers n = 1.6 and 1.2, mL N_2/g cat

Greek Symbols

θ	Time-on-stream, h

Abbreviations

AMOCO	American Oil Company
ASTM	American Society for Testing and Materials
ATOF	Area Turnover Frequency
BET	Brunauer, Emmett and Teller
BT	Benzo(b)thiophene
CCRL	Consumers' Co-operative Refineries Ltd
CONOCO	Continental Oil Company
DHU	Distillate Hydroprocessing Unit
DMP	2,5 dimethylpyrrole
DPEP	Deoxophylloerythoetioporphyrin
FCC	Fluid Catalytic Cracker
H/C	Hydrogen to Carbon atomic ratio
HDM	Hydrodemetallation
HDN	Hydrodenitrogenation
HDNi	Hydrodemetallation specific to nickel
HDO	Hydrodeoxygenation

HDS	Hydrodesulphurisation
HDV	Hydrodemetallation specific to vanadium
HGO	Heavy Gas Oil
HT	Hydrotreater
ICAP	Inductively Coupled Argon Plasma
ICDD	International Centre for Diffraction Data
JCPDS	Joint Committee on Powder Diffraction Studies
LCO	Light Cycle Oil
LGO	Light Gas Oil
LHSV	Liquid Hourly Space Velocity
LSV	Liquid Space Velocity
MCR	Micro Carbon Residue
Ni-SOD	Nickel-impregnated sodalite
RICO	Ru Ion Catalyzed Oxidation
SOD	Sodalite
TGA	Thermogravimetric Analysis
XRD	X-ray Diffraction

CONTENTS

LIST OF TABLES

LIST OF FIGURES

CHAPTER ONE

1.0 INTRODUCTION

1.1 SCOPE OF RESEARCH

The object of this work was to improve the colour of the diesel fuel fraction which is produced by hydrocracking Lloydminster heavy oil at the Consumers' Cooperative Refineries Ltd (CCRL) in Regina Saskatchewan. The effect of Ni-impregnated sodalite as a catalyst component was studied by measuring data on hydrodemetallation (HDM), hydrodesulphurization (HDS) and hydrodenitrogenation (HDN) as well as on catalyst deactivation. This is an extension of investigations by Minja and Ternan on hydrocracking of heavy oil with Co-Mo catalysts containing a zeolite component (Minja, 1990). In their study, they used Boscan (Venezuela) heavy oil and obtained HDS, HDN and MCR experimental results using Co-Mo catalysts containing various amounts of HY zeolite (Minja, 1990) and H-mordenite (Minja and Ternan, 1991, 1991a).

The fact that zeolites act as molecular sieves offers a significant advantage over the amorphous alumina-silica. The uniformity and the size of its pores allow a reliable selectivity of reaction as only molecules small enough to enter the pores will reach the

active sites. This principle was emphasized in this work as sodalite was used for its small pores. Nickel ions were deposited inside those pores using both ion exchange methods and impregnation methods. After reduction of the nickel oxide (NiO), potassium ions (K^+) were exchanged on the sodalite to be positioned at the pore mouths. The intent was to reduce the size of the pores to allow only the small hydrogen molecules to reach the Ni active sites while the larger hydrogen sulphide molecules remained outside the zeolite pores. As a result, the active sites were to be protected from sulphur poisoning and remained available for hydrogen dissociation. Once the dissociation by reduced nickel was achieved, the hydrogen atoms would spillover on the sulphided Co-Mo-alumina pore surface and become available for the hydroprocessing reactions.

1.2 THE OIL INDUSTRY

Today's petroleum industry has evolved significantly from the mid 1800's when the first modern petroleum well, the Drake well, was drilled near Titusville, Pensylvania in 1859 (Egloff and Alexander, 1951). Initially petroleum refining involved simple fractionation of the components already present in the oil to obtain kerosine for lamps. Later the market for more specialized products broadened and crude quality became more varied (Shreve and Brink, 1977). Today, as the worldwide supply of high quality, low-sulphur crude oil decreases and product specifications become more stringent, (Søgaard-Andersen et al., 1992), the refining industry is under increasing pressure to convert heavier, more challenging feedstocks into higher quality finished products. This

is particularly true for Canada as it has one of the largest proven deposits of oil sands bitumen and heavy oils in the world (Ouwerkerk et al., 1982). Since fossil fuels will continue to be the predominant source of energy for several decades to come, modern scientists must develop more efficient technologies capable of meeting today's challenges.

1.2.1 PETROLEUM CHEMISTRY

1.2.1.1 Crude Oil

The feedstock for refineries comes from petroleum or crude oil from various reservoirs throughout the world. In Canada, conventional petroleum is supplemented by synthetic crude oil derived from oil sand bitumen, etc. Conventional crude oil can contain between 20% to 50% of atmospheric residuum. In contrast, synthetic crude oil contains only distillate. Table 1.1 shows the properties of various atmospheric residua (Quann et al., 1988).

Petroleum is a complex, wide-boiling-range mixture of hydrocarbons and non-hydrocarbon organic compounds that extends from the simplest alkanes to highly complex structures with molecular weights in the thousands. With increasing boiling point, the concentration of cyclic and aromatic compounds increases (up to 80%) as does the complexity of the mixture. The heavier fractions contain a significant amount of impurities such as sulphur, nitrogen, oxygen and metals. Although it was found that

Table 1.1 : **Properties of Various Atmospheric Residua** (Quann et al., 1988)

Crude Oil Origin	Gravity (°API)	Sulphur (wt%)	Nitrogen (wt%)	MCR (wt%)	Asphalt. (wt%)	Nickel (ppm)	Vanadium (ppm)
Iranian Heavy	14.7	2.52	0.47	9.5	6.7	57	166
Kuwait	14.6	4.1	0.22	11.1	3.5	22	77
Arabian Heavy	12.7	4.24	0.28	12.3	10.2	28	78
Maya (Mexico)	8.8	4.5	0.54	18.3	15.0	70	433
Asthmus (Mexico)	15.7	2.84	0.24	8.6	2.1	14	86
Alaskan North Slope	15.4	1.58	0.34	8.3	1.7	16	43
Hondo (California)	8.5	6.49	0.87	13.5	14.2	130	249
France-Wilmimgton (California)	10.0	2.18	0.79	13.0	5.9	73	84
Santa-Maria (California)	5.3	6.43	0.86	17.0	17.6	156	318
Kern River (California)	10.2	1.16	0.94	9.3	3.3	88	47
Jobo (Venezuela)	6.8	4.24	0.54	16.2	14.4	93	450
Bachaquero (Venezuela)	10.1	2.79	0.57	14.3	8.4	61	507
Honogas/Morichal (Venezuela)	8.6	3.54	0.51	13.8	11.1	114	387
Boscan (Venezuela)	6.3	5.9	0.69	18.2	13.5	130	1553
Athabasca (Canada)	5.9	4.9	0.41	14.9	11.4	86	167
Cold Lake (Canada)	10.0	4.4	0.39	12.8	10.8	62	164
Lloydminster (Canada)*	10.1	3.74	0.45	13.4	14.6	56	123

*Data measured in laboratory

nearly half of the metals of the periodic table can be found in trace amounts in petroleum, Ni, V and Fe are normally the major constituents. It is generally agreed that the elemental composition of petroleum varies within the following ranges (Francis and Peters, 1980):

carbon	80 to 89 %
hydrogen	12 to 14 %
nitrogen	0.3 to 1.0%
sulphur	0.3 to 3.0 %
oxygen	2.0 to 3.0%

1.2.1.2 Asphaltenes

By definition, asphaltenes are the precipitate obtained when a petroleum of bitumen is mixed with 40 volumes of a relatively light paraffin, usually pentane. Asphaltenes constitute a solubility class consisting primarily of highly polar and aromatic species which may be quite varied on a molecular basis (Quann et al., 1988). Asphaltenes are thought to be the most complex, high-molecular-weight, high-boiling components in petroleum. Heteroatom impurities tend to concentrate in disproportionate amounts in the asphaltene fraction of the crude. Sulphur content was determined to be 8.0%, oxygen 3.0% and nitrogen 1.0%. The hydrogen/carbon atomic ration was about 1.24 (Mojelsky et al., 1992). The diameter of these molecules, as determined using analytical and preparative gel permeation chromatography, is in the range of 38-55 Å for sulphur containing species, 41-72 Å for nickel, and 40-65 Å for vanadium (Hall and Herron, 1981). Mojelsky et al. (1992) characterized the Athabasca oil sand asphaltene

fraction as a dark brown amorphous solid having an average molecular weight number of 3600 with a broad molecular weight distribution ranging from a few hundreds to tens of thousands. The structural details were further studied by Mojelsky and co-workers using the Ru Ion Catalyzed Oxidation (RICO) technique which revealed numerous bridges varying in lengths between heavily branched aromatic carbons. A simplified asphaltene structure can be found in Figure 1.1.

1.2.2 PETROLEUM REFINING

Petroleum refining is probably one of the most complex industries as it can supply in excess of 2000 different products (Gary and Handwerk, 1984). Each refinery is specifically designed to operate under different constraints such as accessibility of feedstock, products slate, product quality, capital investment, environmental regulations and by-product disposal. As an example, a simplified block diagram of the Consumers' Co-operative Refineries Ltd (CCRL) heavy crude oil upgrader in Regina, Saskatchewan is shown in Figure 1.2. In most refineries, crude oil is first separated by an atmospheric fractionator into several distillate fractions having specific boiling-point ranges. While light fractions such as straight run gasoline are sold without further processing, naphthas are hydrotreated and reformed into light aromatics to improve their octane number. Middle distillate and light gas oil fractions are hydrotreated to meet environmental specifications.

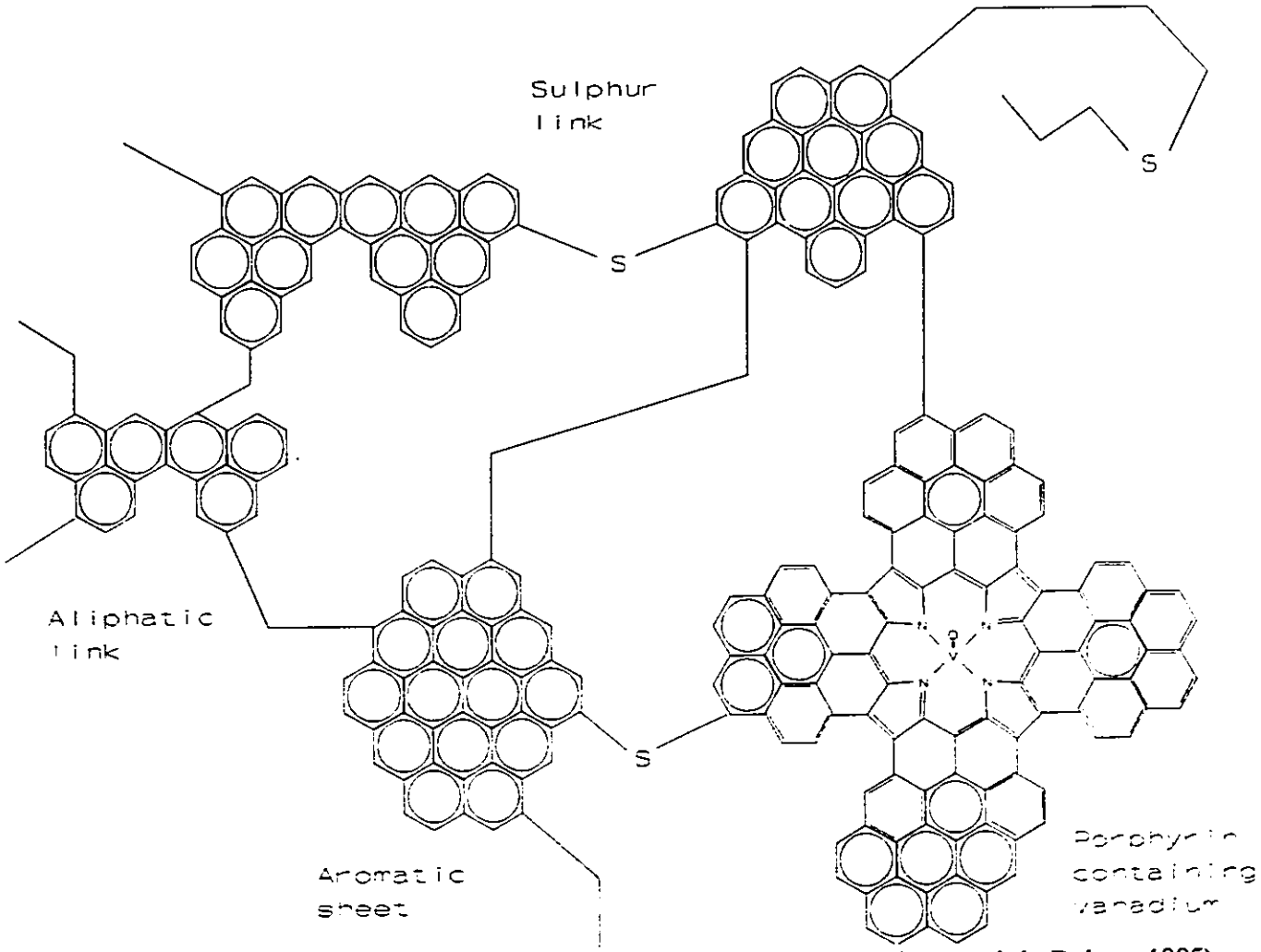

Figure 1.1 : **Model of aromatic cluster found in the asphaltene fraction** (Dautzenberg and de Deken, 1985).

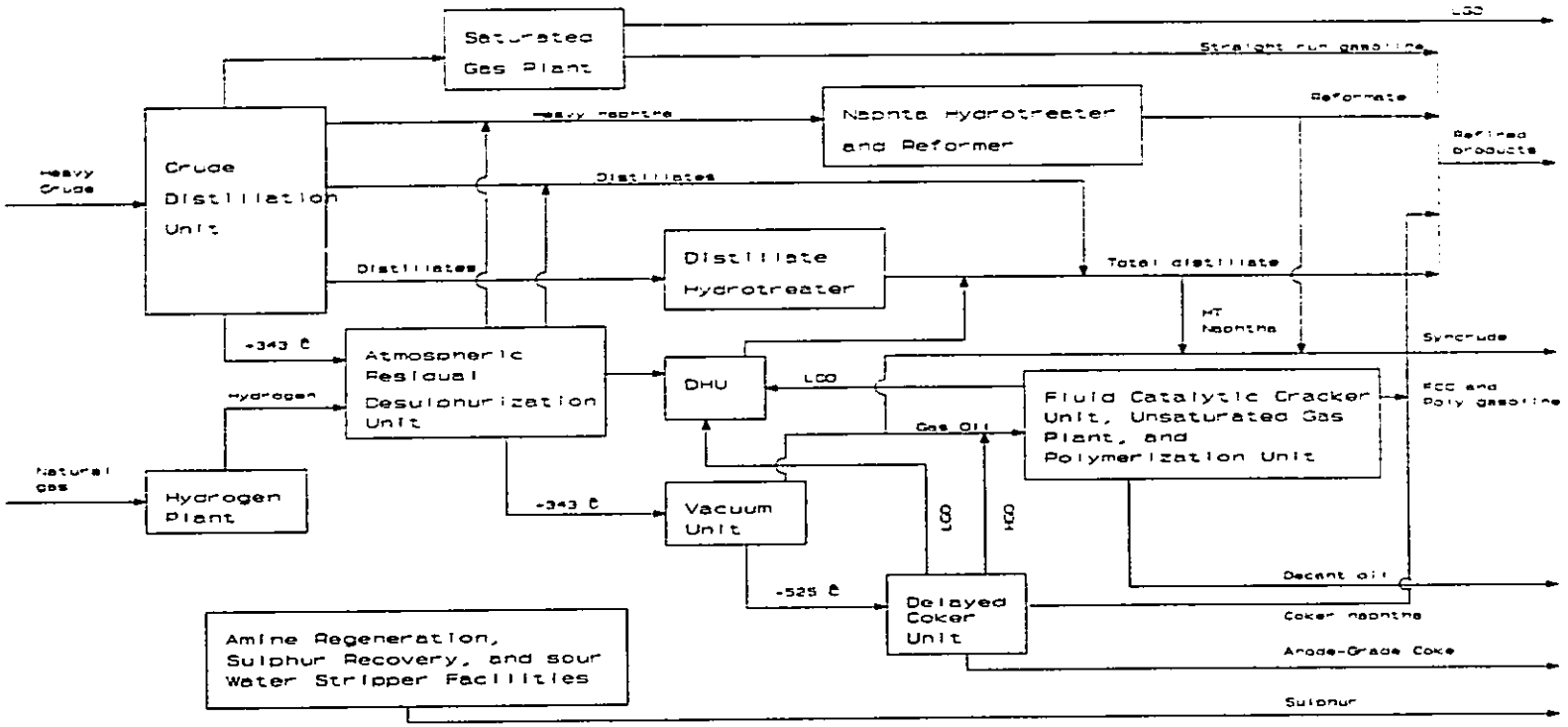

Figure 1.2 : **Block Flow Diagram of the CCRL Refinery and Heavy Oil Upgrader** (Court and Smith, 1989).

The high-boiling residue (typically +343°C) from the atmospheric fractionator called *atmospheric residuum* undergoes a number of different processes. First, it is fractionated under vacuum up to a normal boiling-point of 525°C. Each vacuum tower distillate fraction is redirected depending on boiling point range, quality of feed and market influences. The heavy, least desirable fraction, the *vacuum residuum* is converted into more valuable products using a number of different methods. The residuum conversion processes, most commonly used by the Canadian petroleum industry (delayed coking and hydrocracking) will be described further. Details on petroleum refining processes can be found in reviews by Shreve and Brink (1977), Langhout et al. (1980), Aalund (1984), Gary and Handwerk (1984), Chase (1989), Court and Smith (1989) and Oelderik et al. (1989). Outlines of some of the most common refining processes, such as catalytic cracking and hydroprocessing (hydrotreating and hydrocracking) are presented below.

1.2.2.1 Hydrotreating

As discussed earlier, most petroleum fractions contain an excess of heteroatoms. Because of environmental concerns and economical aspects, the heteroatom content in petroleum products must be minimized. Sulphur and nitrogen are responsible for SO_x and NO_x emissions which contribute to acid rain. Furthermore, sulphur and nitrogen species poison hydroprocessing catalysts by eliminating active sites. Consequently, hydrotreating must he performed on most lighter product streams for better performance.

Numerous studies have been conducted in an attempt to describe the mechanisms of hydrotreating. However, because of the complexity of petroleum feedstocks, it is almost impossible to isolate each reaction taking place during hydroprocessing. Consequently, model compounds are studied in relatively pure environments in order to help understand their reaction mechanisms. Caution must be exerted in the interpretation of these studies as they cannot represent the true behaviour of these heteroatom compounds in such complex mixtures like petroleum. However, they provide the best available quantitative foundation for process modelling and catalyst development.

1.2.2.1.1 Hydrodesulfurization (HDS)

Thiophenic compounds are considered the least reactive organosulphur compounds in petroleum and other fossil fuels (Gates et al., 1979). Some examples of these compounds are shown in Figure 1.3a. Of those, methyl-substituted dibenzothiophenes are recognized as the organosulphur compounds with the slowest conversion, consequently they are the most representative of the HDS in heavy fossil fuels.

Kolboe (1969) presented evidence that the first C-S bond on the adsorbed thiophene compound is broken before a random hydrogenation of the remaining radical takes place in parallel with the cleavage of the second C-S bond. In contrast however, Girgis and Gates' (1991) review of catalytic hydroprocessing reactions revealed that for most HDS proposed mechanisms, hydrogenation of the organosulphur molecule had to

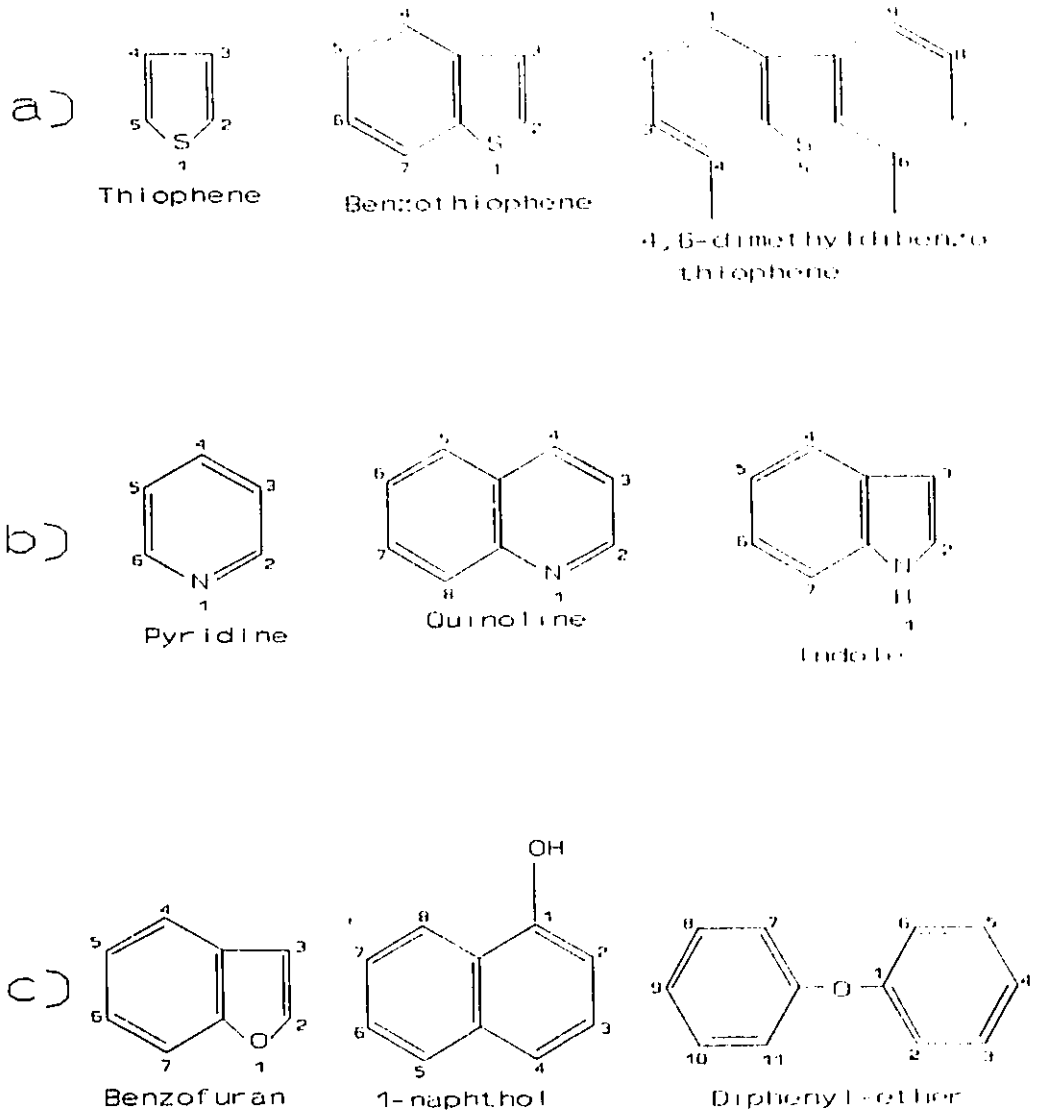

Figure 1.3 : **Typical heteroatom-containing molecules present in crude oil a) Sulphur containing molecules b) Nitrogen containing molecules c) Oxygen containing molecules.**

take place to a certain extend, thereby weakening the C-S bond strength before bond cleavage and sulphur elimination as H_2S could occur. Huckett and co-workers (1988), in their study of deuterium exchange of benzo(b)thiophene (BT) reported that, as for thiophene, BT was adsorbed via π-thiophene ring. In the activated form it would then undergo deuterium exchange on the H2 and H3 positions. Girgis and Gates (1991) also suggested that, because of their relatively rapid hydrogenation, some compounds such as benzonaphthothiophenes would be adsorbed flat on the catalyst to form π-bonded species to which hydrogen could be added.

1.2.2.1.2 Hydrodenitrogenation (HDN)

Nitrogen in heavier feedstocks is present predominantly in heterocyclic aromatic compounds. Nonheterocyclic organonitrogen compounds such as aliphatic amines and nitrites are also present, but in considerably smaller amounts. They are denitrogenated much more rapidly than the heterocyclic compounds (Katzer and Sivasubramanian, 1979). Examples of nitrogen compounds are shown in Figure 1.3b. Quinoline is considered to be a good model for higher molecular weight compounds found in heavier hydroprocessing feeds (Satterfield and Yang, 1984).

Nitrogen compounds definitely must be hydrogenated before scission of the nitrogen- carbon bond and formation of NH_3. HDN is virtually irreversible under typical reaction conditions. Because of stearic hindrance, it is believe that end-on adsorption

through the nitrogen atom is unlikely and that an adsorption through the π-bonds of the aromatic rings is more probable (Girgis and Gates, 1991). The HDN conversion decreases dramatically if the sulphur content of the catalyst decreases.

1.2.2.1.3 Hydrodeoxygenation (HDO)

The content of oxygen complexes in the original crude is normally lower than that of sulphur and nitrogen. The oxygen compounds of main interest are furanic-ring-containing compounds, phenols and aryl ethers. In addition, prolonged exposure of feedstocks to air will increase the amount of oxygen through autoxidation (Furimsky, 1983). Large quantities of oxygen compounds can be rather unstable and form deposits on exposure to air. Examples of these compounds are shown in Figure 1.3c.

Very few studies have been reported on HDO in comparison with the extend of the literature covering HDS and HDN. HDO reviews indicate that oxygen removal may occur either with or without prior hydrogenation of the complex (Furimsky, 1983; Girgis and Gates, 1991). Although the mechanism of HDO is not well understood, it was found that the reaction will not take place in the absence of active hydrogen even if the molecule is adsorbed in a proper position. It was assumed that for example, on an acidic surface, the phenols tend to be adsorbed in a flat position while on a nonacidic surface, the interaction of a phenolate form with the surface via the oxygen anion occurs

(Furimsky, 1983). It was also concluded that a sufficient amount of S-donating species must be continuously supplied to avoid replacement of sulphur in the catalyst by oxygen (Furimsky, 1983).

1.2.2.1.4 Hydrodemetallation (HDM)

HDM studies are extensive in the literature as metals, namely nickel and vanadium are probably the most troublesome heteroatoms in petroleum. It is desirable to remove metal compounds to prevent poisoning of the cracking catalyst and erosion of the furnace linings and turbine blades (Quann et al., 1988).

Nickel and vanadium in petroleum exist either as metal porphyrins and nonporphyrin metal complexes. The basic skeleton of porphyrin is porphine ($C_{20}H_{14}N_4$), a closed ring of four pyrrole groups bridged by methine-carbon atoms at the α-carbon which is shown at Figure 1.4 along with the two basic groups of metallopetroporphyrins: DPEP (deoxophylloerythoetioporphyrin) and etioporphyrin (etio). Nonporphyrinic metal complexes are simply heteroatom aromatic ring structures resembling porphyrins, except that they contain sulphur and nitrogen or chelated metal complexes in various proportions. Dean and Whitehead (1963) performed molecular distillation to temperatures as high as 705°C without severe cracking of the feedstock. Their study revealed that the majority of Ni and V appeared in the + 650°C fraction, normally as nonporphyrins. Only a small percentage of metals was present in the 500-650°C fraction,

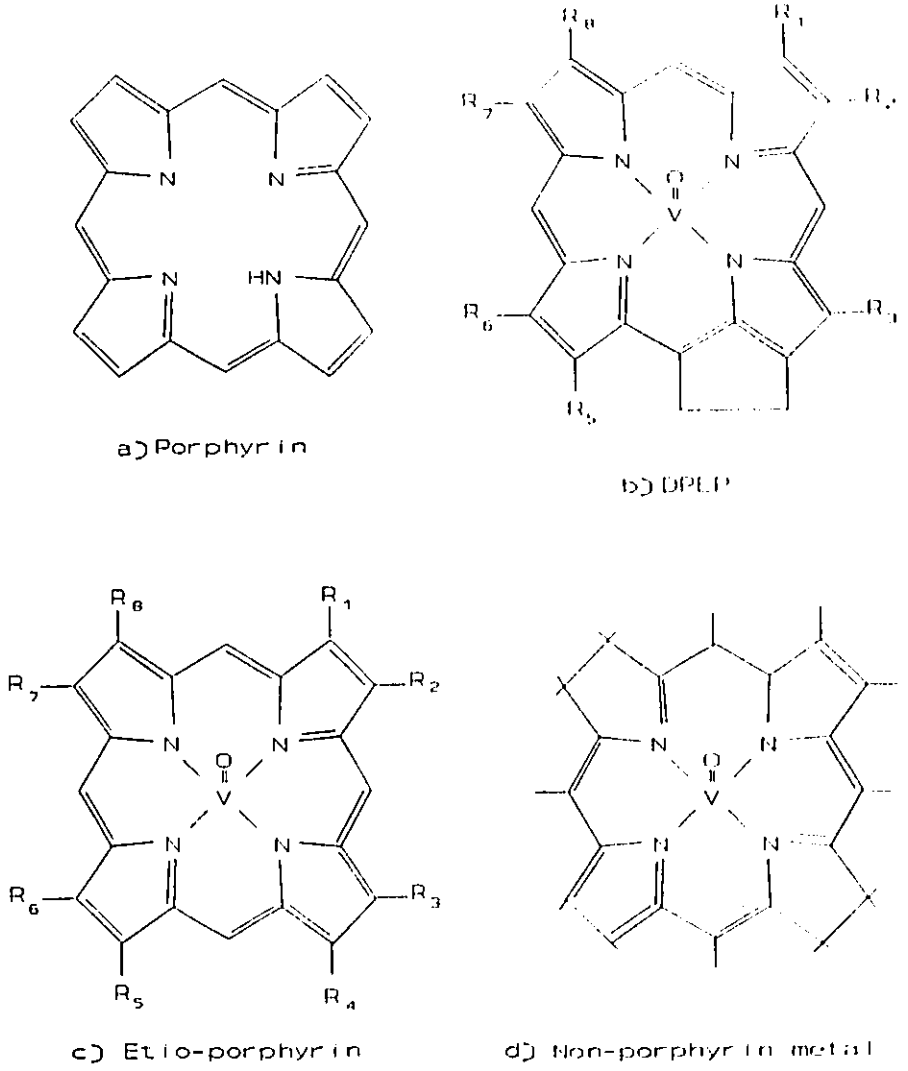

Figure 1.4 : **Typical porphyrins and metal complexes present in crude oil.**

but within this fraction, most of the metal (70%) was in the form of porphyrins. It would appear that the metal porphyrins are more volatile and, therefore, have lower molecular weight or lower polarity resulting in fewer intermolecular associations (lower boiling-point) than the nonporphyrin metals.

Ware and Wei studied the mechanism of hydrodemetallation of Ni-porphyrins both in a reaction mixture without sulphur (Ware and Wei, 1985a) and in a reaction mixture having both competing sulphur and nitrogen reactions (Ware and Wei, 1985b). Both studies revealed that reversible hydrogenation of methine bridges in Ni-porphyrins molecules occurred twice to form the tetrahydro species before the ring was opened and the metal deposited. This conclusion from both studies indicated that the HDM mechanism for Ni-porphyrins was not catalyst dependent but changed with the type of porphyrins.

1.2.2.2 Hydrocracking

The hydrocracking process is normally effected on heavier fractions such as gas oil or residue from the atmospheric fractionator, and is often combined with hydrotreatment. Hydrocracking converts high boiling compounds into desired lower boiling molecules by hydrogenation and pyrolysis without producing large amounts of coke by-product. The use of hydrogen allows saturation of heavier complexes, carbon bond cleavage and heteroatom removal. Hydrotreating is performed in the first stage

where a more resistant, less active catalyst such as Co-Mo or Ni-Mo complexes are used to eliminate most of the heteroatoms in the feed and hydrogenate aromatic structures. Hydrodemetallation is normally performed as well at that stage since metals tend to concentrate in heavier fractions. Metals are well known for depositing on catalyst surfaces, thereby causing pore plugging, rapid deactivation and higher catalyst costs. In the second stage, further hydrotreating but mainly hydrocracking take place. More expensive, less heteroatom resistant bifunctional catalysts such as Ni/W/zeolite complexes are more suitable for this function (Bhatia, 1988).

Hydrocracking is also performed on the vacuum fractionator heavier fractions. Because of the higher molecular weight and the higher heteroatom content of these fractions, only CoMo/NiMo complexes are used. Despite the poor quality of the feed, these catalysts can still perform both functions of heteroatom removal and pyrolysis.

1.2.2.3 Catalytic Cracking

Catalytic cracking is the most important and widely used refinery process for converting heavy gas oils into more valuable products (Bhatia, 1988). The advent of catalysis significantly improved the yield of higher boiling fractions over thermal cracking, therefore almost eliminating the use of thermal cracking in modern refineries. Because catalytic cracking does not use hydrogen, feedstocks to catalytic crackers are usually of higher quality such as products from a crude distillation unit or a

hydrocracking unit. The main purpose of catalytic cracking is to reduce molecular weight and aromatic content.

Catalytic cracking is normally performed using moving bed or fluidized bed units both of which are similar in principle. Moving bed units operate on the first-in-first-out basis with catalyst particle size up to about 3 mm in diameter. Fluidized bed reactors, for their part use a lighter catalyst (particle size less than 5Oμm in diameter) which is rapidly circulating between the reactor and the regenerator until the desired yield is obtained. Hydrocarbons and residual oil are steam stripped before the catalyst enters the regenerator where deposited coke will be burned with air. Coke and metal deposition on the catalyst surface quickly reduces catalytic activity, making regeneration essential for longer life cycles. For this reason, a constant flow of catalyst must be maintained between the reactor and the regeneration unit. Residual coke may vary between 0.2 and 0.4 wt% (Bahtia, 1988). The heat generated by the regeneration process is recycled to the reactor.

1.2.2.4 Delayed Coking

The delayed coking process was developed to convert large residuum molecules into smaller distillate molecules by severe thermal cracking. High velocities of feed in the furnace tubes and transfer lines (minimum retention time) avoid the formation of solid coke at temperatures above the coking point, consequently *delaying* coking until the feed

has reached insulated coke drums where it remains for long residence times. Lighter fractions formed by pyrolysis reactions are separated as they enter the vapour phase and leave the coking drum. (Gary and Handwerk, 1984). Delayed cokers can be used in conjunction with hydroprocessing to process the unconverted +525°C fraction from a residuum hydrocracker (Chase, 1989). With extensive hydroprocessing it is possible to produce more valuable high grade coke (low sulphur, low metals) which can be used as carbon anodes in electrochemical plants (Quann et al., 1988; Pereira et al., 1987).

An example of an efficient combination of hydroprocessing and coking is the world's largest residuum hydrocracker which was brought on stream by the AMOCO refinery in Texas City, Texas in 1984. A comparison between total coking and a combination of hydroprocessing and coking was performed at the AMOCO plant and revealed that the combination produced an increase of more than 30% in valuable distillate product yield while decreasing undesirable coke production by 70%. Furthermore, the coke produced in the second option was entirely high grade. The AMOCO residuum hydroprocessing unit consists of three trains, each having three backmixed reactors in series, followed by an atmospheric fractionator and a vacuum tower. The process produces gasoline, distillate and gas oil. It is capable of processing 60 000 barrels per stream day and has a conversion level in excess of 70%. Finally, a downstream coker produces high grade coke. The AMOCO process was thoroughly reviewed by Beaton and Bertolacini (1991).

1.3 FUEL STORAGE STABILITY

The storage instability of fuels is a function of their composition. Middle distillates originating from thermally or catalytically cracked stocks are known to be much less stable than straight-run distillates (Bhan et al., 1986; Taylor and Frankenfeld, 1986; Pedley et al., 1988; Batts and Fathom, 1991; Beaver 1991; Baron et al., 1992). Unfortunately, straight-run distillate yields are no longer sufficient to match the steady increase in middle distillate demand. The petroleum industry has been forced to increase the proportion of light cycle oil (LCO) in their final product blends, thereby causing the storage stability of the fuel to diminish.

The stability of a fuel is measured from its capacity (or lack thereof) to form gum and sediments, as well as to maintain its translucent colour. Although no correlation has been established between the colour of diesel and engine performance (Taylor and Frankenfeld, 1986; Baron et al., 1992), consumers associate dark colours with poor fuel grades. On the other hand, sediments and gum can cause real problems, such as nozzle or injector clogging, filter plugging and ultimately, engine failure (Batts and Fathoni, 1991). Consequently, colour darkening, sediment and gum formation are undesirable.

1.3.1 CAUSES OF INSTABILITY

Nitrogen, sulphur and oxygen compounds are the principal sources of fuel

instability (Taylor and Frankenfeld, 1986; Batts and Fathoni, 1991; Mushrush et al., 1991). However, the specific heteroatom compounds directly responsible for instability are not normally well known because of the multiplicity of reaction possibilities and the synergistic actions of those reactions (Stirling et al., 1991). However, several categories of compounds have been identified. Some examples are non-basic nitrogen heterocycle compounds such as pyrroles (2,5 dimethylpyrrole (DMP) (Tort et al., 1991) and indoles, particularly alkyl indoles (Hiley and Pedley, 1988), carbazole (Beaver, 1991; Marshman, 1991), and 2-methylindole (Tort et al., 1991). Sulphonic compounds which are known to have an effect on sediment formation and fuel coloration include aromatic thiols (Taylor and Frankenfeld, 1986) such as thiophenols (Henry, 1986; Hazlett, 1988). Aliphatic thiols, sulfides, disulfides, condensed thiophenes (Hiley and Pedley, 1986; Taylor and Frankenfeld, 1986; Mushrush et al., 1991), and more specifically benzo and dibenzothiophenes (Fathom et al., 1991) do not play a significant role in fuel instability.

Not all investigators agree on the effects of nitrogen compounds. Bhan and co-workers (1987), in their extensive study on fractionated marine diesel fuels, observed no relation between the content of nitrogen compounds and sediment production or development of colour. This observation suggests that nitrogen compounds may not necessarily be sediment precursors. Bhan et al emphasize the ease of oxidation of certain nitrogen compounds, such as the well documented DMP (Mushrush et al., 1991), as being the cause of sediment formation instead of the presence of the nitrogen component itself. Many more authors concur with the importance of oxidation, often as a first step

towards sediment and gum formation (Taylor and Wallace, 1967; Cooney et al., 1985; Batts and Fathoni, 1991; Mushrush et al., 1991). Beaver (1991) proposed an extensive series of oxidation mechanisms on the degradation of petroleum distillates. It was proposed that various organosulphur and organo-oxygen are readily oxidized to the corresponding sulphonic acid or carboxylic acid by hydroperoxide species (Mushrush et al., 1991). Sulphonic acids from the oxidation of mercaptans (Marshman, 1991) or aromatic thiols (Hiley and Pedley, 1988; Mushrush et al., 1991) are known to be particularly deleterious to storage stability. They function as both a catalyst and a radical initiator but are not normally incorporated into the deposits (Hazlett, 1988). Carboxylic and phenolic acids have also been reported to exert a catalytic effect on fuel instability and on the quantity of sediments formed (Dorbon et al., 1990). Finally, traces of metallic copper complexes act as catalysts for sediment and gum formation (Henry, 1986; Batts and Fathoni, 1991; Beaver, 1991; Tort et al., 1991).

1.3.2 MECHANISM

Among the number of mechanisms for sediment formation proposed (Mushrush et al., 1991a; Taylor and Frankenfeld, 1986; Tort et al., 1991), the one developed by Pedley and co- workers (1988, 1989) has gained general acceptance by a number of authors. It consists of the oxidation of phenalene to phenalenone, followed by the reaction of phenalenone with alkyl indoles to form a complex called indolylphenalenes which are soluble in middle distillate. Under the influence of sulphonic acids resulting

from the oxidation of thiols however, these indolylphenalenes yield coloured precipitates. Figure 1.5 depicts a simplified version of a precursor reaction involved in the mechanism for sediment formation. Although the amount of insolubles formed during a storage period could not be correlated directly with the concentration of alkylindole and phenalene species, the stable fuels were nevertheless characterized by the absence of one or both of these species, and both species were present in the unstable fuels (Pedley et al., 1990). Furthermore, a world-wide storage stability survey was conducted by Marshman and Pedley (1991) and revealed a good correlation between the presence of phenalene or phenalenone species in fuels from various sources and the presence of the typical storage stability sediments. Further work by Marshman (1991) revealed that the formation of sediments during storage of fuels containing light cycle oil required the presence of at least three chemical species: phenalenes, indoles and acids. The removal of one or more of these species resulted in a stable fuel. Finally, a study performed by Stirling and co-workers (1991) revealed that the distillate fraction boiling in the 240-330°C range which includes both indole (254°C) and phenalene (295°C) species did not form appreciable quantities of sediments. Although no relation with the presence or absence of acids in the latter boiling fraction was made in this case, a separation of the middle distillate into acidic, neutral and basic components revealed that acids had a major impact on fuel stability.

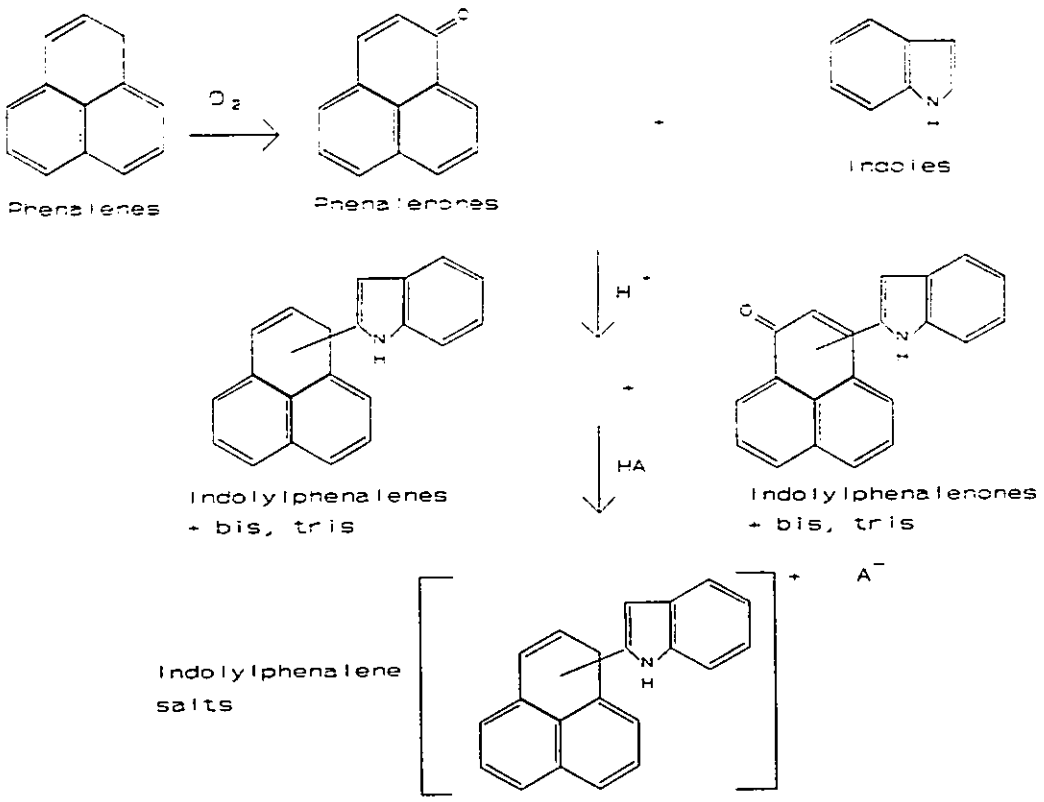

Figure 1.5 : **Reaction mechanism for sediment formation proposed by Pedley** (Marshman, 1991).

1.3.3 COLOUR FORMATION

Diesel colour is of particular importance for this investigation. In addition to the compounds reported previously, Taylor and Frankenfeld (1986) noted that alkyl amines will produce colour under storage conditions, but no measurable sediment. Bhan and co-workers (1986) reported that colour-causing species were concentrated in the acid fraction and that oxidation of neutral components to polar intermediates could be a major pathway for darkening of diesel fuels. Fuel concentrates were obtained using nonaqueous ion exchange liquid chromatography. Finally, exposure of fuel to light or oxygen was reported detrimental to diesel fuel colour stability (Baron et al., 1992).

In some countries like Australia and Japan, fuel colour specifications are particularly stringent. Consumers have been used to lighter fuel colour in the past and continue to expect it despite the changes in crude oil supplies. For instance, colour specifications in Australia or Japan call for ASTM colour of no more than L1.0 while it is not uncommon to see ASTM colour specifications of 3.0 in the United States (Baron et al., 1992). ASTM colour ranges from 0 (colourless) to 8.0 (dark red).

In order to meet those requirements, a Japanese feasibility study (Takatsuka et al., 1991) was performed to examine colour improvements from a deep desulphurization HDS processing unit. The desired sulphur level was 0.05 wt%. Interesting observations have been made which show that the yellow colour of straight-run diesel first disappeared

up to a desulphurization level of 80 %. Then the yellow-green fluorescence appeared again when the conversion reaches 95 %. This phenomenon was explained as follows: in the desulphurization mechanism, sulphur is removed from the oil onto the catalyst, and the remainder of the molecule is quenched by hydrogen. If the molecule is not easily quenched for reasons such as steric hindrance, it is left as an active radical and a condensed aromatic structure can be formed. It was suspected that colour bodies could be derived from this new structure of polyaromatics.

After deep desulphurization, distillate fractions boiling below 250°C did not contain colour bodies as they were clear. In contrast colour existed in distillates boiling above 250°C since those fractions were darker in colour. Finally, it was found that colour bodies were not caused by molecules having structures such as $> C = C <$, $> C = NH$, or $> C = S$ bonded to aromatics since those compounds are removed by the deep desulphurization process (Takatsuka et al., 1991).

1.3.4 IMPROVING FUEL STABILITY

Although the problem of fuel stability is complex, it can be alleviated. The most popular method of stabilizing diesel fuels is probably the use of low cost additives. It is very important that antioxidants be added to cracked components before oxygen exposure. Hindered phenols and dialkyl phenylenediamines are used as antioxidants to prevent peroxide accumulation (Henry, 1986) but their efficiency has been questioned

(Hazlett, 1988). On the other hand, organic amines such as tertiary alkyl amine which are basic compounds are considered to be quite effective. It has been proposed that they counteract the deposit inducing ability of acids, which catalyses condensation and polymerization reactions involving components in light cycle oils (Hazlett, 1988). Tort and co-workers (1991) also recommended the use of basic and nucleophilic compounds to avoid condensation of alkylindoles and/or formation of sulfonic acids. Metal deactivators are also used to neutralize traces of dissolved metal salts. They form chelates with the metal salts which are generally less active as oxidation catalysts (Henry, 1986).

Caustic scrubbing is used for sweetening of the fuel by removing thiophenols. It does not stabilize the cracked material completely. Therefore a combination of scrubbing and additives is recommended (Batts and Fathoni, 1991). Excellent reduction of deposit formation tendencies have been obtained (Smith and Palmer, 1986).

Although these methods have some influence on sediment and gum formation, they cause very little improvement on colour stability. The most effective and the most costly process to stabilize diesel fuel colour is hydrotreatment (Palmer and Copson, 1986; Smith and Palmer, 1986; Batts and Fathoni, 1991). As discussed earlier, such process are expected to produce a fuel with little or no olefinic unsaturation and a low sulphur content (Batts and Fathoni, 1991). Palmer and Copson (1986) showed that for colour stabilization, hydrotreating was clearly the superior method.

1.4 CATALYSIS

1.4.1 Co-Mo CATALYST

The most widely used catalysts for heteroatom removal are $CoMo/Al_2O_3$ or $NiMo/Al_2O_3$ (Pereira et al., 1987; Quann et al., 1988; Girgis and Gates, 1991). However, some tungsten compounds (Girgis and Gates, 1991; Wilson and Kriz, 1984) are also used and a number of catalysts containing germanium, chromium, salts of lanthanum and boron phosphate have been patented (Pereira et al., 1987). Although some studies have been performed using molybdenum in its oxidized form (Ware and Wei, 1985a; Girgis and Gates, 1991), industrial molybdenum hydroprocessing catalysts are in their sulphided form (MoS_2) as they are more reactive as sulphides. Cobalt or nickel are used as promoters on Mo catalysts where cobalt is used for HDS and nickel for HDN. Prins et al. (1989) compiled an extensive review of the structure, mechanism and the role of the cobalt promoter in Co-Mo/γ-Al_2O_3 hydrodesulphurization (HDS) catalysts.

1.4.2 THE PHYSICAL STRUCTURE

The Co-Mo/γ-Al_2O_3 catalysts extrudates are usually made by impregnating a γ-Al_2O_3 support with aqueous solutions of ammonium paramolybdate $(NH_4)_6Mo_7O_{24}.4H_2O$ and cobalt nitrate $Co(NO_3)_2.6H_2O$. In its oxide form, Mo is highly dispersed and occurs

in a 6+ oxidation state. As loading increases, the Mo oxide structure changes to a three-dimensional morphology. These clusters are anchored to the support through Mo-O-Al linkages having a distribution of strengths (Hayden and Dumesic, 1987). On an industrial scale, sulphiding occurs in a stream of H_2S produced either from a sulphur compound such as CS_2 or directly from a mixture of H_2 and the feedstock. The reaction environment is highly reducing with H_2S always present and thermodynamics predicts that under those conditions, molybdenum and cobalt or nickel reside in their respective sulphided forms, MoS_2, and Co_9S_8, or Ni_3S_2 (Prins et al., 1989). Sulphiding leads to the breakup of large, bulky MoO_3 crystallites and to the conversion of the highly dispersed oxide layer into MoS_2 crystallites. At normal sulphiding temperatures (400°C), the oxygen anions not connected to the support such as oxygens terminally bound to Mo or bridging between molybdenum atoms are converted, leaving the more resistant Al-O-Mo links intact. At low molybdenum loading, higher sulphiding temperatures (500°C) will increase the average size of the particles, but also break more Al-O-Mo links allowing the MoS_2 crystallites to assume a 90° orientation, perpendicular to the basal plane. At higher loading however, the number of strong Al-O-Mo links is reduced to cause the larger particles (30 nm) to lay with the MoS_2 basal plane parallel to the support. In this state, these crystallites have little or no interaction with the support and are stabilized by weak van der Waals forces between their basal planes and the alumina surface (Hayden and Dumesic, 1987). Since sulphur anions in the basal planes are more strongly bonded to the Mo cations than those at the edges or corners of the platelets, catalysis is believed to occur at edges and corners as opposed to occurring on the basal planes as postulated

by Voorhoeve and Stuiver in their study of nickel promoted tungsten catalyst (1971b).

It was found that cobalt could be present in the catalyst under three different forms, each one being dependent on the original oxidic precursor form. As precursors, cobalt ions can occupy octahedral sites just below the Al_2O_3 surface or tetrahedral sites in the Al_2O_3 bulk. During sulphiding, the cobalt ions migrate to the MoS_2 crystallites to form the Co-Mo-S phase, while those in the tetrahedral sites remain in the γ-Al_2O_3 structure. At higher loadings, cobalt can form separate solid phases Co_3O_4 crystallites in the oxide form on the surface of the support which in turn become Co_9S_8 in the sulphidic form (Topsøe et al., 1981). It was shown that the promoter effect was not caused by separate Co_9S_8 crystallites but by cobalt ions in the CoMoS phase (Wivel et al., 1981). Furthermore, an infrared study confirmed that the cobalt ions were located at the edges of a MoS_2 layer, (on the molybdenum plane) covering the molybdenum ions (Topsøe and Topsøe, 1983), rather than between the edge sulphur anions of subsequent layers of MoS_2 (Farragher and Cossee, 1973) or intercalated between alternating MoS_2 layers (Voorhoeve, 1971).

1.4.3 SURFACE MECHANISM

The mechanism for heteroatom removal remains at this time open for speculation (Prins et al., 1989). It has been suggested that there are two types of active sites on the catalyst. Electron holes created by an excess of sulphur anions (Aoshima and Wise,

1974) or by cobalt cations (Wentrcek and Wise, 1976) dissociating H_2. Sulphur compounds react at sulphur anion vacancies (Kogan et al., 1990). These sites adsorb the heteroatoms of a carbonaceous molecules (end-on) and subsequently hydrogenation and bond cleavage take place (Ternan, 1983; Furimsky, 1983; Bahtia, 1988; Prins et al., 1989). However, Prins and co-workers (1989) in their review demonstrated that several authors no longer agree with this proposed mechanism and have suggested a number of other possibilities. Kwart et al. (1980) proposed that adsorption of thiophene, for example takes place via π-bonds (side-on) where the number of "contact points" varies on the size of the molecule adsorbed, while others prefer a model involving the formation of ligands (Rakowski-Dubois et al., 1980). None of these models have been rejected by recent findings, therefore they cannot be ignored.

1.4.4 PORE DIFFUSION

The diffusion of large molecules though small pores can be prohibitively slow. Unfortunately small pores are necessary to maximize the catalyst surface area and the number of reaction sites. Consequently, there is an optimum pore size for each catalyst which is dependent upon the purpose of the catalyst and the feedstock processed. Maximum activity for Ni and V removal from Athabasca bitumen occurred with catalysts characterized by median pore diameters of 200 Å (Quann et al., 1988). Bimodal catalysts with mesopores and macropores are often used to improve the rate of diffusion. Hydrodemetallation takes place in the larger macropores which are also used as highways

for the carbonaceous molecules to reach the smaller mesopores which contain most of the catalyst surface area accessible to the carbonaceous molecules. The mesopores are large enough to allow the large carbonaceous molecules inside, however their diffusion rate is much slower in mesopores than in macropores.

1.4.5 CATALYST POISONING

The worst poison for hydrocracking catalysts is probably metal deposition from heteroatom removal reactions. Products from HDN and HDO reactions, NH_3 and H_2O are also known to be poisonous to the catalyst by occupying reaction sites on its surface. The presence of H_2S, the product of the HDS reaction, helps maintain the surface in a sulphided form (Furimsky, 1983) and competes with other gas molecules for anion vacancies (Kogan et al, 1990). Poisoning by these species is limited by their partial pressure in the vapour phase. On the other hand, metals continue to deposit on the catalyst surface and poison active sites, as long as they are in the reactor. If the reaction rate on the catalyst surface is rapid compared to the diffusion rate, metals quickly build up at the pore mouths causing fouling and pore mouth plugging, thereby forbidding access to active sites within the catalyst pores. It is sometimes desirable to reduce activity of the catalyst using dopants such as Cs or Na (Ware and Wei, 1985c, 1985d) in order to favour a more uniform intraparticle deposition of metal and subsequently increasing catalyst life. In unimodal catalysts, increasing pore size in an attempt to avoid pore mouth plugging reduces the total surface area of the catalysts, and at the same time

the number of available active sites. Bimodal catalysts are a compromise. They allow rapid diffusion to the centre of the catalyst through macropores, but still provide large surface area in mesopores.

Another poison for catalysts are carbonaceous deposits or coke. Formation of coke is due to oligomerization of large molecules which cover active sites by depositing uniformly on the catalyst surface throughout the hydrocracking reaction. Under reactor operating conditions, coke builds up quickly at first but slows down after the initial deactivation period (Pereira et al., 1987). In hydrotreating, accumulation of coke is normally dealt with through catalyst regeneration.

1.5 ZEOLITES

1.5.1 HISTORY

Zeolites were first discovered in 1756 by the Swedish mineralogist A.F. Cronstedt when he observed that the mineral stilbite gave off steam when heated. From that result came the term zeolite, which is derived from the two Greek words "zeo", to boil, and "lithos", stone (Davis, 1991). More than 40 different natural species of zeolites are now found in a broad range of geological environments, and at least 100 synthetic species have been made in laboratories for commercial applications (Zoltai and Stout, 1984). It was not until the 1960's that the first zeolites were used in petroleum processing but

zeolite catalysis has since then undergone rapid and dynamic advances (Bahtia, 1988).

1.5.2 STRUCTURE

Zeolites are porous crystalline aluminosilicates. Their framework consists of SiO_4 and AlO_4 tetrahedra called *primary building blocks* which are joined together through shared oxygen atoms in various regular arrangements called *secondary building blocks*. These secondary building blocks form an open crystal lattice containing pores of a precise uniformity with no distribution of pores size. Because of this unique feature, zeolites can be used as molecular sieves. Each aluminum atom introduces one negative charge on the SiO_4 framework which must be balanced by an exchangeable cation. The particular cation will influence the properties of the structure.

For the purpose of this research, sodalite was chosen for its small pores and tri-dimensional pore network. Its structure consists of secondary building blocks in the form of aluminosilicate cube-octahedral cages creating cavities 6.6 Å in diameter (Carr et al., 1968). Each sodalite cage is composed of 8 six-member rings of oxygen atoms resulting in an approximate free pore diameter of 2.8 Å. The actual pore size depends on the exchangeable cation present (Bhatia, 1988).

Figure 1.6a represents the primary building blocks of the zeolite while the sodalite cage structure is shown in Figure 1.6b. Each vertex represents the location of an Si or

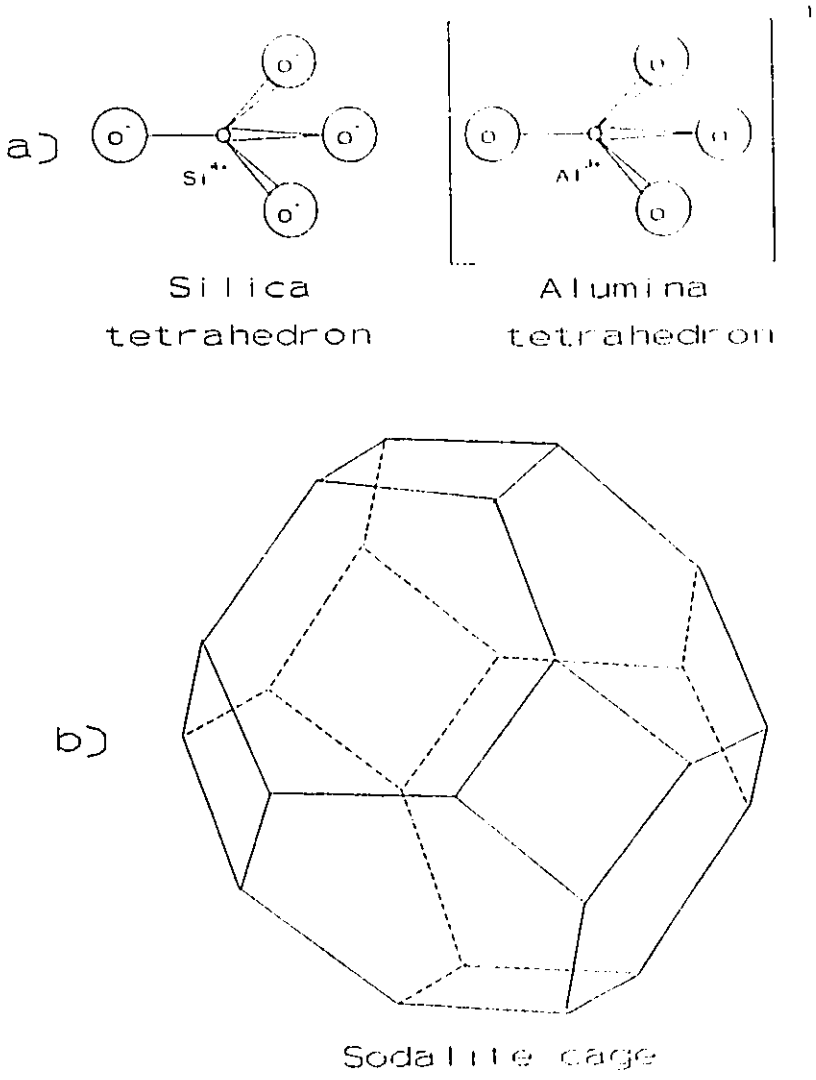

Figure 1.6 : **Zeolite structure a)** Primary building blocks of zeolites **b)** Sodalite cage structure (Bhatia, 1988).

Al atom while the lines represent, approximately, the diameters of the oxygen atoms or ions plus the bond length between atoms. Oxygen ions are very much larger than the tetrahedral Si or Al atoms.

1.5.3 SYNTHESIS OF SODALITE

Barrer and White (1952) have studied the conditions for crystalline sodium aluminosilicate synthesis extensively and concluded that the pH of the sodium hydroxide solution was a determinant factor in the synthesis of the desired crystalline structure. They showed that a solution of less than 150% of the minimum amount of NaOH required to provide the Na cations to make up the missing positive charge of the aluminum cations would yield *nepheline* while 150-300% NaOH yields *cancrinite*. Nepheline and cancrinite are two zeolite structures very closely related to sodalite. Their crystallisation is competitive as they are often precursors to sodalite. (Deer et al., 1975). Only in a highly basic solution will the same specified reactant proportions (Na_2O,Al_2O_3,$n$$SiO_2$,$m$$H_2O$) yield the desired sodalite structure. They found that "basic" sodalite (sodalite without chlorine) was grown at temperatures between 350°C and 450°C in the complete absence of sodium chloride but in the presence of a large excess ($\sim$300%) of sodium hydroxide (NaOH). Figure 1.7 shows a diagrammatic representation of the approximate formation regions for products obtained by the crystallisation of gels in the presence of excess NaOH.

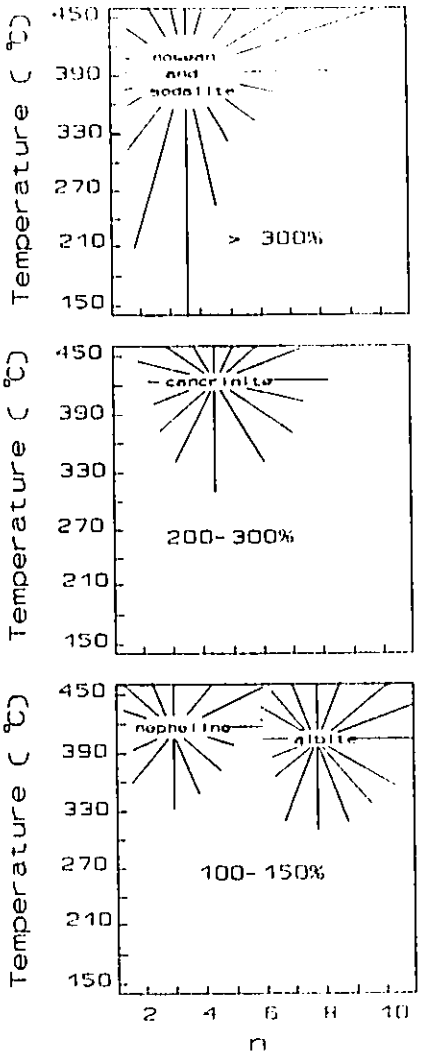

Figure 1.7 : **Approximate combinations of T°C and chemical composition for the crystal formation obtained from $Na_2O,Al_2O_3,nSiO_2$ with excess NaOH (%)** (Barrer and White, 1952).

CHAPTER TWO

2.0 METHODOLOGY

This chapter describes the methodology employed to perform all analysis on the various samples. The results from those analysis were used either to characterize original samples or to determine the performance of the catalysts developed in laboratory. They can be found in "Properties of Materials" Chapter 3 or in Appendix B.

Various analysis were performed . X-ray diffraction of the synthesized sodalite powders were compared with those in the literature (von Ballmoos, 1984; Hermeler et al., 1991) to ensure that the correct zeolite structure was obtained. Surface areas and pore size distributions were measured on all fresh and used catalysts. Analysis for carbon, hydrogen, nitrogen, sulphur, metals and Micro Carbon Residue (MCR) contents were performed on all liquid product samples as well as on the feedstock. A manual distillation (ASTM D-1160) was performed on all the samples collected during time-on-stream period θ = 5.8h-9.8h. ASTM colour readings were taken on the middle distillate fraction (288°C- 343°C) as well as analysis for nitrogen and sulphur contents, while the +343°C fraction was analyzed for sulphur, MCR and metal contents. Finally, the used catalysts were analyzed for metals and carbon contents only. The procedures used for each analysis follow.

2.1 ANALYSIS ON CATALYSTS

2.1.1 BET SURFACE AREA

The Brunauer-Emmett-Teller (BET) method (Bond, 1987) is the most widely used procedure for the determination of the surface area of solid materials. The equipment performing the surface area measurements on fresh and used catalysts was a computer-controlled AUTOSORB1 Gas Sorption System using the Quantachrome Autosorb Data Acquisition Software. The preferred range of the apparatus for total surface area was 5-50 m^2, so the weight of the sample was adjusted accordingly. Before analysis, the sample was freed of adsorbed gases by filling the sample holder with helium at 300°C under atmospheric pressure, and then slowly bringing it to vacuum over a period of 12 h. The data for the full isotherm were obtained by admitting or removing a known quantity of nitrogen into the sample cell maintained at a constant temperature near 77 K (boiling point of liquid nitrogen at atmospheric pressure). As adsorption occurred, the pressure in the sample cell changed until equilibrium was established. An adsorption isotherm was obtained point by point by admitting successive known volumes of nitrogen to the sample and measuring the equilibrium pressure. Similarly, desorption isotherms could be obtained by measuring the quantity of gas removed from the sample as the relative pressure was lowered. Isotherm plots can be found in Appendix C. The BET surface area was calculated using the adsorption data points in the $0.05 < p/p^\circ < 0.30$ according to the following equation:

$$\frac{p}{X\,(p^{o}-p)} = \frac{1}{X_m C} + \frac{(C-1)}{X_m C}\left(\frac{p}{p^{o}}\right)$$

where C is a constant, p and p^{o} are the partial pressure and the saturated vapour pressure of N_2 respectively, X is the amount of N_2 adsorbed and X_m is the amount of N_2 adsorbed in one monolayer. The surface area is calculated from

$$SA_{BET} = \frac{X_m\, N\, SA_{N_2}}{MW} * 10^{-20}$$

where SA_{BET} is the BET surface area in m^2/g cat, N is the Avogadro number, M, the molecular weight of nitrogen and SA_{N2} the surface area of one nitrogen molecule.

2.1.2 CHEMISORPTION

Chemisorption measurements were performed on Ni-impregnated sodalite and on fresh catalysts using a Micromeritics Chemisorb 2500 unit. In this study, preparation of the samples weighing 0.4 - 1.0 g was performed by exposing each one to a H_2 gas flow of 45 cm^3/min for a minimum of 2 hours at 450°C and then to an identical flow of N_2 for 1 hour, also at 450°C. The sample was allowed to cool to room temperature before it was tested for hydrogen adsorption. In chemical adsorption measurements, a known amount of active gas (normally hydrogen or carbon monoxide) is injected as a pulse into an inert carrier gas (nitrogen or helium) flowing at a rate of 15 mL/min over the sample to be tested. The amount of active gas in the carrier gas is measured as a peak by a thermal conductivity detector. The difference in the amount of active gas that

enters the sample chamber and the amount that leaves is the amount of gas chemisorbed by the catalyst. Peak area calculations are performed by the Chemisorb 2500 unit. A minimum of eight injections of hydrogen (or until three consecutive injections revealed the same peak area in the exit gas) were made from a sample loop of a volume of 0.11 cm^3 containing the active gas.

2.1.3 MERCURY POROSIMETRY

The pore size and distributions of the catalysts were determined using a Micromeritics AutoPore II 9220 System which measured the pore size and the pore distribution in samples by mercury intrusion and extrusion. A sample of approximately 0.5 g was placed in a glass cell at room temperature. The mercury pressure was increased first from vacuum to 30 psia to measure macro pores ($d_p > 50$ nm) and then from 30 to 60 000 psia to measure mesopores (2 nm $\leq d_p \leq$ 50 nm) and micropores ($d_p < 2$ nm). Pressure was then reduced slowly to obtain extrusion data. This process was repeated once to insure that all pores had been filled. The pore diameters (d_p) of the catalysts were calculated using the Young & Laplace equation as described by Moore (1966). The pressure at which mercury enters the pores is inversely proportional to the pore diameter. The volume of mercury which enters the pores is a direct measurement of the pore volume. The data are reported graphically and can be found in Appendix D.

2.1.4 THERMOGRAVIMETRIC ANALYSIS

Thermogravimetric analysis were performed on selected fresh catalysts using a Perkin-Elmer TGA 7 Thermogravimetric Analyzer which permits the measurement of weight changes in a sample material as a function of temperature or time. The samples were heated at a rate of 1°C/min from room temperature to 100°C in a platinum wound microfurnace using either a nitrogen or an air purge. A typical sample weight was approximately 21 mg. One major component of the TGA 7 is a sensitive ultramicrobalance which is capable of detecting weight changes as small as 0.1 μg. The null balance design of this microbalance uses a servo-controlled torque motor to automatically compensate for weight changes in the sample material. The amount of current necessary to maintain the system in the "null" state is directly proportional to the weight change in the sample.

Thermogravimetric analysis were also performed on selected fresh catalysts and on sodalite powders using ammonia gas to determine the relative strength of acid sites. Samples weighing about 40 mg were heated to 500°C at 5°C/min and maintained at 500°C for 60 min before they were cooled to 100°C at a rate of 5°C/min. Samples were exposed to a flow of 30 cm^3/min of NH_3 for 4 h and then flushed with nitrogen for another 4 h to eliminate all trace of physisorption. Finally, the temperature was raised by 2°C/min to 500°C and maintained at 500°C for 60 min to desorb the ammonia. The weight change is a measure of the number of acid sites and the ammonia desorption

temperature is a measure of the strength of the acid sites. The weight variations were recorded throughout the whole temperature profile. TGA diagrams can be found in Appendix E.

2.1.5 X-RAY DIFFRACTION

A SIEMENS D500TT automated X-ray diffractometer (XRD) was used to characterize the sodalite powder. XRD spectra can be found in "Properties of Material", section 3.1. Each sample was mounted in an aluminum holder using the side-loading method technique and diffraction data were collected over the angular range of 5° to 75° (2θ) in 0.02° steps with a counting time of 1 s per step. The X-rays were generated by Cu($K\alpha$) radiation. The generator voltage and current setting were 45 kV and 40 mA, respectively.

The spectra were identified using the SIEMENS "DIFFRAC 500" software package and compared with the Powder Diffraction File patterns from the International Centre for Diffraction Data (ICDD), formerly known as the Joint Committee on Powder Diffraction Studies (JCPDS). Literature was also used to identify the spectra (see section 3.1).

2.2 ANALYSIS ON LIQUID SAMPLES

2.2.1 ASH

To determine the ash content in the feed, the ASTM D-482 method was used. 30 g of the feed (sufficient to provide up to 20 mg of ash) was weighed to the nearest 0.1 % in a crucible, It was then ignited using a bunsen burner and allowed to burn until only ash and carbon remained. The carbonaceous residue was reduced to an ash by heating in a muffle furnace at 775°C, cooled and weighed. The heating and weighing were repeated until consecutive weighings differed by not more than 0.5 mg.

2.2.2 CARBON AND HYDROGEN

To determine the carbon and the hydrogen content in the liquid product samples, a Perkin-Elmer PE-2400 CHN Elemental Analyzer was used. The sample (2 mg) was sealed in tin capsule and deposited in a furnace heated at 950°C. The carbon and hydrogen present in the sample were oxidized to gases (CO_2, H_2O) in a pure oxygen environment. The product gases separated through columns under steady-state conditions were measured by a thermal conductivity detector with a repeatability of 0.3%..

The feed sample was analyzed in the same fashion but using a LECO CHN-600 analyzer. The larger sample holder (70-100 mg), allowed for heavier, more viscous

fractions to be analyzed. The sample was dropped in a furnace at 950°C where the carbon and the hydrogen were oxidized to $CO_2$and H_2O in a pure oxygen environment. The resulting gases were then circulated through an infra-red detector and reported in parts per million (ppm).

2.2.3 DISTILLATION

A manual ASTM D-1160 distillation procedure was performed on the feedstock to obtain 5 distillate fractions as follows: initial boiling point (IBP) to 176°C, 176°C-288°C, 288°C-343°C, 343°C-525°C and +525°C. The distillation was performed under constant magnetic stirring from a boiling flask containing 165-200 g of the feed. The simple set-up also included a 750 W controllable heating jacket, a flash column, a condenser and a vacuum pump. Boiling fractions up to a boiling point of 288°C were obtained at atmospheric pressure. The diesel fraction was obtained under a low vacuum (10 mm Hg), but a higher vacuum of 0.1 mm Hg (accuracy 1 % of absolute pressure) was established to separate the higher boiling fractions. The heating rate was 3°C/min. Between each fraction, the flask was cooled and the receiving vessel was emptied and cleaned.

The distillation performed on the product samples obtained during time-on-stream θ = 5.8h - 9.8h of the catalyst testing experiments was performed manually. Only three boiling point fractions were obtained which were as follows: IBP to 288°C, 288°C to

343°C and +343°C. The liquid product samples were centrifuged before distillation as described in section 2.2.4.

2.2.4 CENTRIFUGING

In spite of using a magnetic stirrer, on several occasion when performing a distillation on the product samples (section 2.2.3), the contents of the boiling flask were carried out of the flask directly into the receiving vessel under vacuum when the vapours reached a temperature around 235°C. Since water evaporates at much lower temperatures, it was assumed that the rapid vaporization of some other species such as ammonium sulphide were responsible for this phenomenon. Therefore, in an attempt to remove any trace of solid ammonium sulphide each product sample was centrifuged at room temperature for 20 minutes at 3500 rpm in a centrifuge apparatus. 3 to 4 g of residue were left in each of the centrifuging cups.

2.2.5 COLOUR

The ASTM D-1500 method was used to quantify the colour of the diesel fraction (288°C- 343°C) obtained from the distillation performed as described in section 2.2.6. A colorimeter equipped with an artificial light source possessing spectral characteristics similar to northern day light was used. The sample, normally stored at room temperature, was poured into a cylindrical clear glass jar with a flat bottom of

approximately 30 to 33.5 mm internal diameter and 115 to 125 mm in height. The jar was placed in the colorimeter next to standard tinted glasses and both containers were covered to exclude all exterior light. The colour of the sample was then compared to the standard glasses graded from ASTM Colour 0.5 to 8.0. If an exact match was not possible, the glass which possessed the next darker colour was used preceded by the letter L. The colour test was performed daily for one week immediately after the sample was distilled and then weekly for a period of approximately 120 days. Distillate fraction samples were stored in the dark, in amber borosilicate bottles and at room temperature.

2.2.6 DENSITY

The density of the feedstock was measured at 15°C using a pycnometer (ASTM D-70). The sample was carefully heated until it had become fluid enough to pour (≈50°C), avoiding incorporation of air bubbles. After the pycnometer was calibrated with distilled water maintained at 15°C (0.1°C) in a water bath, it was filled with the sample to about three fourths of its capacity. It was then allowed to cool to room temperature for at least 40 min and the total weight was recorded to the nearest mg. Once the pycnometer reached room temperature, it was then topped with distilled water and placed in the bath at 15°C for 30 min. Finally, the pycnometer was wiped dry and weighed to the nearest mg. The specific gravity was expressed in terms of the ratio of the mass of a given volume of sample at 15°C to that of an equal volume of water at the same temperature. The density was the specific gravity multiplied by the density of

water at test temperature.

The density of the liquid product samples was also measured at 15°C but using a Digital Density Meter Paar Model DMA40 (ASTM D-4052). Approximately 0.7 mL of liquid sample was introduced into an oscillating borosilicate glass sample tube of 2-mm inside diameter whose temperature was maintained by a water-circulating bath (±0.05°C). The change in oscillating frequency caused by the change in the mass of the tube was used in conjunction with calibration data to determine the density of the sample.

2.2.7 NICKEL AND VANADIUM CONTENTS

The nickel and vanadium contents of all liquid samples were determined simultaneously by Inductive Coupled Argon Plasma, using an ICAP9000. About 3 g of the liquid product was poured into a platinum crucible and covered with 0.2g of fusion flux (50% lithium tetraborate and 50% lithium metaborate). The mixture was then reduced to ashes by slowly heating the sample l°C/min to successive temperature plateaus as follows: 250°C for 2 h, 500°C for 1 h, 750°C for 3 h and finally 1050°C for 20 min. The sample was heated slowly in order to avoid spilling. The ashes containing metal oxides (V_2O_5, NiO, Fe_2O_3) were cooled at room temperature in a desiccator and dissolved in 50 mL of nitric acid (HNO_3, 3.5% vol). The resulting solution was then fed through a nebulizer in the ICAP9000 at a rate of 2 mL/min and excited in a plasma flame (T° = 10 000 K). The specific wavelength of the emissions produced by each oxide was

detected by a photomultiplier and quantified by a computer.

2.2.8 MICRO CARBON RESIDUE (MCR)

The MCR test was performed according to ASTM D-4530 procedure using a Micro Carbon Residue Tester ALCOR MCRT-120. The MCR quantification provides an indication of the relative coke forming tendency of the sample material. A sample weighing 0.15 g $\pm$0.05 was placed in a 2 mL glass sample vial. The vial was placed in an air-tight furnace equipped with a nitrogen purge. Nitrogen was flowed at a rate of 600 mL/min for at least 10 min and then the sample was heated to 500°C $\pm$2°C at a rate of 10°-15°C/min under a nitrogen purge of 15° mL/min. The 500°C temperature was maintained for 15 min, and then the oven was cooled gradually to 250°C under a nitrogen purge of 600 mL/min. The carbonaceous residues were weighed at room temperature and expressed as a percentage of the original sample within 0.3 wt%.

2.2.9 NITROGEN CONTENT

The nitrogen content of the liquid samples were determined by oxidative combustion and chemiluminescence detection (ASTM D-4629) using a Dohrman Nitrogen Analyzer DN-1000. The sample (5 μL) was injected into a stream of inert gas (helium). It was then vaporized and carried into a high temperature zone (inlet 850°C, outlet 950°C) where oxygen was introduced and organically bound nitrogen was converted to

nitric oxide (NO). The NO contacted ozone, and was converted to excited nitrogen oxide (NO_2). The light emitted as the excited NO_2 decays was detected by a photomultiplier tube. The resulting signal was a measure of the nitrogen contained in the sample. Repeatability was within 2% of the weight of the sample.

2.2.10 PENTANE INSOLUBLES

The percentage of pentane insolubles was determined using the ASTM D-2042M procedure modified for pentane. A feed sample weighing 1.5-2.0 g was heated to 100°C in a crucible and dissolved by hand in 125 mL of pentane. The crucible was deposited in a sonic bath for 20 min and allowed to sit overnight. The solution was then filtered under vacuum using a Millipore Cellulose filter paper (8 μm) and washed with at least 50 mL of pentane. The contents of the filter paper were then dried at 100°C for 20 min, cooled to room temperature and weighed. Pentane insolubles were reported as percentages of the original sample weights within $\pm 10\%$.

2.2.11 SULPHUR CONTENT

The sulphur content of the feed was measured using the ASTM D-1552 method using a LECO SC432 instrument. 100-120 mg of feed was weighed in a combustion boat, introduced in a resistance furnace and burned in a stream of oxygen at a sufficiently high temperature to convert about 97% of the sulphur to sulphur dioxide (SO_2) (135°C).

The combustion products were flowed through 2 drying tubes containing magnesium perchlorate before they entered a infra-red detector for quantification. Repeatability was within 0.02%.

The liquid product samples were analyzed using an OXFORD LabX 1000 with an X-ray fluorescence detection system. A sample size of 1-2 mL was poured in a sample cup which was closed with a polyethylene film. The sample, surrounded by a purge of helium to eliminate interference, was exposed to an iron-55 X-ray source. The fluorescence of the sulphur contained in the sample was quantified against a calibration curve.

2.2.12 TOLUENE INSOLUBLES

The percentage of toluene insolubles was determined by using the general procedure described for pentane insolubles except that toluene was the solvent. The ASTM D-2042M procedure was used and modified for toluene. Because toluene was a much better solvent than pentane, a slightly heavier feed sample weighing 2.0 -2.5 g was heated to 100°C in a crucible and dissolved by hand in 100 mL of toluene. The crucible was deposited in a sonic bath for 20 min and allowed to sit overnight. The solution was then filtered under vacuum using a Millipore Cellulose filter paper (8 μm) and washed with at least 50 mL of toluene. The contents of the filter paper were then dried at 100°C for 20 min, cooled at room temperature and weighed. Toluene insolubles were reported

as percentages of the original sample weights within 10%.

2.3 ANALYSIS ON USED CATALYSTS

2.3.1 SOXHLET EXTRACTION

Prior to performing analysis on used catalyst, a soxhlet extraction using toluene was performed. Approximately 10 g of used catalyst was deposited in a cellulose extraction thimble and into a soxhlet extraction tube. The tube was placed between a boiling flask containing approximately 300 mL of toluene and an Allihn condenser for reflux of the toluene. The boiling flask was maintained at constant temperature so that the toluene would vaporize then condense and finally wash all the oil residue from the catalyst as it flowed down from the condenser back into the boiling flask. This process was maintained for about two days or until the toluene filtering out of the thimble was colourless.

2.3.2 CARBON AND HYDROGEN CONTENTS

The carbon and hydrogen contents of the used catalysts were analyzed using the same method that was described for the feedstock in section 2.2.2 using a LECO CHN-600 analyzer. The sample (70-100 mg) was dropped into a furnace at 950°C where the carbon and the hydrogen were oxidized to CO_2 and H_2O in a pure oxygen

environment. The resulting gases then flowed through an infra-red detector and reported in parts per million (ppm).

2.3.3 NICKEL AND VANADIUM CONTENTS

The nickel and vanadium contents of all used catalysts were determined using the same method described for liquid samples in section 2.2.7 using an ICAP9000, Inductive Coupled Argon Plasma Spectrometer. About 0.1 g of the used catalyst was deposited in a platinum crucible and covered with 0.2 g of 50% lithium tetraborate 50% lithium metaborate. The mixture was then reduced to ash at 1050°C for 20 min. The ashes containing metal oxides (V_2O_5, NiO) were allowed to cool at room temperature in a desiccator and dissolved in 50 mL of nitric acid (HNO_3 3.5 % vol). The resulting solution was then fed to a nebulizer in the ICAP9000 at a rate of 2 mL/min and excited in a plasma flame (10 000 K). The emissions produced by the oxides were detected by a series of 50 photomultipliers and quantified by a computer.

CHAPTER THREE

3.0 PROPERTIES OF MATERIALS

Chemical and physical properties of all materials used in this study are described in this chapter. They consisted mainly of the prepared catalysts containing synthesized basic sodalite and Co-Mo/Al_2O_3, the reference catalyst AC 1442B as well as the Lloydminster atmospheric resid as feedstock.

3.1 ZEOLITE CHARACTERIZATION

3.1.1 SODALITE

3.1.1.1 Crystal Structure

Powder X-ray diffraction was used to identify the crystal structure of the synthesized zeolite powders. The XRD powder diffraction spectrum for the basic sodalite prepared during this research are shown in Figure 3.1a. The spectrum was compared with those reported by Hermeler and co-workers (1991) as well as with the simulated patterns for basic sodalite obtained by Von Ballmoos (1984). The line pattern shown in Figure 3.1a was reconstructed from the data published by Hermeler and

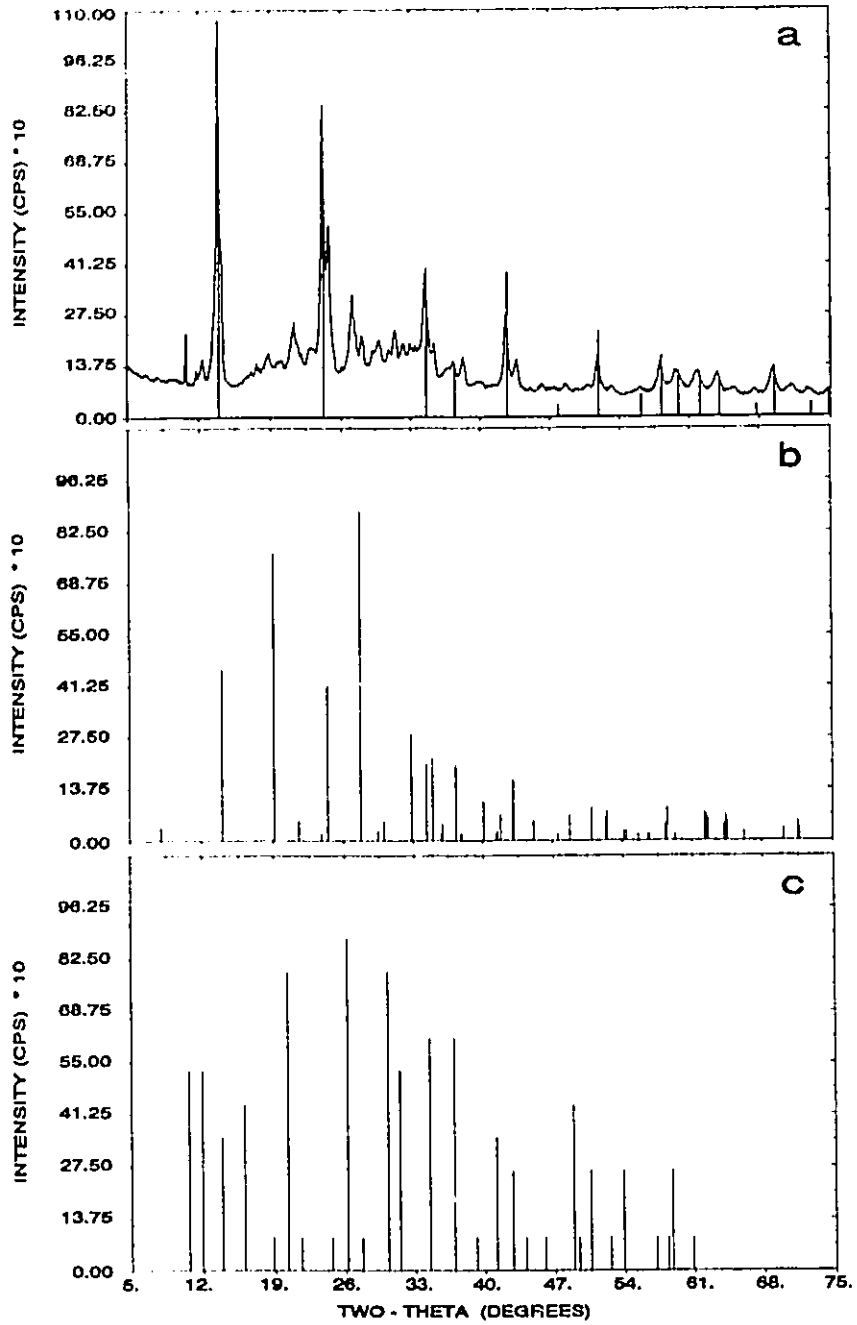

Figure 3.1 : **XRD Powder Diffraction Spectra a)** Basic sodalite with pattern (Hermeler, 1991), **b)** Cancrinite (#34-176) **c)** Nepheline (#10-460).

co-workers (1991). The main characteristics of the basic sodalite pattern are two strong peaks at two-theta values of 13.96° and 24.30° as well as four fingers between 58° and 64°. As discussed in section 1.5.3, cancrinite and nepheline are two crystalline structures very close to sodalite. All three structures are derived from one another and are often present together. Figures 3.1b and 3.1c show the patterns for cancrinite (#34-176) and nepheline (#10-460) respectively. Pattern numbers refer to the International Centre for Diffraction Data (ICDD) listing, formerly known as the Joint Committee on Powder Diffraction Studies (JCPDS). The most obvious difference between the cancrinite pattern and the sodalite pattern are two strong peaks at two-theta values of 19.15° and 27.77°. For the nepheline pattern, the pair of peaks at 10.65° and 11.95° as well as the three strong peaks at 13.86°, 20.21° and 26.19° cannot be found in the sodalite pattern. A comparison of the line pattern and the sample spectrum in Figures 3.1a,b and c confirms the high purity of the sodalite crystal prepared in the course of this work.

3.1.1.2 Acidity

The acidity of sodalite was compared with that of HY and H-mordenite zeolites using thermogravimetric measurements in presence of ammonia. The respective weight variation curve can be found in Appendix E, Figures E-1 to E-3. Table 3.1 gives a comparison of adsorption data for all three zeolites. The total ammonia adsorption for sodalite was less than 20% of that of either HY or H-mordenite. The ammonia intake on sodalite was also much slower due to the smaller pores in sodalite. Finally, ammonia

Table 3.1: **Thermogravimetric analysis**

	SOD	H-mordenite	HY	$CoMo/Al_2O_3$	39% Ni in 10% Ni-SOD	39% Ni in 26% Ni-SOD
Physisorption (%)	0.18	2.6	3.1	1.0	1.0	1.0
Chemisorption (%)	1.0	2.7	3.4	1.8	1.4	1.2
Total adsorption (%)	1.18	5.3	6.5	2.8	2.4	2.2

was completely eliminated from the sodalite at around 270°C (800 min) while weight loss was still occurring up to 500°C in H-modernite and HY zeolites. These results indicate that sodalite has fewer accessible acid sites that H-mordenite or HY zeolites and that its sites are weaker since they can be removed at much lower temperatures.

3.1.2 NICKEL IMPREGNATED SODALITE (Ni-SOD)

The X-ray powder diffraction spectrum for the nickel impregnated sodalite before reduction is shown in Figure 3.2a. The three strong peaks at two-theta values of 37.28°, 43.30° and 62.92° are attributed to the presence of a high concentration of nickel in the sodalite (39 wt%) which formed nickel oxide or *bunsenite* (pattern # 4-0835). Figure 3.2b shows the same pattern on an expanded scale (3 times), where the sodalite pattern can be seen more clearly. On a full scale, its intensity is significantly attenuated by the presence of the nickel oxide peaks.

3.1.3 EFFECT OF REDUCTION AND K^+ ION EXCHANGE

3.1.3.1 Crystal Structure

After the reduction of nickel, the remaining ions were exchanged with potassium ions in a solution of potassium hydroxide (section 4.1.2.4). Although the ion exchange was successful, it was found to have altered to crystal structure of the zeolite from

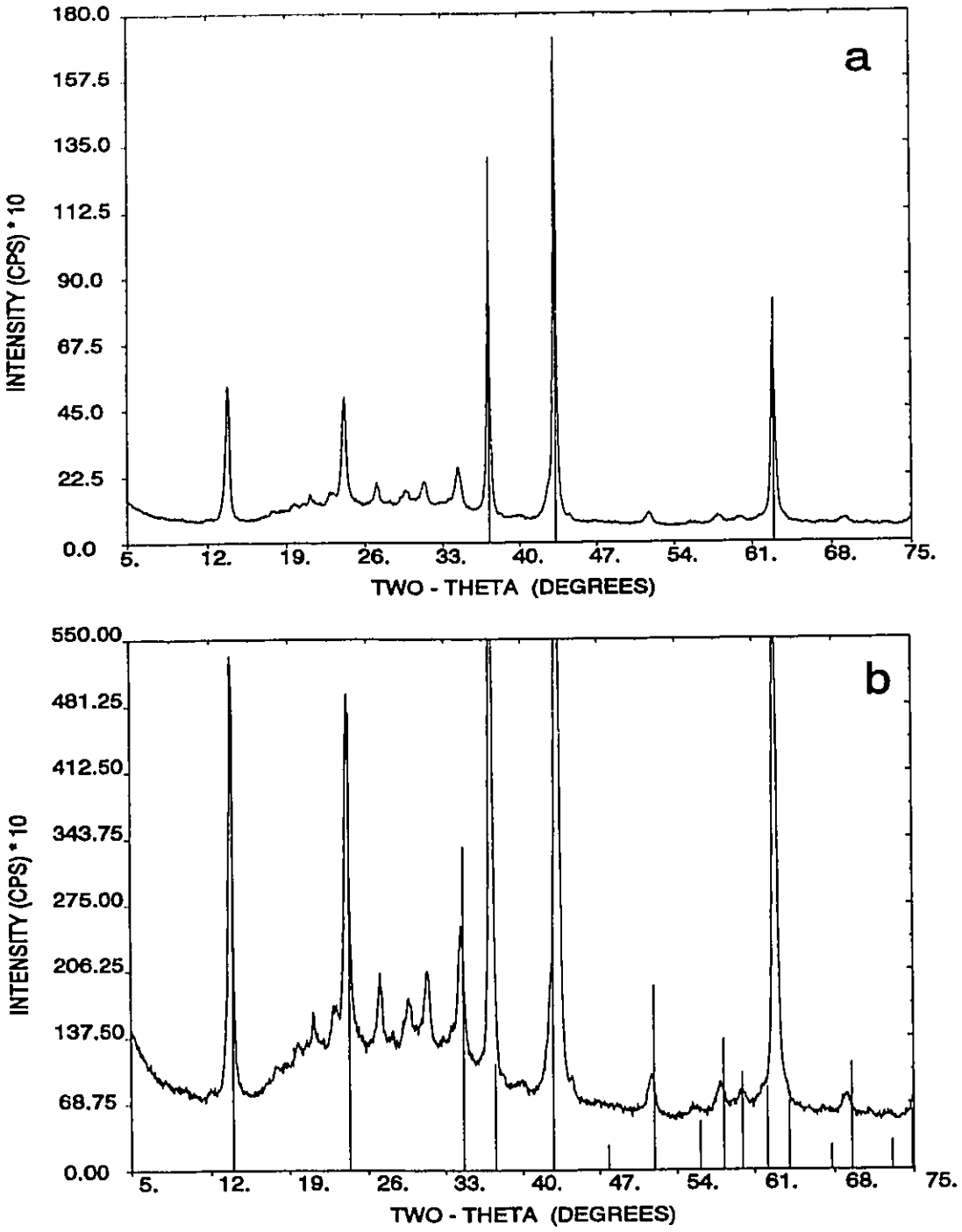

Figure 3.2 : **XRD Powder Diffraction Spectra a)** Ni-SOD with pattern for NiO (#4-0835) **b)** Ni-SOD with basic sodalite pattern (Hermeler, 1991).

sodalite to nepheline in some cases. Since the basic nature of the solution (pH 12) was so critical to the synthesis of the sodalite structure, it was believed that the reduced pH value of the exchange solution (pH 8) could have been the cause for the reversion in crystalline structure. Figure 3.3a shows the X-ray powder diffraction spectrum for a sample with modified crystalline structure. The form of nepheline in this figure is different from that of Figure 3.1 as it contains potassium (ICDD pattern #9-0338). The crystals still contain a large amount of bunsenite with a small amount of nickel in the metallic state characterized by the presence of two peaks at 44.51° and 51.85° as shown in Figure 3.3b. In cases where the crystal structure was not altered (Figure 3.4), the amount of amorphous material increased significantly, reducing the overall intensity of the spectrum. This can be seen by comparing Figure 3.4a with Figure 3.1a. The sodalite structure can still be noted, however, as well as the presence of the nickel oxide and the reduced nickel.

3.2 CATALYST COMPONENTS

3.2.1 SILICA

The silica used in the preparation of sodalite was the Cab-O-Sil M-5 grade manufactured by Cabot Corporation, Massachusetts. Cab-O-Sil is a three-dimensional network structure with a purity of more than 99.8% SiO_2. It's versatile properties such as thickening, and ease of fluidizing are used in a number of industries from chemical

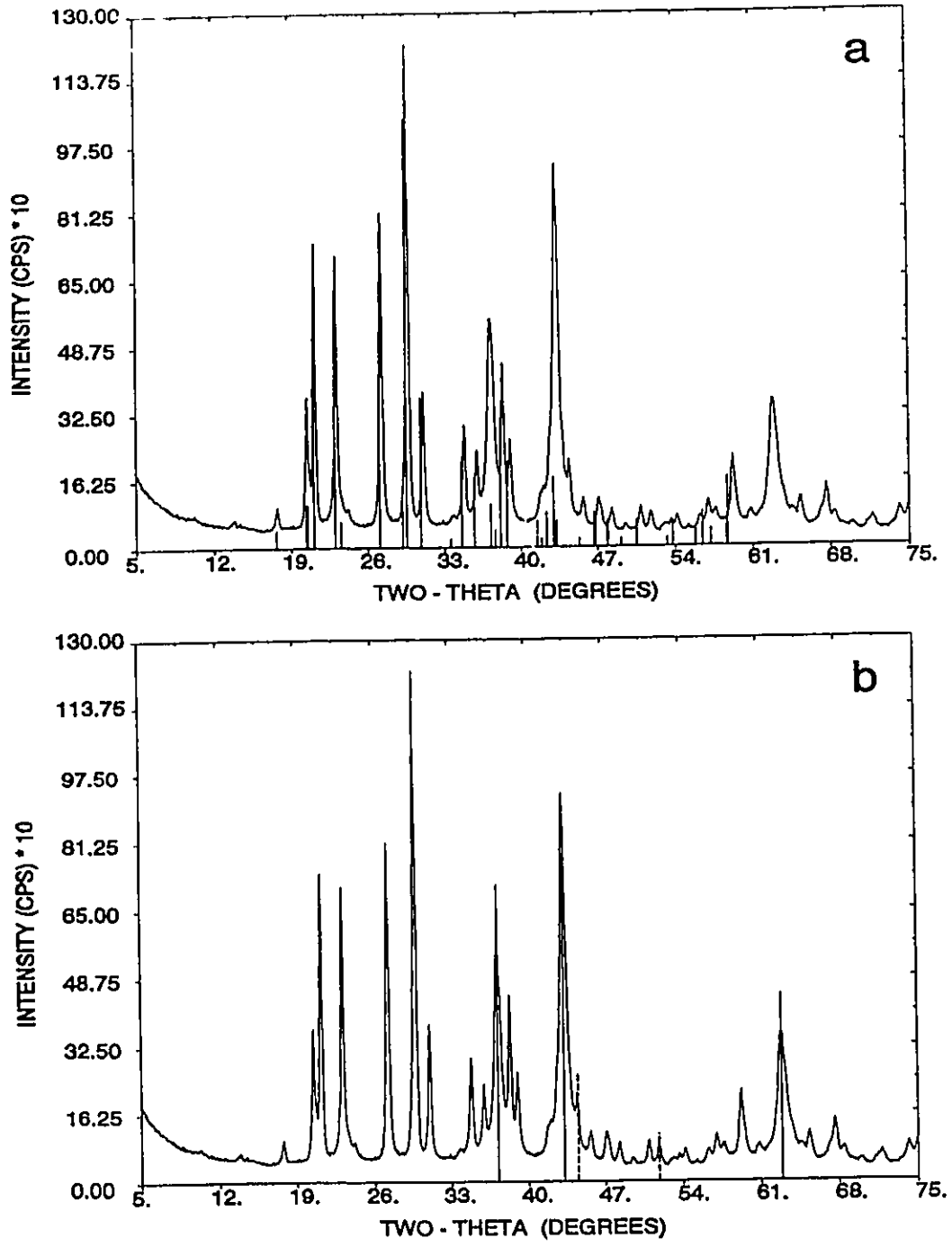

Figure 3.3 : **XRD Powder Diffraction Spectra** a) Nickel impregnated nepheline after reduction and potassium ion exchange (#9-0338) b) (—) NiO (#4-0835), (----) Ni° (#4-0850).

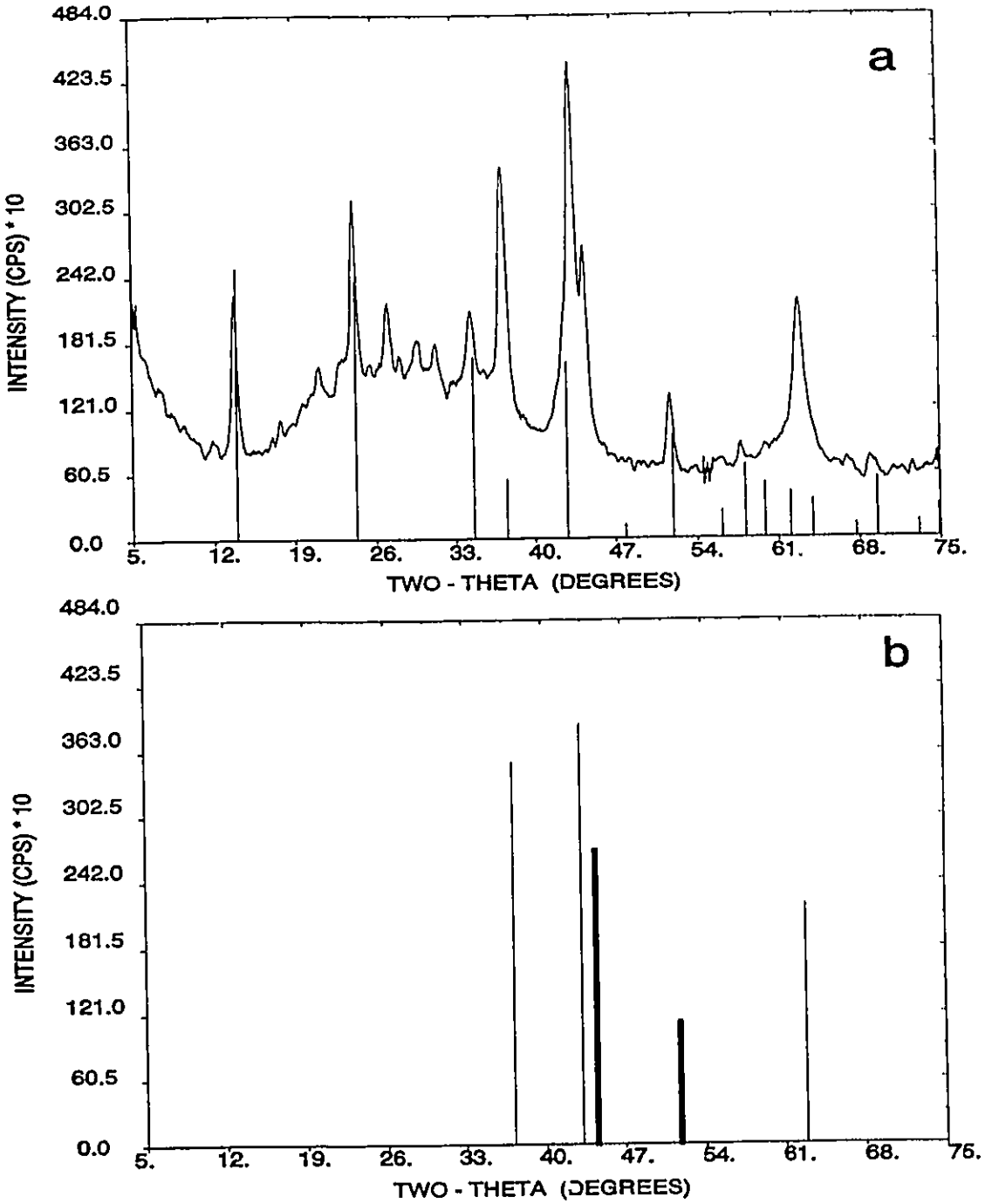

Figure 3.4 : **XRD Powder Diffraction Spectra** a) Ni-SOD after reduction and potassium ion exchange (pattern from Hermeler, 1991) **b)** (—) NiO (#4-0835),(▬) Ni° (#4-0850).

and pharmaceutical plants to food production. Some physical and chemical properties of Cab-O-Sil can be found in Table 3.2.

3.2.2 MONOMODAL ALUMINA MONOHYDRATE

The alumina material used in the preparation of sodalite was the Catapal SB Alumina monohydrate manufactured by the Continental Oil Company (CONOCO) in New Jersey. The Catapal SB Alumina is a spray dried material with good particle size uniformity, good porosity and excellent flow properties. Catapal SB Alumina crystal structure is alpha aluminamonohydrate (boehmite) which becomes gamma alumina after calcination for 3 h at 482°C. Catapal SB Alumina is used in specific catalytic applications such as hydrotreating, reforming, and auto exhaust catalysts. Physical and chemical properties can be found in Table 3.3.

3.2.3 BIMODAL ALUMINA MONOHYDRATE

The alumina support used in catalyst preparation was gamma alumina made from Versal-250 (calcined pseudoboehmite) manufactured by Laroche Chemicals Inc. in Baton Rouge, Louisiana. Versal-250 is a *bimodal* alumina monohydrate because it contains two different groups of pore sizes. Versal-250 has a narrow micropore distribution (d_p < 120 Å) and a medium macroporosity (d_p > 350 Å). It also has good strength and high total pore volume. Versal-250 is available as a fine powder and is normally used in

Table 3.2: **Properties of Cab-O-Sil**

Surface area (m^2/g)		200 ± 25
Bulk density (g/cm^3)		0.032
Nominal particle size (μm)		0.014
Chemical properties (wt %):	SiO_2	99.8
(ppm):	Al	8
	Co	< 20
	Fe	< 2
	Mo	< 2
	V	< 2
	Na	20-40
	Ni	< 0.4

Table 3.3 : **Properties of Catapal SB Alumina**

Alumina phase		Boehmite
Alumina phase -- calcined at > 482°C		gamma
Loose bulk density (g/cm^3)		0.69
BET surface area (m^2/g)		250
Pore volume (cm^3/g)		0.53
Particle size distribution	< 45 μm	48
	> 90 μm	11
Chemical composition (wt%)	Al_2O_3	75
	Ignition loss	25
	Carbon*	0.3
	SiO_2	0.008
	Fe_2O_3	0.005
	Na_2O	0.004
	Sulphur	0.01

*as primary alcohol, completely removed during calcination

manufacturing, catalyst supports, for washcoating, catalyst and ceramic binders or anti-slip coatings. Physical and chemical properties of Versal-250 can be found in Table 3.4.

3.2.4 ZERICE OIL

A fine hydrocarbon distillate oil referred to as *zerice* was used in the preparation of the catalysts as described in section 4.1.3.1 to preserve the porosity of the zeolite. Zerice was selected for its boiling range to ensure that it is completely vaporized during calcination. Table 3.5 shows the properties of zerice oil.

3.3 PROPERTIES OF FRESH CATALYSTS

Chemical compositions and physical properties of the fresh catalysts prepared in the laboratory can be found in Table 3.6. The amounts of molybdenum and cobalt in the alumina support was maintained constant while the amount of sodalite varied. The percentage of nickel reported was calculated on the basis of the weight of nickel impregnated divided by the weight of sodalite as opposed to divided by the total weight of catalyst.

Table 3.4 : **Properties of Versal-250**

Alumina phase		p-boehmite
Alumina phase -- calcined at > 500°C		gamma
Calcined loose bulk density (600°C) (g/cm^3)		0.21
Surface area (calcined at 600°C) (m^2/g)		300
Chemical composition (wt%):	Na_2O	0.02
	SiO_2	0.10
	Fe_2O_3	0.03
	TiO_2	<0.01
	Carbon	0.15
	SO_4	0.02
	Cl	0.07

Table 3.5: **Properties of Zerice Oil**

Specific Gravity at 15°C	0.889
Carbon (wt%)	86.3
Hydrogen (wt%)	13.3
Nitrogen (ng/μL)	85.8
Boiling Range (°C)	245-553
H/C Atomic Ratio	1.85

Table 3.6 : **Properties of Fresh Catalysts**

Chemical Composition						
Sodalite (wt%)	10.2	10.2	9.6	10.2	10.2	10.2
Nickel in sodalite (wt%)	0	13.1	25.5	34.1	38.5	44.8
Al_2O_3 (Wt%)	73.3	73.3	73.8	73.3	73.3	72.0
MoO_3 (Wt%)	13.8	13.8	13.9	13.8	13.8	15.0
CoO (wt%)	2.7	2.7	2.7	2.7	2.7	3.0
Physical Properties						
BET Specific Surface Area SA_{BET} (m^2/g)	281.6	295.3	294.9	265.1	292.1	302.0
t-curve Surface Area $(SA)_t$ (m^2/g)	342.3	358.2	358.0	316.5	351.9	357.7
Total Pore Area SA_{Hg} (m^2/g)	293.7	270.6	262,1	264.7	272.1	246.3
Total Pore Volume V_p (mL/g)	0.6313	0.6614	0.4568	0.6299	0.6447	0.4565
Average Pore Diameter (nm)	9.3	9.8	7.0	9.5	9.5	7.4
Bulk Density (g/mL)	1.014	0.9603	1.0274	1.0192	1.0387	0.9456
Skeletal Density (g/mL)	3.2799	2.6317	1.9358	2.847	3.1448	1.664
Porosity (%)	69.08	63.51	46.93	64.20	66.97	43.17

Table 3.6 : **Properties of Fresh Catalysts** (cont'd)

Chemical Composition						AC-1442B
Sodalite (wt%)	0	5.1	10.2	20.0	25.9	0
Nickel in sodalite (wt%)	0	38.5	38.5	38.5	38.5	0
Al_2O_3 (Wt%)	83.1	78.2	73.3	63.9	56.7	80.1
MoO_3 (Wt%)	14.1	13.9	13.8	13.5	14.5	16.4
CoO (wt%)	2.8	2.7	2.7	2.7	2.9	3.5
Physical Properties						
BET Specific Surface Area SA_{BET} (m^2/g)	294.8	318.9	292.1	288.2	252.4	319.8
t-curve Surface Area $(SA)_t$ (m^2/g)	353.8	377.1	351.9	339.1	295.2	401.7
Total Pore Area SA_{Hg} (m^2/g)	313.2	262.1	272.1	201.8	215.8	333.8
Total Pore Volume V_p (mL/g)	0.382	0.4328	0.6447	0.3865	0.4152	0.6863
Average Pore Diameter (nm)	4.9	6.6	9.5	7.7	7.7	8.2
Bulk Density (g/mL)	1.3567	1.1474	1.0387	1.0753	1.0238	0.8245
Skeletal Density (g/mL)	2.816	2.2793	3.1448	1.8399	1.7807	1.8992
Porosity (%)	51.82	49.66	66.97	41.56	45.0	71.0

3.3.1 SURFACE AREA

The surface areas of the catalysts are shown in Figures 3.5 and 3.6 as a function of sodalite content in the catalyst and as a function of nickel content in the sodalite. The surface area diminishes as the amount of sodalite in the catalyst increases but remains unchanged with changing nickel content in the sodalite. Since the N_2 surface area of the pure sodalite is only 15 m^2/g of sodalite, it does not contribute significantly to the total surface area. Consequently, the total surface area of the catalyst decreases as the concentration of sodalite increases. Small pores normally contribute the largest surface area per unit pore volume. However, in the case of sodalite, the pore mouths are too small (2.2 A, Breck, 1974) to accommodate nitrogen molecules (3.0 Å, Weast et al., 1989) so that only the external surface area of the crystals was measured.

The BET surface area calculations reveal the surface area available on the catalyst in all pores by simple adsorption of nitrogen on the surface. The method is known to be applicable to data points for which $P/P^o < 0.35$, prior to occurrence of capillary condensation of nitrogen. P is the partial pressure of N_2 and P^o is the saturated vapour pressure of N_2. Another method called *t-curve* introduced by Shull can be used for the determination of surface area of the catalysts. Shull developed an empirical formula to determine the statistical number of adsorbed monolayers of nitrogen. It can be used to verify the surface area calculated using the BET method. Detailed calculations of the surface area using the t-curve method can be found in Appendix A.

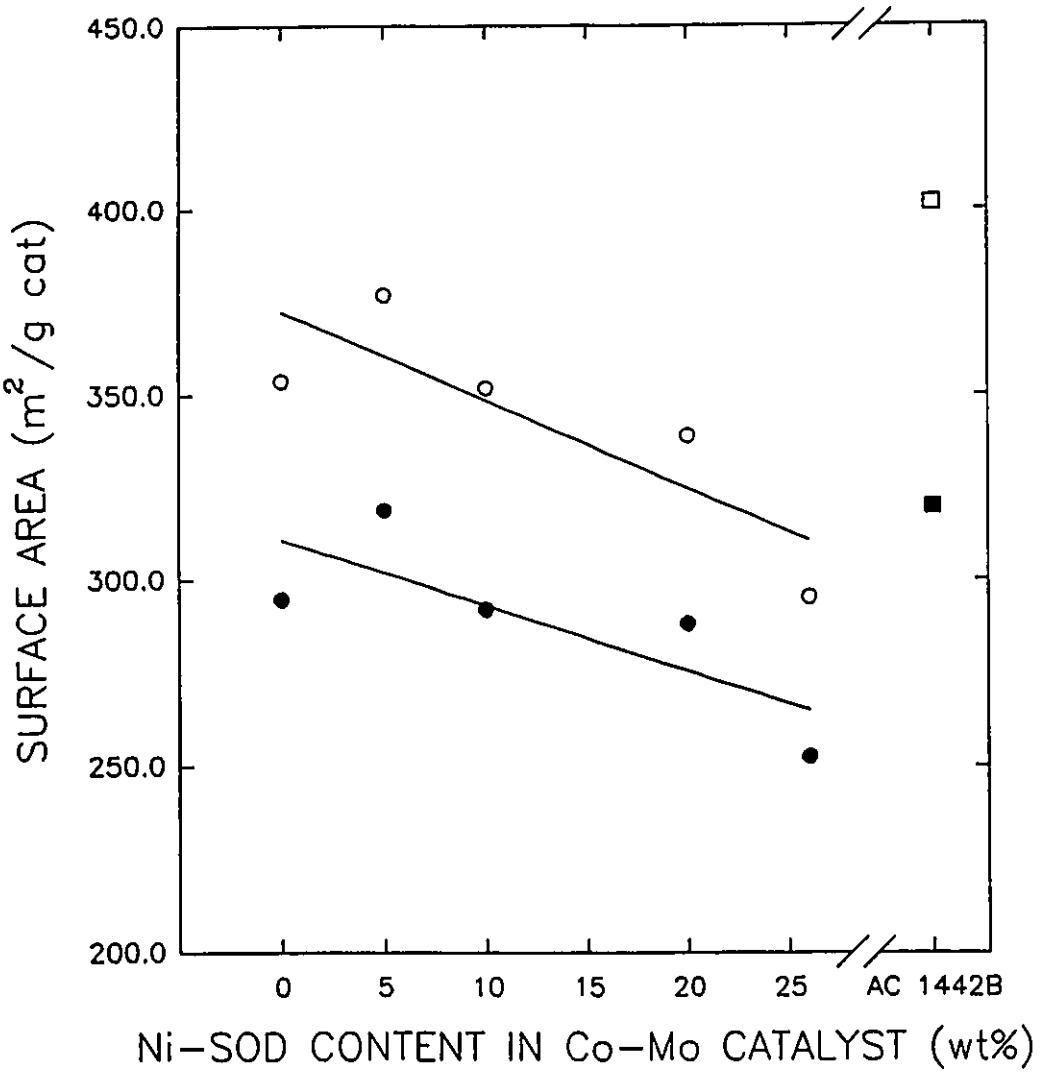

Figure 3.5 : **Catalyst surface area (m^2/g cat) as a function of Ni-SOD content in the Co-Mo catalyst (wt%).** Solid and open data points represent the BET and the t-curve methods respectively.

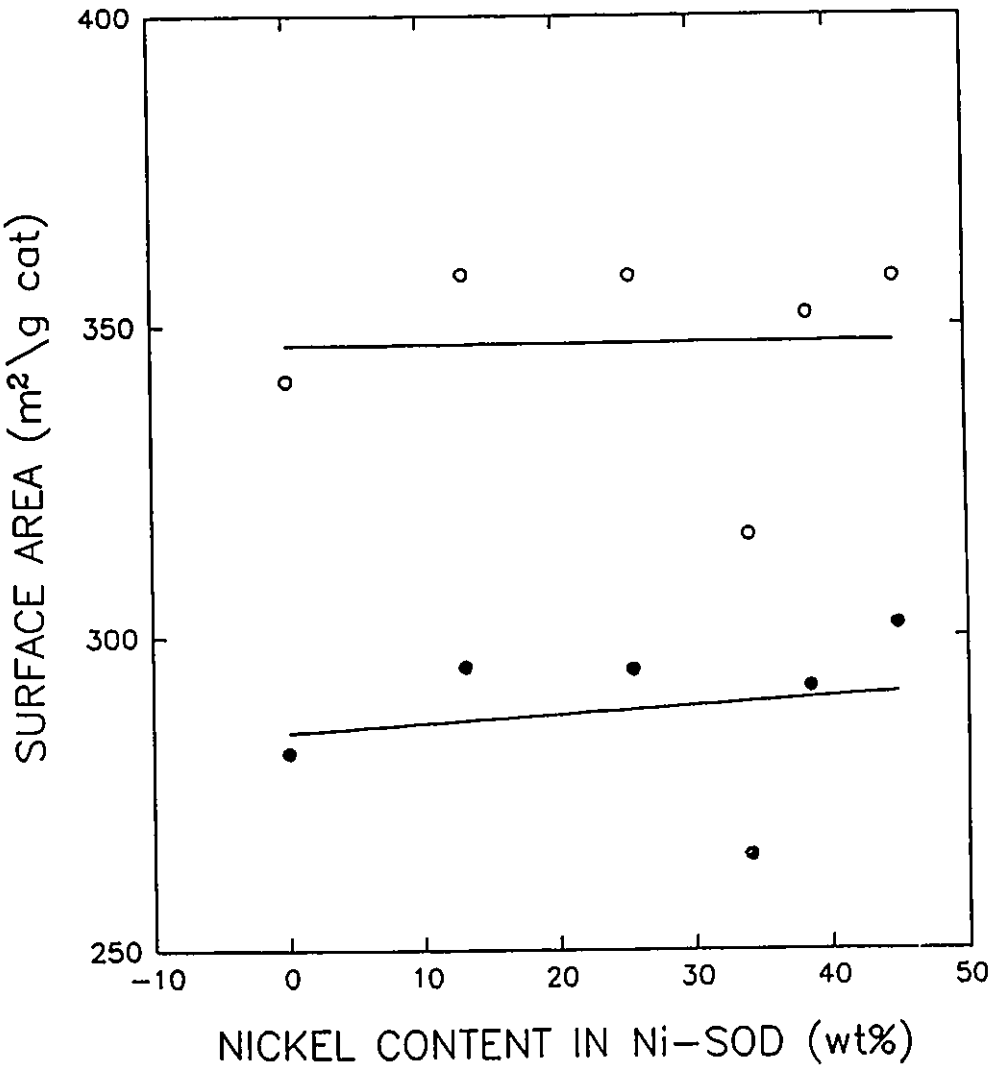

Figure 3.6 : **Catalyst surface area (m^2/g cat) as a function of nickel content in the sodalite component of the Co-Mo catalyst (wt%).** Solid and open data points represent the BET and the t-curve methods respectively.

The t-curve procedure used here is based on the amount of nitrogen adsorbed between the 1.2 and 1.6 statistical layers of adsorption. Therefore the nitrogen molecules on the first layer of the surface are not considered in the calculation. Consequently, when there are micropores that are completely filled by the first layer, the t-curve method often produces a surface area value smaller than that calculated using the BET method. The surface areas of the prepared catalysts were also calculated using the t-curve method and results are shown along with the calculations from the BET method in Figures 3.5 and 3.6. It is of interest to note that the values of surface area calculated using the t-curve method are 15-20% higher than those calculated using the BET method. One explanation would be that the first layer of adsorbed molecules include some adsorption sites that behave like type III or type V isotherms. That is, nitrogen molecules prefer to interact with other nitrogen molecules rather than the solid surface. A more extensive study of the phenomenon would be required in order to confirm this hypothesis.

3.3.2 MERCURY POROSIMETRY

Mercury porosimetry measurements were performed on all catalysts in order to compare their pore size distribution. Some catalysts were found to be bimodal while the others were unimodal. Bimodal catalysts contain both macropores and mesopores while unimodal catalysts have mainly mesopores. This phenomenon is characterised by the distinct shoulder at a pressure above 110 psig on plots for the cumulative intrusion

volume as a function of mercury pressure. Porosity plots for each catalyst can be found in Appendix D. The difference in modality of the prepared catalysts was attributed to the different calcination procedures as described in section 4.1.3.3. All bimodal catalysts were calcined according to the short calcination procedure while most of the unimodal catalysts were calcined according to the long calcination procedure. An extended calcination period probably caused most of the large pores in the alumina to collapse, leaving mainly mesopores in the final catalyst. Bimodal catalysts presented a much higher porosity (about 50%) as well as a significant increase in mesopore volume. Their average pore size was greater by almost 30% (Table 3.6). The reference catalyst is bimodal and has a significantly higher number of mesopores than the prepared unimodal catalysts.

3.3.3 PORE VOLUME DISTRIBUTION

Figure 3.7 is a pore volume distribution for a catalyst typical of the bimodal group. The diagram of the pore volume distribution is the first derivative of the plot of the cumulative intrusion volume (the pore volume) with respect to the logarithm of the pore diameter versus the logarithm of the catalyst pore diameter. It shows the pore sizes in which the pore volume is distributed. The data used to plot the pore volume distribution were generated from plot 1 from the graph of the cumulative intrusion volume of the catalyst containing 10% sodalite impregnated with 39 % of nickel as a function of pressure which can be found in Figure 3.8. It can clearly be seen in Figure

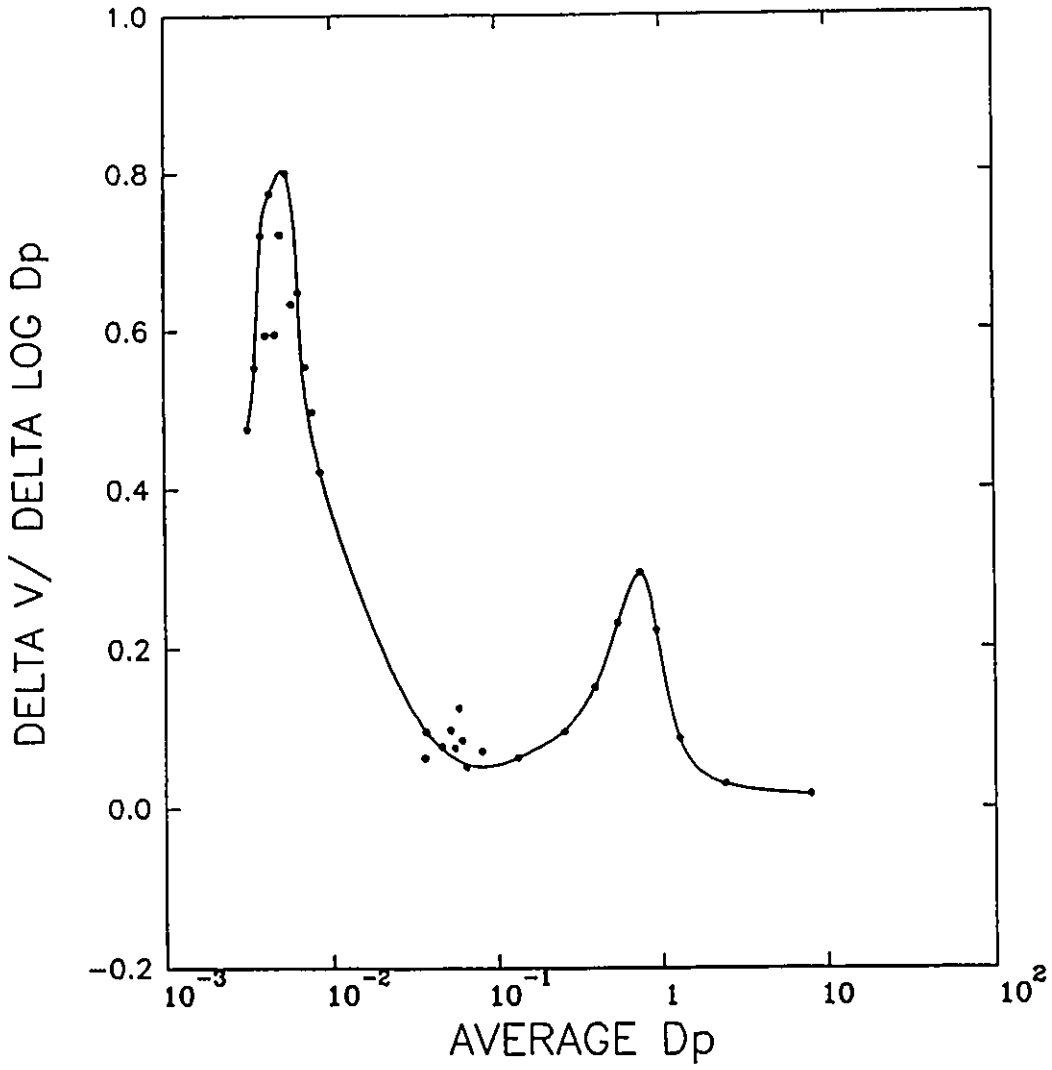

Figure 3.7 : **Pore volume distribution for Co-Mo catalyst containing 10% Ni-SOD impregnated with 39% nickel.**

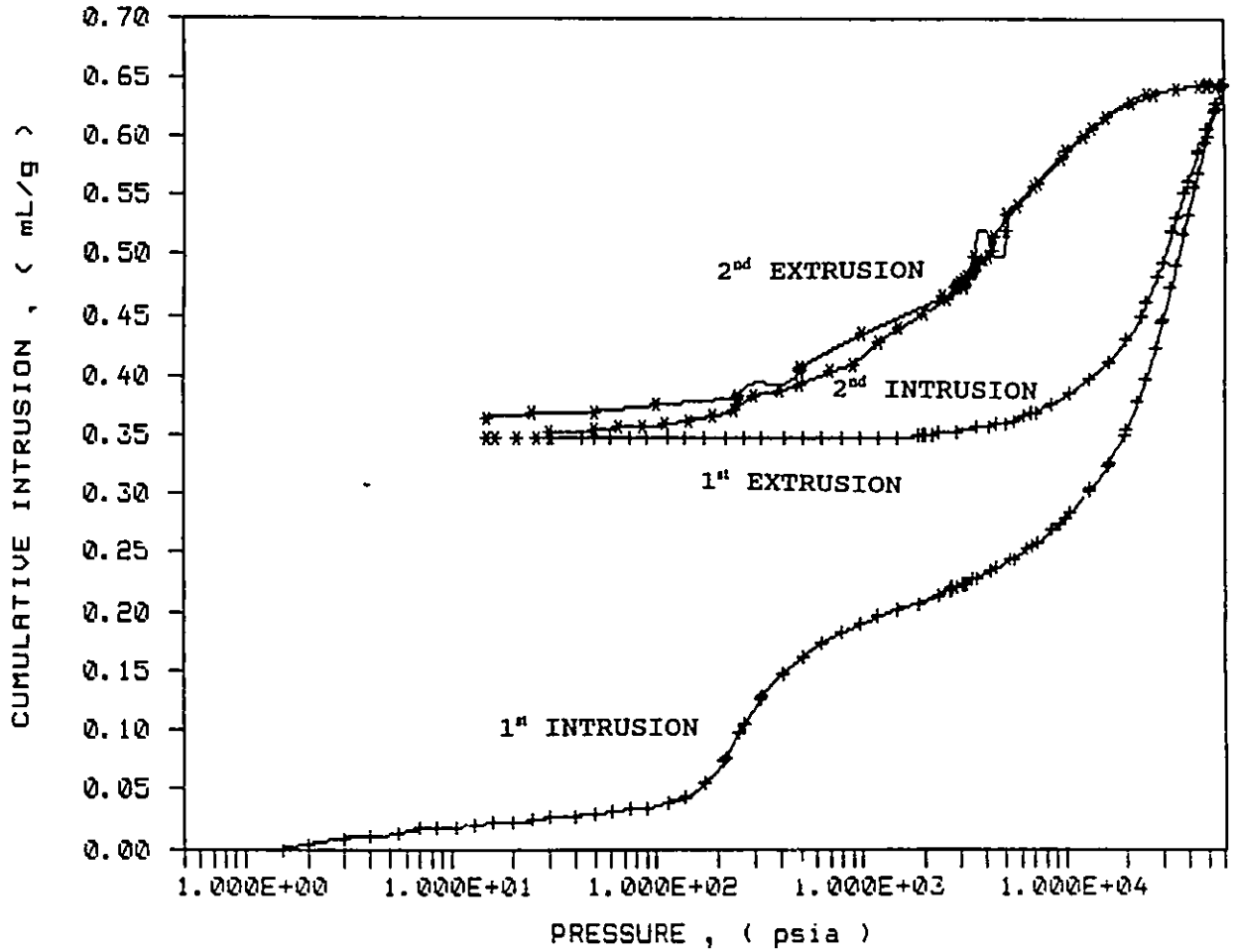

Figure 3.8 : **Cumulative mercury intrusion volume (mL/g) versus pressure (psia).** Fresh catalyst containing 39% impregnated Ni in SOD and 10% SOD in the Co-Mo catalyst.

3.8 that two groups of pores are present in the catalyst, one with an average size of about 700 nm (macropores) and the other averaging about 5 nm (mesopores). In Figure 3.9, however, only one type of pores is present at an average pore diameter size of about 6 nm which is typical of a unimodal catalyst. The catalyst used as an example of a unimodal catalyst was composed of 10% sodalite impregnated with 45% nickel whose plot of cumulative intrusion volume vs pressure is located in Figure 3.10.

3.3.4 PORE SURFACE AREA DISTRIBUTION

The pore surface area distribution of the two catalysts used in Figures 3.7 and 3.9 are depicted in Figures 3.11 and 3.12. The diagram of the area distribution is the first derivative of the plot of the cumulative catalyst surface area with respect to the logarithm of the pore diameter versus the logarithm of the catalyst pore diameter. It indicates which pore sizes contain the surface area (Figure 3.11 and 3.12). The pore surface area distributions clearly demonstrate that contribution to the surface area from the macropores is minimal as only the mesopore peak is present in both diagrams. The low surface area in the macropores indicates that the number of active sites in the large pores is limited. The presence of macropores however greatly assists in the diffusion of molecules towards the active sites located in the smaller mesopores.

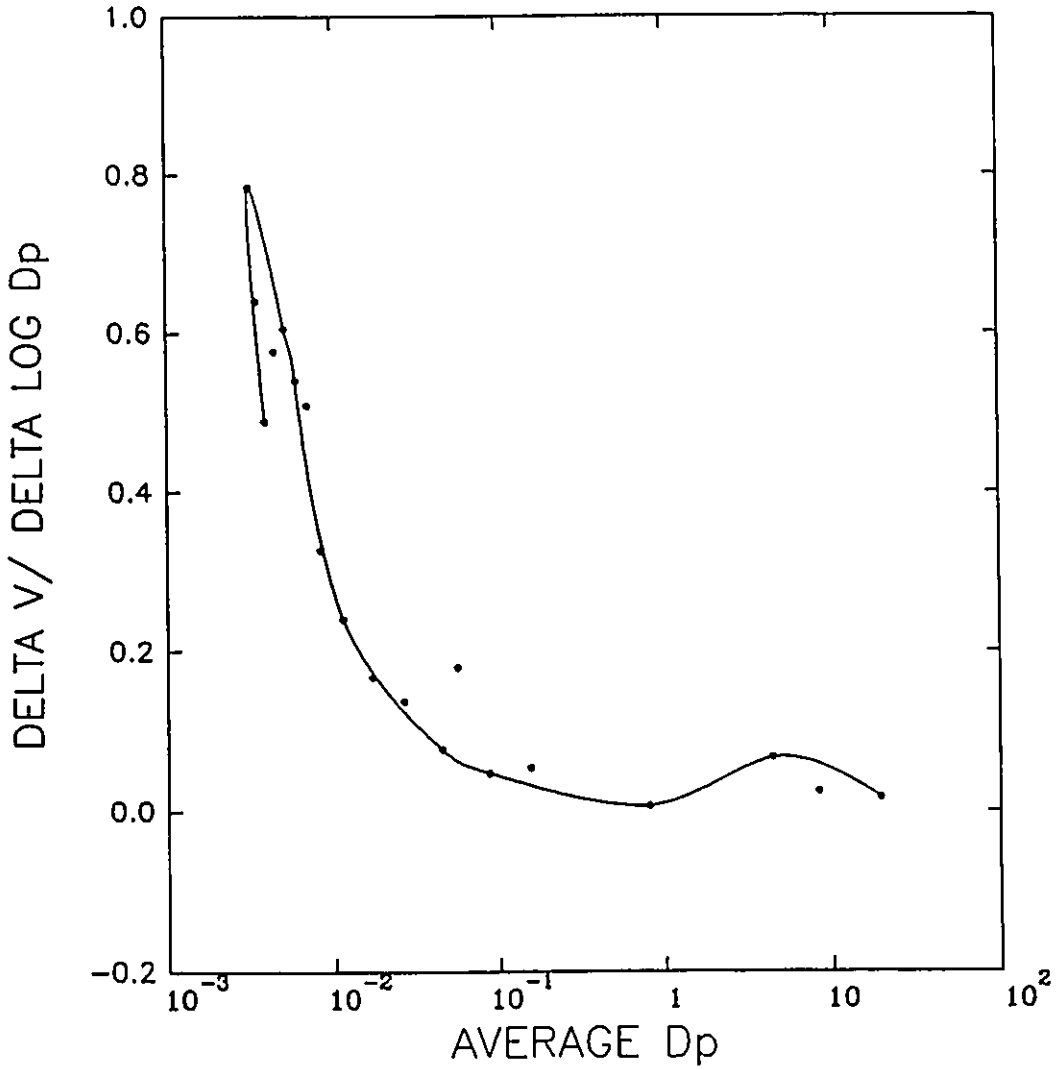

Figure 3.9 : **Pore volume distribution for Co-Mo catalyst containing 10% Ni-SOD impregnated with 45% nickel.**

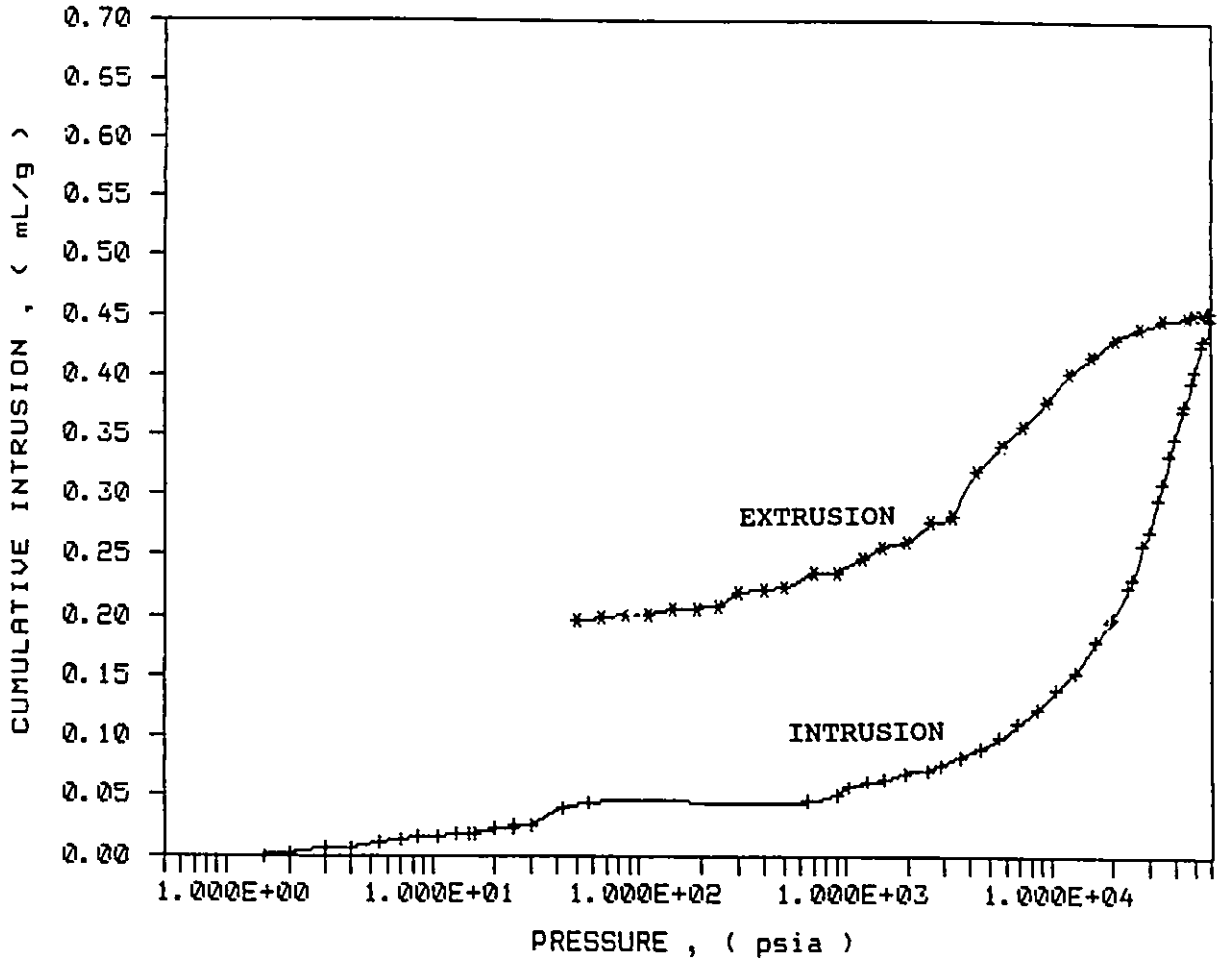

Figure 3.10 : **Cumulative mercury intrusion volume (mL/g) versus pressure (psia).** Fresh catalyst containing 45% impregnated Ni in SOD and 10% SOD in the Co-Mo catalyst.

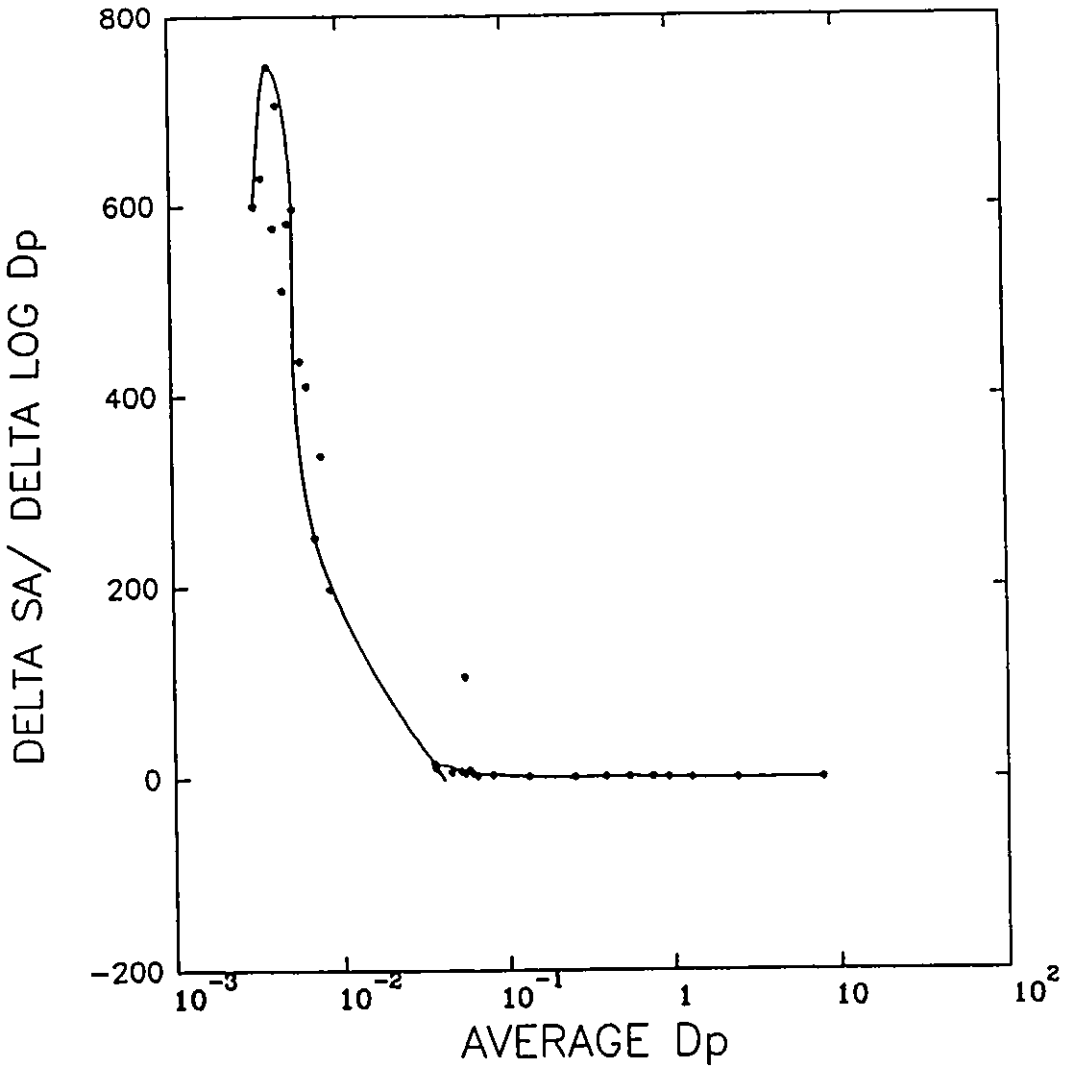

Figure 3.11 : **Surface area distribution for Co-Mo catalyst containing 10% Ni-SOD impregnated with 39% nickel.**

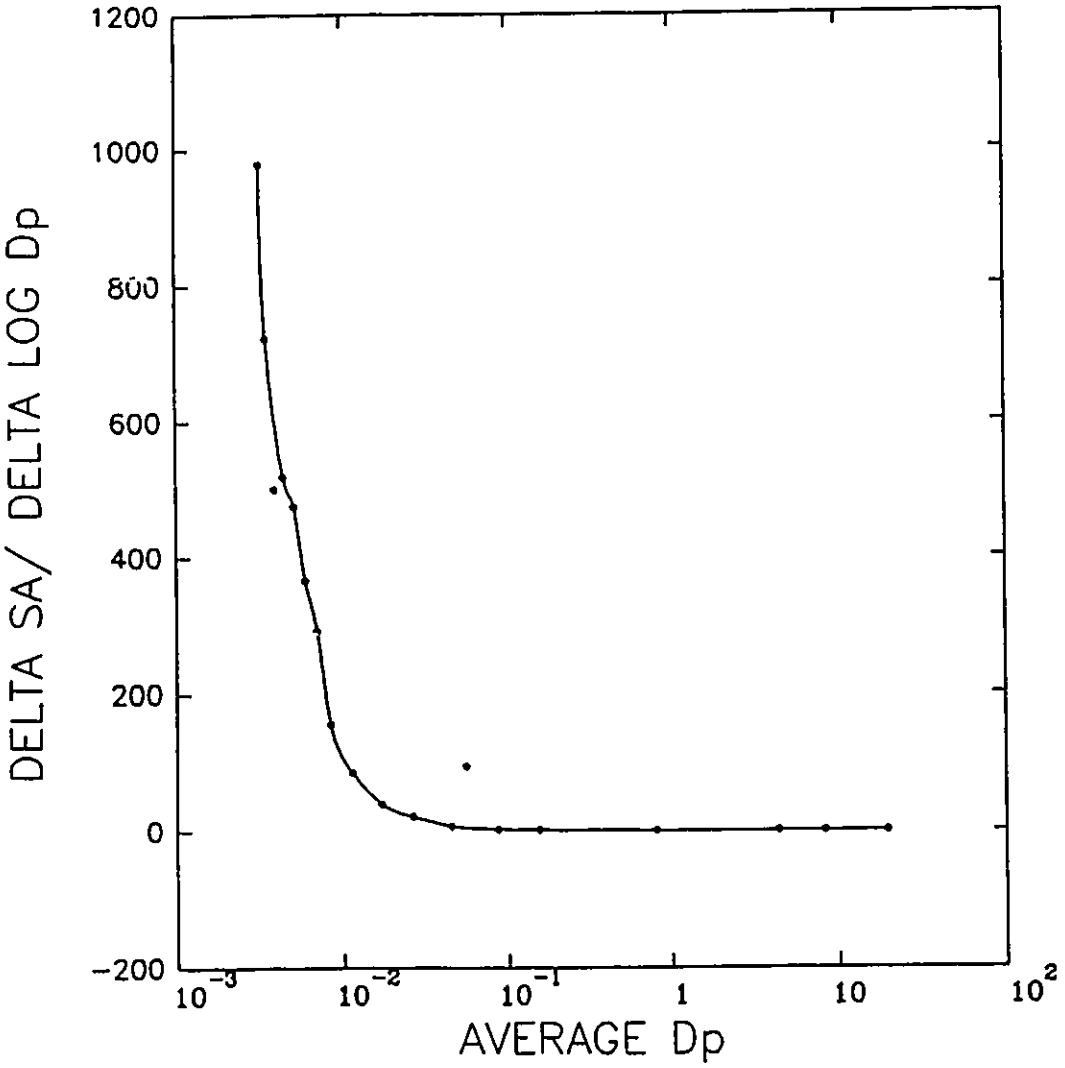

Figure 3.12 : **Surface area distribution for Co-Mo catalyst containing 10% Ni-SOD impregnated with 45% nickel.**

3.3.5 ACIDITY

The acidity of three laboratory prepared Co-Mo/Al_2O_3 catalysts containing 0%, 10% and 26% Ni-SOD impregnated with 39% nickel was compared using thermogravimetric analysis in presence of ammonia. The weight variation curves as a function of time are located in Appendix E, Figures E-4 to E-6 and a comparison can be found in Table 3.1. The percentage of physisorption was the same in all three catalysts, but chemisorption was less as the amount of Ni-SOD increased. This observation implies that fewer acid sites could be reached by ammonia molecules as the content of Ni-SOD increased due to the slow diffusion of ammonia through sodalite cages. The strength of acid sites, however, was greater with increasing sodalite contentsince the ammonia was desorbed at higher temperature as the Ni-SOD content increased. Although high purity sodalite (Figure E-1) has weaker acidity than 100% Co-Mo/Al_2O_3 (Figure E-4), a combination of sodalite with the Co-Mo/Al_2O_3 catalyst increases the strength of acid sites which results in stronger acidity than for each of the components separately.

3.4 FEEDSTOCK

The feedstock used for all experiments was the Lloydminster atmospheric residuum supplied by Consumers' Co-operative Refineries Ltd (CCRL), Regina, Saskatchewan. The Lloydminster atmospheric residuum has a small amount of heteroatoms and MCR when compared with most of the feedstock listed in Table 1.1.

Its asphaltene fraction (insolubles in 1/40 pentane) is larger however and it has a relatively low API gravity. Lloydminster atmospheric residuum was used in order to establish a comparison between the hydrocracked products produced in laboratory and hydrocracked products produced at CCRL. The feedstock properties can be reviewed in Table 3.7.

Table 3.7 : **Properties of Lloydminster Atmospheric Residuum**

Density at 15°C (kg /m^3)	999.2
API gravity	10.11
IBP to 176°C (wt%)	0
176°C - 288°C (wt%)	1.05
288°C - 343°C (wt%)	2.99
343°C - 525°C (wt%)	42.76
+525 residue (wt%)	52.9
Carbon (wt%)	84.4
Hydrogen (wt %)	11.4
Sulphur (wt%)	3.74
Nitrogen (wt%)	0.45
Vanadium (ppm)	123
Nickel (ppm)	56.7
Iron (ppm)	7.7
Silicon (ppm)	16.5
Titanium (ppm)	2.4
Calcium (ppm)	30.5
Magnesium (ppm)	4.9
Sodium (ppm)	17.3
Ash (wt%)	0.04
Micro Carbon Residue (wt%)	13.4
Pentane insolubles (wt%)	14.6
Toluene insolubles (wt%)	0.08
H/C Atomic Ratio	1.6

CHAPTER FOUR

4.0 EXPERIMENTAL

4.1 CATALYST PREPARATION

A detailed account of catalyst preparation and the experimental procedures for hydrocracking experiments follows. All relevant tables can be found in Appendix B.

4.1.1 SYNTHESIS OF SODALITE

Sodalite was synthesized by using methods and reaction parameters based on work by Barrer et al. (1952), Carr et al. (1968) and Hermeler et al. (1991) The initial sodalite samples were prepared in a small stainless steel autoclave with a volume of approx 100 mL. A colloidal suspension consisting of 16.4g NaOH in 100 mL H_2O (4.1M), 8.2 g Al_2O_3 (CATAPAL SB Alumina) and 7.0 g SiO_2 (Cab-O-Sil) was placed in the sealed autoclave and heated at 160°C for 120 h. It was important that no vapour loss from the autoclave occurred during the course of the experiment in order to maintain the total volume of solution in the autoclave and its pH as explained in section 1.5.3. No external pressure was added to the mixture except for the normal vapour pressure built-up inside the sealed autoclave which was estimated to be approx 6 atm (Perry et al., 1984). After

5 days, the autoclave was quenched and the resulting crystalline powder filtered with copious amounts of deionized water (3-4 L). The filter was then dried for 10 h at 105°C and calcined for 4 h at 350°C. The experiment resulted in 12.3 g of a white, fluffy powder.

In order to obtain the sodalite in sufficient quantity to conduct all our hydrocracking experiments, a larger scale operation was set up. A four-litre autoclave was fitted with an inner sleeve having a volume of 1.1 L which was made of stainless steel SS-316 to avoid permanent damage to the autoclave walls. It is known that hot concentrated NaOH solutions will corrode stainless steel. However, after one experiment, the inside wall of the inner sleeve was permanently coated with a thin layer of sodalite crystal preventing corrosion products from entering the solution. 150 g of sodalite powder were obtained when 89.2 g of Al_2O_3, 77.0 g of SiO_2 and 188 g of NaOH were mixed in 1028 g of deionized water and heated at 160°C for 5 days. The mixture was allowed to sit at room temperature for 20 hrs before heating started. The product was washed with 5 L of deionized water in an attempt to reduce the pH value of the resulting crystals from pH 12 to pH 8. The sodalite crystals were dried for 10 h at 105°C. Then, the temperature was increased to 350°C at a rate of 5°C/min for calcination for a period of 4 h.

4.1.2 ZEOLITE PREPARATION

Once the sodalite powder was obtained, it received additional processing before it was combined with the Co-Mo mixture to form the final catalysts. Ni cations were inserted inside the sodalite cages, through ion exchange and impregnation. Then, the resulting nickel oxide (NiO) was reduced and the pores were partially blocked by potassium ions (K^+) during a subsequent ion exchange.

4.1.2.1 Ion Exchange Ni^{2+}

The method used for metal loading was that described by Linde (LINDE Technical Bulletin #F-09). Three 1L boiling flasks each equipped with a magnetic stirrer and a heating jacket were used to conduct ion exchanges in parallel. Each of the flasks was loaded with 40 g of sodalite slurried in 80 g of deionized water. The exchange solutions were prepared using 2.48g $Ni(NO_3)_2$ (2 wt% Ni) dissolved in 800g of deionized water (300-400 times the weight of salt). Each 40 g load of sodalite was exchanged with three separate nickel exchange solutions. The green exchange solution was added at the rate of about 150 mL once every hour, to each of the rapidly agitated molecular sieve slurries and maintained at reflux temperature (100°C). Slow addition and thorough mixing were required to insure a uniform distribution of the metal cations. The stirring was maintained for 20 h after the addition was complete to establish exchange equilibrium. The slurry was then filtered and the metal-loaded molecular sieve washed

free of all soluble salts. The conductance meter (YSI model 32) that was used to test the wash water for presence of nickel salt showed a concentration of $< 5 \times 10^{-4}$ mol Ni^{2+}. The wash water was colourless while the powder had taken a light green shade. Finally, the powders were dried for 400 min at 120°C. The temperature was raised 550°C at the rate of 1°C/min and maintained for calcination for 4 h. The Ni-loaded powders turned to an earth brown colour upon calcination. This experiment was repeated twice for a total of 240 g of sodalite.

4.1.2.2 Impregnation Ni^{2+}

Five crucibles each containing 20 grams of pre-exchanged sodalite were prepared for nickel impregnation. The amount of nickel species impregnated in the sodalite was calculated on the basis of weight percent of sodalite. The sodalite samples contained 13%, 26%, 34%, 39% and 45% Ni atoms or Ni^{2+} cations. A nickel nitrate ($Ni(NO_3)_2.6H_2O$) solution of the desired concentration was prepared and slowly added to the sodalite powder using a 5 mL Pasteur pipette until the powder was moist but not wet. The volume of solution added was sufficient to fill the pore volume of the sodalite, but insufficient to permit excess liquid to be present. Each cup was covered with a paraffin film and allowed to stand at about 40°C for 24 h to reach equilibrium before it was dried at 105°C for 10 h and calcined at 350°C for 4 h. The impregnated powders were originally bright green but after calcination turned from light to dark grey.

4.1.2.3 Reduction of NiO

The impregnated powder was placed in 4 fine-meshed traps which were loaded into a 155 mL autoclave equipped with a gas inlet and outlet. Reduction of nickel oxide (NiO) to its metallic state Ni° was attempted at 435°C with a constant hydrogen flow of 3.4 L H_2 (STP)/min under a pressure of 17.3 MPa for a period of 4 h. The traps were also used to prevent the sodalite powders containing different amounts of Ni^{2+} from mixing. 10 wt% of powder was lost during the process. The reduced sodalite was charcoal black.

4.1.2.4 Ion Exchange K^+

The last step was to replace Ni^{2+} that had not been reduced to Ni metal by ion exchange with K^+ cations. The goal was to locate as much as possible of the K^+ ions at the pore mouths, According to LINDE (Bulletin #F-09), if small amounts of metal are loaded by ion exchange, nearly all of the metal will be located near the periphery. An amount of potassium nitrate (KNO_3) equivalent to 4 wt% of potassium cations (K^+) was used. The reduced sodalite powder was slurried in twice its weight of deionized water in a 1L boiling flask equipped with a magnetic stirrer and a heating jacket. The exchange solution was composed of 0.10lg KNO_3/g reduced sodalite dissolved in 300-400 times its weight of deionized water and was added to the rapidly agitated slurry over a period of 4 h in 5 separate additions. The resulting exchanged powders were dried for

10 h at 105°C and calcined at 350°C for 4 h. The temperature was increased at the rate of 5°C/min. The charcoal black colour turned to a dark grey after calcination. This final ion exchange completed the sodalite treatment.

4.1.3 EXTRUDATE PREPARATION

Two series of catalyst were created, one composed of a fixed sodalite content with varying amounts of impregnated Ni^{2+} and the other composed of fixed amounts of Ni^{2+} in the sodalite with varying sodalite contents. The quantities of material in each catalyst can be found in Table B-4. The first series six catalysts were prepared with 90% Co-Mo-Al_2O_3 catalyst and 10 wt% of the sodalite impregnated with 0%, 13%, 26%, 34%, 39% and 45% Ni^{2+} as per methods described in sections 4.1.2. Those catalysts were tested in a hydrocracking experiment as per section 4.2. Following preliminary analysis of the first samples, the Ni^{2+} content in the sodalite for the second series was chosen at 39 % while the sodalite content varied at 0%, 5%, 20% and 26% respectively.

4.1.3.1 Preparation of Pastes

The catalysts were prepared by combining two pastes, an oil paste and an alumina paste, before extrusion. The alumina pastes were prepared using Versal 250 pseudoboehmite alumina support mixed with an aqueous solution of ammonium paramolybdate (APM) ($NH_{46}Mo_7O_{24}.4H_2O$) (Baker Analyzed Reagent) and a solution of

cobalt nitrate hexahydrate (CN) ($Co(NO_3)_2.6H_2O$) (Baker Analyzed Reagent). The APM solution contained ammonium hydroxide (30% NH_4OH) (Allied Chemicals) to improve its solubility and both solutions were placed in a fixed-temperature oven at 125°C for 10 min for faster dissolution. Mixing was done manually using a stainless steel spatula. HNO_3 (concentration 70% Baker Analyzed Reagent) was slowly added to the mixture. Subsequently, about half of a diluted HNO_3 solution (H_2O:70% HNO_3 = 25:1) was then added to increase the pH of the acidic paste (see Appendix B for amounts in grams). Concurrently, an oil paste contained an equal weight of treated sodalite powder and of light hydrocarbon distillate oil (Imperial Oil, Zerice) was prepared. The composition of the oil can be found in Table 3.5. The purpose of the zerice oil was to prevent water from being trapped into the pores of the zeolite as well as to prevent the alumina paste from acting like a glue and blocking access to the sodalite pores. The zerice oil was removed by burning during calcination of the extrudates. The oil paste was incorporated into the alumina paste which was fairly consistent but still powdery. Thorough mixing was performed after each addition. The remainder of the diluted HNO_3 solution was finally added. The combined paste, firm but not dry was then ready for extrusion.

4.1.3.2 Extrusion Equipment

Extrudates were formed using a 10 cm diameter, vertically mounted stainless steel cylinder with a perforated bottom onto which the combined paste was deposited. The paste was then forced through 1 mm diameter holes using a piston displaced by a thick

screw equipped with long handles. The combined paste was passed through the extruder twice for better mixing. The spaghetti-like extrudates were dried first for a minimum of 18 h in a fixed-temperature oven at 110°C and transferred into a temperature-programmed oven for calcination.

4.1.3.3 Calcination Procedures

The first group of catalysts was dried and calcined over a period of 15 h. They were dried for 10 h at 105°C and then calcined at 450°C for 4 h. The rate of temperature increase was 5°C/min. Throughout this first series, as much as 100% of the catalyst extrudates was reduced to powder. The rapid evaporation of water trapped in the catalyst pores may have caused the extrudate to crumble. In an attempt to solve the problem, a series of tests using thermogravimetric analysis were performed to determine the critical temperatures at which the largest weight loss occurred (see Appendix E). It was noted that, for both catalysts tested, there was a sharp weight loss around 200°C followed by a constant decrease up to about 580°C. As a result, the calcination period was extended to 64 h for the second group to insure a slow and gradual elimination of water and zerice light oil. The catalysts were first allowed to sit at 110°C overnight, then heated through two plateaux of 10 h in duration at 190°C, 200°C. The temperature was raised again to 220°C and maintained for 20 h. Two more plateaux were established at 285°C and 365°C for 7.5 h each and finally calcination was effected at 450°C for 4 h. All temperature increases were made at the rate of 1°C/min. A slow rate of heating was

essential in order to avoid bursting of the extrudates. Catalysts in the first group were: Ni-SOD content: 10%, nickel content in sodalite: 0%, 13%, 26%, 34% and 39%, as well as 100% $CoMo/Al_2O_3$. Catalysts in the second group were: nickel content: 39%, Ni-SOD content: 5%, 20% and 26%.

4.2 CATALYST TESTING

4.2.1 HYDROCRACKING EQUIPMENT

Hydrocracking experiments were performed to test each catalyst for both heteroatom conversion and catalyst deactivation. A schematic of the experimental setup can be found in Figure 4.1. It consists of a 1L double-barrel Ruska (2217 NI) constant feed metering pump, an upward-flow fixed-bed reactor (155 mL) equipped with a three-section heating sleeve and two reservoirs (1L and 2L) for sample collection and waste collection. All connecting tubing conduits as well as the pump barrels were heated at 90°C using Brisk Heat flexible electric heating tapes (1.5 cm).

The feed was preheated in the reactor inlet conduit from 160°C to 260°C as it approached the reactor and the reservoirs were maintained at 150°C to eliminate water from the products. The hydrogen and the bitumen feed were combined at the reactor inlet and all outlet gases flowed through a gas-liquid separator, a pressure let down regulator and a scrubber containing 500g of KOH in 2L of H_2O before exiting through

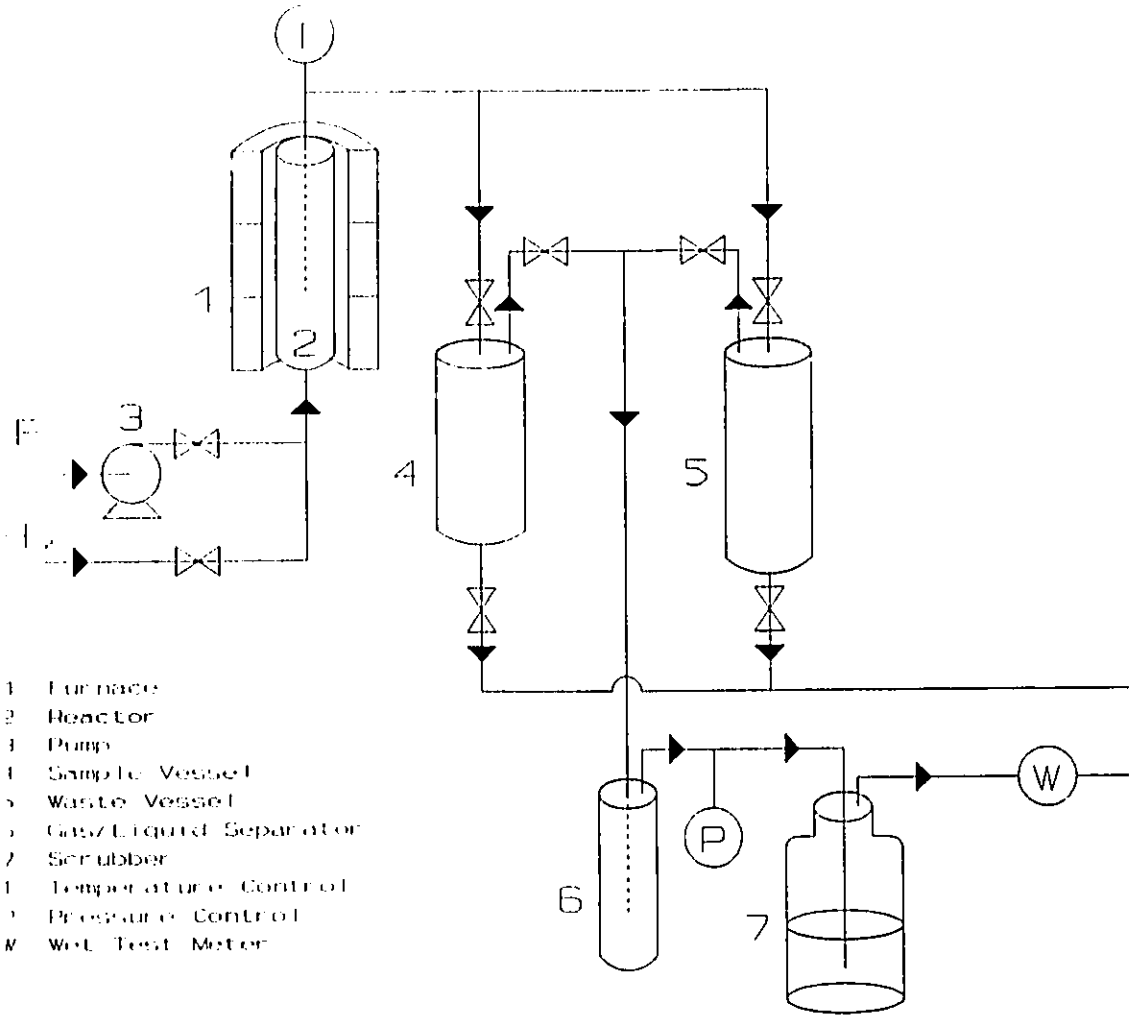

Figure 4.1 : **Hydrocracking Equipment.**

flow wet test meter (American Meter Company No. 803). The outlet pressure was set at 0.31 MPa and the gas flow was regulated by a needle valve controller. No gas product was collected for analysis.

4.2.2 OPERATING PROCEDURES

The feed used for all experiments was Lloydminster atmospheric resid +343°C supplied by Coop Refineries, Regina, Sask. Properties of the feed can be found in section 3.4. The reactor was loaded with approximately 60g of catalyst extrudates measuring 2-15 mm in length. Each experiment was run in the course of 3 days for a total time-on-stream of 12.5 h. Presulphiding was performed on the catalyst for 4 h at 415°C at the beginning of the experiment. The feed rate was set at a rate of 160 mL/h for time-on-stream θ = 3.5h - 4.25h and θ = 11.8h -12.5h and at 88 mL/h for time-on-stream θ = 5.8h-9.8h. A liquid product sample was collected during each time-on-stream period. A large sample was collected after the second time-on-stream period for distillation (ASTM 1160) and colour testing (ASTM 1500) of the second boiling point fraction of that sample as described in the methodology section. The third time-on-stream period was compared with the first and used for deactivation quantification. The reaction temperature was maintained at 415°C within 1°C throughout the testing period. Table 4.1 shows the reaction conditions for the hydrocracking experiments. Two experiments were performed as references, one with a standard catalyst (American Cyanamid 1442B) (74 % Al_2O_3, 15.2 % MoO_3, 3.2 % Co_3O_4) and

the other with 0.5 cm diameter steel balls was a non-catalytic thermal hydrocracking experiment. Identical reaction conditions were used for both the laboratory prepared catalysts and for the standard catalyst but only the reaction conditions for θ = 5.8h-9.8h and θ = 11.8h-12.5h were used for the thermal cracking experiment with steel balls as presulphiding was not required.

Table 4.1 : **Hydrocracking Conditions**

Time-on-stream (θ) (h)	**3.5 - 4.25**	**5.8 - 9.8**	**11.8 - 12.5**
Feed Rate (mL/h)	160	88	160
LHSV (h^{-1})	1.07	0.59	1.07
H_2 Flow Rate ($L\ H_2$ (STP)/L feed)	536.3	567.3	536.3
Temperature (°C)	415	415	415
Pressure (MPa)	17.3	17.3	17.3
Heating time (h)	1.5	1.5	1.5
Presulphiding time (h)	2.5		
Time to steady state (h)	1	1.66	1
Sample time (h)	0.75	4 0	.75
Cool down time (h)	1	1	1

CHAPTER FIVE

5.0 RESULTS AND DISCUSSION

Evaluations of several sulphided Co-Mo/Al_2O_3 catalysts containing a zeolite component (Ni-sodalite) were made by hydrocracking Lloydminster Atmospheric Residuum. Two series of Co-Mo catalysts were prepared to establish both the effects of sodalite content in the catalyst and nickel content in the sodalite on hydrocracking. The first series of catalysts contained increasing amounts of sodalite which had been impregnated with a fixed amount of nickel while the other series contained a fixed amount of sodalite with varying amounts of impregnated nickel. Catalysts preparation is described in chapter four.

5.1 COLOUR FORMATION IN THE DIESEL FRACTION

Rapid colour formation in the diesel boiling fraction (288°C - 343°C) is a major concern for Consumers' Co-operative Refineries Ltd (CCRL), Regina, Sask. As a result, a study of colour formation in the diesel fraction produced by hydrocracking CCRL's feedstock, Lloydminster atmospheric residuum, was performed. Lloydminster atmospheric residuum was hydrocracked using bench-scale equipment. Colour measurements of the various diesel fractions were made. The relationship between the

sulphur and nitrogen contents of the diesel fractions and colour were determined.

The ASTM colour changes of the diesel fractions from the laboratory prepared catalysts, the reference catalyst (manufactured by American Cyanamid) and the thermal cracking (non-catalytic) experiment are compared in Figures 5.1 - 5.4 over a storage period of 120 days. Colour data are available in Table B-5. The colour formation at the beginning of the test period for all catalysts is shown more clearly in Figures 5.5 - 5.7. The colour of the diesel fractions obtained using the laboratory prepared catalysts develop rapidly in the first 20 days of storage. The values at which colour stabilizes increase as the catalyst content of sodalite increases as shown in Figure 5.5. However, the time required for the colour to reach its plateau (Figure 5.5) decreases as the catalyst sodalite content increases. Both of these observations suggest that sodalite increases the rate at which the colour plateau is attained.

In contrast, the rate of colour formation decreases as the catalyst nickel content in the sodalite increases (Figures 5.3, 5.4, 5.6 and 5.7). Furthermore, greater ASTM colour readings values were obtained for each plateau by varying the nickel content than by varying the sodalite content in the catalyst. Although nickel retards the rate of colour formation, the value at which colour stabilizes to a plateau is generally greater .

The laboratory prepared catalysts were compared with the reference catalyst and with thermal hydrocracking without a catalyst. The reference catalyst was more effective

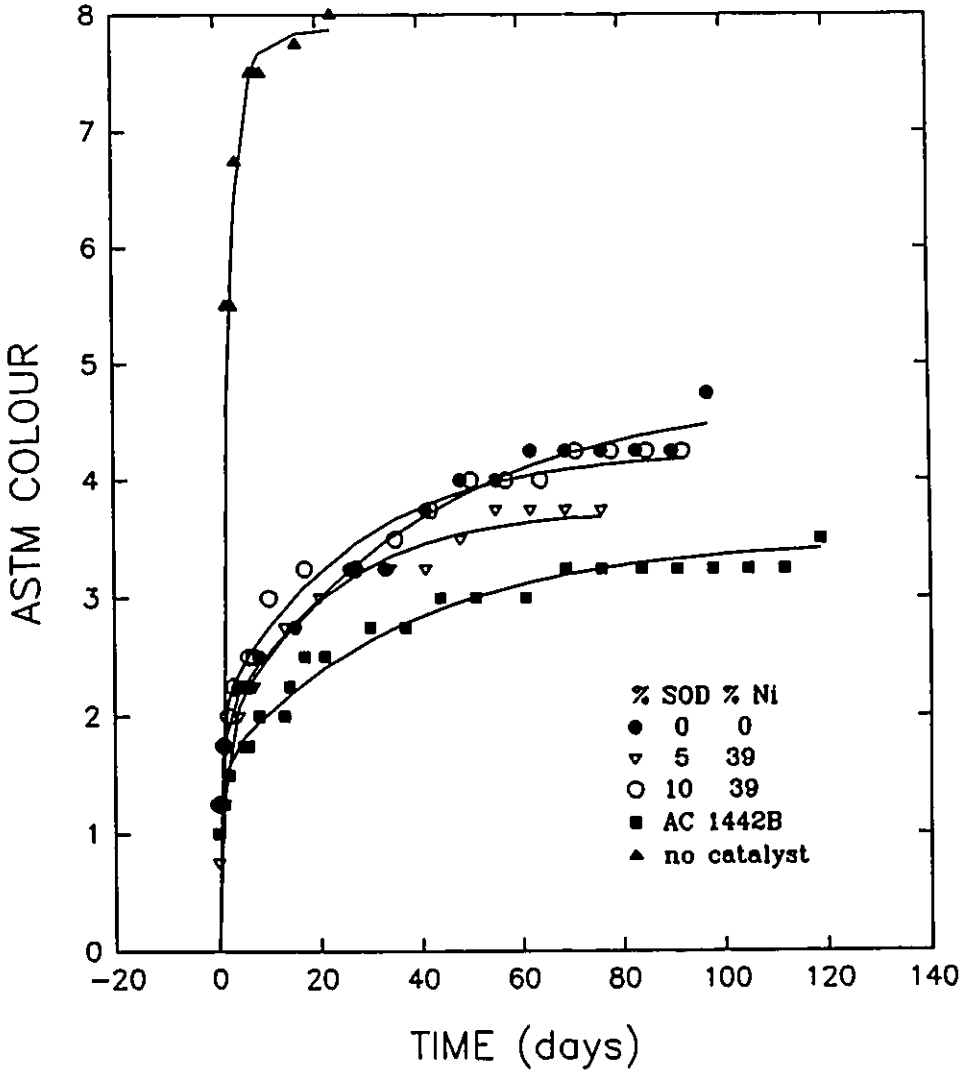

Figure 5.1 : **ASTM colour of the diesel fraction over a storage period of 120 days.** Co-Mo catalysts containing 0%, 5% and 10% Ni-SOD impregnated with 39% nickel.

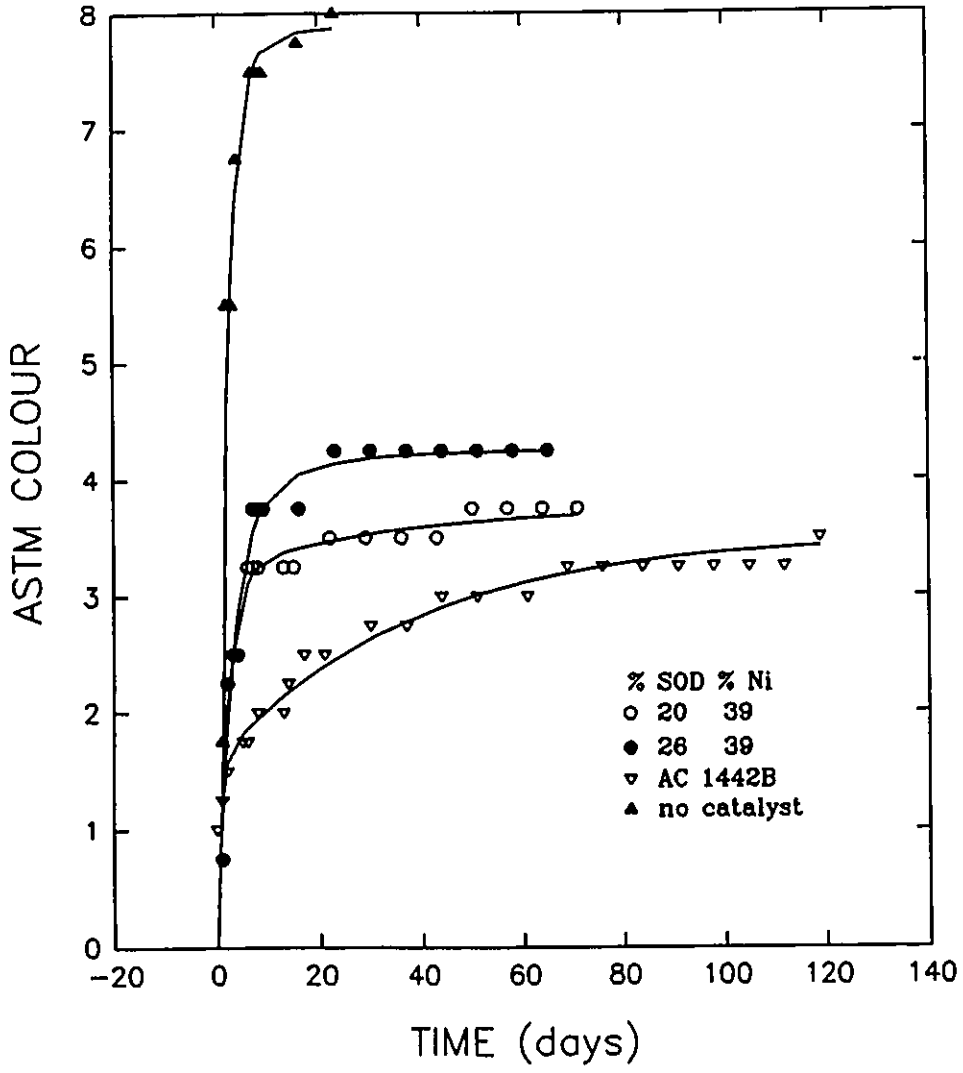

Figure 5.2 : **ASTM colour of the diesel fraction over a storage period of 120 days.** Co-Mo catalysts containing 20% and 26% Ni-SOD impregnated with 39% nickel.

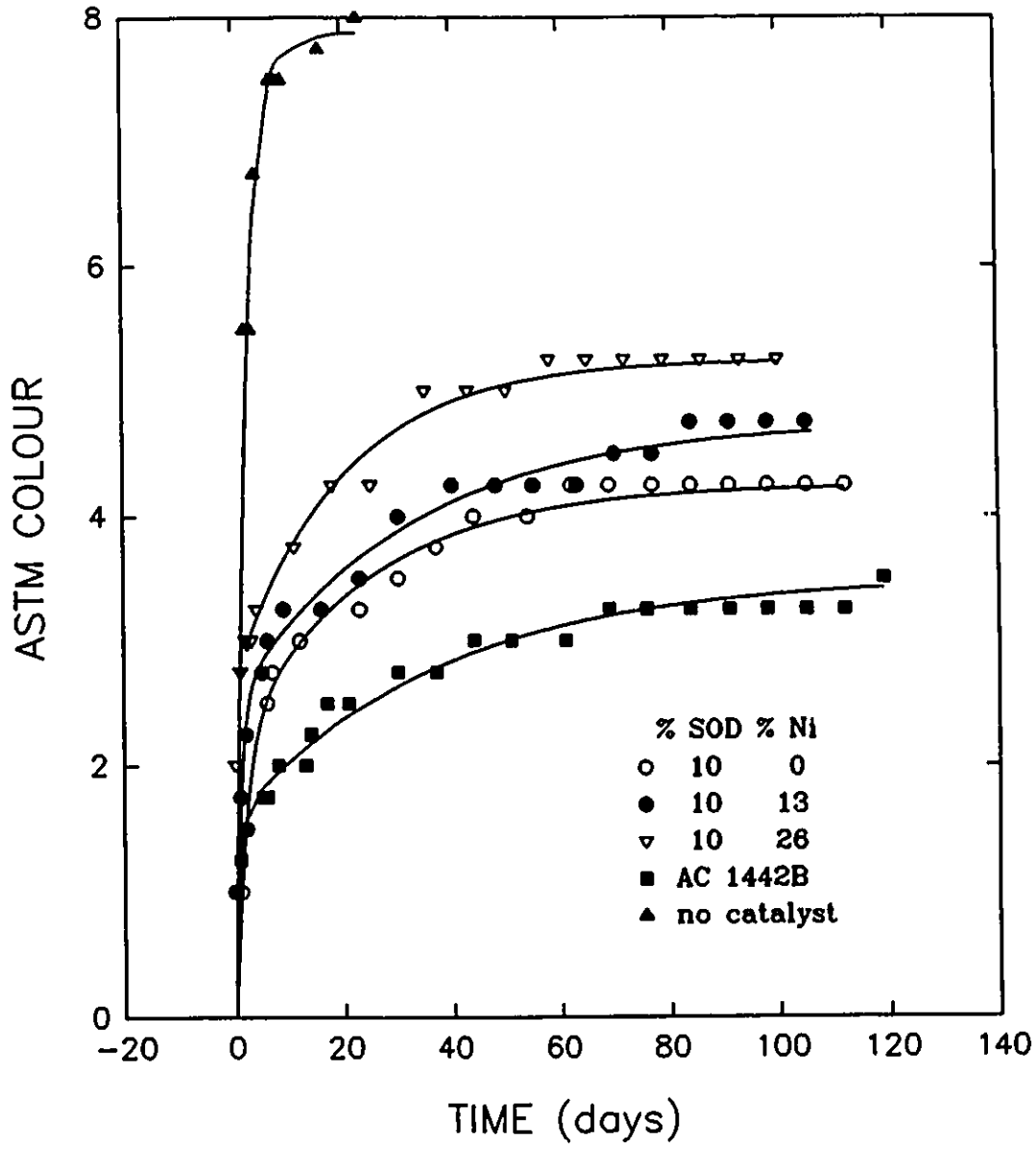

Figure 5.3 : **ASTM colour of the diesel fraction over a storage period of 120 days.** Co-Mo catalysts containing 10% Ni-SOD impregnated with 0%, 13% and 26% nickel.

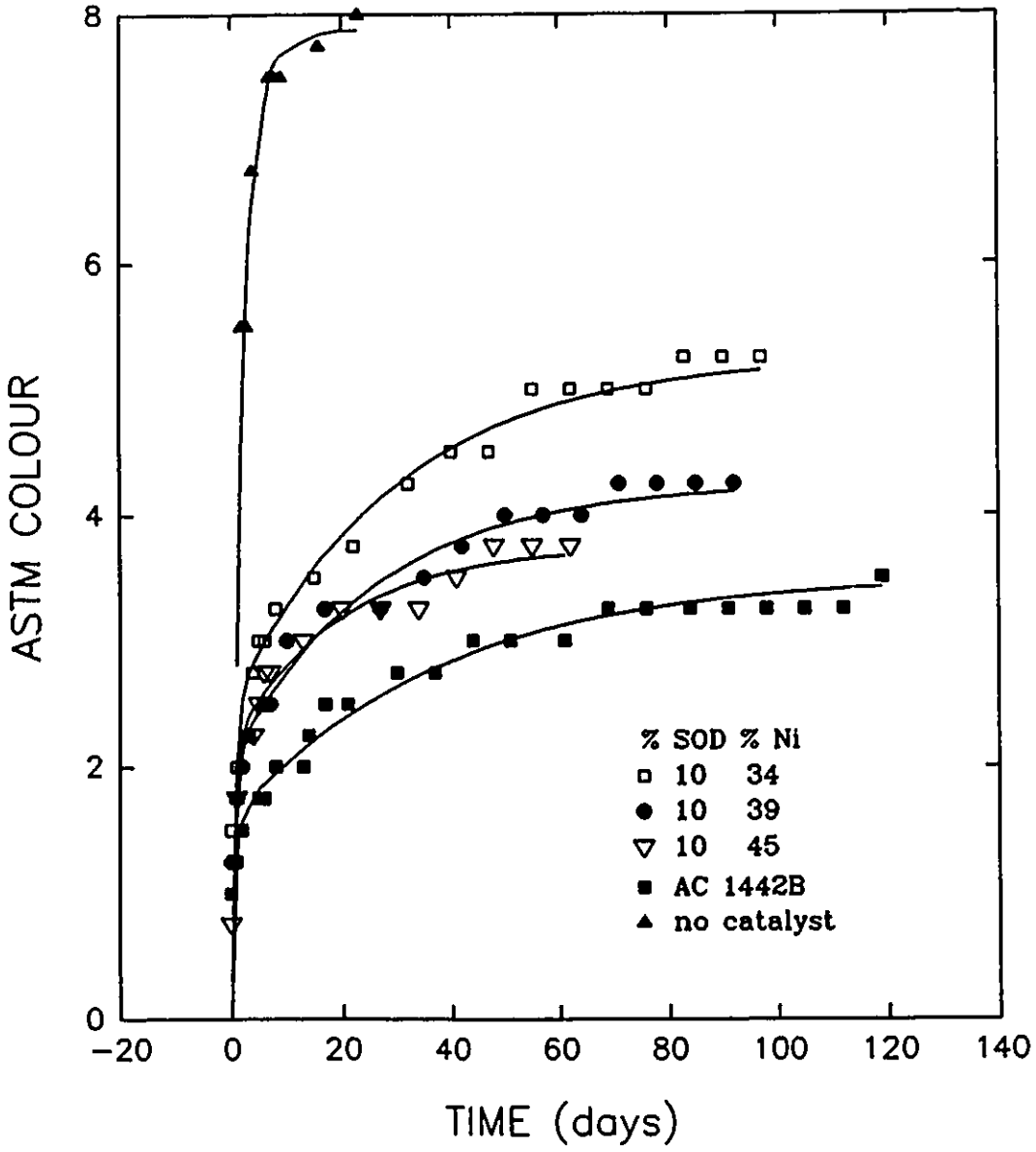

Figure 5.4 : **ASTM colour of the diesel fraction over a storage period of 120 days.** Co-Mo catalysts containing 10% Ni-SOD impregnated with 34%, 39% and 45% nickel.

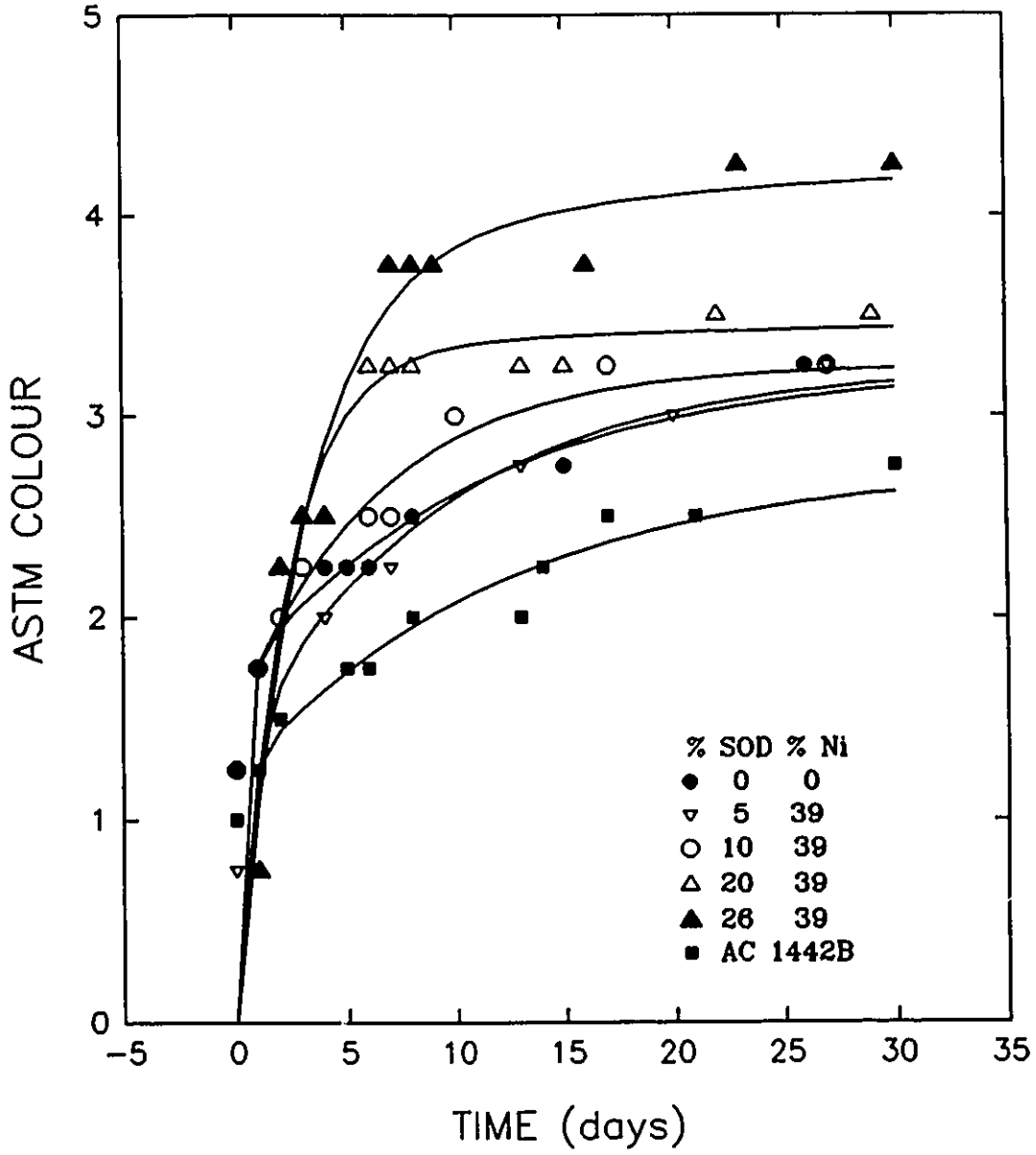

Figure 5.5 : **ASTM colour of the diesel fraction over a storage period of 30 days.** Co-Mo catalysts containing various amounts of Ni-SOD impregnated with 39% nickel.

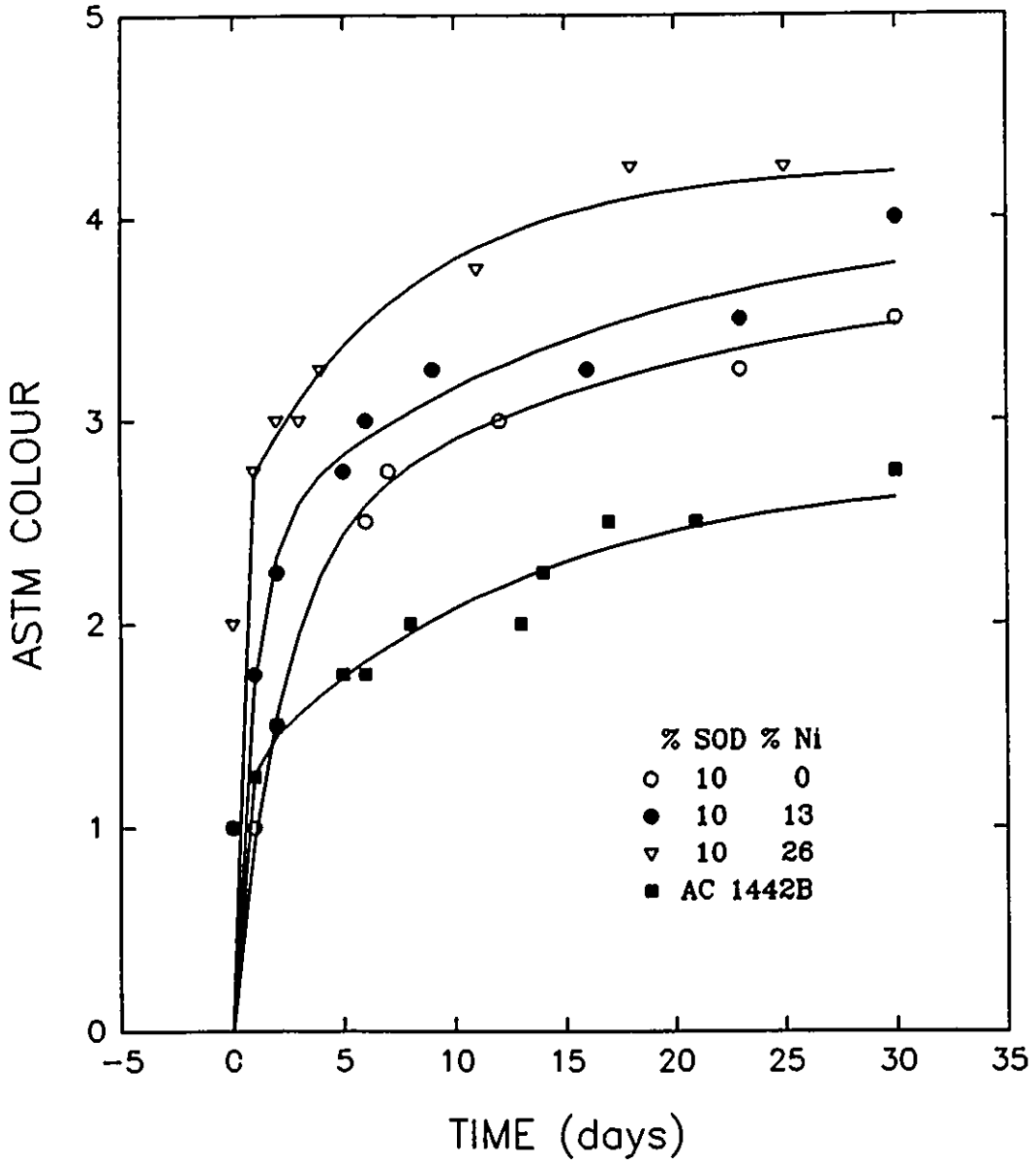

Figure 5.6 : **ASTM colour of the diesel fraction over a storage period of 30 days.** Co-Mo catalysts containing 10% Ni-SOD impregnated with 0%, 13% and 26% nickel.

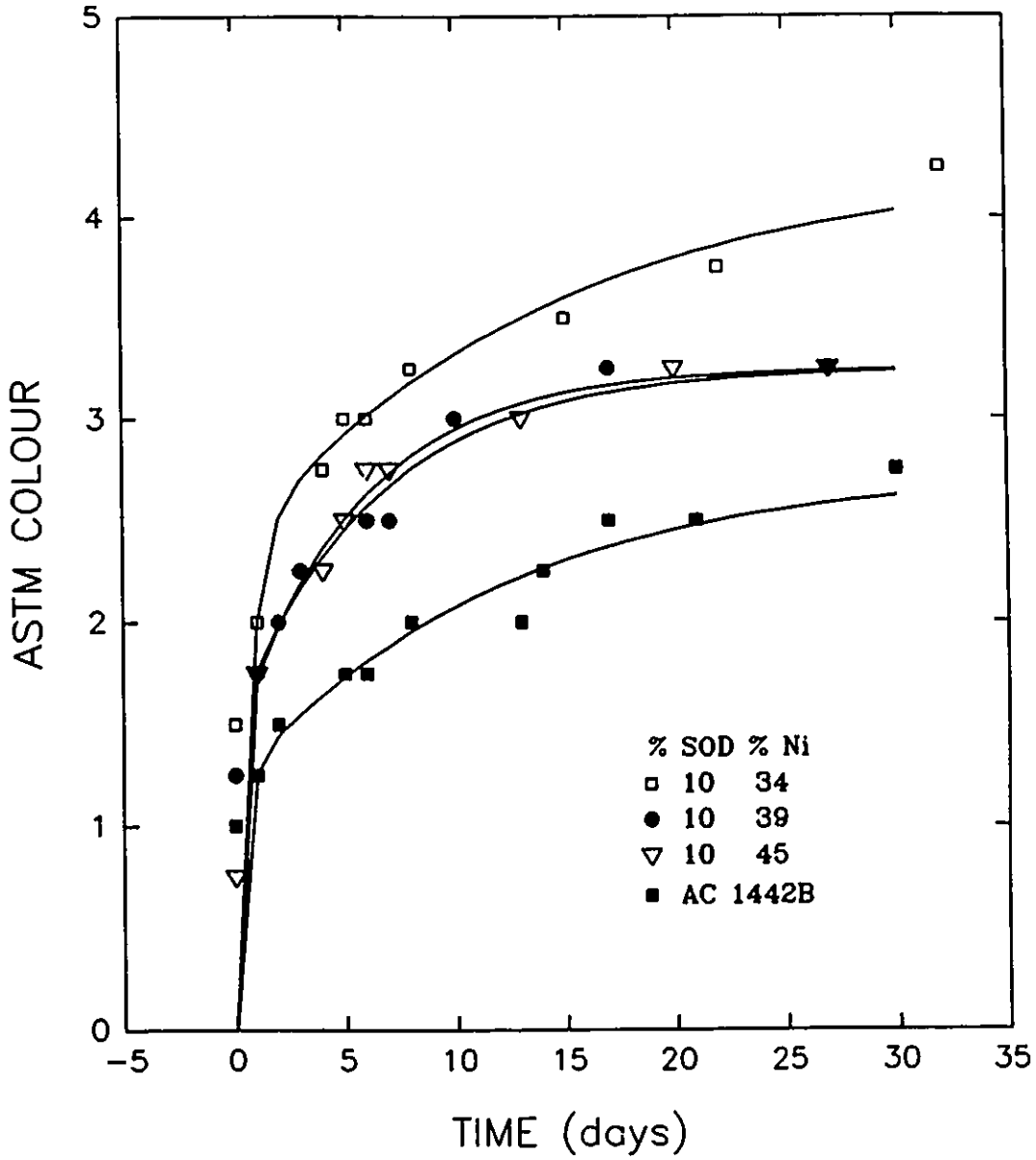

Figure 5.7 : **ASTM colour of the diesel fraction over a storage period of 30 days.** Co-Mo catalysts containing 10% Ni-SOD impregnated with 34%, 39% and 45% nickel.

at controlling colour formation in the diesel fraction than any of the laboratory prepared catalysts. Both the rate of colour development and the colour value of the plateau were lower. The colour of the diesel fraction obtained from thermal hydrocracking, however, develops more rapidly over a shorter period of time than that of the fractions obtained from the laboratory prepared catalysts. In less than 25 days the thermally hydrocracked fraction reached an ASTM colour reading of 8, which is the maximum measurable ASTM colour. It is obvious that hydrocracking catalysts improve the initial colour of the middle distillate fraction as well as its stability over time.

The development of coloured species has been attributed to carbonaceous molecules containing heteroatoms such as nitrogen (CM_N) and sulphur (CM_S). As it is widely agreed that oxidation leads to colour formation, a first order reaction between the heteroatom species and oxygen dissolved in the diesel fuel (perhaps from air or already present in the diesel fraction) can be expressed as (using CM_N as an example):

$$CM_N + \frac{1}{2}O_2 \rightarrow CM_N\text{-}O \ (coloured) \qquad (5\text{-}1)$$

The final concentration of the coloured species will be proportional to the initial concentration of the heteroatom species $[CM_N]_o$. The rate of this reaction will be expressed as

$$r = -\frac{d[CM_N]}{dt} = k\,[CM_N] \qquad (5\text{-}2)$$

where k is the reaction rate constant. Equation 5-2 can be integrated to obtain

$$[CM_N] = [CM_N]_o \, e^{-kt} \tag{5-3}$$

The concentration of coloured species C at any time t can then be written as

$$C = [CM_N]_o - [CM_N] = [CM_N]_o \, (1 - e^{-kt}) \tag{5-4}$$

which can be written as

$$C = A \, (1 - e^{-Bt}) \tag{5-5}$$

Data generated using Equation 5-5 did not agree Figures 5.1 to 5.7. However, colour degradation curves were found to behave exponentially, as per the following equation:

$$C = A - A_1 \, e^{-B_1 t} - A_2 \, e^{-B_2 t} \tag{5-6}$$

where C is the ASTM colour value at time t days, and A is the maximum ASTM colour value achieved. A_1, A_2, B_1 and B_2 are constants where

$$A_1 + A_2 = A \tag{5-7}$$

The value for A_1, A_2, B_1 and B_2 for storage periods of 120 days and 30 days were compiled for each catalyst in Tables B-6 and B-7. The lines for the above equation using the constants in Tables B-6 and B-7 are shown in Figures 5.1 to 5.7. An excellent correspondence between the data points and the lines was achieved which suggests that two different species contribute to colour formation.

The colour of the diesel fraction after 60 days of storage is shown as a function of sodalite content in the Co-Mo catalyst in Figure 5.8 and as a function of nickel content in the sodalite in Figure 5.9. For this comparison, the measurement period was limited to 2 months (60 days) in order to include all catalysts. The addition of small amounts of sodalite appears to cause a small decrease in colour value after 60 days of storage according to Figure 5.8. In contrast there is an increase in colour value as the nickel content of the catalyst increases up to 26 % as shown in Figure 5.9. The colour reading of the fraction obtained from thermal hydrocracking (filled inverted triangle in Figure 5.8) is shown at ASTM colour 8 although it is likely that after 60 days of storage, the colour reading is much greater than the maximum measurable value on the ASTM colour scale. The colour of the diesel fraction obtained from the catalytic hydrocracking using the reference catalyst is represented by an inverted hollow triangle.

The sulphur content in the diesel fraction is shown as a function of the sodalite content in the Co-Mo catalyst in Figure 5.10 and as a function of the nickel content in the sodalite in Figure 5.11. The shapes of both of these curves generally correspond to those of Figures 5.8 and 5.9 respectively, which indicates a possible relation between sulphur content and colour. Furthermore, both the sulphur content and the colour of the diesel fraction obtained from thermal hydrocracking are much greater than all of the other fractions. Similarly, the diesel fraction obtained using the reference catalyst has both lesser sulphur content and colour value than all of the other fractions. To confirm this observation, plots of the colour readings after a storage period of 25 days and 60

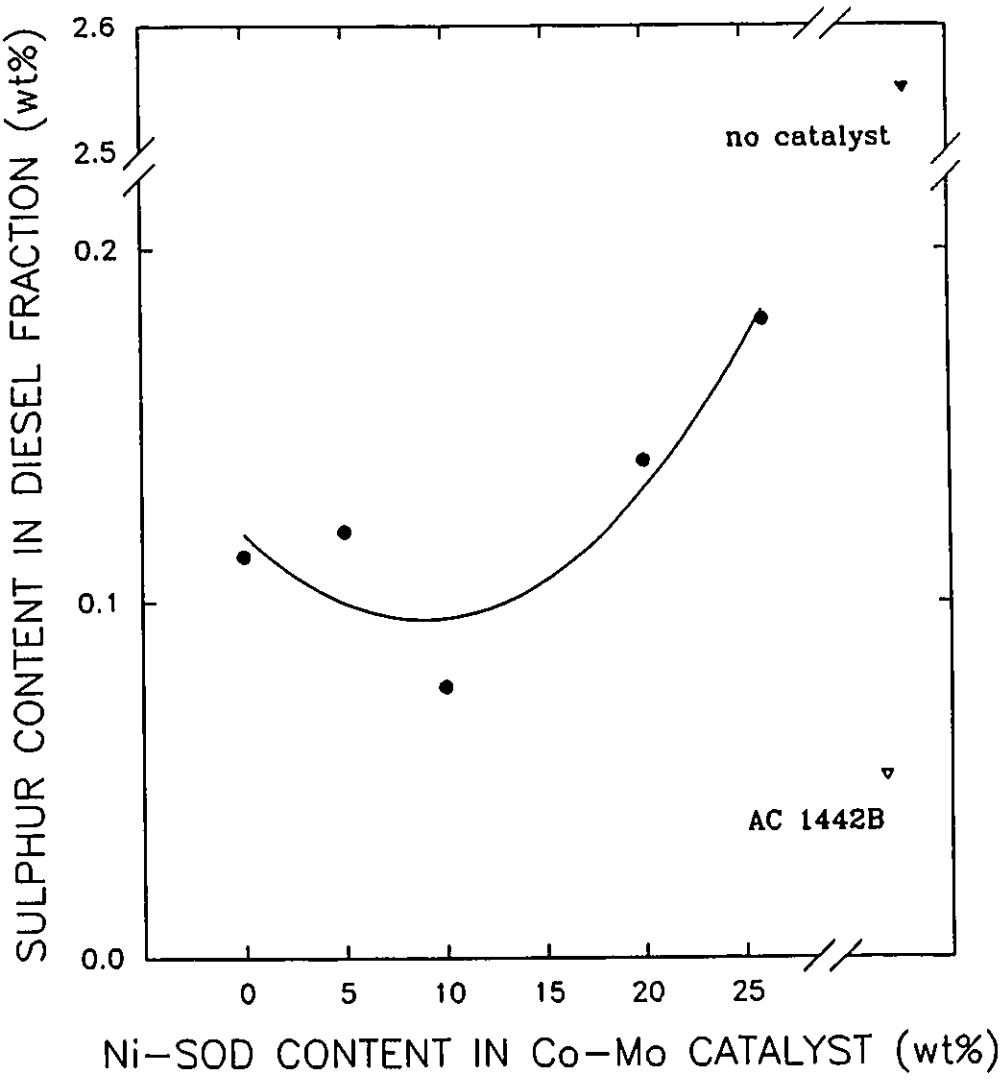

Figure 5.8 : **Sulphur content (%) of the diesel fraction as a function of Ni-SOD content in the Co-Mo catalyst (wt%).**

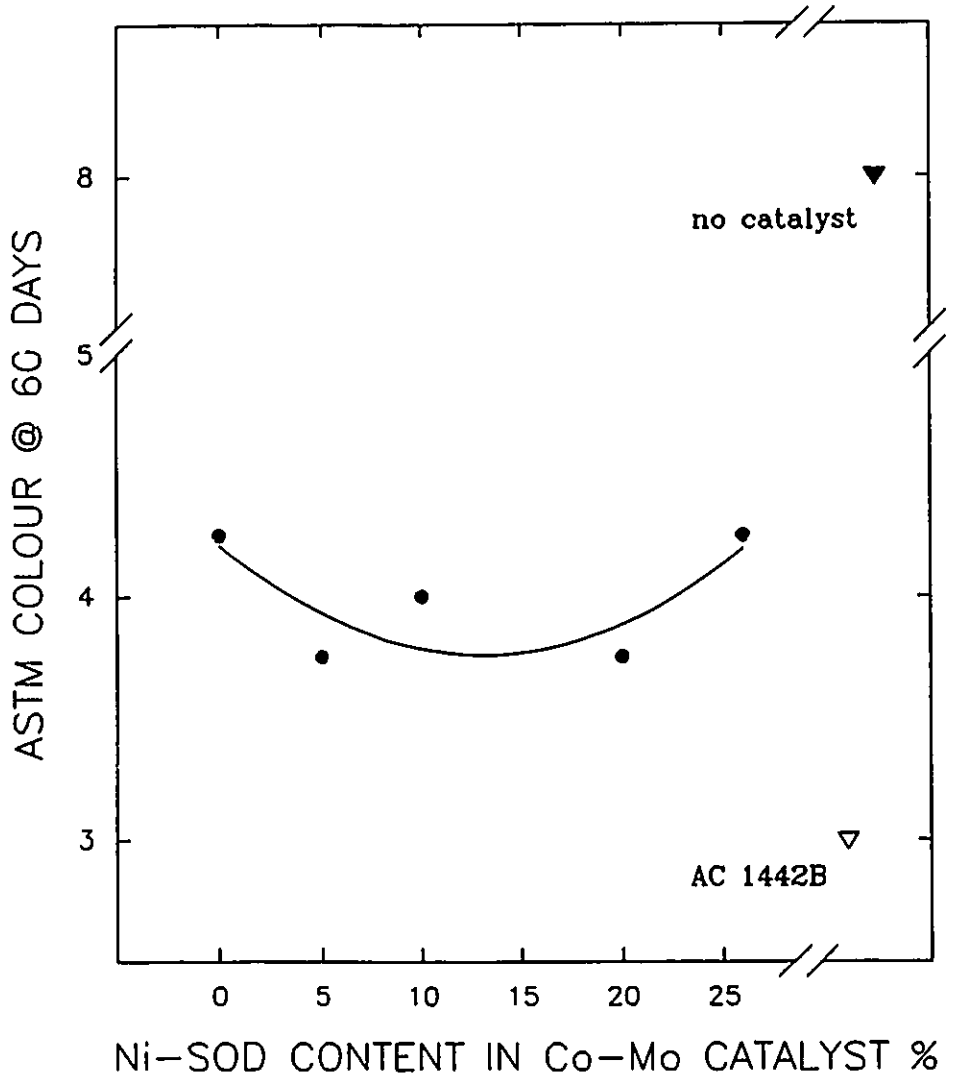

Figure 5.9 : **ASTM colour after 60 days of storage as a function of Ni-SOD content in the Co-Mo catalyst (wt%).**

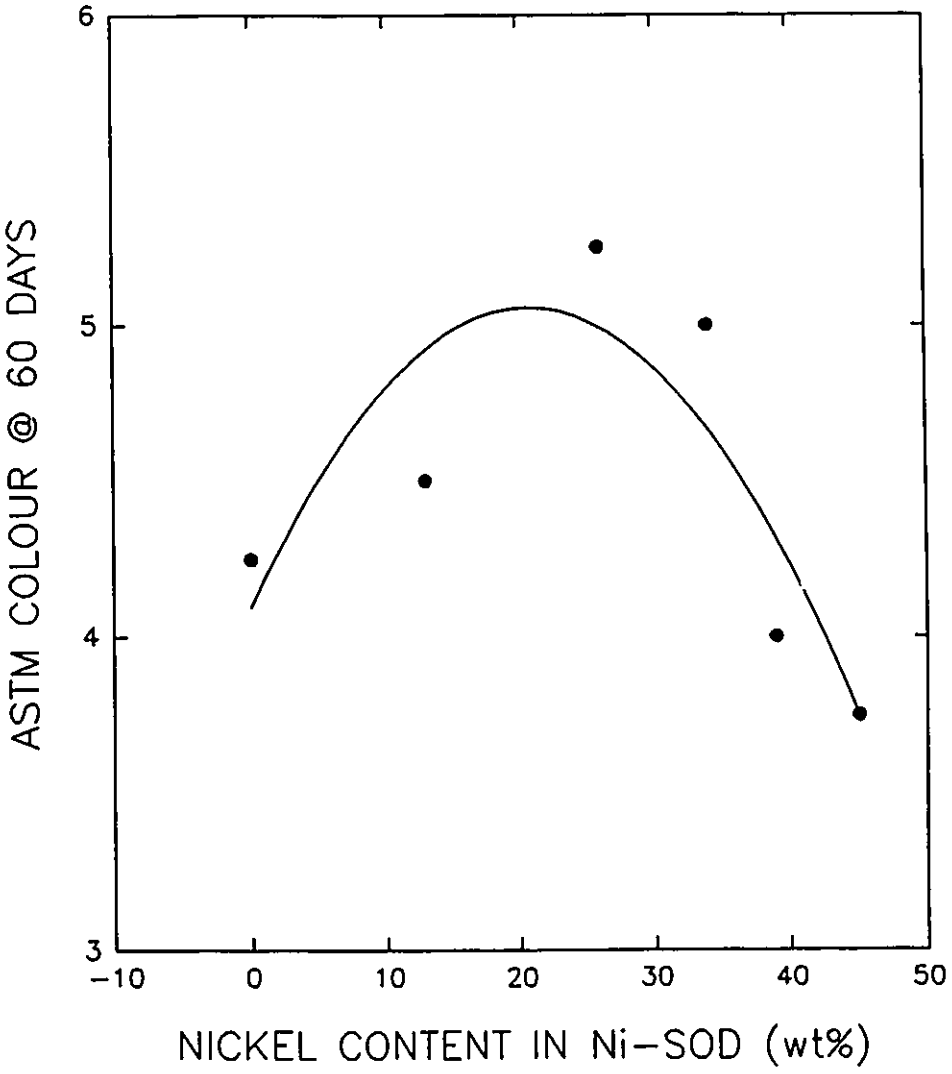

Figure 5.10 : **ASTM colour after 60 days of storage as a function of nickel content in the sodalite component of the Co-Mo catalyst (wt%).**

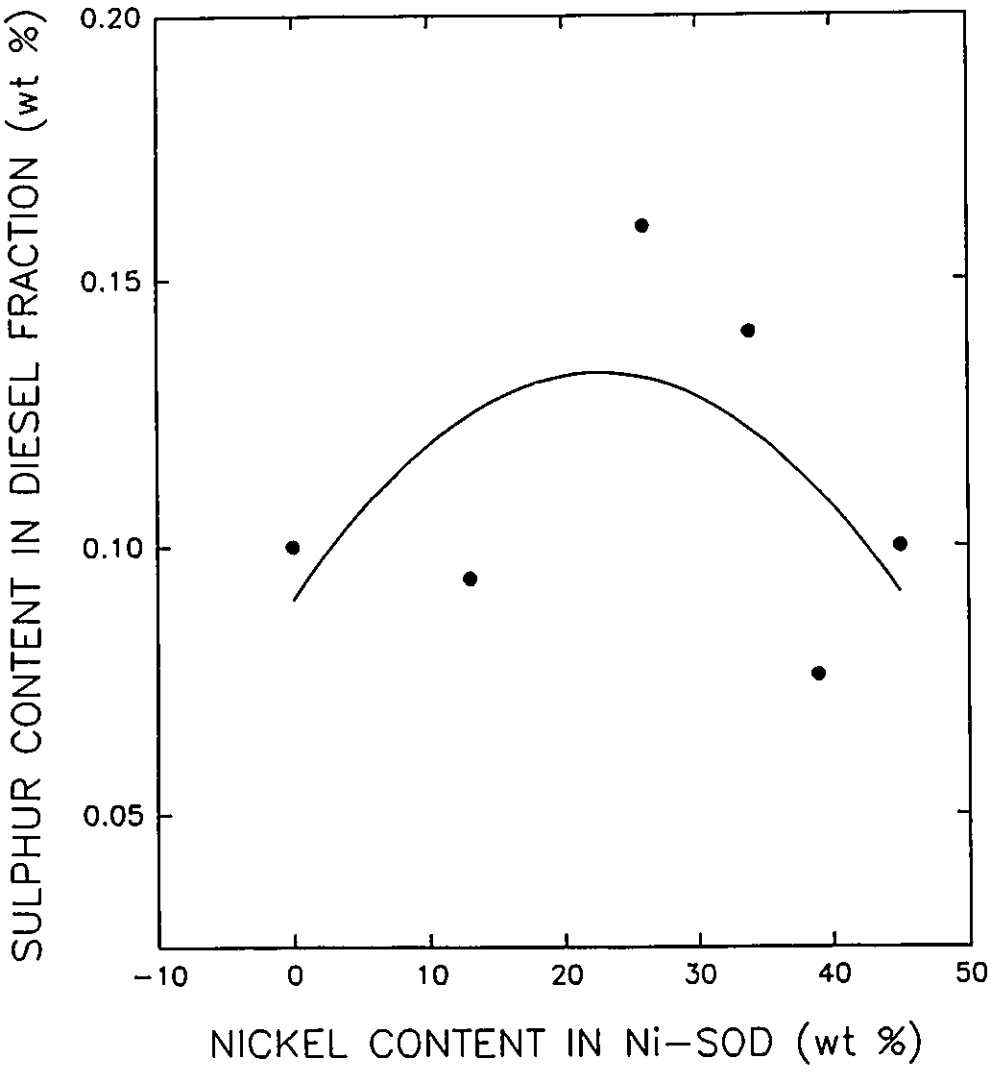

Figure 5.11 : **Sulphur content (%) in the diesel fraction as a function of nickel content in the sodalite component of the Co-Mo catalyst (wt%).**

days as a function of sulphur content in the diesel fractions are shown in Figures 5.12 and 5.13. Because of the limitations in the precision of the ASTM colour readings, a range of colour values is indicated on those plots in order to depict a more realistic picture of the relation between sulphur contents and colour values. The correlation between colour and sulphur content is good after 25 days with a correlation coefficient of 0.76 but deteriorates slightly after 60 days of storage with a correlation coefficient of 0.69.

In order to improve the correlation between sulphur content and colour formation, the sulphur components present in the diesel fraction could be separated in classes of compounds using such techniques as Solid Phase Extraction, Gas Chromatography and Mass Spectrometry (Jokuty and Gray, 1991). By eliminating those sulphur compounds which have little influence on colour formation, a closer relation could be established both with the ASTM colour readings and with the factors of the exponential equation presented earlier. A number of authors have identified sulphur components as being a principal cause of fuel instability and colour development (Taylor and Frankenfeld, 1986; Batts and Fathoni, 1991; Mushrush et al., 1991).

The presence of nitrogen compounds has also been identified as a principal cause for fuel instability and colour formation (Taylor and Frankenfeld, 1986; Batts and Fathoni, 1991; Mushrush et al., 1991). The nitrogen content of the diesel fraction is presented as a function of sodalite content in the catalyst in Figure 5.14 and as a function

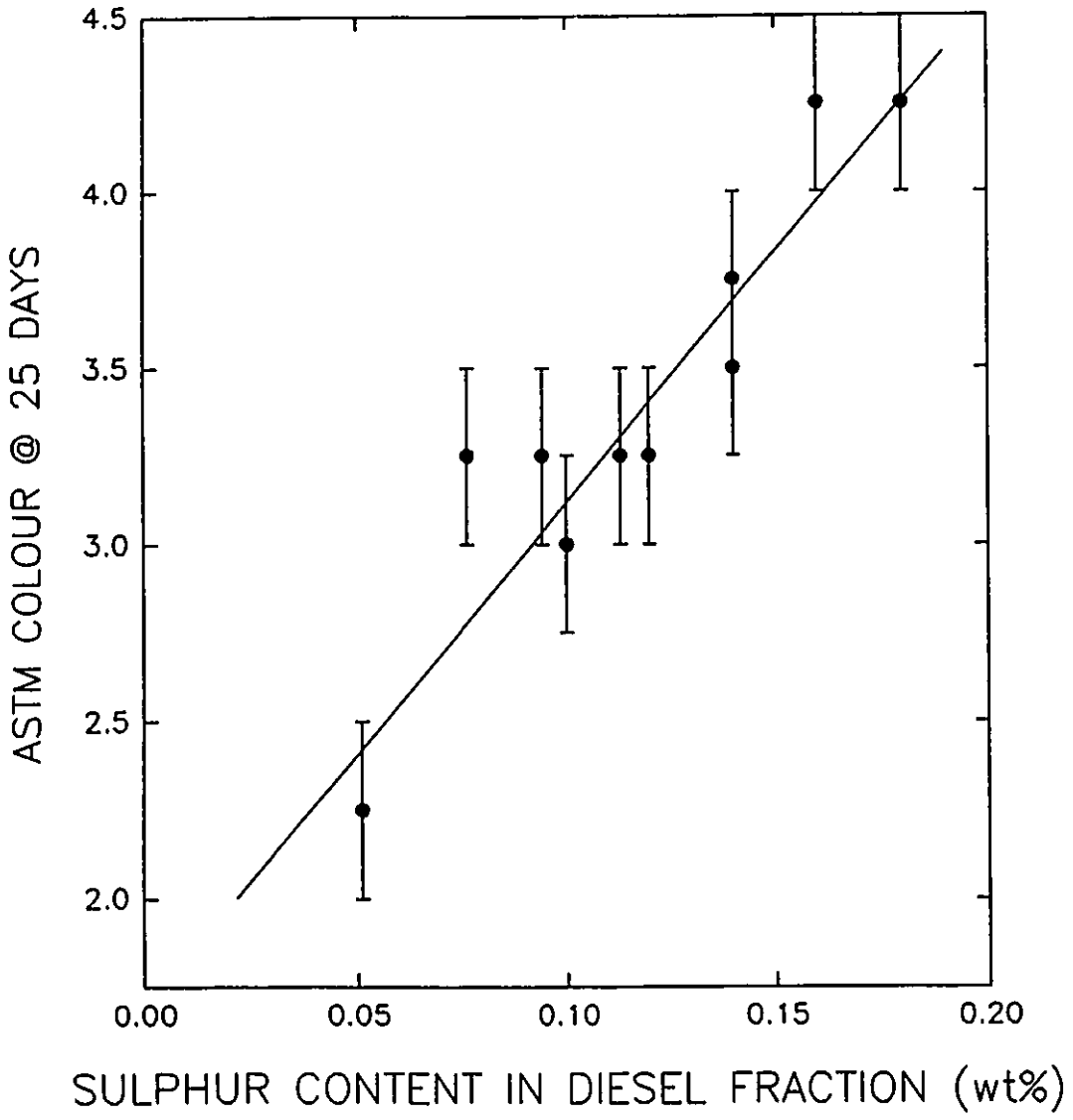

Figure 5.12 : **ASTM colour of diesel fraction after 25 days of storage as a function of its sulphur content.**

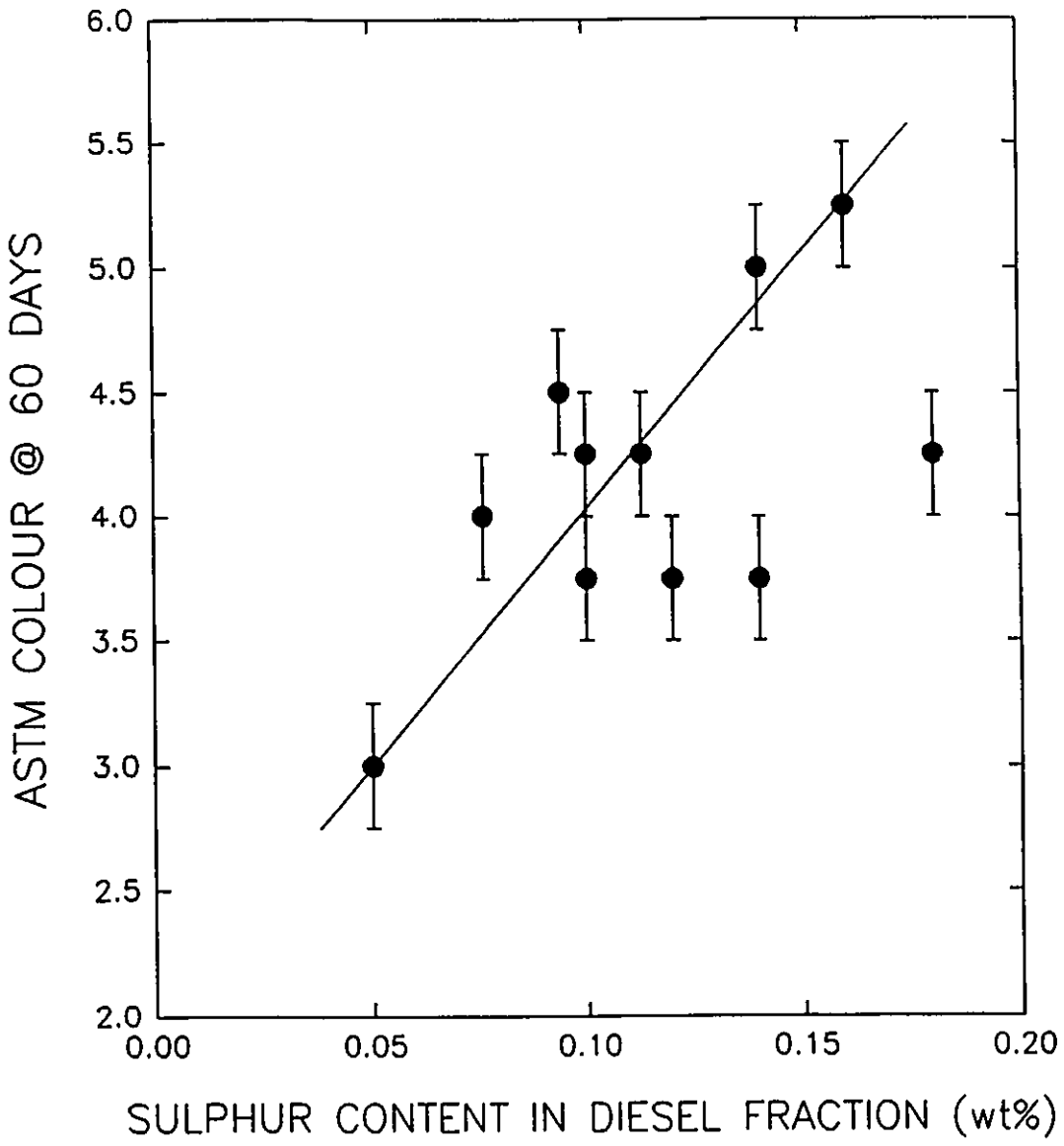

Figure 5.13 : **ASTM colour of diesel fraction after 60 days of storage as a function of its sulphur content.**

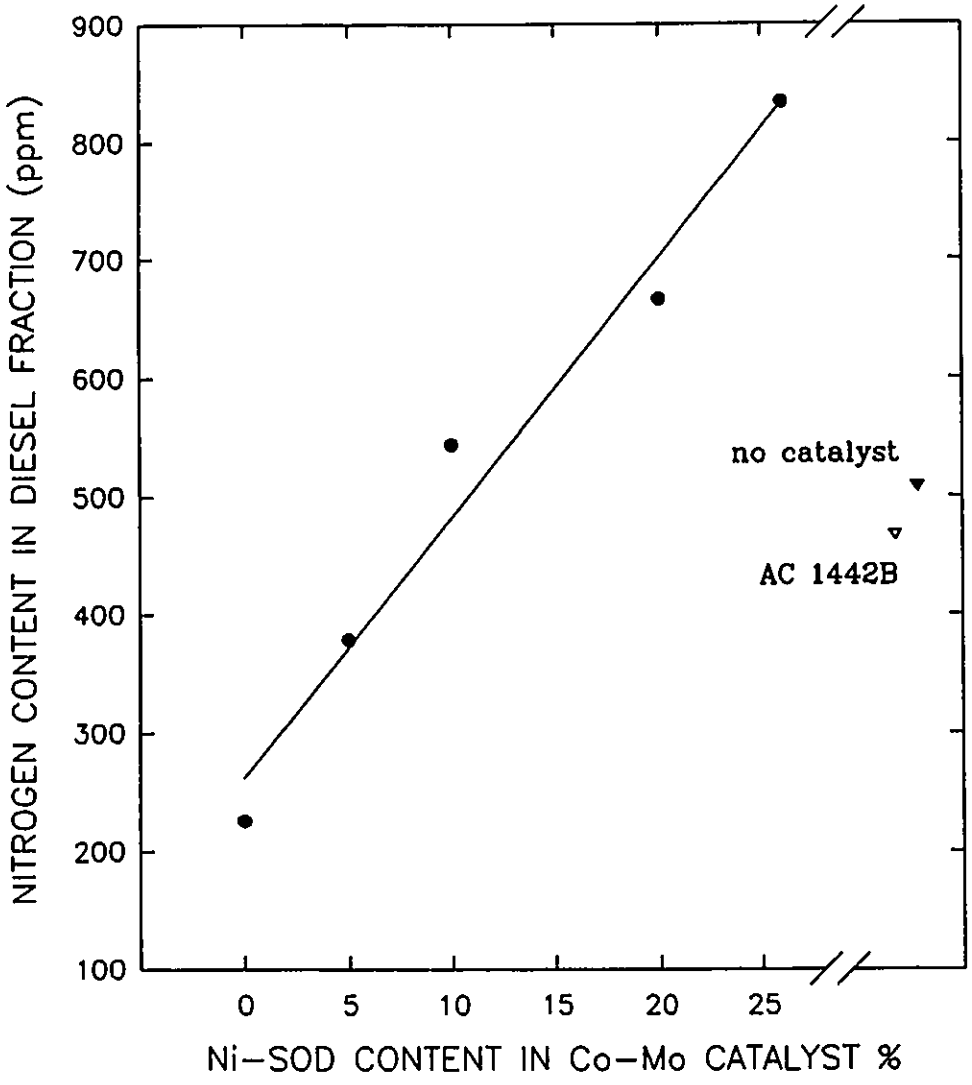

Figure 5.14 : **Nitrogen content (%) of the diesel fraction as a function of Ni-SOD content in the Co-Mo catalyst (wt%).**

of nickel content in the sodalite in Figure 5.15. The nitrogen content shows a steady increase with increasing sodalite content while it shows a steady decrease with increasing of nickel content. The shape of these two curves are different than those for colour in Figures 5.8 and 5.9. Also, the nitrogen content of the diesel fraction obtained from thermal hydrocracking and that obtained from catalytic hydrocracking with the reference catalyst are almost identical but their colour difference is the greatest among all of the fractions. This would indicate that nitrogen compounds contained in the diesel fractions did not influence their colour. The lack of correlation between nitrogen content and colour is confirmed in Figures 5.16 and 5.17. The correlation coefficient of the plot for the colour of the diesel fraction after 25 days of storage as a function of nitrogen content is 0.51 while that for the colour after 60 days of storage as a function of nitrogen content is 0.15. The two corresponding correlations with sulphur are definitely better. The fact that no correlation was observed between nitrogen content and colour is in accordance with statements by Bahn and co-workers (1987) who were first to report a lack of correlation between nitrogen content and colour degradation. In their report, the cause of colour degradation and sediment formation was attributed not to specific elements such as nitrogen or sulphur, but rather to the instability or ease of oxidation of certain compounds in general. The fact that some of those unstable compounds contain nitrogen is incidental.

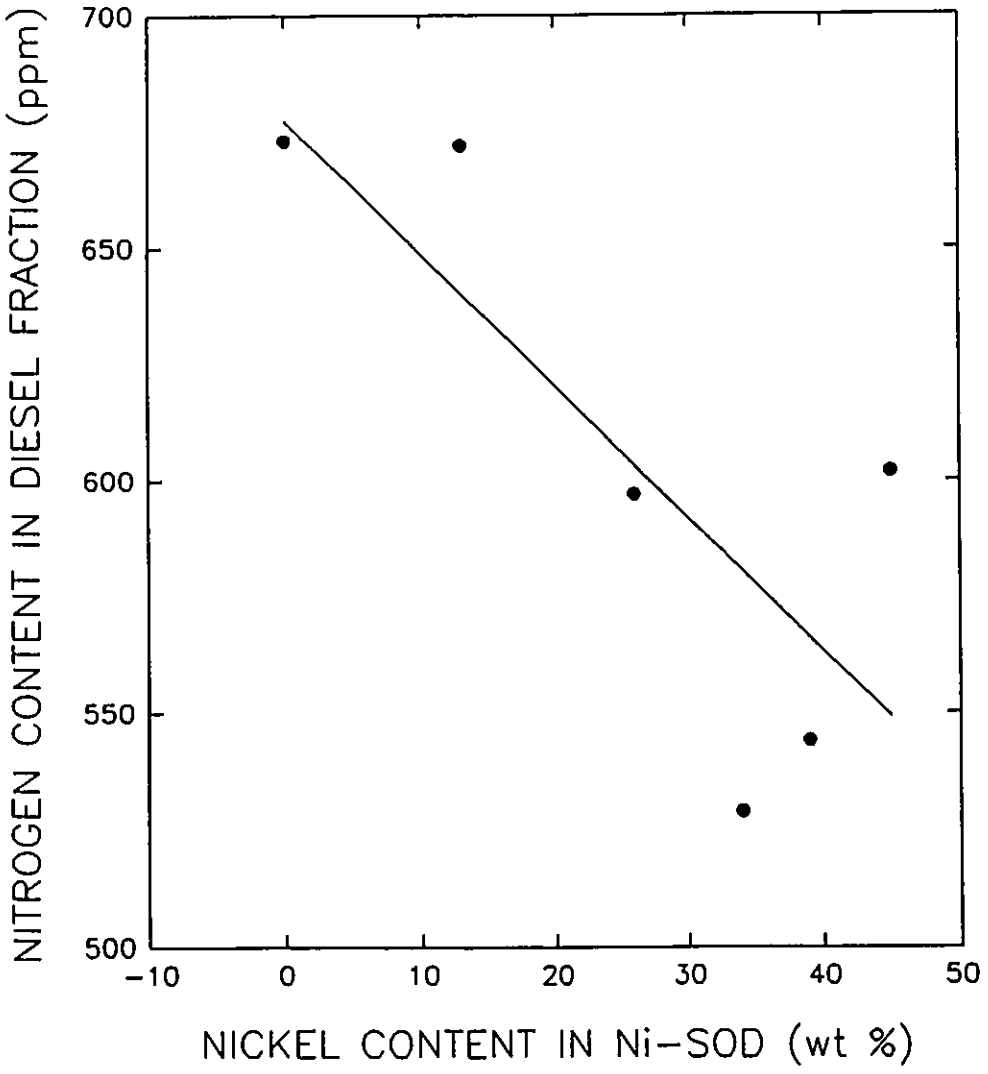

Figure 5.15 : **Nitrogen content (%) in the diesel fraction as a function of nickel content in the sodalite component of the Co-Mo catalyst (wt%).**

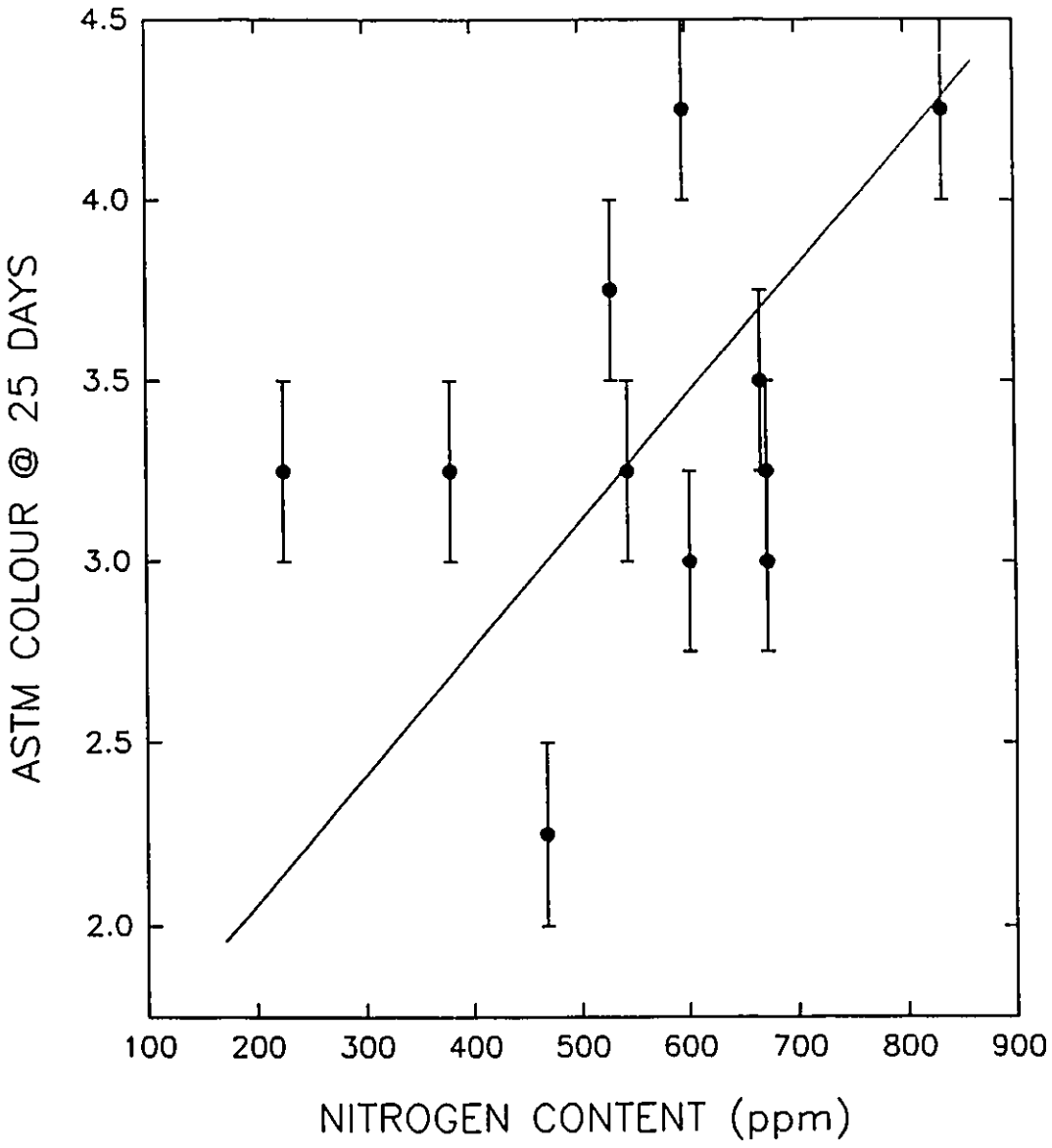

Figure 5.16 : **ASTM colour of diesel fraction after 25 days of storage as a function of its nitrogen content.**

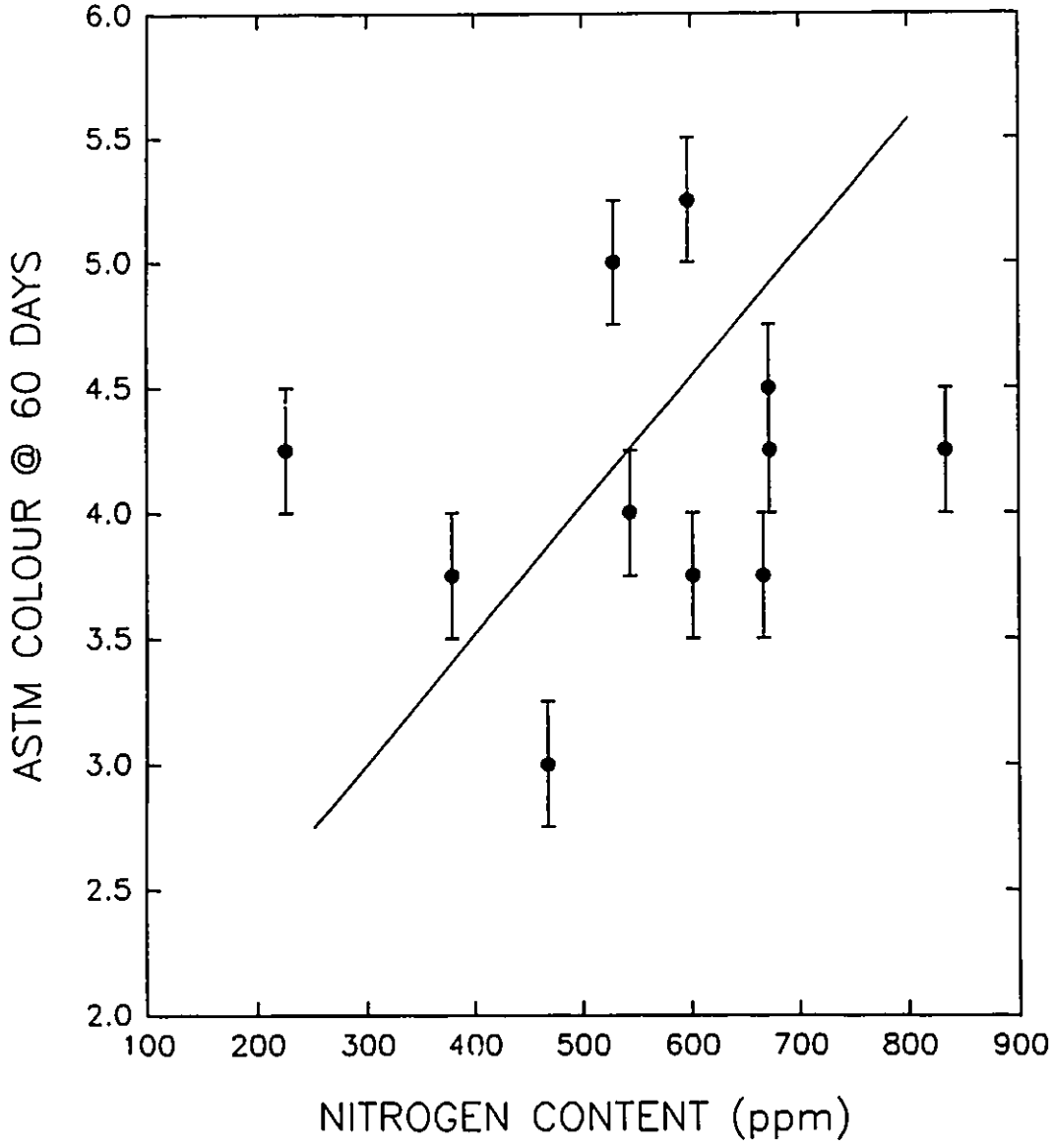

Figure 5.17 : **ASTM colour of diesel fraction after 60 days of storage as a function of its nitrogen content.**

5.2 HETEROATOM REMOVAL FROM THE TOTAL LIQUID PRODUCT

Based on the previous correlations, it would appear that there is a relationship between colour and heteroatom content, specifically the sulphur content of the diesel boiling point fraction. Therefore, the influence of the catalyst properties on heteroatom removal may provide some indirect understanding of colour change.

Heteroatoms can be removed from the diesel fraction by HDS, HDN, and HDM. However, they can also be added to it. Heteroatom addition occurs when a molecular fragment produced by cracking a large molecule has the correct boiling point to be in the diesel fraction. If the molecular fragment contains one or more heteroatoms, then heteroatom addition has occurred. The first part of the discussion will eliminate the complexity of combined addition and substraction by considering only heteroatom removal from the total reactor product liquid. Only heteroatom removal can occur when the total liquid product is considered. Heteroatom content of the boiling point fractions (diesel and +343°C) will be discussed in a later part of this chapter.

5.2.1 EFFECT OF SODALITE

Heteroatom conversions using two catalysts are compared at different times-on-stream (θ) and different space velocities in Figures 5.18 - 5.20. One catalyst

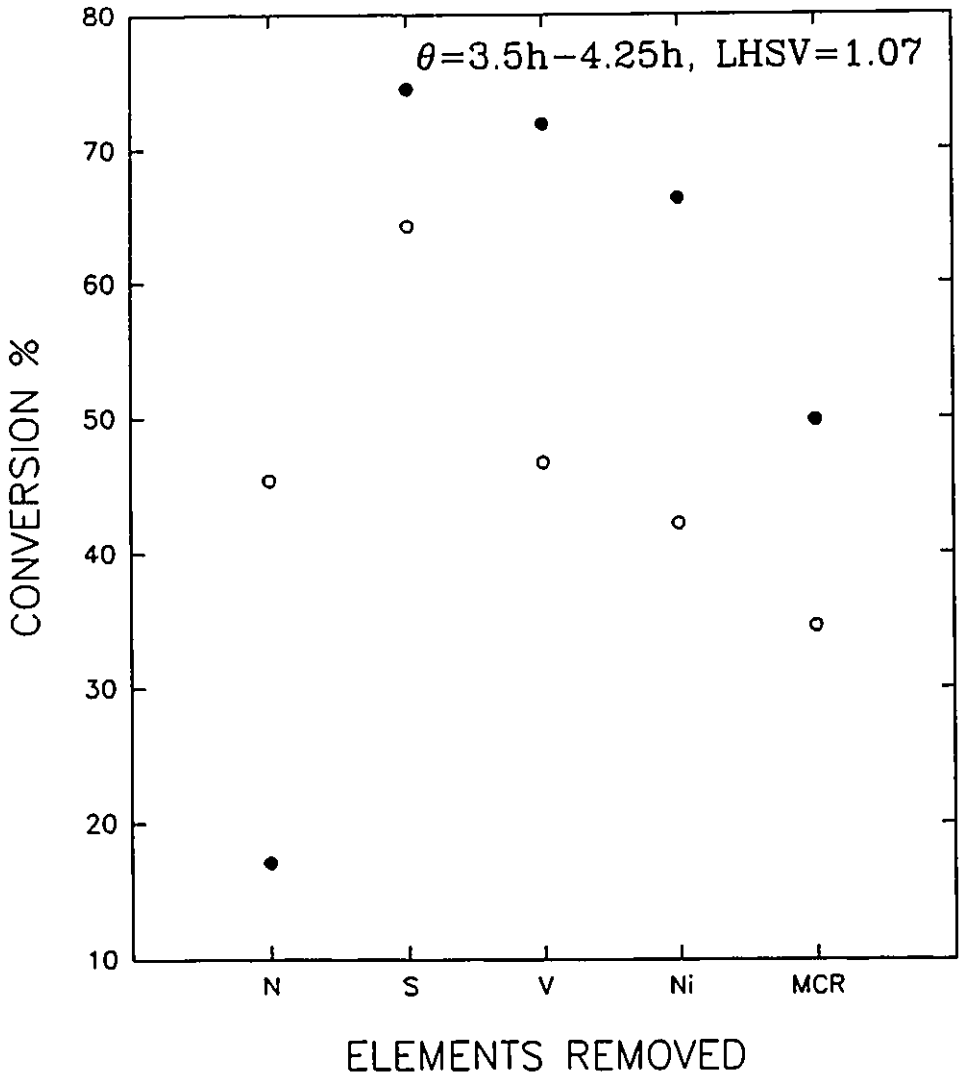

Figure 5.18 : **Heteroatom conversion comparison.** θ=3.5h-4.25h, LHSV=1.07
○ Co-Mo catalyst containing 0% Ni-SOD, ● Co-Mo catalyst containing 10% Ni-SOD.

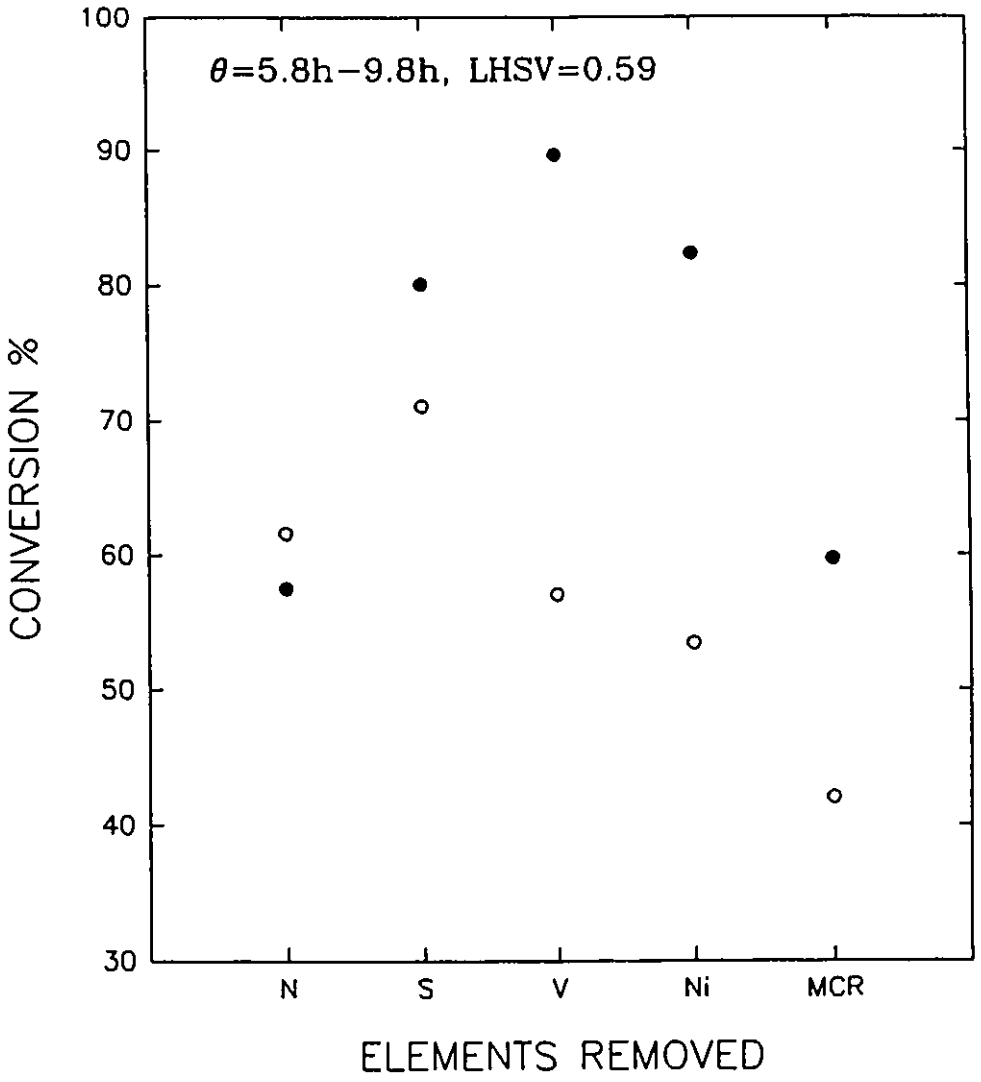

Figure 5.19 : **Heteroatom conversion comparison.** θ=5.8h-9.8h, LHSV=0.59 ○ Co-Mo catalyst containing 0% Ni-SOD, ● Co-Mo catalyst containing 10% Ni-SOD.

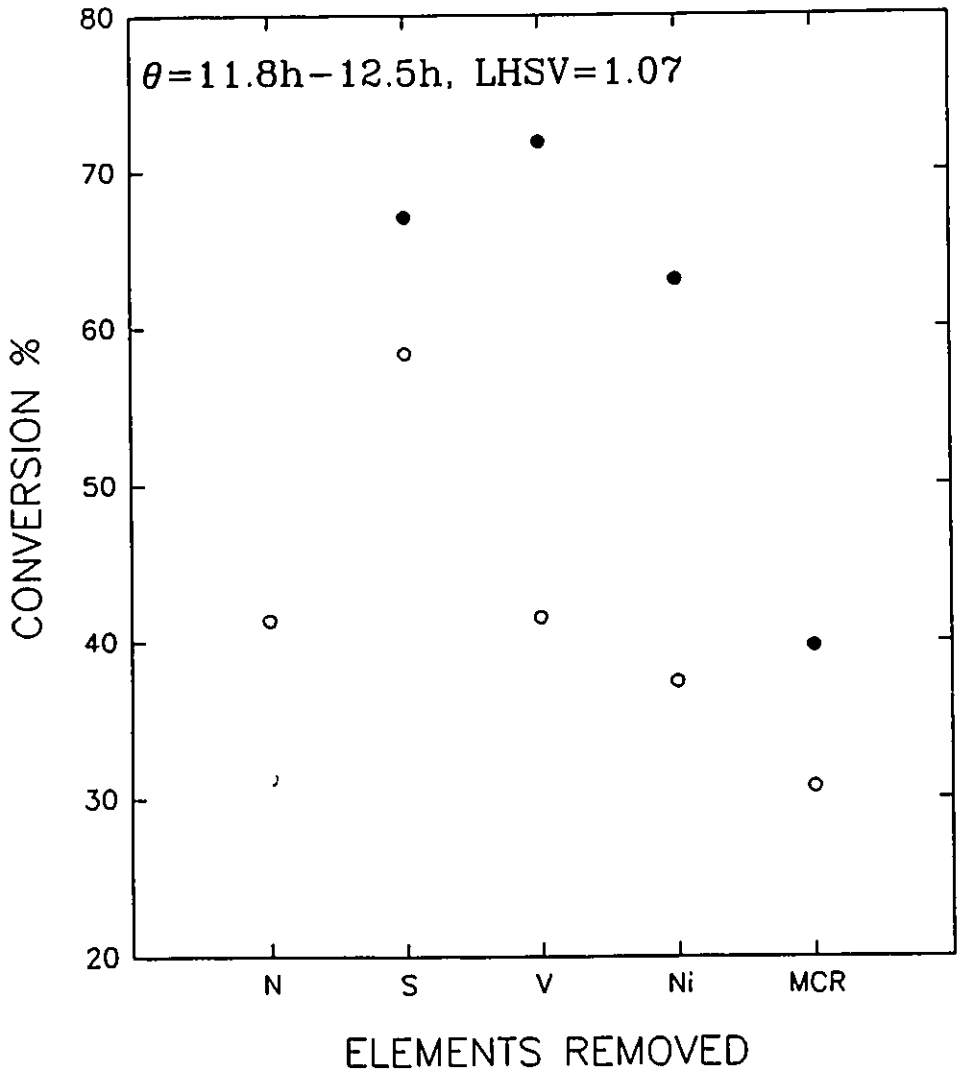

Figure 5.20 : **Heteroatom conversion comparison.** θ=11.8h-12.5h, LHSV=1.07 ○ Co-Mo catalyst containing 0% Ni-SOD, ● Co-Mo catalyst containing 10% Ni-SOD.

was a sulphided Co-Mo/Al_2O_3 catalyst and the other was identical except that it also contained 10 wt% sodalite. The sodalite did not contain any impregnated nickel. The conversion of N, S, V, Ni and MCR are shown. For this discussion, the MCR conversion will be considered along with heteroatom removal since MCR conversion requires hydrogenation to increase the hydrogen/carbon atomic ratio. The positive effect of sodalite observed here is similar to that reported for H-mordenite by Minja and Ternan (1991) and for HY zeolite by Minja (1990). With the exception of nitrogen, the conversion of each element improved with addition of sodalite. HDM displayed the most significant improvement in Figure 5.18 - 5.20. The influence of sodalite on catalyst deactivation can be examined by comparing the data in Figure 5.18, for θ = 3.5h - 4.25h, with that in Figure 5.20, for θ = 11.8h - 12.5h. It is noticeable that for some reactions, the catalyst with sodalite is more resistant to deactivation than the catalysts without sodalite. The HDM conversion for vanadium using the catalyst with sodalite remains unchanged between 4 and 12 h on stream for the same LHSV value. The deactivation of the sodalite catalyst for nickel conversion is half of the deactivation of the catalyst without sodalite. However, the improvement noted in the deactivation caused by the sodalite component in a Co-Mo/Al_2O_3 catalyst is within experimental error.

The first step for HDM, HDS and HDN is hydrogenation of the molecule followed by heteroatom removal via hydrogenolysis of the bond immediately adjacent to the heteroatom (Furimsky, 1983; Ware and Wei, 1985; Quann et al., 1988; Girgis and Gates, 1991). Hydrogenation involves the saturation of one or more multiple bonds with

hydrogen while hydrogenolysis involves the rupture of a bond between two atoms as each of those atoms will form a new bond with a different hydrogen atom. The fact that an increase in sodalite content improves HDM, HDS, and not HDN is consistent with bonding energies of the species involved. On the basis of bond strengths of diatomic molecules, nitrogen is attached more strongly to carbon (184 $\pm$1 kcal mol^{-1}) than it is to vanadium (114 $\pm$ 4.1 kcal mol^{-1}) or than sulphur is to carbon (170 $\pm$0.3 kcal mol^{-1}) making hydrogenolysis more difficult (Weast et al., 1989). This would to suggest that sodalite might enhance the removal of sulphur and metals but not the removal of nitrogen, on the basis of the nitrogen-carbon bond strength being stronger than the other bonds. This implies that if sodalite has no positive effect on HDN, nitrogen removal is only caused by the Co-Mo/Al_2O_3 portion of the catalyst. Because an increase in catalyst's sodalite content causes a decrease in the amount Co-Mo/Al_2O_3 portion of the catalyst, it would also cause a decrease in HDN activity.

5.2.2 EFFECT OF NICKEL IMPREGNATED SODALITE (NI-SOD) AS A CATALYST COMPONENT

The effect of the sodalite component in the Co-Mo/Al_2O_3 was studied further using a series of catalysts containing different amounts of sodalite that had been impregnated with 39 wt% nickel. The nickel was added in an attempt to improve activity of the catalyst.

5.2.2.1 Conversion

The conversions of nickel, vanadium, nitrogen, sulphur and microcarbon residue (MCR) as a function of the sodalite content in the catalyst are shown in Figures 5.21 to 5.25. That for the reference catalyst AC 1442B for a time-on-stream (θ) of 5.8h to 9.8h is represented on all figures as a filled square. The slower Liquid Hourly Space Velocity (LHSV) (17.3MPa, 415°C, 0.59 h^{-1}) caused the conversion at θ = 5.8h - 9.8h to improve over that of θ = 3.5h - 4.25h and θ = 11.8h - 12.5h. A longer residence time (lower LHSV) produces higher conversion. In all cases, conversions increased as the liquid space velocity LSV decreased from 1.07 h^{-1} to 0.59 h^{-1}. Hydrodemetallation (Figures 5.21 and 5.22) shows the sharpest increase of all heteroatoms as the amount of sodalite in the catalyst increases. The metal conversion reaches a maximum at a sodalite content of 10%. The same phenomena were observed for hydrodesulphurization (Figure 5.24) and MCR conversion (Figure 5.25). Nitrogen conversion (Figure 5.23), however, shows a constant decrease with increasing sodalite content. The shape of the curves is similar for each of the time-on-stream periods, which demonstrates the consistency of the results. The decrease in conversion from θ = 3.5h - 4.25h to θ = 11.8h - 12.5h for all heteroatoms and for MCR was attributed to the deactivation of the catalyst. Both experiments were conducted under the same conditions (17.3 MPa, 415°C, 1.07 h^{-1}) as described in chapter four.

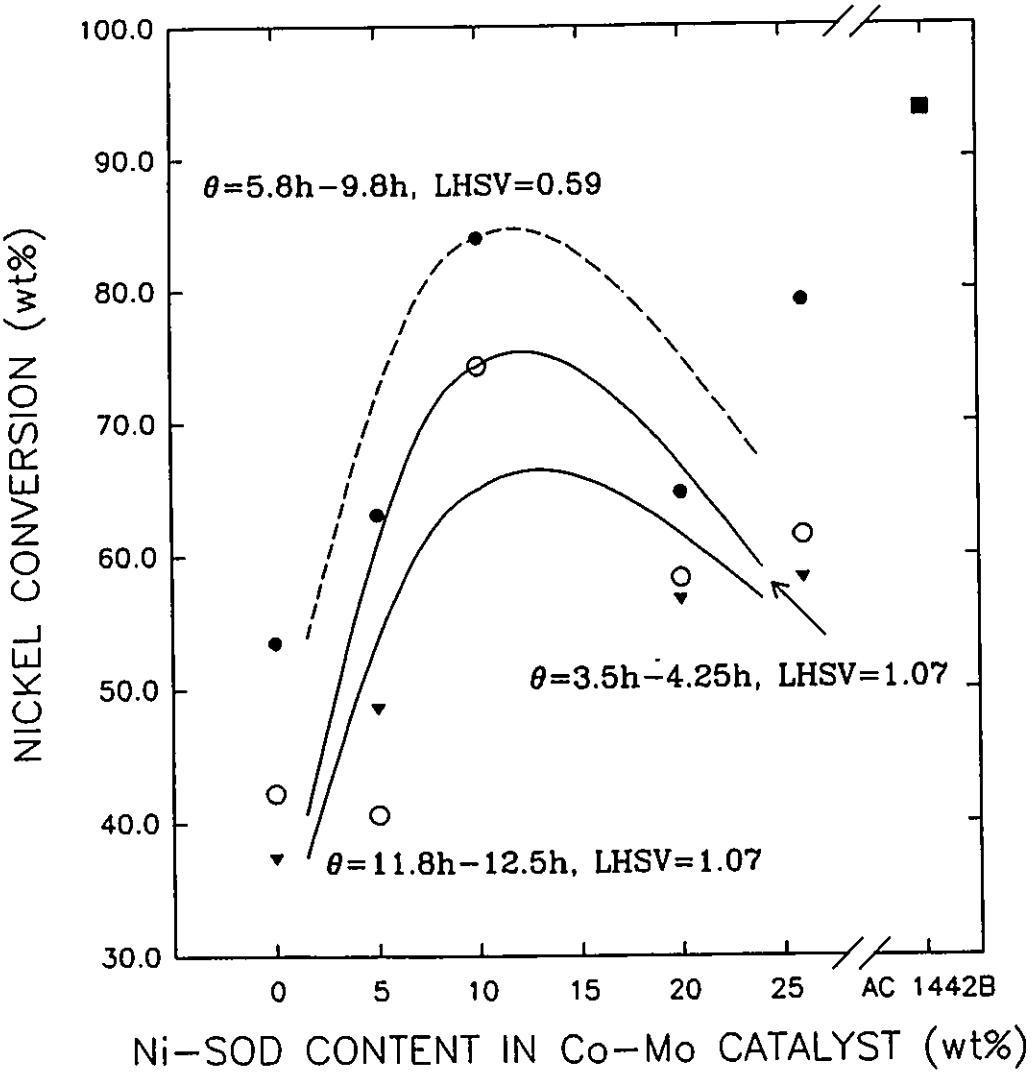

Figure 5.21 : **Nickel conversion (%) as a function of Ni-SOD content in the Co-Mo catalyst (wt%).**

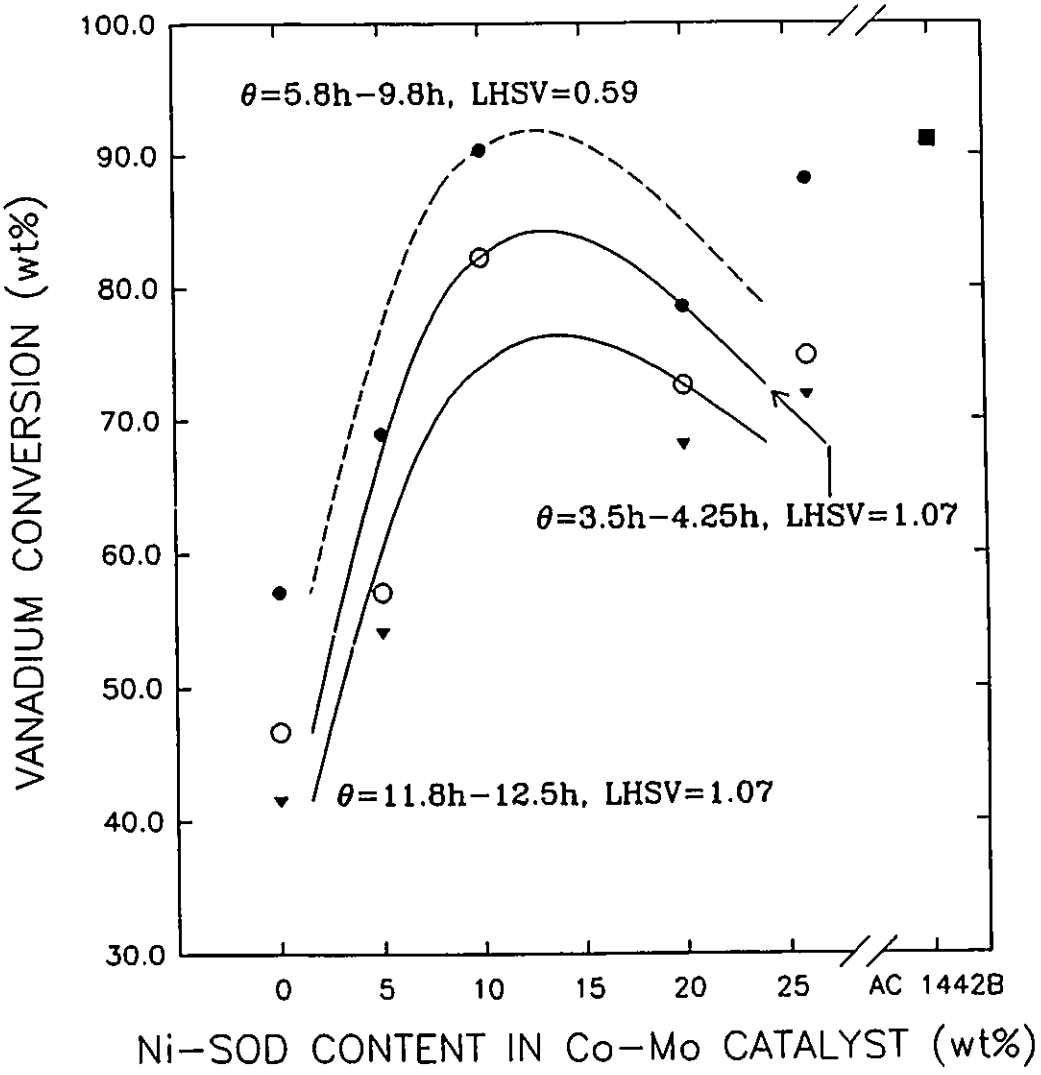

Figure 5.22 : **Vanadium conversion (%) as a function of Ni-SOD content in the Co-Mo catalyst (wt%).**

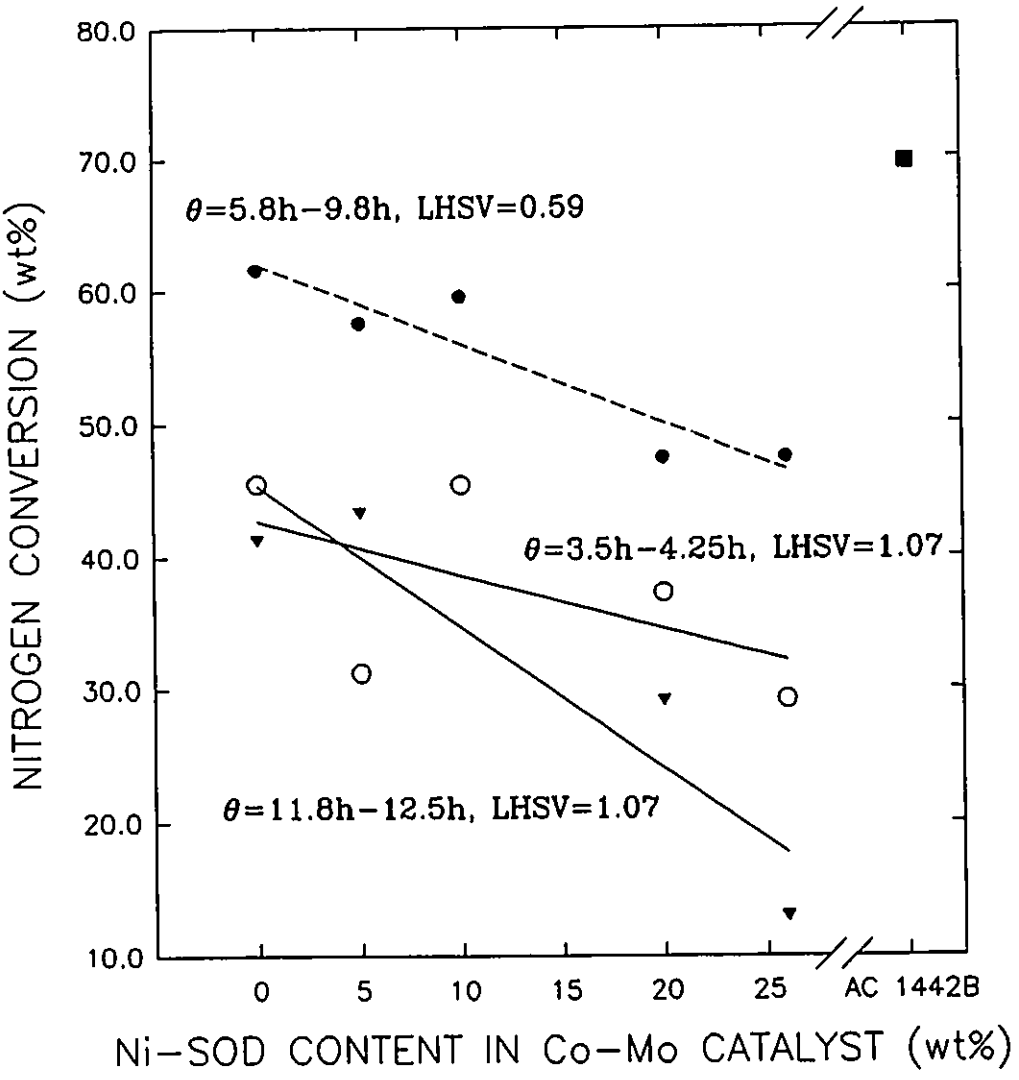

Figure 5.23 : **Nitrogen conversion (%) as a function of Ni-SOD content in the Co-Mo catalyst (wt%).**

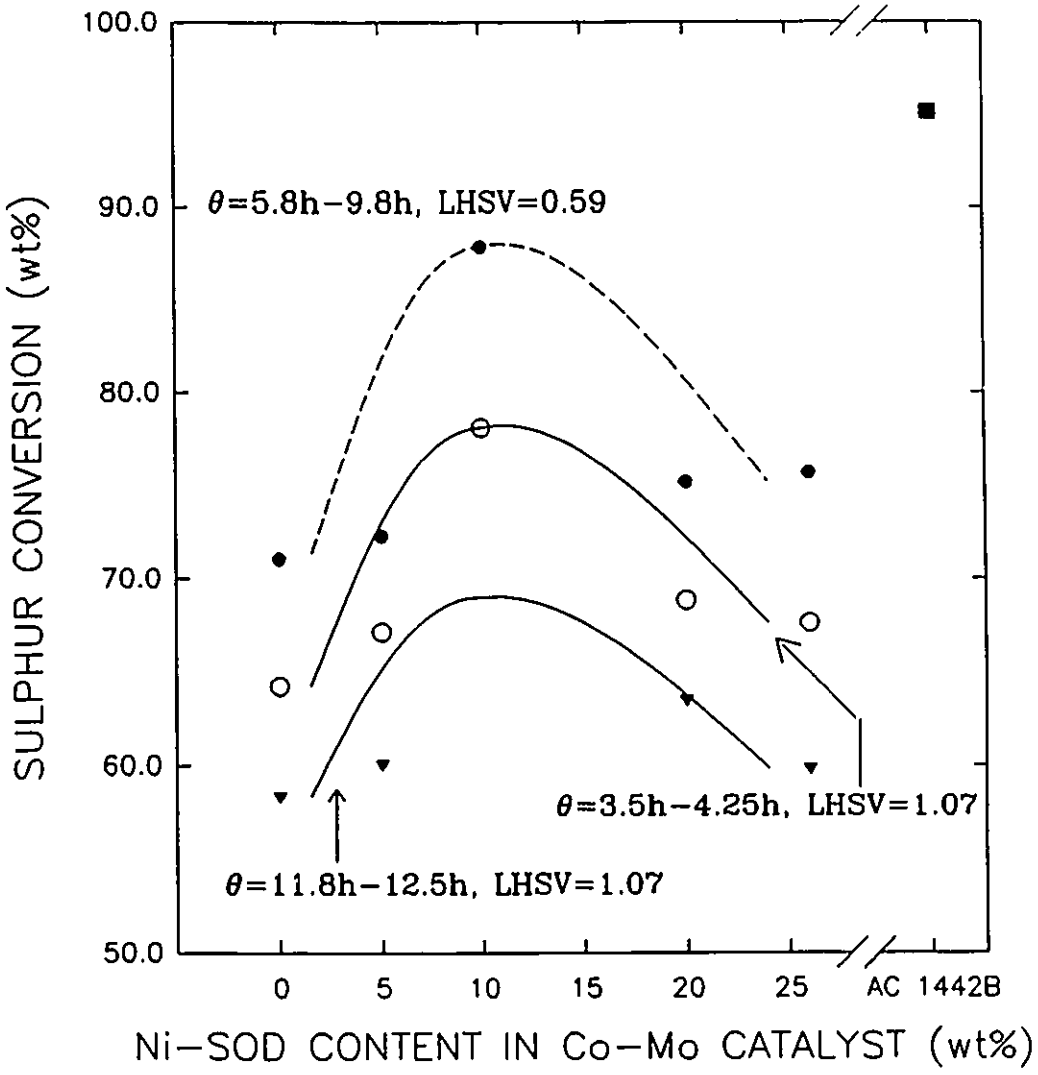

Figure 5.24 : **Sulphur conversion (%) as a function of Ni-SOD content in the Co-Mo catalyst (wt%).**

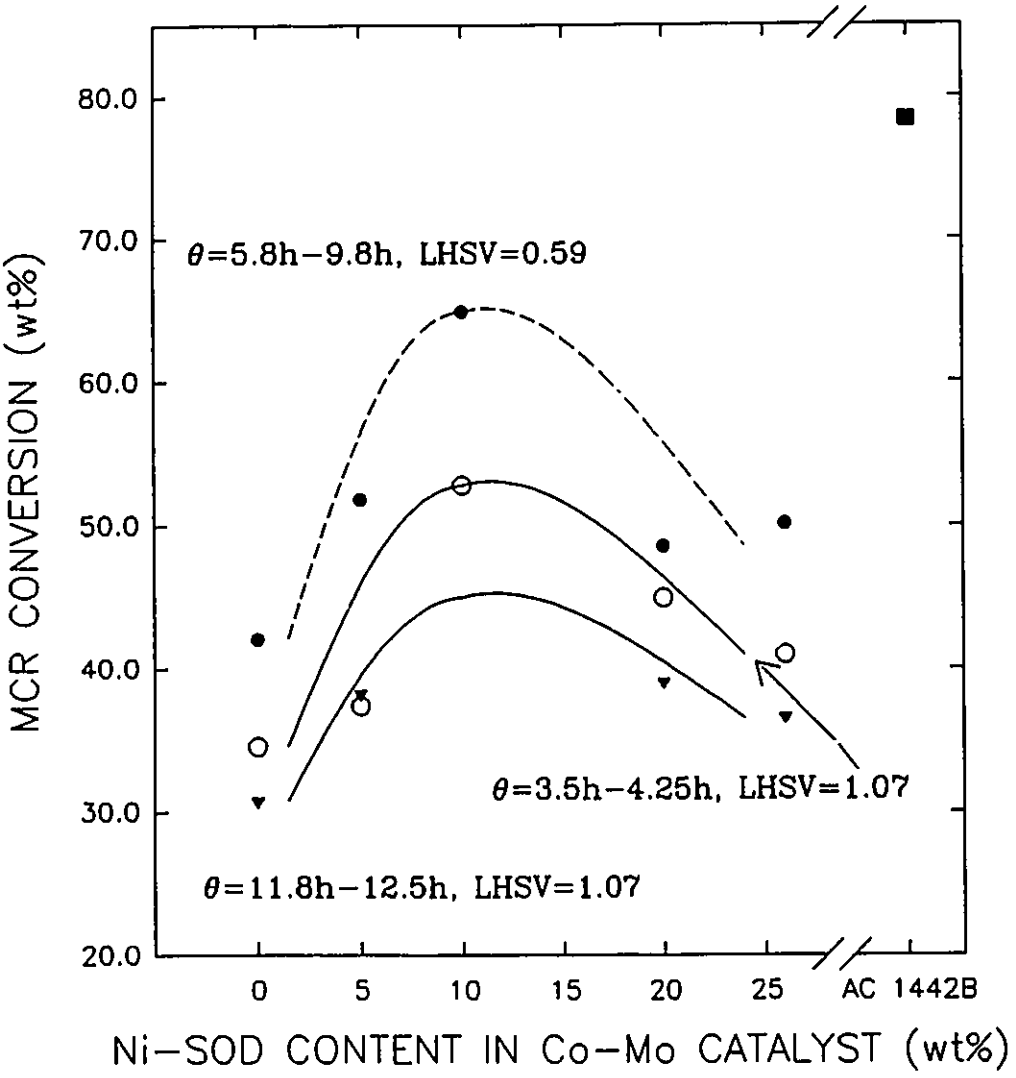

Figure 5.25 : **MCR conversion (%) as a function of Ni-SOD content in the Co-Mo catalyst (wt%).**

5.2.2.2 Area Turnover Frequency (ATOF)

There are different ways to compare catalysts. Conversion at the same processing conditions is a practical comparison because it indicates the amount of reaction that occurs in one unit of reactor volume. When the catalyst properties are different, different amounts of catalyst surface area can be loaded into the same unit of reactor volume. This is caused by different catalysts having different bulk densities (g/mL) and different specific surface areas (m^2/g). Since catalysis occurs on surfaces, it is often interesting to compare catalyst performance on the basis of unit surface area. It must be emphasized that unit surface area comparisons are of scientific interest only. Practical comparisons are based on reactors of the same size and not on catalysts of the same surface area. The area turnover frequency (ATOF) is probably the best quantity to compare heterogeneous catalysts on a unit surface area basis. For this work ATOF is represented by the number of heteroatoms removed in the reactor per unit time divided by the total catalyst surface area (atoms removed/nm^2.s). Sample calculations are given in Appendix A.

To calculate the total surface area in the reactor, both the catalyst bulk density and the catalyst specific surface area are required. The bulk density of the Co-Mo catalyst as a function of its sodalite content is shown in Figure 5.26. The catalyst specific surface area was given in Figure 3.7 in chapter 3. The total surface area of the Co-Mo catalyst as a function of sodalite content is shown in Figure 5.27. It shows that

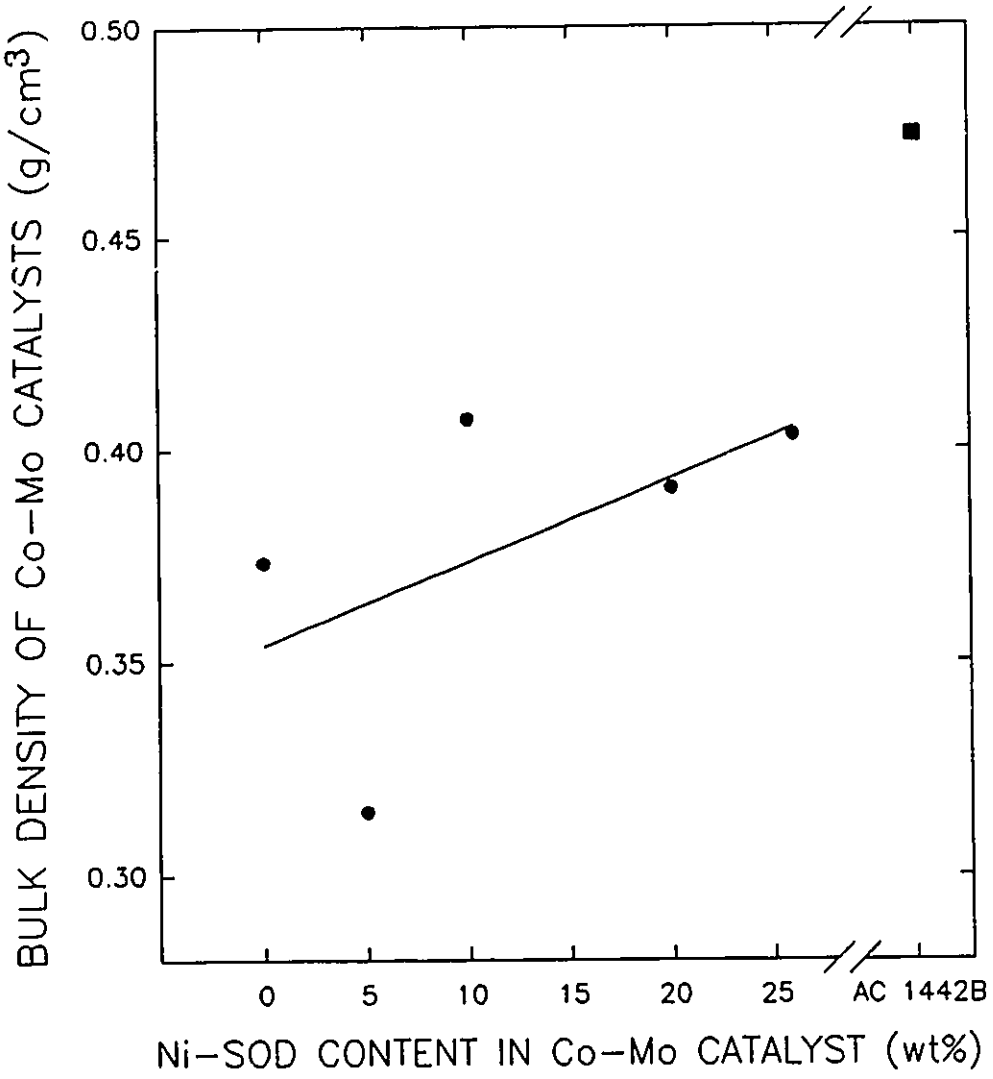

Figure 5.26 : **Bulk density of the Co-Mo catalsyt (g/cm^3) as a function of Ni-SOD content in the Co-Mo catalyst (wt%).**

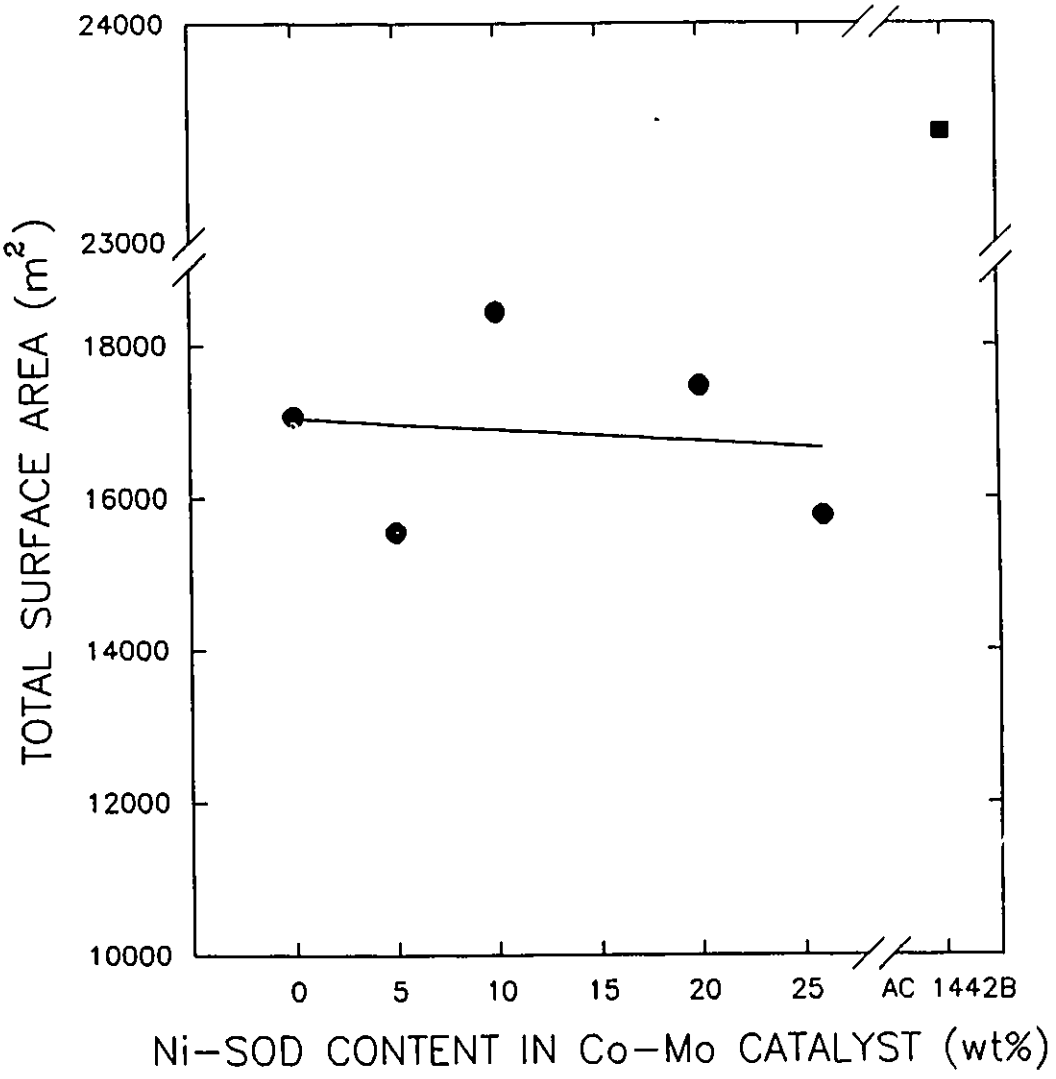

Figure 5.27 : **Total surface area (m^2) as a function of Ni-SOD content in the Co-Mo catalyst (wt%).**

the individual effects of bulk density and specific surface area tend to cancel one another.

The area turnover frequencies for the removal of nickel, vanadium, nitrogen and sulphur are shown as a function of sodalite content in Figures 5.28 to 5.31. ATOF for the reference catalyst AC 1442B is also shown. Normalisation of the conversion with regards to the total surface area improved data correlation. It is apparent that an increase of the sodalite component in the catalyst improved HDM (Figures 5.28 and 5.29) and HDS (Figure 5.31). These data suggest that the addition of up to 10 wt% sodalite improves catalyst activity. Finally, an increase in sodalite content in the catalyst clearly reduced HDN (Figure 5.30). These figures are consistent with the conversion results previously discussed.

Metals removed from heteroatoms containing vanadium and nickel were deposited on the catalyst surface as demonstrated in Figure 5.32. The shape of the curve is similar to that of metal ATOFs (Figures 5.28, 5.29) which confirms that metals deposit directly onto the catalyst surface during heteroatom removal. Since the number of active sites engendering HDM is dependant upon the surface area of the catalyst, the amount of metal deposited is directly proportional to the number of atoms removed/m^2s^{-1} (ATOF).

Because fewer heteroatoms are fed to each active site at lower LHSV, fewer heteroatoms are converted, causing the ATOF values to be lower than at the greater LHSV. A similar phenomena is responsible for the difference in vanadium and nickel

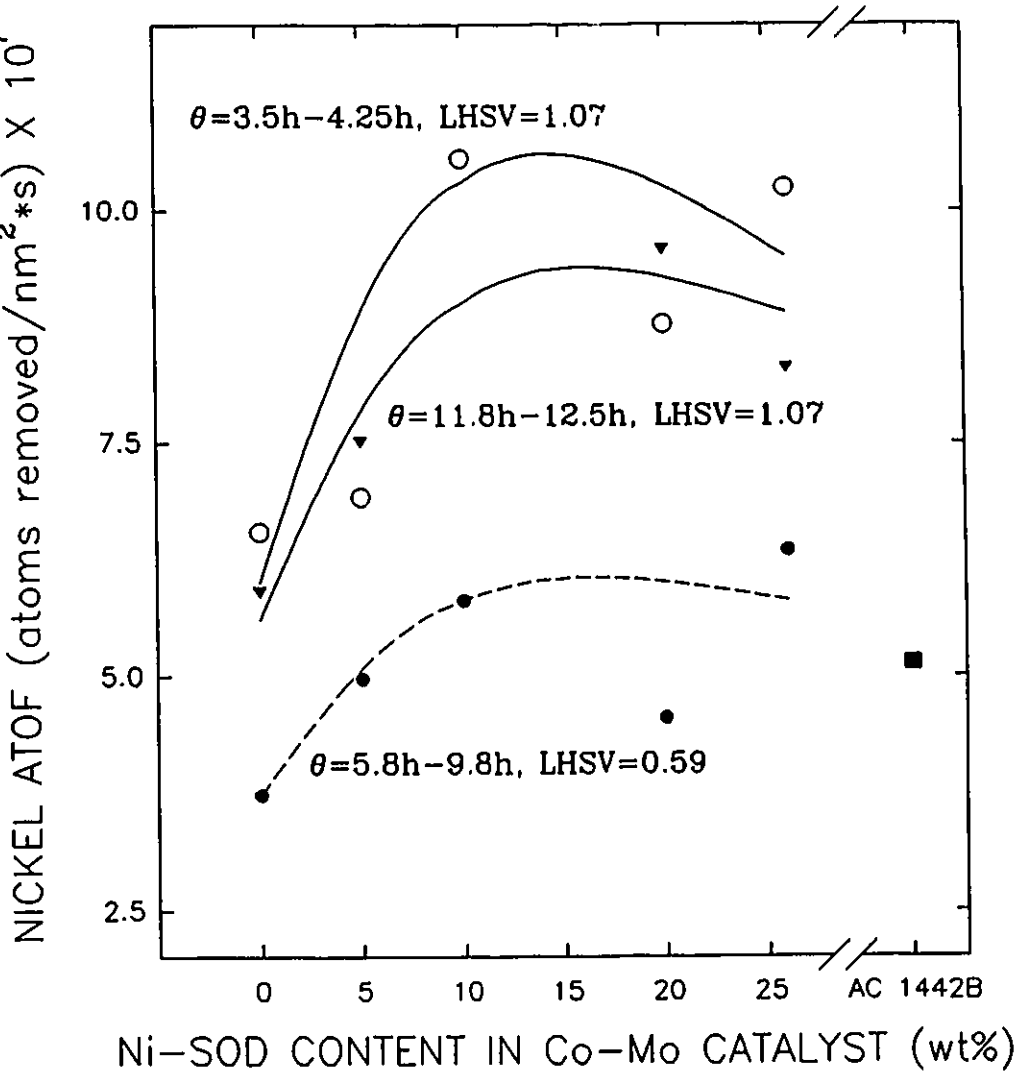

Figure 5.28 : **Nickel ATOF (atoms removed/nm^2. s) as a function of Ni-SOD content in the Co-Mo catalyst (wt%).**

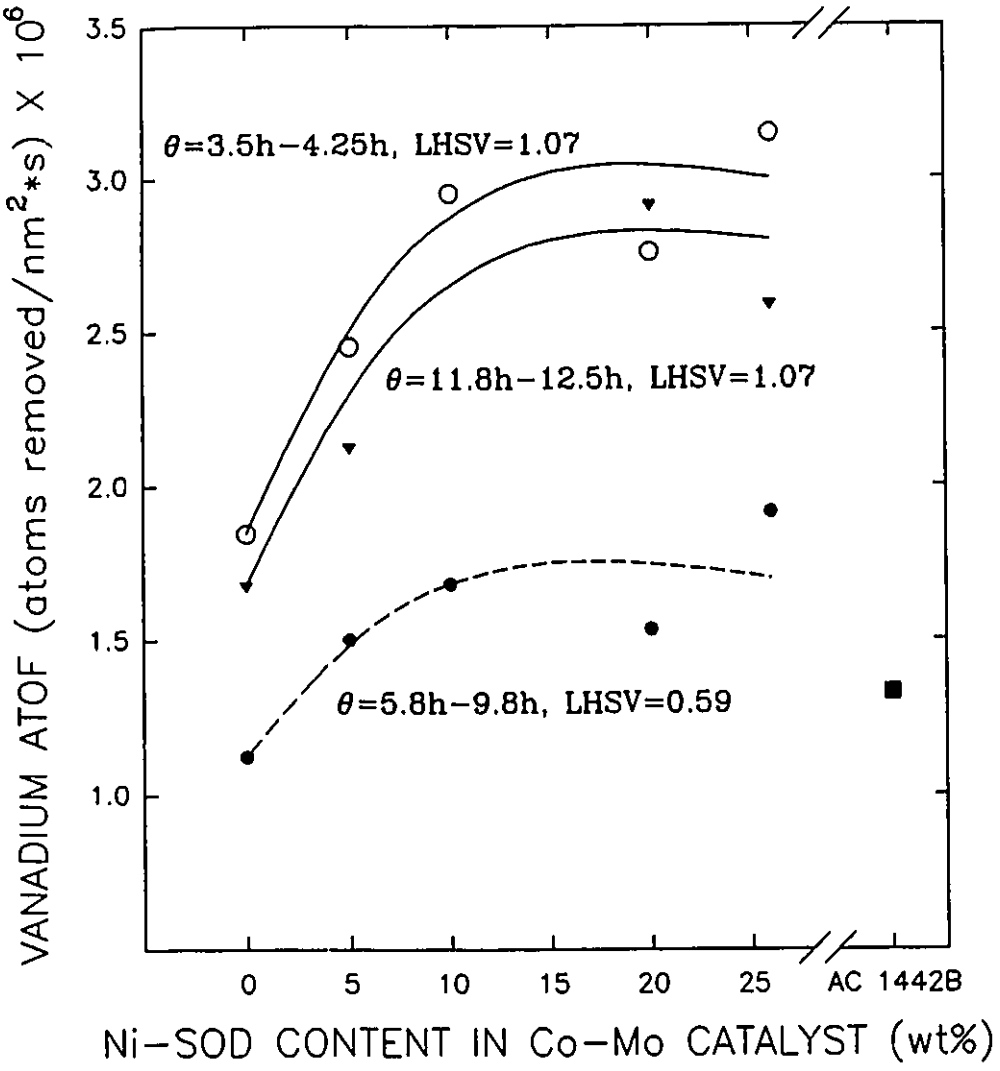

Figure 5.29 : **Vanadium ATOF (atoms removed/nm^2. s) as a function of Ni-SOD content in the Co-Mo catalyst (wt%).**

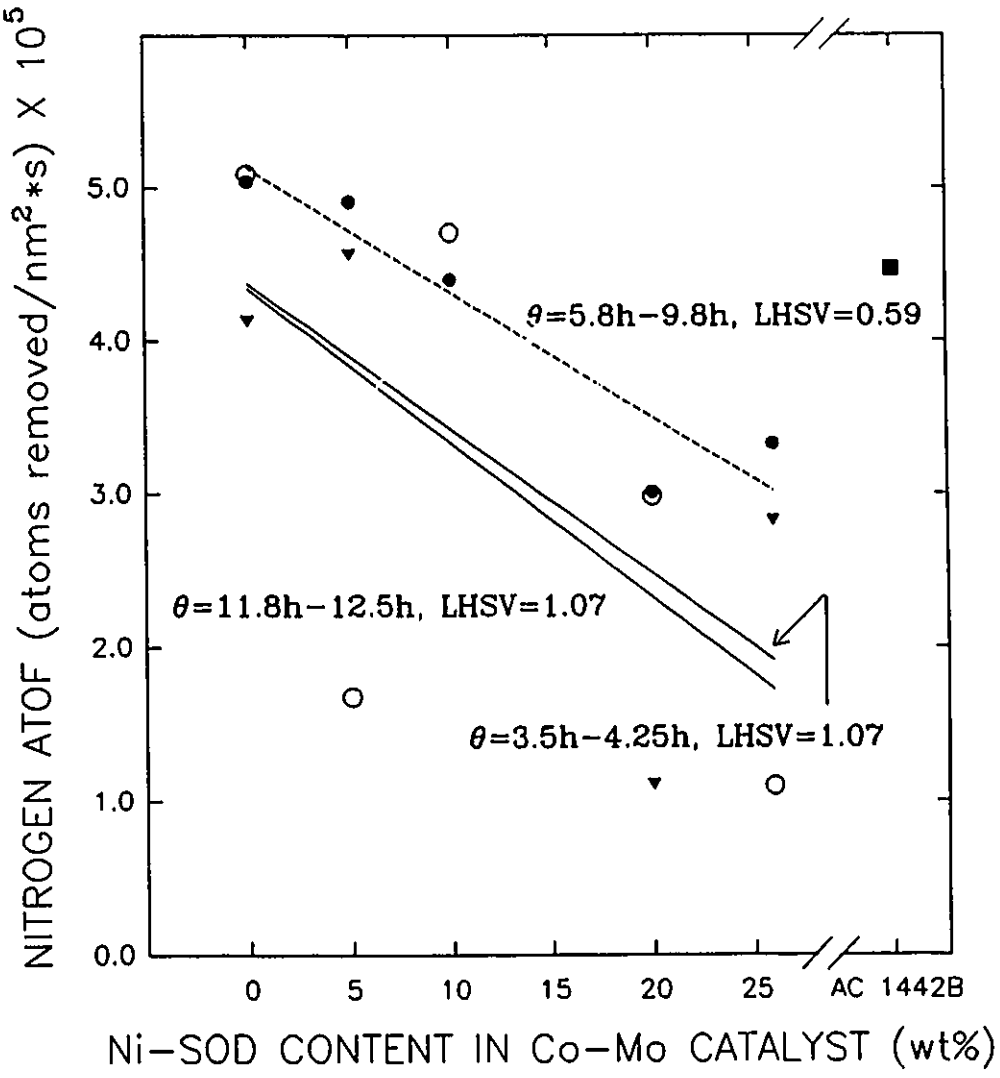

Figure 5.30 : **Nitrogen ATOF (atoms removed/nm². s) as a function of Ni-SOD content in the Co-Mo catalyst (wt%).**

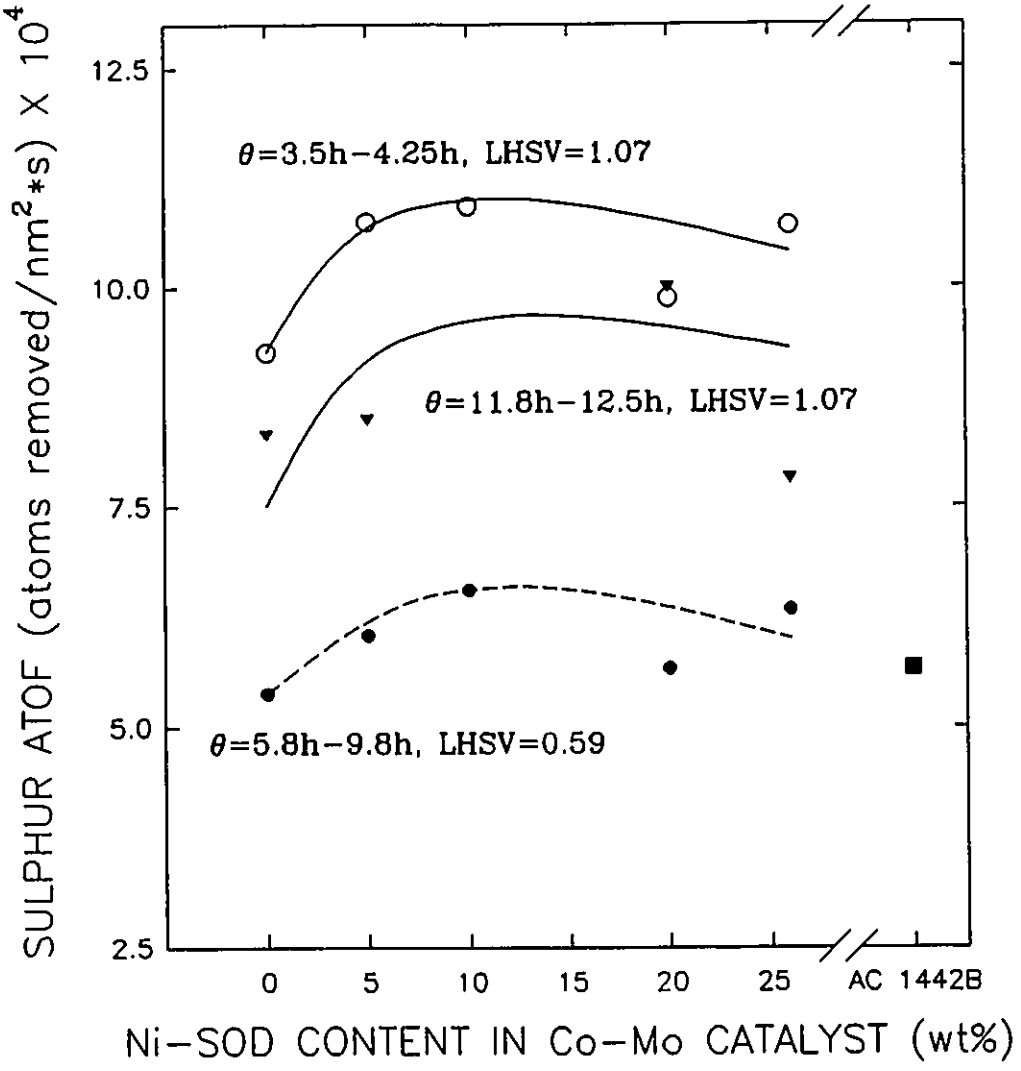

Figure 5.31 : **Sulphur ATOF (atoms removed/nm^2. s) as a function of Ni-SOD content in the Co-Mo catalyst (wt%).**

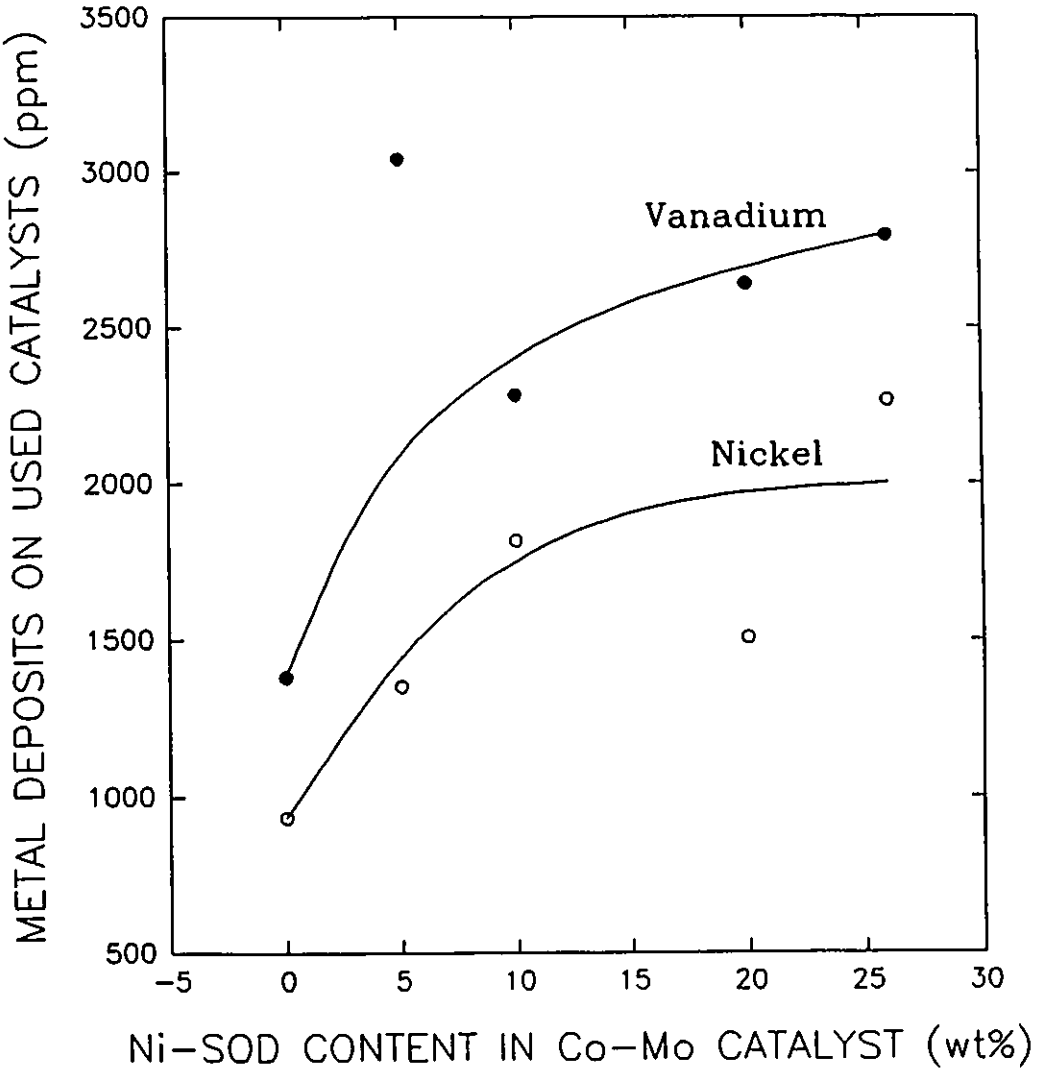

Figure 5.32 : **Metal deposits on used catalysts (ppm) as a function of Ni-SOD content in the Co-Mo catalyst (wt%).**

ATOF values. The concentration of vanadium in the feed is higher than that of nickel, causing the availability of atoms to be converted to be less, thereby the lower nickel ATOF values.

Comparisons of the reference catalyst with the laboratory prepared catalysts are different using ATOF than using conversion. The conversion by the AC 1442B catalyst, at equal LHSV and on the basis of one reactor volume was consistently better than for the laboratory prepared catalysts (Figures 5.21 - 5.25). However, some of the prepared catalysts were more active, than the reference catalyst on the ATOF basis (Figures 5.28 -5.31). This phenomena was attributed in part to the higher surface area of the reference catalyst (Figure 3.5, chapter 3). Also, the reference catalyst extrudates had shorter lengths compared to those of the prepared catalysts and could be compacted more closely in the reactor volume for greater bulk density (Figure 5.26). These two factors resulted in a much higher total available surface area in the reactor for the reference catalyst (Figure 5.27) yielding more active sites than for the laboratory prepared catalysts.

These results are consistent with those of Minja and Ternan (1991) who reported an increase of HDM, HDS and MCR conversion with an increase in H-mordenite component in the catalyst. Minja also found the same effect when the HY component of the catalyst was increased (Minja, 1990). However, they reported an increase in HDN as well, which is contrary to the effect of sodalite on HDN which was found in this study. The improvements in catalyst activity were attributed to greater catalyst acidity

brought about by the presence of the zeolite component. The acidity of the sodalite was compared with those of the HY zeolite and the H-mordenite using temperature programmed desorption of ammonia (TGA) discussed in chapter 3. The sodalite was found to be less acidic than either HY or H-modernite which could explain the different effect of sodalite on HDN. A more acidic catalyst would be more active, thereby more capable of breaking the strong nitrogen-carbon bonds. It is possible that the sodalite may not be sufficiently acidic to break the bonds.

5.2.3 THE EFFECT OF NICKEL CONCENTRATION IN A NI-SOD CATALYST COMPONENT

A second series of sulphided Co-Mo/Al_2O_3 catalysts was used to distinguish between the conversion caused by impregnated nickel and that caused by sodalite. As described in chapter four, catalysts containing a fixed amount of sodalite impregnated with various amounts of nickel were prepared.

5.2.3.1 Conversion

For all heteroatoms, the conversions in Figures 5.33 to 5.37 at the lower LHSV (θ = 5.8h - 9.8h) were greater than those at the higher LHSV, which is consistent with the previous results in Figures 5.21 - 5.25. Metal conversion as a function of nickel content in the sodalite component of the Co-Mo/Al_2O_3 catalyst is shown in Figures 5.33

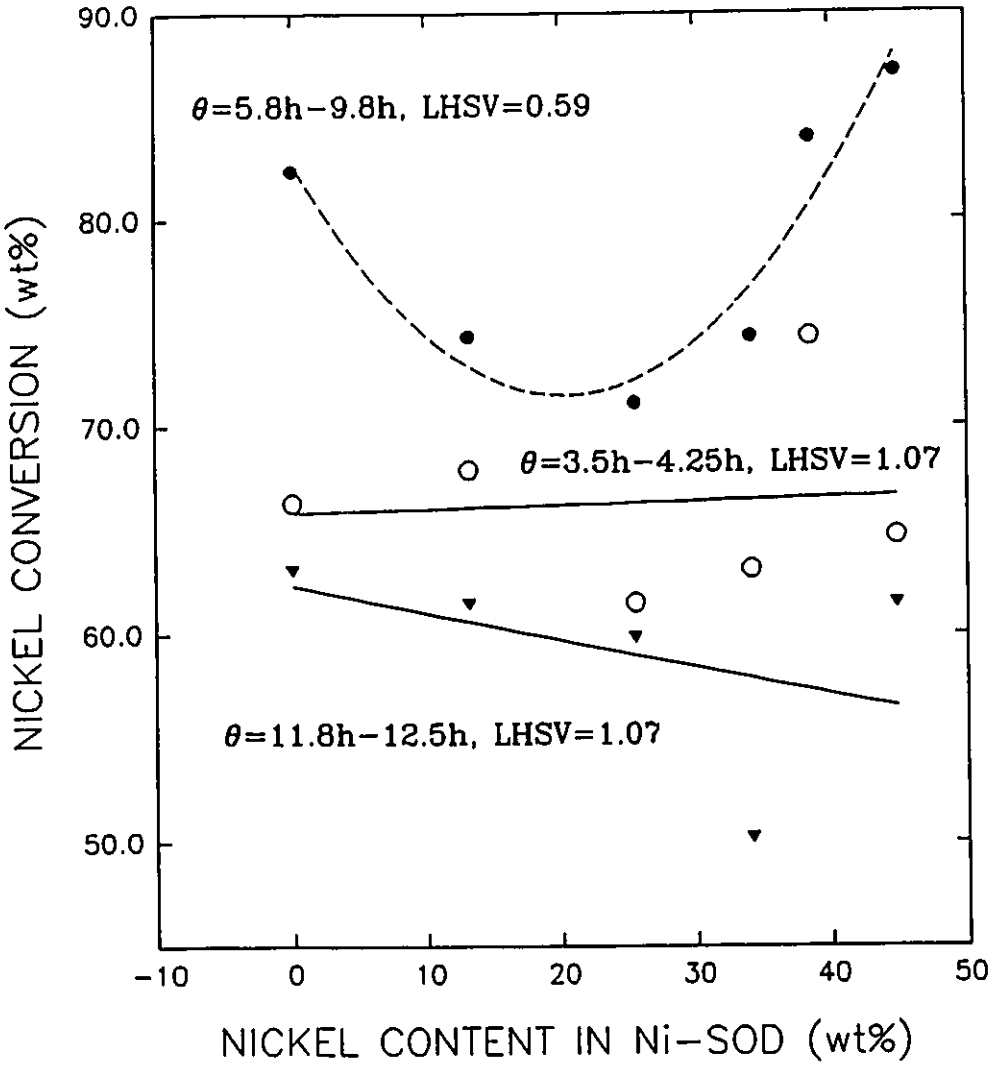

Figure 5.33 : **Nickel conversion (%) as a function of impregnated nickel content in the sodalite component of the Co-Mo catalyst (wt%).**

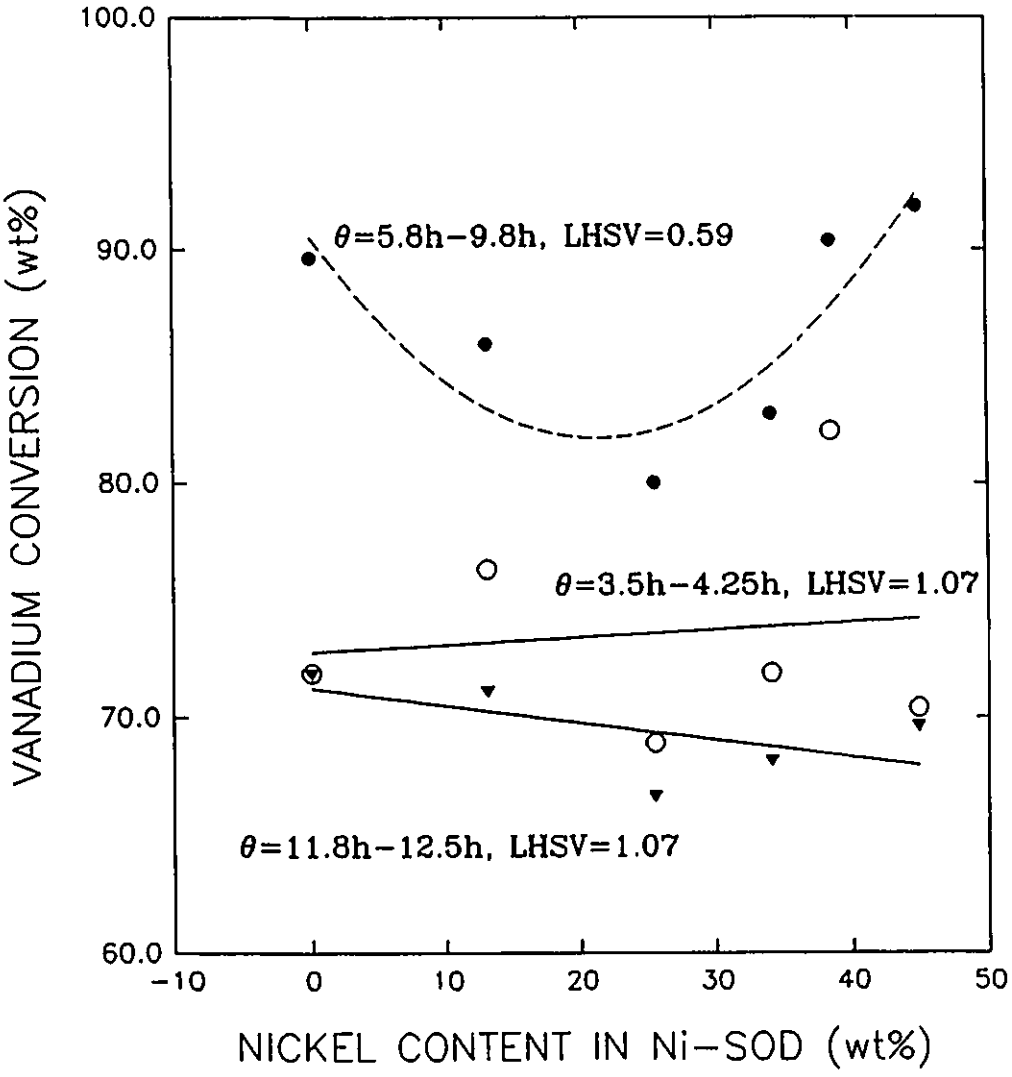

Figure 5.34 : **Vanadium conversion (%) as a function of impregnated nickel content in the sodalite component of the Co-Mo catalyst (wt%).**

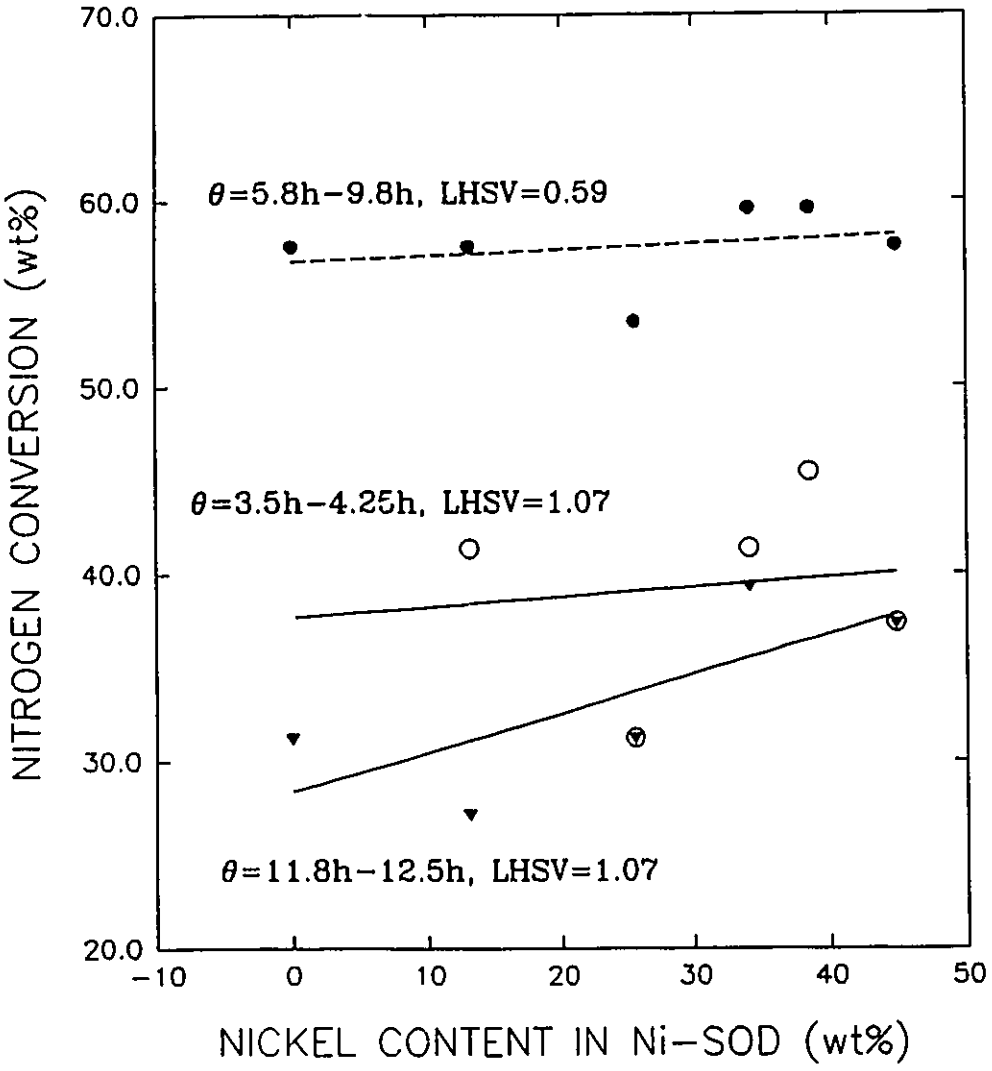

Figure 5.35 : **Nitrogen conversion (%) as a function of impregnated nickel content in the sodalite component of the Co-Mo catalyst (wt%).**

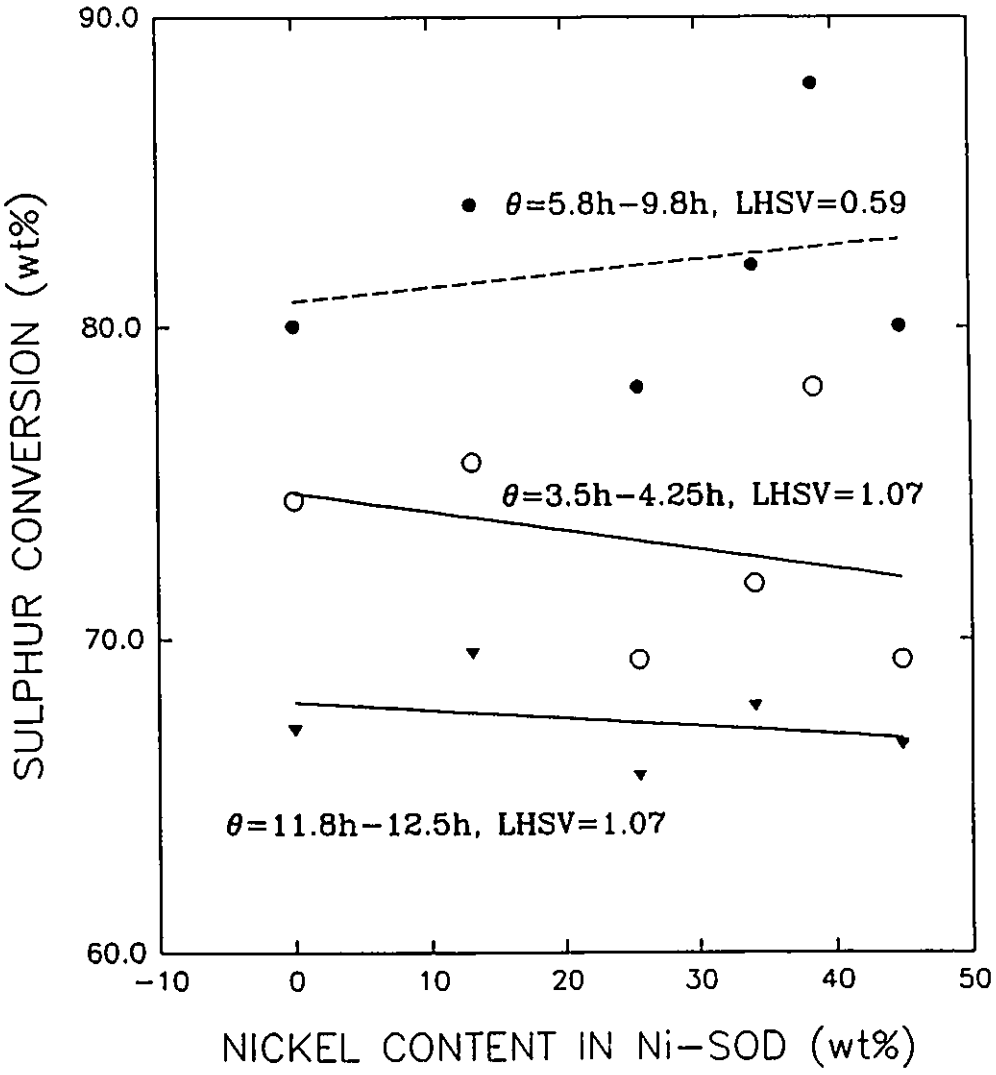

Figure 5.36 : **Sulphur conversion (%) as a function of impregnated nickel content in the sodalite component of the Co-Mo catalyst (wt%).**

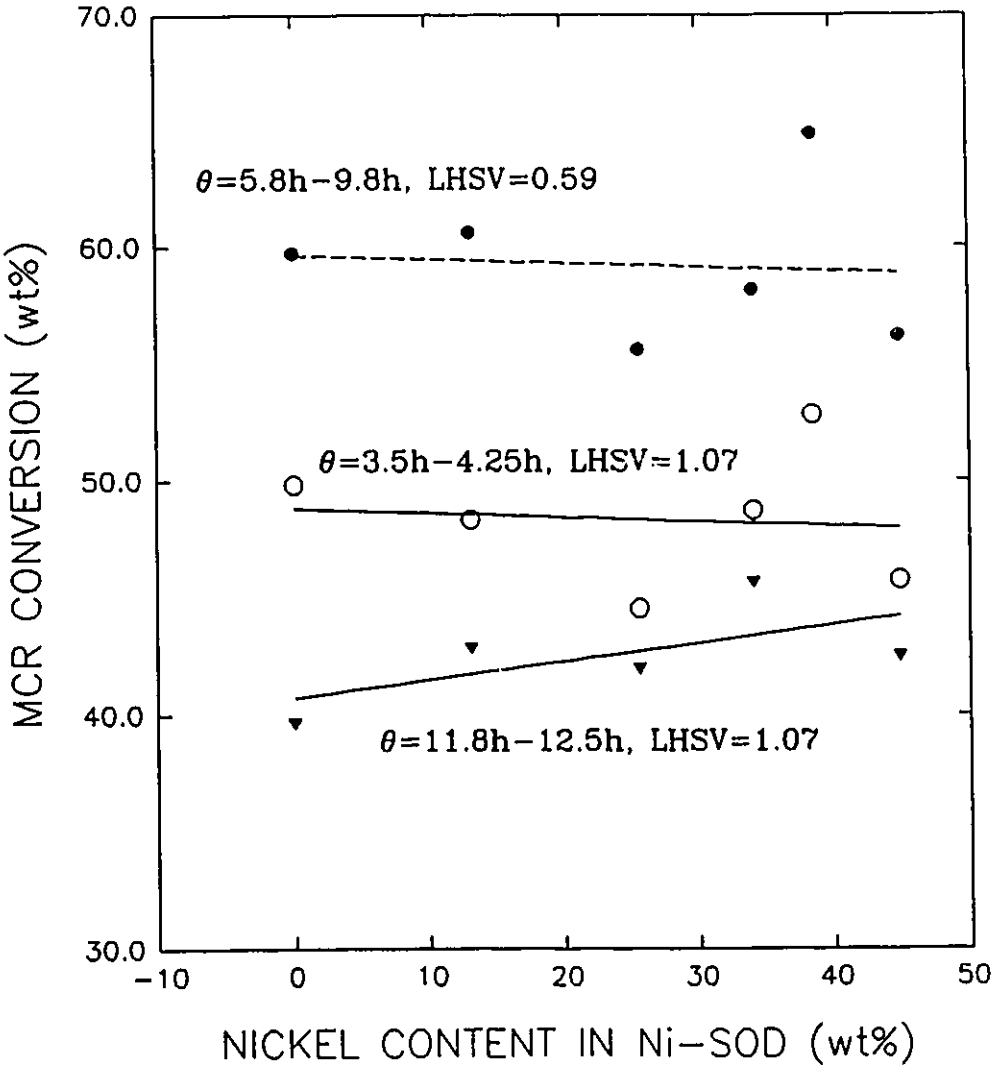

Figure 5.37 : **MCR conversion (%) as a function of impregnated nickel content in the sodalite component of the Co-Mo catalyst (wt%).**

and 5.34. Sodalite nickel content has very minimal effect on metal conversion at the higher LHSV. At lower LHSV, metal conversion went through a minimum at 26% nickel content in the sodalite. For nitrogen, sulphur and MCR conversions (Figures 5.35 - 5.37), the effect of nickel is negligible. The difference in conversion between θ = 3.5h - 4.25h and θ = 11.8h- 12.5h indicates that catalyst deactivation occurred. The change in nickel content of the sodalite had no influence on the degree of deactivation.

5.2.3.2 Area Turnover Frequency (ATOF)

As discussed previously, the calculation of ATOF requires the catalyst bulk density (g/mL) and the catalyst specific surface area (m^2/g) to determine the total catalyst surface area in the reactor. The plot of the catalyst bulk density as a function of nickel content in sodalite in Figure 5.38 indicates that the sporadic conversion data discussed above could be attributed to the difference in reactor loading rather than to the presence of the nickel in the sodalite. The multiplication of the relatively constant specific surface area of each catalyst (Figure 3.6, chapter 3) by the scattered reactor loading values results in a relatively scattered total surface area plot (Figure 5.39).

The Area Turnover Frequencies (ATOF) plots for nickel, vanadium, nitrogen and sulphur are shown as a function of nickel content in sodalite in Figures 5.40 - 5.43 respectively. The minimum metal conversion at a sodalite nickel content of 26% for LHSV = 0.59 was not apparent when ATOF was used to represent the reaction data.

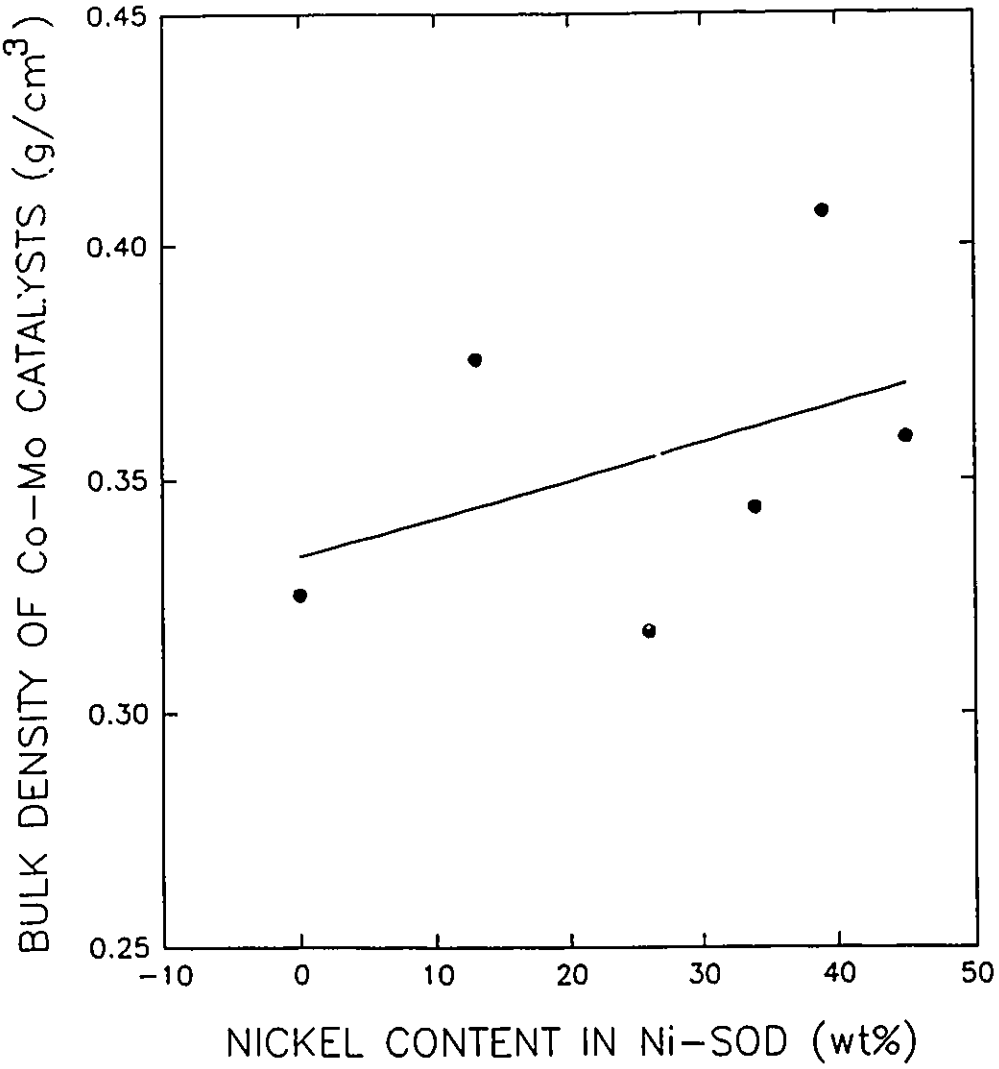

Figure 5.38 : **Bulk density of Co-Mo catalysts (g/cm^3) as a function of impregnated nickel content in the sodalite component of the Co-Mo catalyst (wt%).**

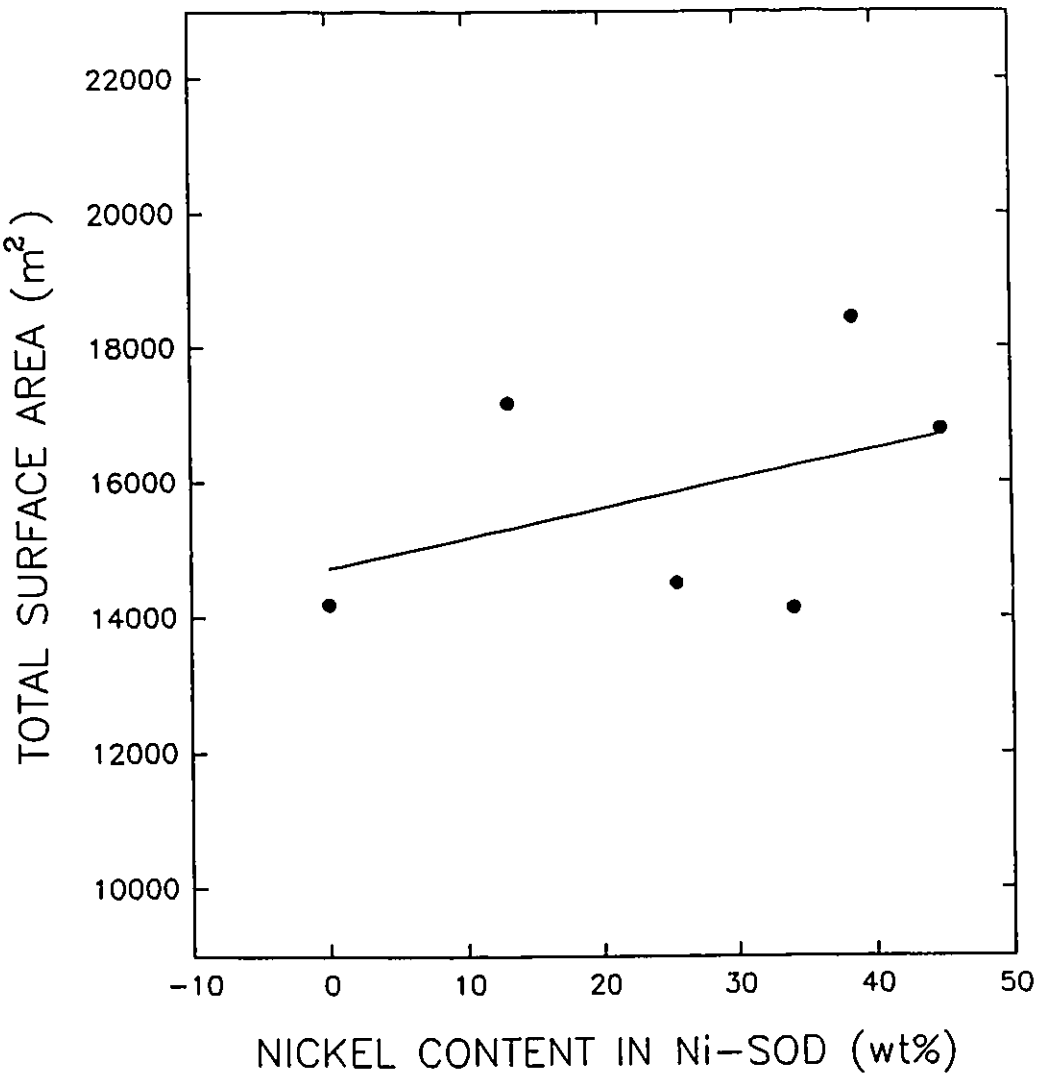

Figure 5.39 : **Total surface area (m^2) as a function of impregnated nickel content in the sodalite component of the Co-Mo catalyst (wt%).**

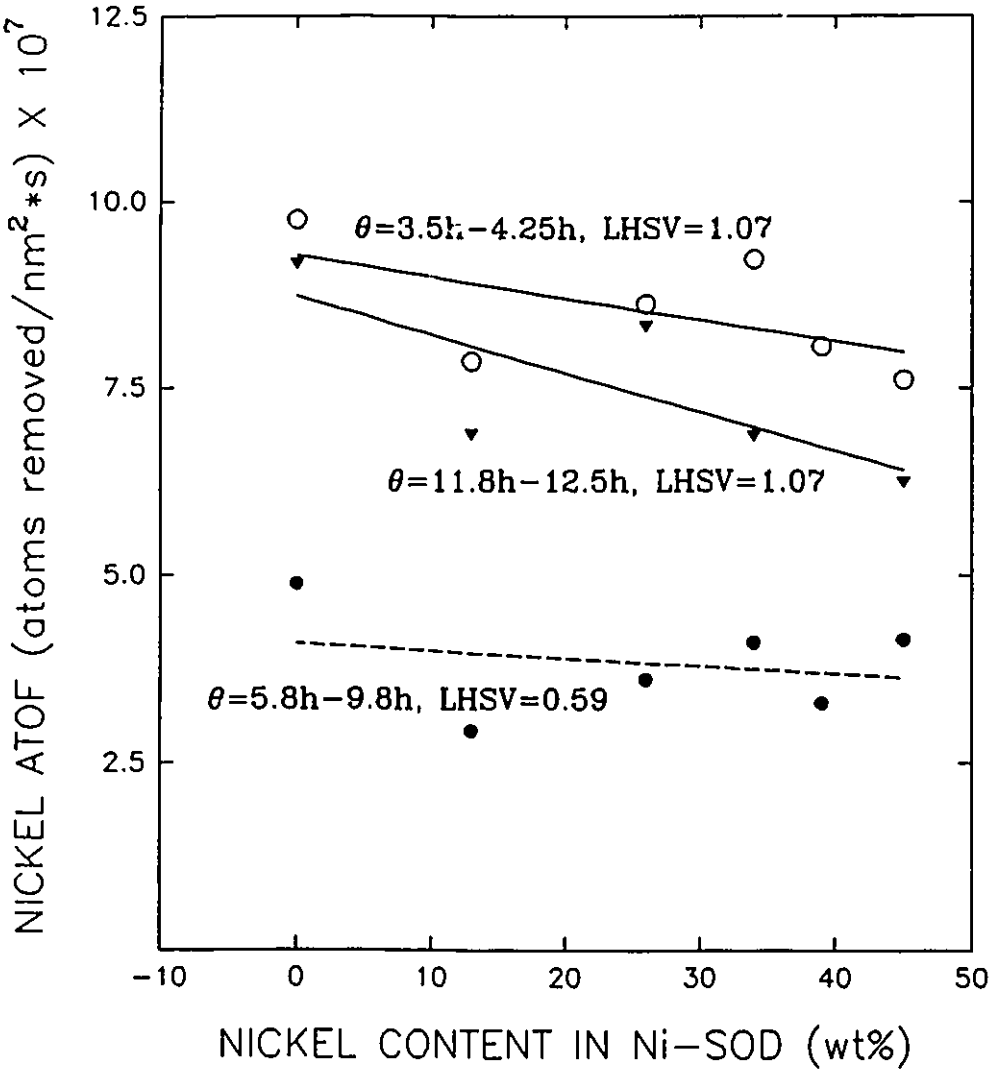

Figure 5.40 : **Nickel ATOF (atom removed/nm². s) as a function of impregnated nickel content in the sodalite component of the Co-Mo catalyst (wt%).**

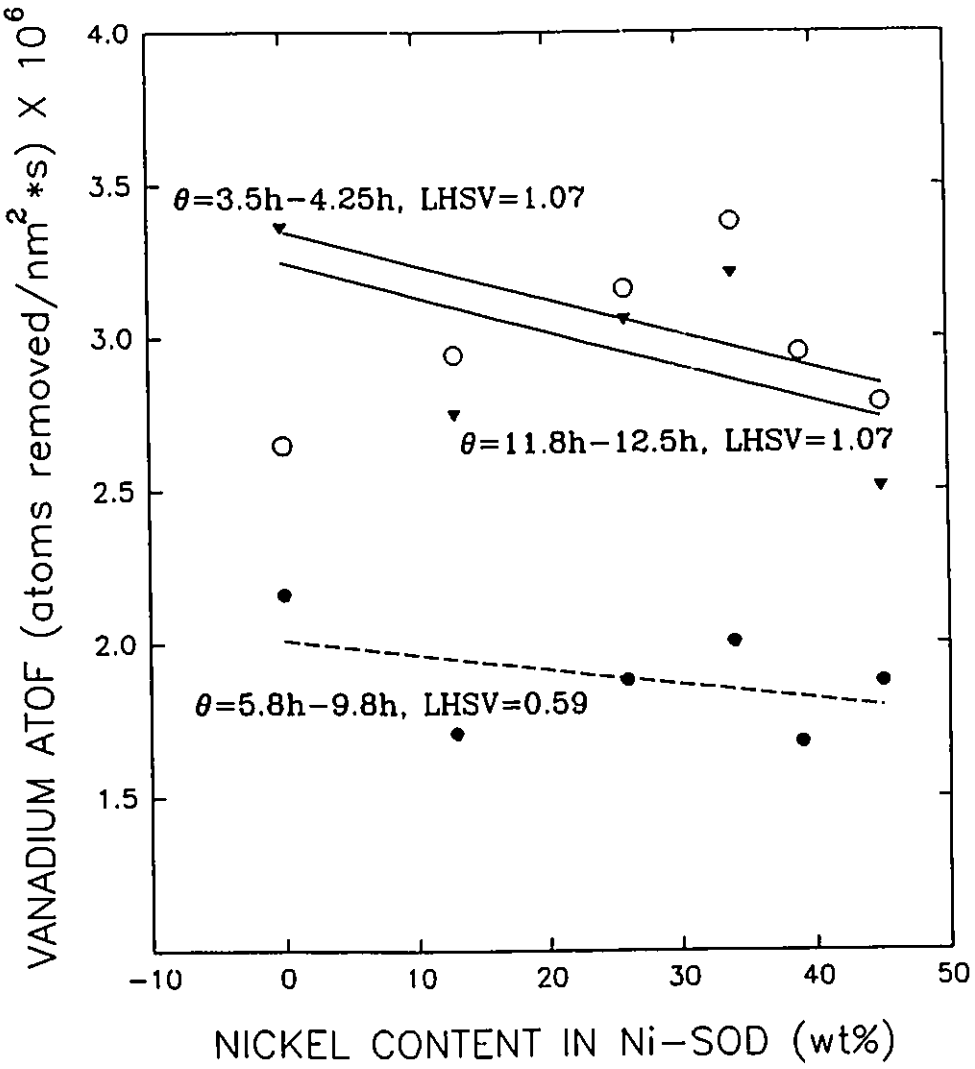

Figure 5.41 : **Vanadium ATOF (atom removed/nm^2. s) as a function of impregnated nickel content in the sodalite component of the Co-Mo catalyst (wt%).**

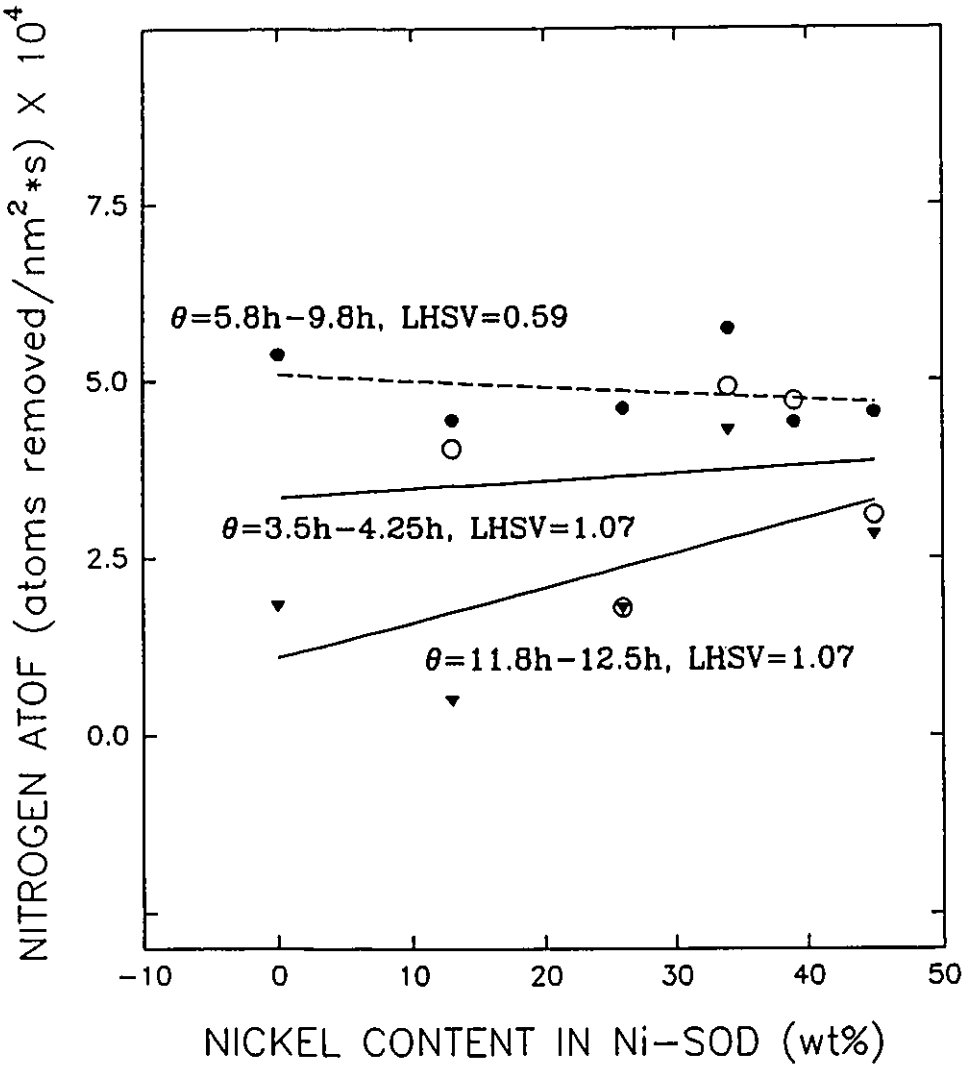

Figure 5.42 : **Nitrogen ATOF (atom removed/nm². s) as a function of impregnated nickel content in the sodalite component of the Co-Mo catalyst (wt%).**

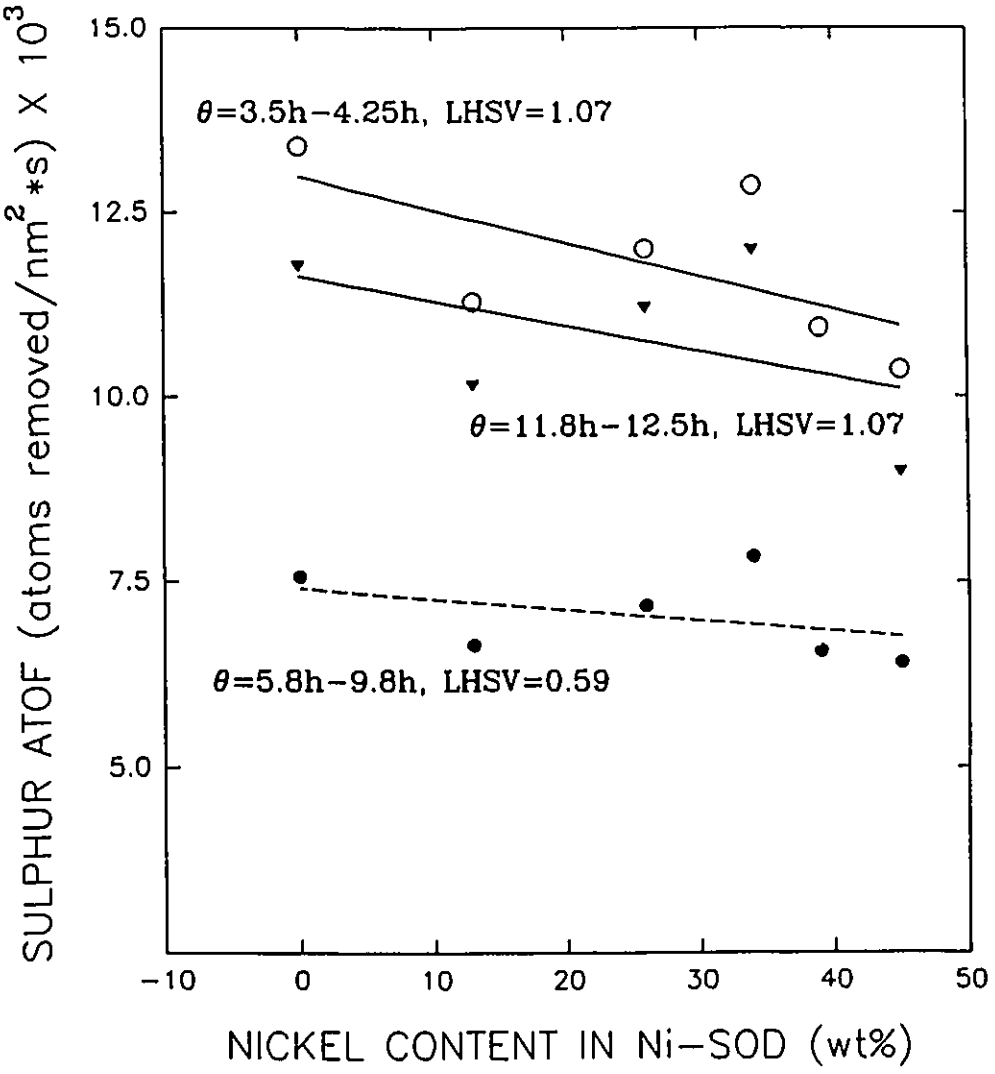

Figure 5.43 : **Sulphur ATOF (atom removed/nm^2. s) as a function of impregnated nickel content in the sodalite component of the Co-Mo catalyst (wt%).**

This suggest that the variation in the reaction data was caused by the different bulk densities of the catalysts as opposed to variations in the sodalite nickel content. Furthermore, the data points in the ATOF format were closer to their correlation lines than when they were in the conversion format. This was especially true for the lower LHSV data θ = 5.8h - 9.8h.

The ATOF results shown in Figures 5.40 - 5.43 as a function of the nickel content insodalite were in agreement with the ATOF results in Figures 5.28 - 5.31 which were a function of the sodalite content in the catalyst. The nickel ATOF (HDNi) was lower than the vanadium ATOF (HDV) because of the lower initial concentration of nickel in the feedstock. Finally, the smaller LHSV caused the ATOF values θ = 5.8h - 9.8h to be less than those at larger LHSV because fewer atoms were available to be converted. Finally, a comparison of the ATOF values for θ = 3.5h - 4.25h and ATOF values for θ = 11.8h - 12.5h indicated that the slopes of the two lines are similar. This suggests that the sodalite nickel content did not affect on the catalysts' deactivation. In all cases, there was catalyst deactivation over the whole utilisation period as shown by the difference in values between θ = 3.5h - 4.25h and θ = 11.8h - 12.5h.

5.2.3.3 Nickel Reduction

Nickel in the form of nickel sulphide has been widely used as a promoter of catalysts in hydrocracking of heavy oil (Pereira et al., 1987; Prins et al., 1989). Wilson

and Kriz (1984) demonstrated superior activity of sulphided nickel tungsten catalysts in comparison with conventional molybdenum catalysts for at least one middle distillate feedstock. Furthermore, reduced nickel catalysts in the form of nickel metal on silica-alumina support required significantly milder reaction conditions than sulphided nickel tungsten catalysts for comparable aromatic conversions, despite the fact that metallic nickel is more sensitive to poisoning (Wilson et al., 1988). For the laboratory prepared catalyst used in this work, an exchange with potassium ions was performed after nickel impregnation and reduction in order to protect the reduced nickel from poisoning. The purpose of this exchange was to prevent the sulphur ions from entering the sodalite cages and contact the reduced nickel.

The lack of noticeable effect from the nickel component in the laboratory prepared catalysts raised immediate concerns. The presence of reduced nickel on sodalite had been confirmed by the XRD spectra during material characterization (Figures 3.3 and 3.4), but chemisorption measurements on fresh catalysts and on reduced Ni-impregnated sodalite revealed that less than 1 % of the nickel available had been reduced using the procedure described in chapter four. Table B-18 shows the percentage of reduced nickel for selected prepared catalysts. The very small amounts of nickel available for chemisorption indicate that nickel reduction was not successful.

Other attempts at reducing the nickel were made using different conditions such as flowing H_2 at atmospheric pressure for 2 h at 450°C and for 3 h at 500°C as well as

for 4 h at 435°C under a pressure of 17.3 MPa without significant improvement in the extent of reduction. The literature reports a wide range of conditions for the reduction of Ni^{2+} on zeolites. Suzuki and co-workers (1982) observed good reduction of nickel on Ni-HY with a flow of hydrogen for 3 h at temperatures varying from 300°C to 500°C with a higher degree of reduction at a higher temperature. Jiang and co-workers (1988) reported using a 5 % H_2/Ar flow at 425°C for 2 h in their study of Ni/faujisite catalysts and Vázquez et al. (1987) reported reducing a series of Ni-Mo/HY ultrastable sodalite catalysts in H_2 flow for 2 h at a temperature of 450°C. Unfortunately, the results from this present study did not reflect the ease of nickel reduction reported by other authors (Mirodatos et al., 1982).

Possible explanations for this phenomenon may be found from the suggestion of other workers. Zhang et al. (1989) reported that the thermodynamics and kinetics of the reduction equilibrium of cobalt and nickel in sodalite cages or hexagonal prisms was unfavourable. Thus, according to these authors, the reduction of cobalt or nickel in sodalite cages can be expected to be difficult. In fact, reduction of cobalt ions in sodalite Y was reported to occur at temperatures as high as 750°C as cobalt or nickel ions tend to be stabilized by the negatively charged sodalite structure (Zhang et al., 1989). A higher temperature also facilitates reduction of nickel ions located in the sodalite cages as thermal vibration allows the small sodalite pore mouths (2.2 Å at room temperature) to stretch to accommodate the larger diatomic hydrogen molecules (2.8 Å) (Jiang et al., 1988). The proximity of a noble metal such as Pt or Pd however facilitates reduction

of transition metals by dissociating H_2 (Feeley and Sachtler, 1991; Zhang et al., 1993). The reduction temperature for Co^{2+} under those conditions is reduced to 500°C with prior calcination at 300°C.

It is believed that failure to obtain metallic nickel in this study was probably caused by the absence of promoter metal such as Pd or Pt. Consequently, the nickel anions could not be freed from the negatively charged sodalite structure at temperature as low as 450°C or 500°C. Also, basic sodalite does not contain supercages as for NaY, faujisite or HY. It is believed that the nickel ions are more accessible and more easily reduced in presence of supercage structures (Jiang et al., 1988).

5.3 HETEROATOM REMOVAL FROM BOILING POINT FRACTIONS

As discussed earlier, the various boiling point fractions can loose heteroatoms by heteroatom removal or gain heteroatoms by heteroatom addition. Rather than express the reaction results as heteroatom conversion, the ratio of heteroatom concentration in the product boiling point fraction to heteroatom concentration in the feedstock boiling point fraction, $(HA)_P/(HA)_P$, is used. When the ratio is greater than unity, it indicates that there has been a net heteroatom addition to the boiling point fraction. When the ratio is less than unity, it indicates that heteroatom removal is the dominant process. The product to feedstock heteroatom ratio can be considered to be an indication of the change

in quality of the boiling point fraction.

The quantity of a boiling point fraction is indicated by its yield. The wt% yield of a product fraction can be compared with the wt% of the same boiling point fraction in the feedstock. The yield of the 288°C - 343°C diesel fraction can increase because molecular fragments in the diesel fraction boiling point range have been formed by cracking some of the molecules in the +343°C residue fraction. In contrast, the diesel fraction yield can decrease if some of its molecules are cracked to the lower boiling IBP - 288°C fraction.

For the total liquid product, heteroatom conversion indicates both quantity and quality. The amount of heteroatom present indicates the quantity as well as the quality because it is a percentage of the amount originally present. For the boiling point fractions, two indicators are required to provide the same information. The product fraction yield is the indicator of quantity while the heteroatom product/feedstock ratio is the indicator of quality

5.3.1 THE EFFECT OF NICKEL IMPREGNATED SODALITE (NI-SOD) AS A CATALYST COMPONENT

5.3.1.1 Quality of Fractions

The liquid product obtained at LHSV = 0.59 for θ = 5.8h - 9.8h from each of the catalytic hydrocracking experiments was distilled into three parts (section 2.2.3). Analysis were performed on two of these fractions (288°C - 343°C and +343°C). In order to determine the quality of the diesel and the residual fractions, their heteroatoms and MCR contents were compared on the basis of the original heteroatoms and MCR contents in the feedstock fractions.

The ratios of nitrogen and sulphur contents for the diesel fraction and of sulphur, nickel, vanadium and MCR contents for the residual fraction are shown in Figures 5.44 - 5.48 as a function of sodalite content in the sulphided Co-Mo/Al_2O_3 catalyst. A ratio higher than one indicates that the fraction has a higher concentration of an element than the same fraction in the feedstock. In the case of nitrogen, for example (Figure 5.44), the ratio is consistently higher than one. This indicates that more nitrogen was added to the diesel fraction than was removed. In other words, the sodalite component in the catalyst puts more nitrogen in the diesel fraction. This is consistent with Figure 5.23 which shows a decrease of nitrogen removal with an increase in Ni-sodalite content. Nitrogen that was initially contained in the heavy fraction was converted into a lighter

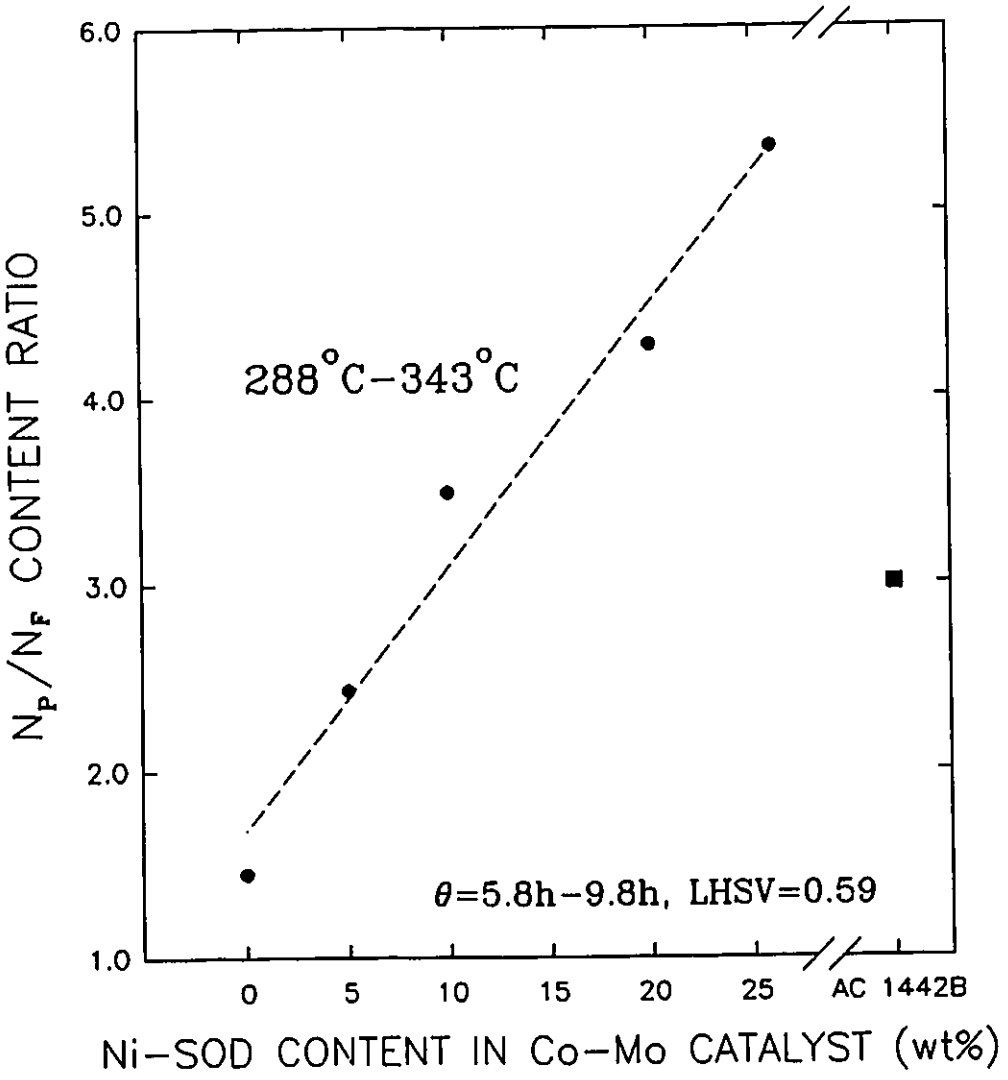

Figure 5.44 : **N_P/N_F ratio for the diesel fraction as a function of Ni-SOD content in the Co-Mo catalyst (wt%).**

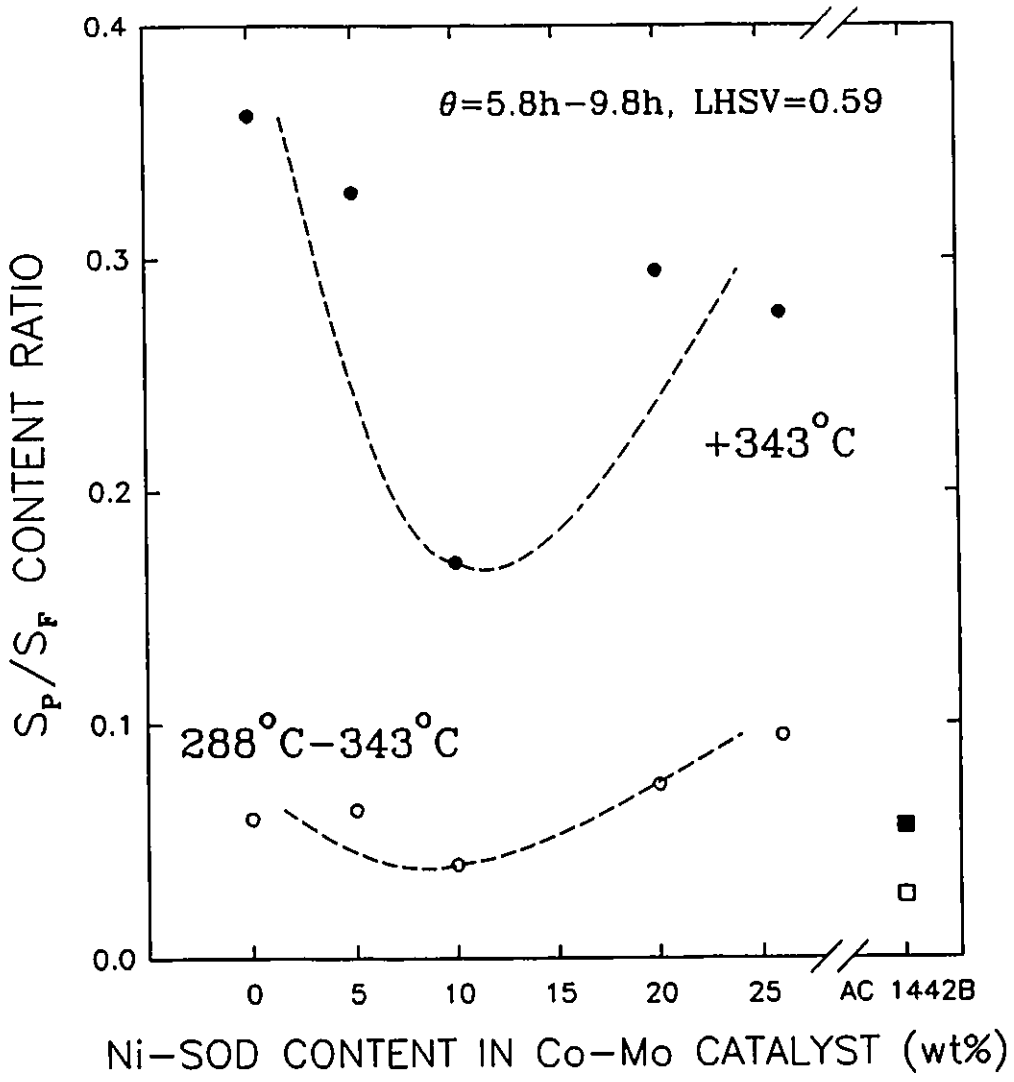

Figure 5.45 : **S_P/S_F ratio for the diesel fraction as a function of Ni-SOD content in the Co-Mo catalyst (wt%).**

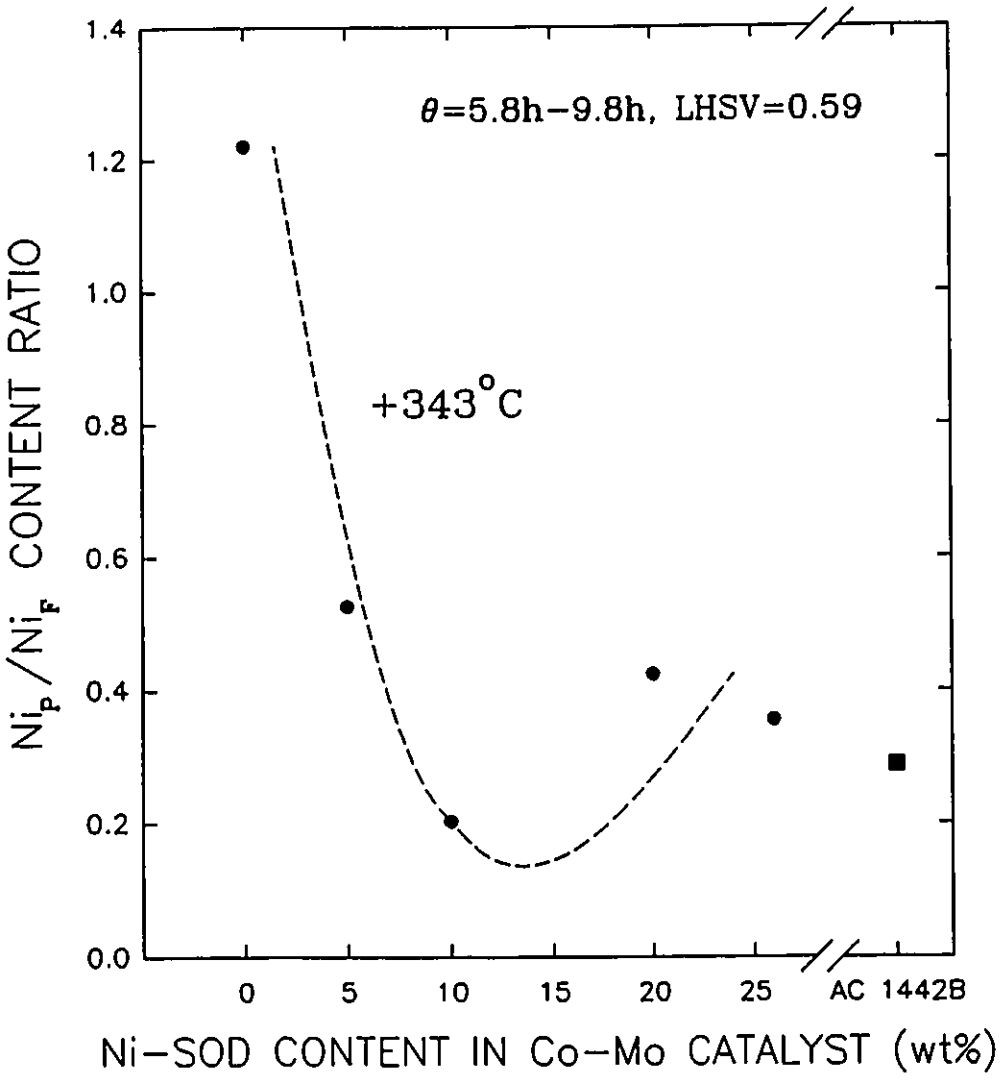

Figure 5.46 : **Ni_P/Ni_F ratio for the diesel fraction as a function of Ni-SOD content in the Co-Mo catalyst (wt%).**

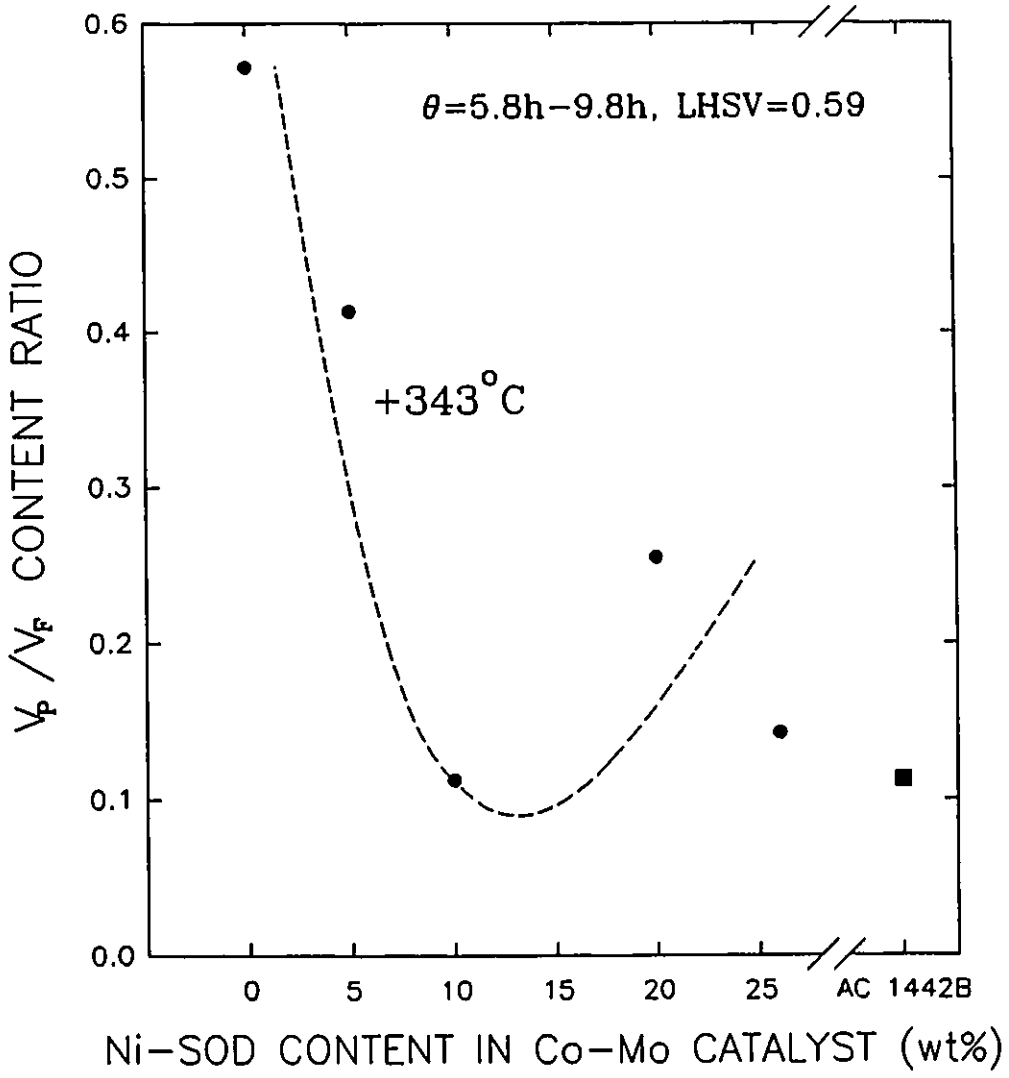

Figure 5.47 : **V_P/V_F ratio for the diesel fraction as a function of Ni-SOD content in the Co-Mo catalyst (wt%).**

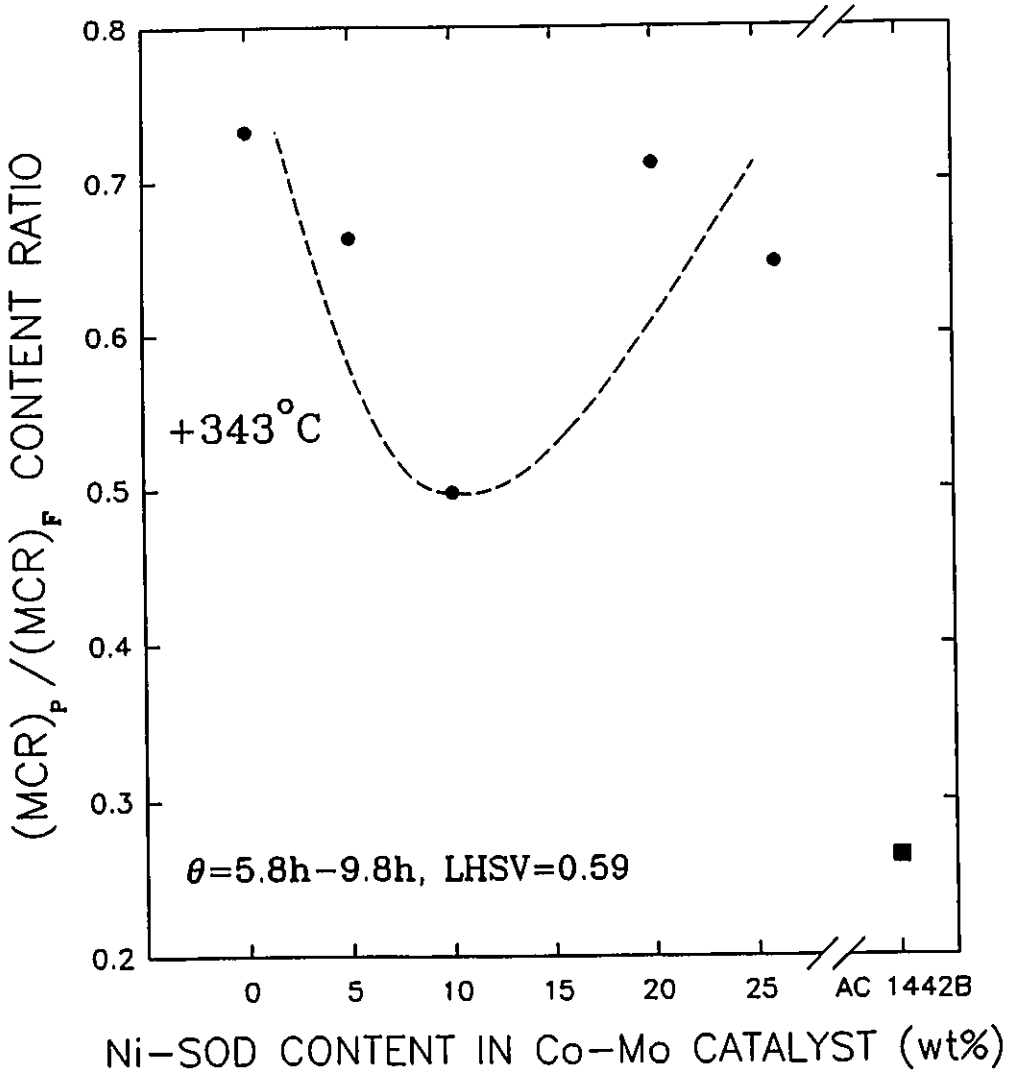

Figure 5.48 : **MCR_P/MCR_F ratio for the diesel fraction as a function of Ni-SOD content in the Co-Mo catalyst (wt%).**

liquid product as opposed to mostly being removed as NH_3. From this observation, it can be postulated that the presence of sodalite changes the product selectivity of the hydrocracking reaction with regards to nitrogen compounds .

In the case of sulphur, shown in Figure 5.45, the S_P/S_F ratio is lower than unity which indicates an improvement in the fraction quality on the basis of sulphur content. The positive effect of sodalite however reaches a maximum at about 10% sodalite content which is demonstrated by a minimum in the S_P/S_F ratio for both fractions. This is consistent with the findings of Figure 5.24. The quality of the diesel fraction is much better than that of the residue because the original concentration of the residue is much higher than in the diesel fraction. Also, the shape of the curve for the residual fraction is a more perfect mirror image of those in Figure 5.24 since most of the sulphur is contained in the heavy fraction. Finally, the same phenomena occur with the ratios for nickel, vanadium and MCR (Figures 5.46 - 5.48 respectively) where each of the curves reach a maximum of quality at about 10 % sodalite content in the Co-Mo catalyst which is consistent with Figures 5.21-5.22 and 5.25.

5.3.1.2 Yield of Fractions

The yield of desirable products (weight percent of feedstock) is an important factor in evaluating the effectiveness of a catalyst. The distributions of boiling fractions in the liquid product are shown in Figure 5.49 as a function of the sodalite content in the

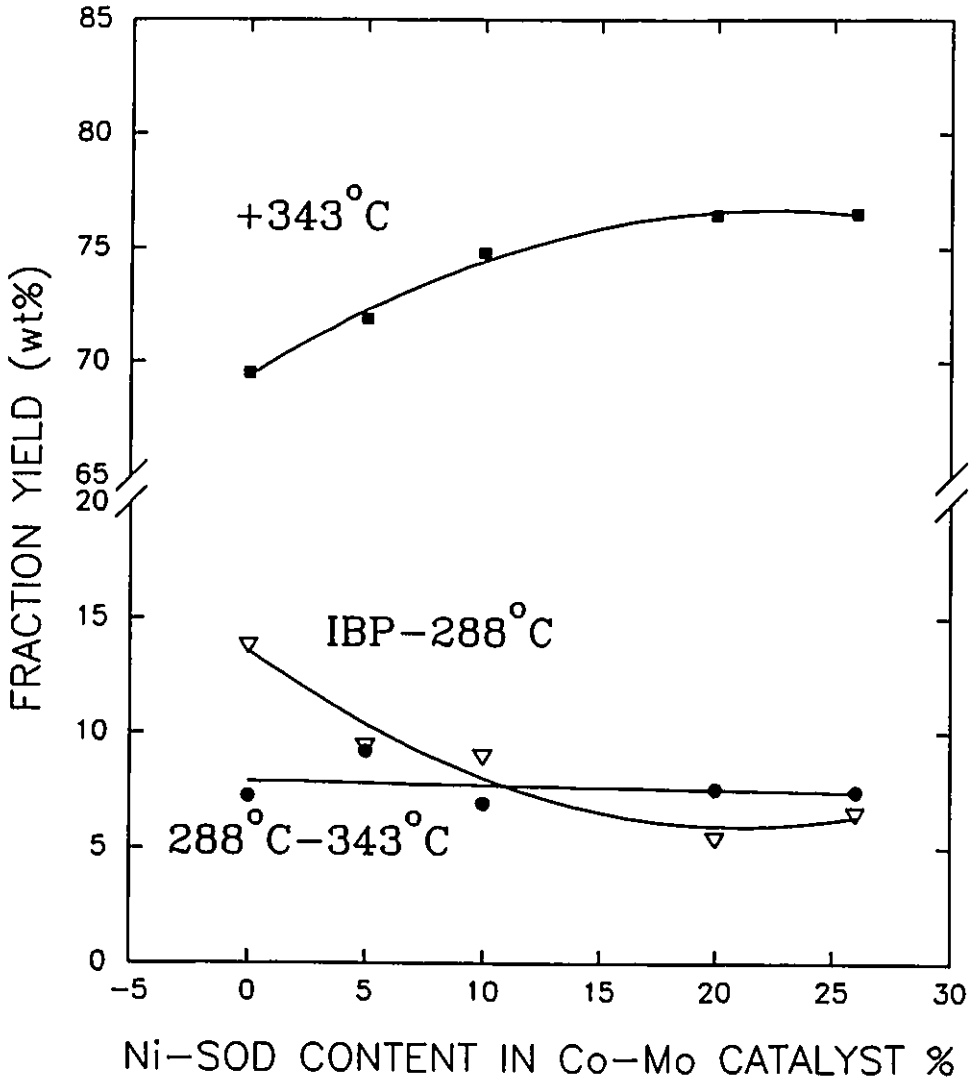

Figure 5.49 : **Liquid product fraction yield as function of Ni-SOD content in the Co-Mo catalyst (wt%).**

sulphided Co-Mo/Al_2O_3 catalyst. As the sodalite component in the catalyst increased, the lower boiling fraction (IBP to 288°C) decreased, the residual fraction (+343°C) increased, while the amount diesel fraction (288°C - 343°C) remained constant. This indicates that, although the amount of heavy nitrogen compounds converted into lighter fractions increased with addition of sodalite to the catalyst as discussed in the previous section, the overall conversion of heavy molecules to lower boiling fractions decreased as the catalyst sodalite content increased. Also, a smaller amount of molecules belonging to the diesel fraction were converted to the lower boiling fraction as the catalyst sodalite content increased. Consequently, the diesel component remained approximately constant as shown in Figure 5.49. The capacity to decrease the molecular weight of heavy molecules is of primary concern in hydrocracking catalysts. It is obvious from this figure that the addition of sodalite somewhat impedes this capacity in the sulphided Co-Mo/Al_2O_3 catalyst. Therefore, it can be said that on the basis of fraction yields, the addition of sodalite does not improve the effectiveness of the Co-Mo catalyst.

5.3.2 THE EFFECT OF NICKEL CONCENTRATION IN A NI-SOD CATALYST COMPONENT

5.3.2.1 Quality of Fractions

Quality comparisons of heteroatom and MCR product to feedstock ratios are shown in Figures 5.50-5.54 as a function of sodalite nickel content for the boiling

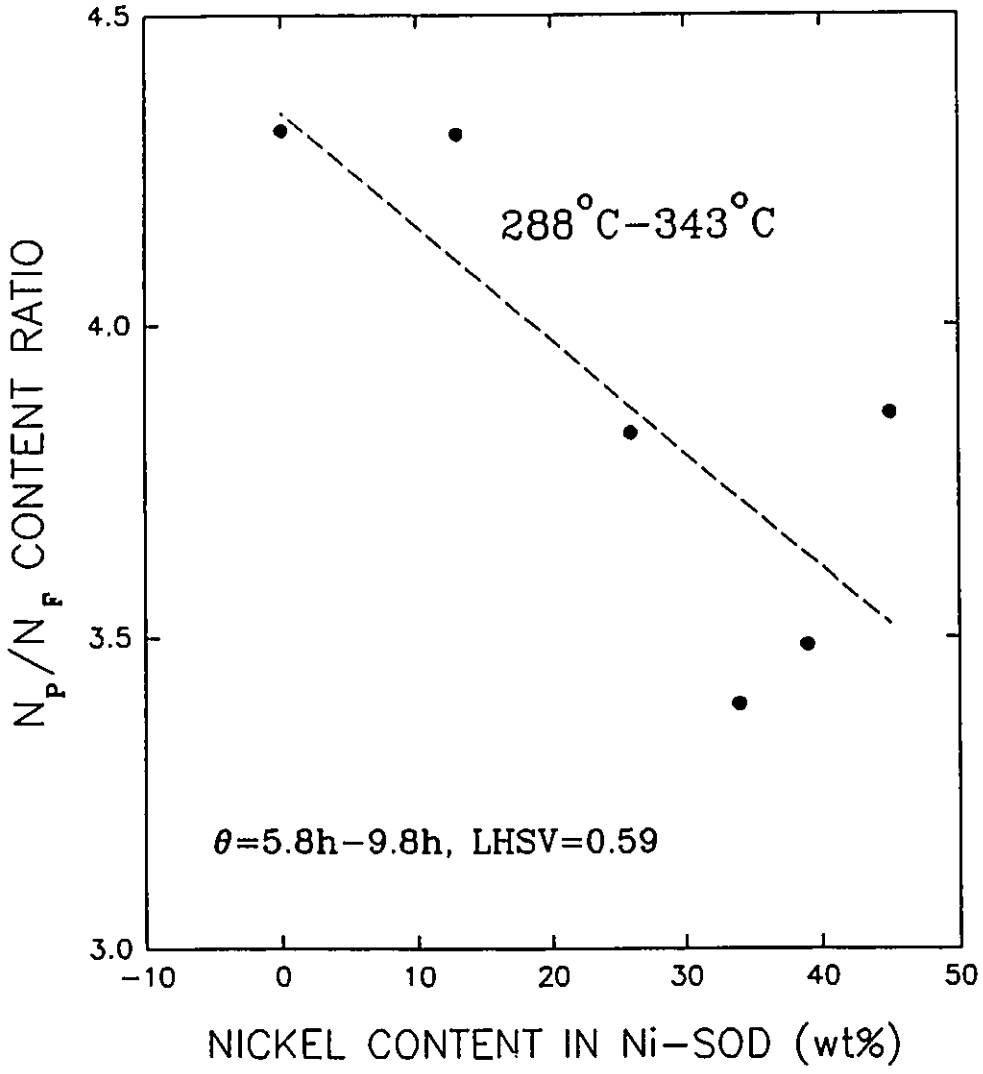

Figure 5.50 : **N_P/N_F ratio for the diesel fraction as function of impregnated nickel content in the sodalite component of the Co-Mo catalyst (wt%).**

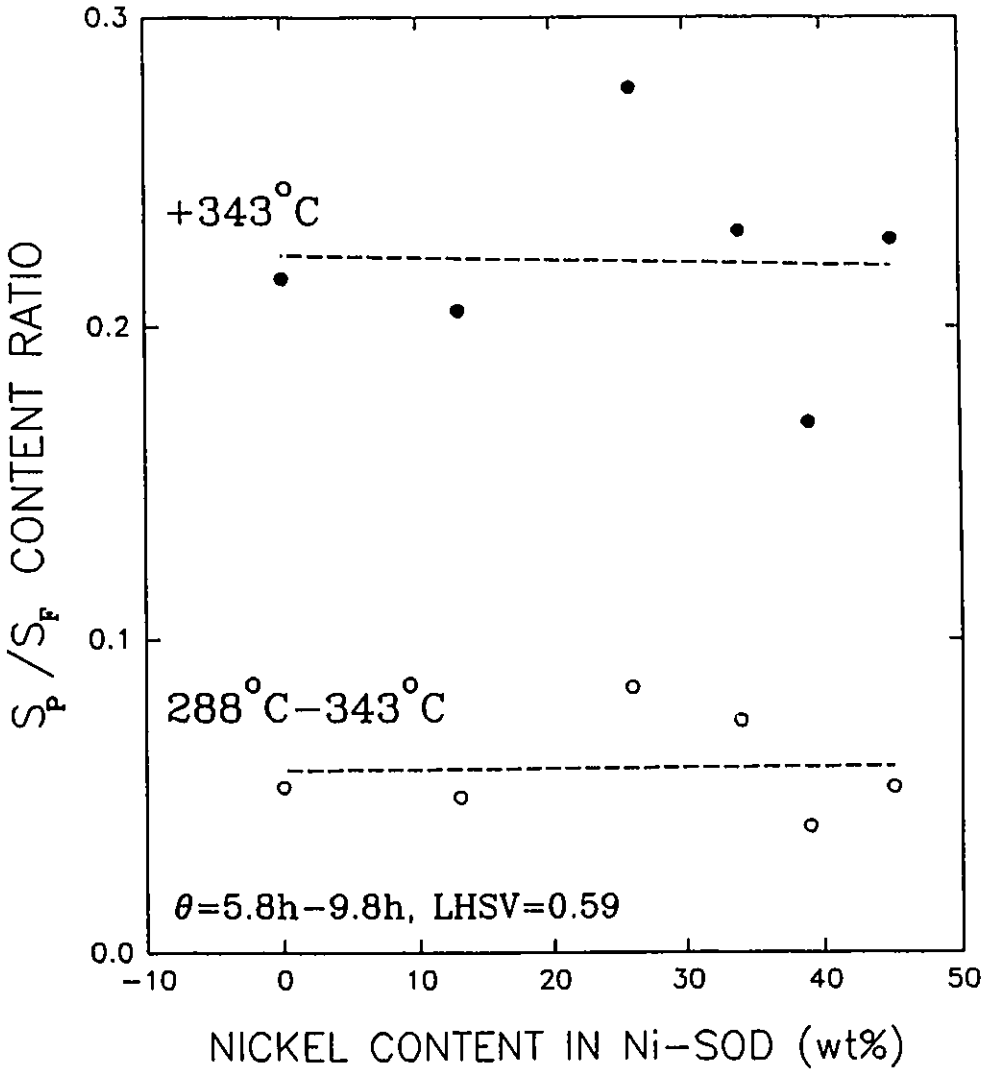

Figure 5.51 : **S_P/S_F ratio for the diesel fraction as function of impregnated nickel content in the sodalite component of the Co-Mo catalyst (wt%).**

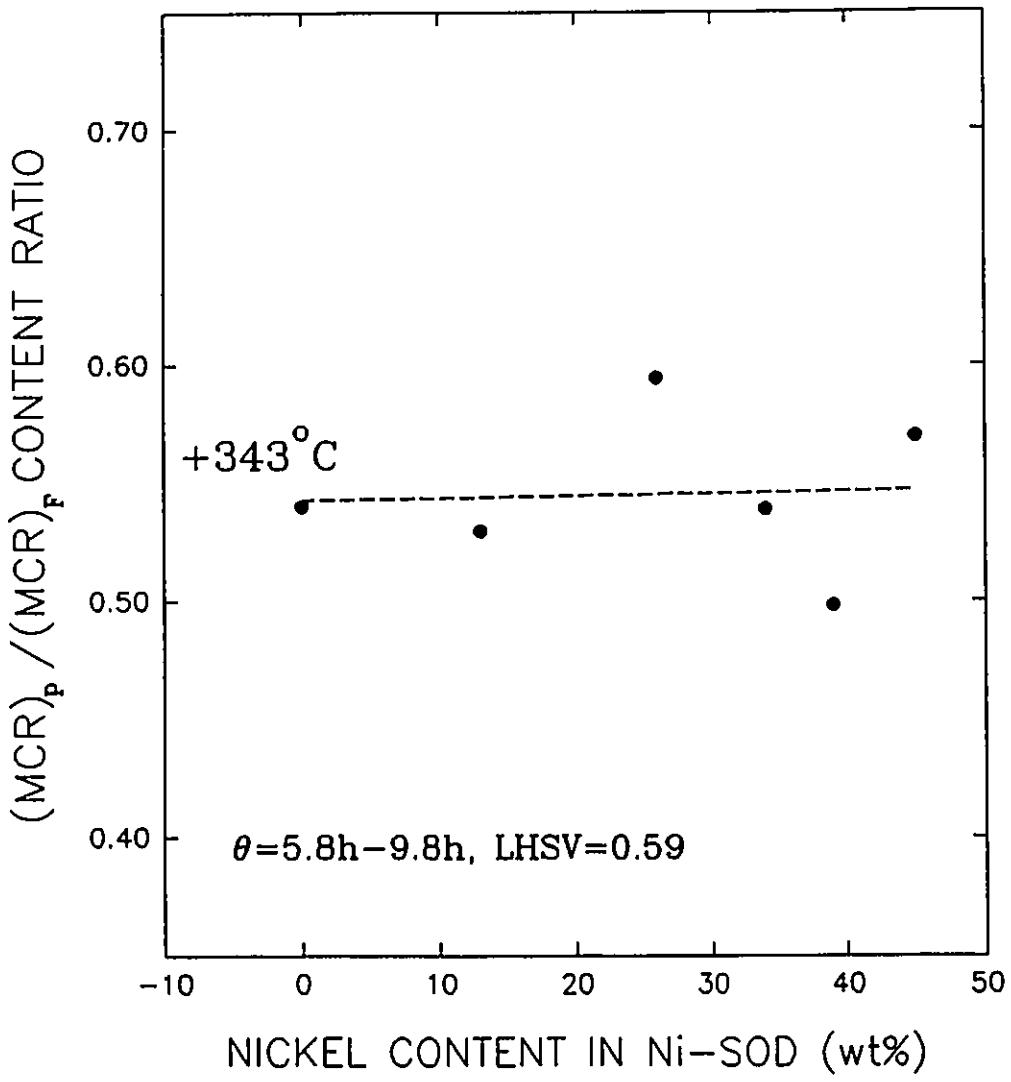

Figure 5.52 : **MCR_P/MCR_F ratio for the diesel fraction as function of impregnated nickel content in the sodalite component of the Co-Mo catalyst (wt%).**

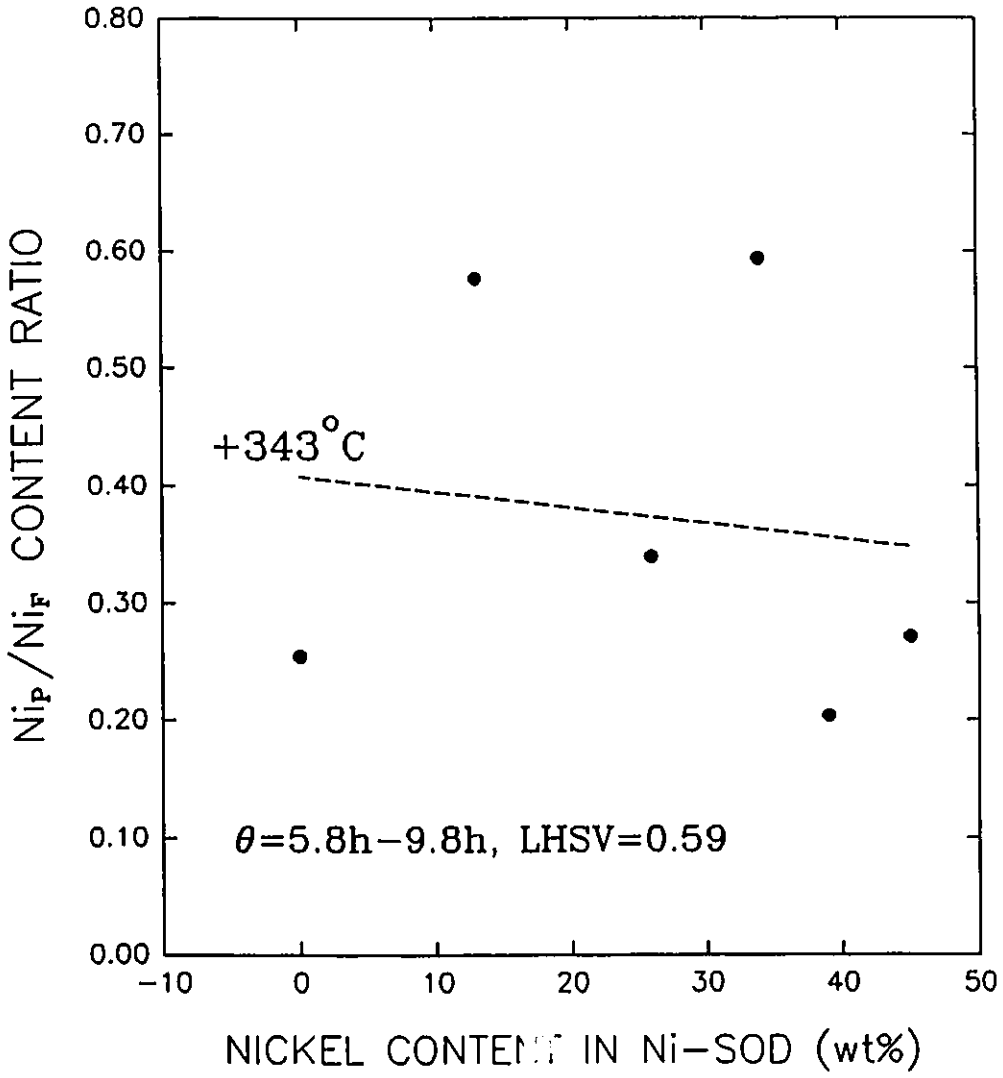

Figure 5.53 : **Ni_P/Ni_F ratio for the diesel fraction as function of impregnated nickel content in the sodalite component of the Co-Mo catalyst (wt%).**

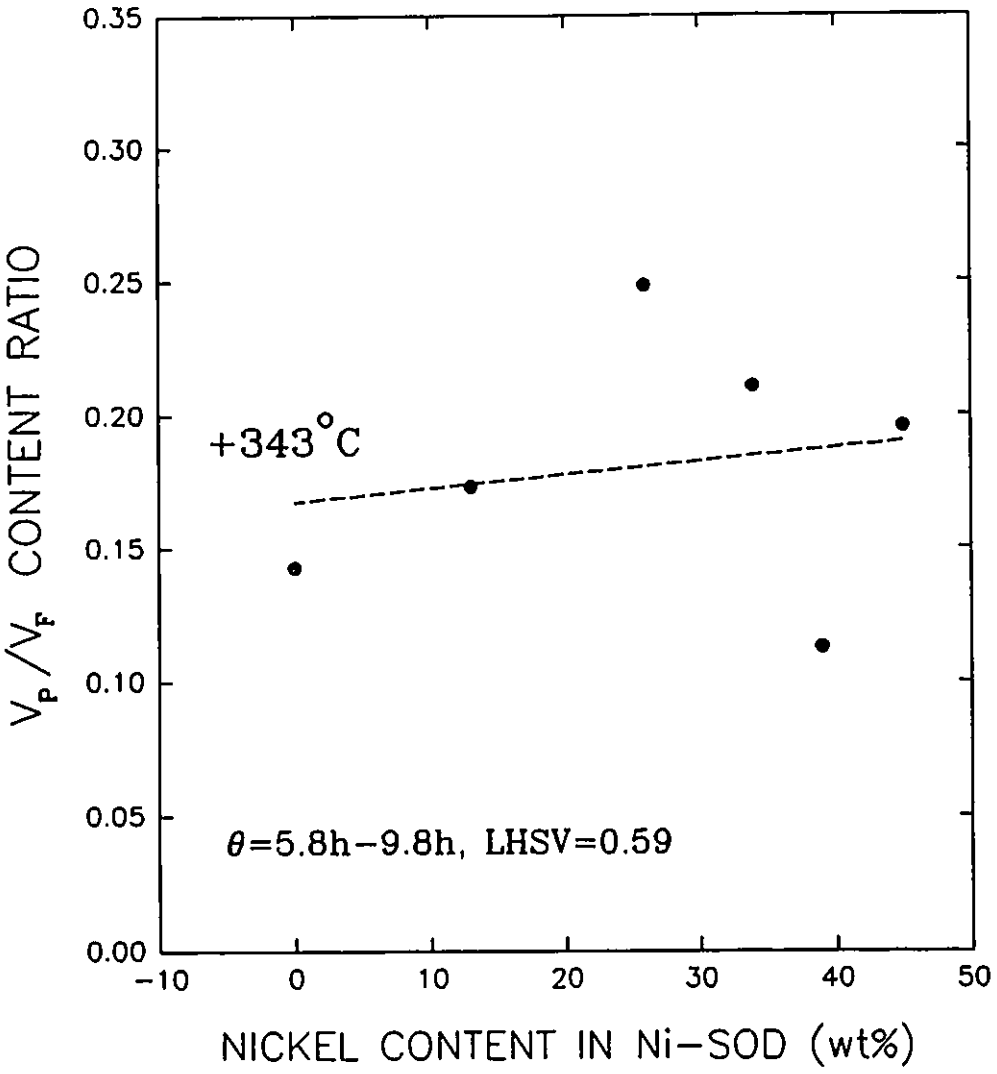

Figure 5.54 : **V_P/V_F ratio for the diesel fraction as function of impregnated nickel content in the sodalite component of the Co-Mo catalyst (wt%).**

fractions of the liquid product collected at LHSV = 0.59 for θ = 5.8h - 9.8h. The N_P/N_F ratios of the diesel (Figure 5.50) are higher than unity. The quality of the product improved with addition of nickel to the sodalite which indicates that the presence of nickel caused more nitrogen compounds to be removed during hydroprocessing. Although the amount of nickel reduced is minimal, it could explain the very slight effect of the nickel sometimes observed in the present study since often only small amounts of nickel in the catalyst are required in order to observe a positive effect (Wilson and Kriz, 1984).

In Figure 5.51, the constant S_P/S_F ratios for the diesel fraction and the residue indicate that the addition of nickel had no effect on the quality of the product based on the sulphur content. The large difference in the S_P/S_F ratios of the diesel fraction and those of the residual fraction is due to the fact that most of the sulphur is contained in the heavy fraction which causes the quality of the residue to be poorer. The same observation on the effect of the sodalite nickel content can be made for the quality of the residual fraction on the basis of MCR_P/MCR_F ratio in Figure 5.52 as the ratio is relatively constant. These results are consistent with the fact that no effect was observed in the whole product shown in Figures 5.35 - 5.37 when the sodalite nickel content increased.

Based on the minimum in metal conversion at around 26 wt% of sodalite nickel content that was observed for the whole product at LHSV = 0.59 (Figures 5.33 and

5.34) a poor quality residual fraction was also expected. However, the $(Ni)_P/(Ni)_F$ and V_P/V_F ratios in Figures 5.53 and 5.54 respectively are very scattered and cannot be correlated with the conversion plots for the whole product (Figures 5.33 and 5.34). The curves in Figures 5.53 and 5.54 would be expected to be a mirror image of those in Figures 5.33 and 5.34 since the organometallic compounds in liquid products are essentially only present in the heavy fraction. Since it is not the case, it was assumed that the curved lines observed in Figures 5.33 and 5.34 were coincidental.

5.3.2.2 Yield of Fractions

The yield of different boiling point fractions is shown in Figure 5.55 as a function of sodalite nickel content in the sulphided Co-Mo/Al_2O_3 catalyst. Nickel appears to have influenced the yields of the two lighter fractions more than the yield of the heavy fraction. In contrast with Figure 5.49, the heavier fraction yield (+343°C) remained constant as the sodalite nickel content increased. The yield of the diesel fraction (288°C - 343°C) however, increased at the expense of the lighter fraction (IBP - 288°C). Therefore, on the basis of fraction yields, the addition of nickel to the sodalite component improves hydroprocessing.

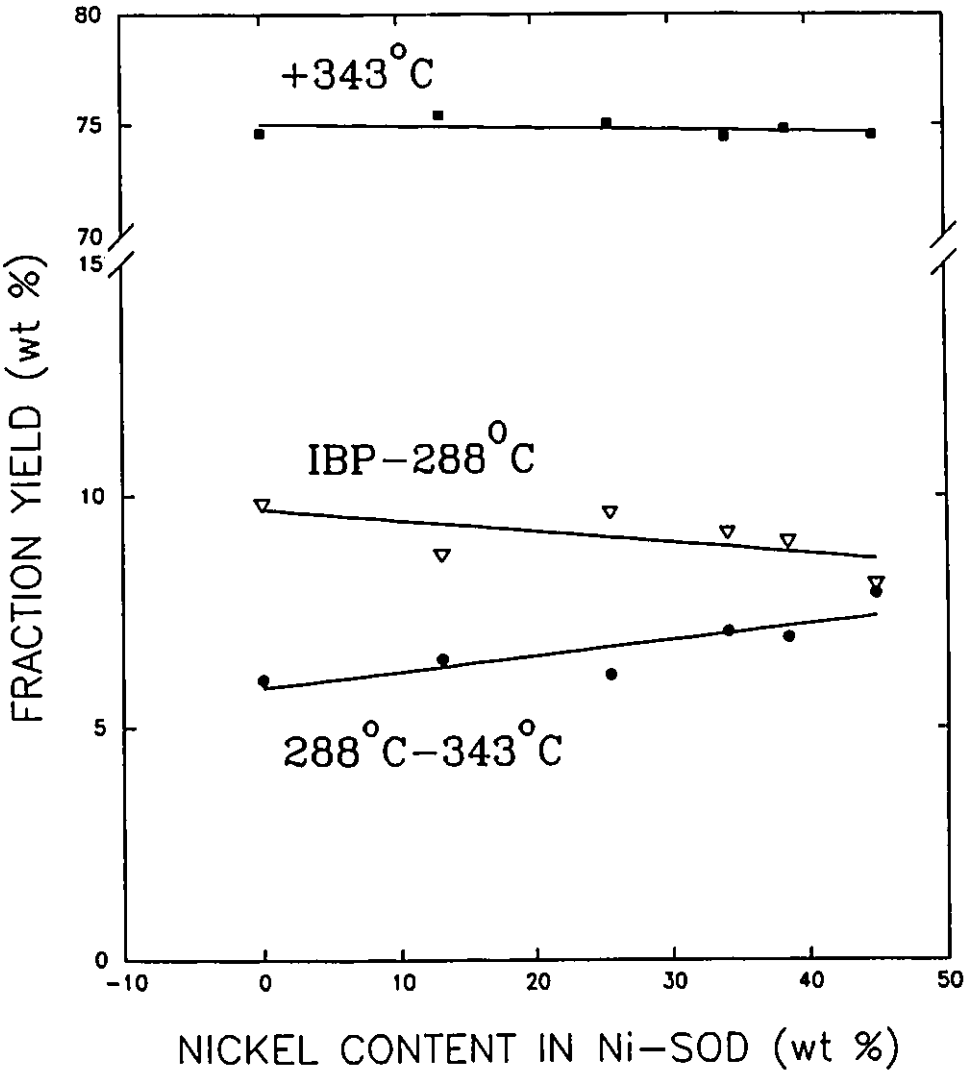

Figure 5.55 : **Liquid product fraction yield (wt%) as function of impregnated nickel content in the sodalite component of the Co-Mo catalyst (wt%).**

CHAPTER SIX

6.0 CONCLUSIONS AND RECOMMENDATIONS

6.1 CONCLUSIONS

6.1.1 Effects on colour formation in the diesel fraction of the liquid product

1. The rate of colour deterioration of the diesel fraction as well as the rate at which the maximum ASTM colour value is attained increases as the content of Ni-SOD in the Co-Mo/Al_2O_3 laboratory prepared catalysts increases.

2. Addition of nickel in the sodalite retards the rate of colour formation in the diesel fraction but develops colour to a greater maximum value.

3. The AC-1442B catalyst is more effective at controlling colour formation in the diesel fraction than any of the laboratory prepared catalysts. All hydrocracking catalysts in this study improved the initial colour of the middle distillate fraction as well as its stability over time when compared to thermal hydrocracking.

4. A correlation exits between colour formation and sulphur content in the diesel fraction, but none could be established with nitrogen content of the diesel fraction.

6.1.2 Effects on catalytic hydrocracking

1. The presence of sodalite as well as that of nickel impregnated sodalite (Ni-SOD) in $CoMo/Al_2O_3$ catalysts improve HDM, HDS and MCR removal. However, their presence reduce HDN, probably because of strong N-C bonds.

2. The highest conversion values for HDM, HDS and MCR removal were achieved at a nickel impregnated sodalite (Ni-SOD) content of 10 wt%. Improvement in conversion was attributed to stronger acid sites with presence of Ni-SOD. However, because the addition of Ni-SOD in the catalyst also caused the loss of reaction sites in the $CoMo/Al_2O_3$ component, more than 10% Ni-SOD did not cause a net improvement.

3. A slower LHSV (longer residence time) improves heteroatom conversion.

4. The AC-1442B reference catalyst is a better hydrocracking catalyst than the laboratory prepared catalysts on the basis of one reactor load, but is worst on the basis of ATOF. Its higher total surface area caused both effects.

5. The presence of Ni-SOD changes the nitrogen compound selectivity in the diesel fraction, but does not improve the effectiveness of the $CoMo/Al_2O_3$ catalyst as it reduces the yield of lower boiling point fractions.

6. The variation of nickel content in the sodalite component of the $CoMo/Al_2O_3$ laboratory prepared catalysts had minimal effect on heteroatom removal due to the difficulty of nickel reduction in the small sodalite cages. However, the presence of nickel in sodalite slightly improves nitrogen removal as well as the yield of the diesel fraction . The small effect sometimes observed was attributed to the high reactivity of

reduced nickel sites.

6.2 RECOMMENDATIONS

The principle of using small zeolite pores partially blocked with a large ion after metal impregnation is a valuable concept as it protects active sites from sulphur poisoning. A zeolite with pores slightly larger than sodalite such as HY or H-mordenite should be considered in order to avoid the difficult reduction problem encountered in the small sodalite cages. Nevertheless, appropriate reduction conditions for NiO located in sodalite cages should be investigated further.

In the preparation of the catalysts, a calcination procedure which maintains the bimodal character of the gamma-alumina support while preventing bursting of the extrudates due to rapid water evaporation should be developed. Also, short straight extrudates should be prepared in order to increase catalyst bulk density.

Finally, further studies on class separation of sulphur and nitrogen components using methods such as Gas Chromatography and Mass Spectrometry should be undertaken in order to identify specific sulphur and nitrogen compounds responsible for colour formation in the middle distillate fraction.

REFERENCES

Aalund, L.R., *"Scotford, Canada's First Grassroots Syncrude Refinery, is Headed Toward Startup Soon"*, ***Oil Gas J.***, Mar 26, 78-80 (1984).

Aoskima, A. and H. Wise, *"Hydrodesulfurization Activity and Electronic Properties of Molybdenum Sulfide Catalyst"*, ***J. Catal.*** **34**, 145-151 (1974).

Ballmoos (von), R. *"Collection of Simulated XRD Powder Patterns for Zeolites"*, Butterworth Scientific lted, on behalf of the Structure Commission of the International Zeolite Association, U.K. (1984).

Baron, K., R.E. Miller, A. Tang and L. Palmer, *"Hydrotreating of Light Cycle Oil"*, in ***Proc. 1992 NPRA Annual Meeting, New Orleans, Louisiana,*** **AM-92-20,** (1992).

Barrer R.M. and E.A.D. White, *"Hydrothermal Chemistry of Silicates. Part II. Synthetic Crystalline Sodium Aluminosilicates"*, ***J. Chem. Soc.*** 1561-1571 (1952).

Batts, B.D. and A.Z. Fathoni, *"A Literature Review on Fuel Stability Studies with Particular Emphasis on Diesel Oil"*, ***Energy Fuels*** **5**, 2-21 (1991).

Beaton, W.I. and R.J. Bertolacini, *"Resid Hydroprocessing at Amoco"*, ***Catal. Rev. Sci. Eng.*** **33(3&4)**, 281-317, (1991).

Beaver, B., *"Long Term Storage Stability of Middle Distillate Fuels from a Chemical Mechanistic Point of View. Part I"*, ***Fuel Sci. Tech. Int.*** **9(10)**, 1287-1335 (1991).

Bhan, O.K., D.W. Brinkman, J.B. Green, and B. Carley, *"Storage Stability of Marine Diesel Fuels"*, ***Fuel 66,*** 1200-1214 (1987).

Bhan, O.K., J.B. Green, D.W. Brinkman, and B. Carley, *"Cause of Colour Change and Sediment Formation in Navy Distillate Fuels"*, in ***Proc. 2nd Int. Conf, on Long-term Storage Stabilities of Liquid Fuels,*** L.L. Stavinoha Ed, San Antonio, Texas. 915-926 (1986).

Bhatia, S., **"ZEOLITE CATALYSIS:** ***Principles and Applications"***, CRC Press, Inc. Florida, (1988).

Bond, G.C., ***"Heterogeneous Catalysis- Principles and Applications"***, 2nd Ed., (Oxford

Chemistry Series), Oxford University Press, New York, (1987).

Breck, D.W., *"ZEOLITE MOLECULAR SIEVES, Structure, Chemistry and Use"*, John Wiley & Sons, NY, (1974).

Carr R.M., P.W. Larking and G.L. Lyon, *"The Synthesis of Basic Sodalite"*, ***Aust. J. Chem.*** **21(10)**, 2555-2559, (1968).

Chase S., *"The Husky Bi-provincial Upgrader"*, ***The Petrol. Soc. CIM,*** paper no 4, Sep (1989).

Cooney, J.V., E.J. Beal, and R.N. Hazlett, *"Mechanism of Synfuel Degradation. 2. Examination of Shale-Derived Polar Fractions and their Effects on the Storage Stability of Shale Diesel Fuel,* ***Ind. Eng. Chem. Prod. Res. Dev.*** **24**, 294-300 (1985).

Court, A.L. and W.H. Smith, *"Canada's First Heavy-oil Upgrader Complex on Stream"*, ***Oil Gas J.,*** Jun 26, 46-58 (1989).

Cyr, N., D.D McIntyre, G. Toth and O.P. Strausz, *"Hydrocarbon Structural Group Analysis of Athabasca Asphaltene and its g.p.c. Fractions by ^{13}C n.m.r."*, ***Fuel*** **66**, 1709-1714 (1987).

Dautzenberg, F.M. and J.C. de Deken, *"Mode of Operation in Hydrodemetallization"*, ***ACS Prepr., Div. Petrol. Chem.,*** **30, No 1,** 8-20, (1985).

Davis, M.E., *"Zeolites and Molecular Sieves: Not Just Ordinary Catalysts"*, ***Ind. Eng Chem. Res.*** **30**, 1675-1683, (1991).

Dean, R.A. and E.V. Whitehead, *"The Composition of High Boiling Petroleum Distillates and Residues"*, ***Proc. 6th World Petrol. Cong.,*** paper V-9, 261-279 (1963).

Deer, W.A., R.A. Howie and J. Zussman, *"An Introduction to the Rock Forming Minerals"*, Longman Group Lted, London, (1975).

Dorbon, M., C. Bernascone, J. Gaillard and J. Denis, *"Storage Stability of Fuels Identification of Nitrogen Compounds and their Evolution during Ageing in Absence and Presence of Additives"*, ***ACS Prepr., Div. Fuel Chem.*** **35, No 4,** 1135-1155 (1990).

Egloff, G.and M.L. Alexander, *"Petroleum Chemistry"*, ***Ind. Eng. Chem.*** **43**, 809-819 (1951).

Fathoni, A.Z., B.F. Batts, R.F. Sprecher and Veloski, *"The Effect of Sulfur Containing Compounds on the Stability of Diesel Fuels"*, in ***Proc. 4th Int. Conf. on Stability and Handling of Liquid Fuels,*** (ed. L.L. Stavinoha), Orlando, Florida. 537-551 (1991).

Farragher, A.L. and P.Cossee, in *"Catalytic Chemistry of Molybdenum and Tungsten Sulfides and Related Ternary Compounds"*, in ***Proc. 5th Int. Cong. on Catal.,*** Palm Beach, 1972, North-Holland, Amsterdam, 1301 (1973).

Feeley J.S. and W.M.H. Sachtler, *" Mechanisms of the Formation of $PdNi_x$ in the Cages of NaY"*, ***J. Catal.*** **131,** 573-581 (1991).

Francis, W. and M.C. Peters, ***"Fuels and Fuel Technology"***, 2nd ed, Pergamon Press, Oxford, (1980).

Furimsky, E., *"Chemistry of catalytic Hydrodeoxygenation"*, ***Catal. Rev. -Sci. Eng.,*** **25(3),** 421-458 (1983).

Gary, J.H. and G.E. Handwerk, ***"PETROLEUM REFINING, Technology and Economics"***, 2nd ed, Marcel Dekker inc, New York, (1984).

Gates, B.C., J.R. Katzer and G.C.A. Schuit, ***"Chemistry of Catalytic Processes"***, McGraw-Hill, New York, (1979).

Girgis, M.J. and B.C. Gates, *"Reactivities, Reaction Networks and Kinetics in High Pressure Catalytic Hydroprocessing"*, ***Ind. Eng. Chem.*** **30,** 2021-2058 (1991).

Hall, G. and S.P. Herron, *"Size Characterization of Petroleum Asphaltenes and Maltenes"*, in ***Chemistry of Asphaltenes,*** Bunger, J.W. and Li, N.C., Ed. ***Adv. Chem. Ser.*** **195,** 137-153 (1981).

Hayden, T.F. and J.A. Dumesic, *"Studies of the Structure of Molybdenum Oxide and Sulfide Supported on Thin Films of Alumina"*, ***J. Catal.,*** **103,** 366-384 (1987).

Hazlett, R.N, *"Acid Base Phenomena in Distillate Fuel Stability"*, ***Fuel Sci. Tech. Int.*** **6(2),** 185-208 (1988).

Henry, C.P., *"Additives for Middle Distillate and Kerosine Fuels"*, in ***Proc. 2nd Int. Conf. on Long-term Storage Stabilities of Liquid Fuels,*** (ed. L.L. Stavinoha), San Antonio, Texas. 807-820 (1986).

Hermeler, G., J.C. Buhl and W. Hoffmann, *"The Influence of Carbonate on the Synthesis of an Intermediate Phase Between Sodalite and Cancrinite"*, ***Catal. Today*** **8,** 415-426, (1991).

Huckett, S.C., R.J. Angelici, M.E. Ekman and G.L. Schrader, *"Deuterium Exchange of Benzo[b]thiophene: Model Complex and Heterogeneous Reactor Studies"*, ***J. Catal.***, **113**, 36-44 (1988).

Hiley, R.W. and J.F. Pedley, *"Storage /stability of Petroleum-derived Diesel Fuel. 2. The Effect of Sulphonic Acids on the stability of Diesel Fuels and a Diesel Fuel Extract"*, ***Fuel***, **67**, 469-473 (1988).

Jiang, H.J., M.S. Tzou and W.H.M. Sachtler, *"Hydrogen Release from Ni/Faujasite Catalysts"*, ***Catal. Let.*** **1**, 99-108 (1988).

Jokuty, P.L. and M.R. Gray, *"Resistant Nitrogen Compounds in Hydrotreated Gas Oil from Athabasca Bitumen"*, ***Energy Fuels*** **5**, 791-795 (1991).

Katzer, J.R. and R. Sivasubramanian, *"Process and Catalyst Needs for Hydrodenitrogenation"*, ***Catal. Rev. - Sci. Eng.*** **20**, 155-208 (1979).

Kogan, V.M., A.A. Greish and G.V. Isagulyants, *"Investigation of the Promotion Effect on the Sulfide Sulfur Mobility and on the Catalytic Activity of Hydrotreating $Co/Mo/Al_2O_3$ Catalysts Using ^{35}S"*, ***Catal. Let.*** **6**, 157-162 (1990).

Kolboe, S. *"Catalytic Hydrodesulfurization of Thiophene. VII. Comparison Between Thiophene, Tetrahydrothiophene. and n-Butanethiol"*, ***Can. J. Chem.***, **47**, 352-355 (1969).

Kwart, H., G.C.A. Schuit and B.V. Gates, *"Hydrodesulfurazation of Thiophenic Compounds: The Reaction Mechanism"*, ***J. Catal.*** **61**, 128-134 (1980).

Langhout (van Zijll), W.C., C. Ouwerkerk and K.M.A. Pronk, *"Development of and Experience with the Shell Residue Hydrocracking"*, presented at the ***88th Nat. Meet. Am. Inst. Chem. Eng.*** Philadelphia, Penns.,**Manuscript # 4234 41C,** June (1980).

LINDE Molecular Sieve Catalysts Bulletin, *"Ion Exchange and Metal-Loading Procedures"*, **F-09**, Union Carbide Adsorbents & Catalysts.

Marcilly, C. and J.P. Franck, *"Use of Zeolite Containing catalysts in Hydrocracking"*, ***Catalysis by Zeolites,*** B. Imelik et al. Eds, Elsevier Scientific Publishing Company, Amsterdam, (1980).

Marshman, S.J., *"Storage Stability of Middle Distillate Fuels: Degradation Chemistry of Catalytically Cracked Gas Oil Blends"* , in ***Proc. 4th Int. Conf. on Stability and Handling of Liquid Fuels,*** (ed. L.L. Stavinoha), Orlando, Florida. 489-502 (1991).

Marshman, S.J.and J.F. Pedley, *"Storage Stability of Middle Distillate Fuels: a World-Wide Survey "*, in ***Proc. 4th Int. Conf. on Stability and Handling of Liquid Fuels,*** (ed. L.L. Stavinoha), Orlando, Florida. 331-339 (1991).

Minja, R.J.A. *"Hydrocracking Boscan Heavy Oil with Catalysts Containing a Zeolite Component"*, M.A. Sc Thesis submitted to University of Ottawa, Ottawa, Canada, (1990).

Minja, R.J.A. and M. Ternan, *"Effect of H-Modernite Zeolite as a Component in Co-Mo-Al_2O_3 Hydroprocessing Catalyst used for the Conversion of Boscan Heavy Oil"*, ***Fuel 70,*** (1991).

Minja, R.J.A. and M. Ternan, *"Hydrocracking Boscan Heavy Oil with a Co-Mo/Al_2O_3 Catalyst Containing an H-Modernite Zeolite Component"*, ***Energy Fuels,*** **5**, 117-122 (1991a).

Mirodatos, C., J.A. Dalmon, E.D. Garbowski and D. Barthomeuf, *"Reduction of Nickel in Mordenite and Silica Catalysts. Influence of Support and Pretreatment"*, ***Zeolites,*** **Vol 2,** 125-130 (1982).

Mojelsky, T.W., T.M. Ignasiak, Z. Frakman, D.D McIntyre, E.M. Lown, D.S. Montgomery and O.P. Strausz, *"Structural Features of Alberta Oil Sand Bitumen and Heavy Oil Asphaltenes"*, ***Energy Fuels,*** **6,** 83-96 (1992).

Moore, W.J. *"Physical Chemistry"*, **4th ed.**, Longman, London, (1966).

Mushrush, G.W., E.J. Beal, R.N. Hazlett and D.R. Hardy, *"Chemical Basis of Instability of Shale-Derived Middle Distillate Fuels: A Model Study of the Interactive Effects between 2,5-Dimethylpyrrole and 3-Methylindole with Sulfonic and Carboxylic Acids"*, ***Energy Fuels,*** **5,** 749-753 (1991).

Mushrush, G.W., D.R. Hardy, R.E. Pellenbarg and R.N. Hazlett, *"Middle Distillate Fuel Instability and Heteroatom Reactions"*, in ***Proc. 4th Int. Conf. on Stability and Handling of Liquid Fuels,*** (ed. L.L. Stavinoha), Orlando, Florida. 461-473 (1991).

Mushrush, G.W., R.N. Hazlett, R.E Pellenbarg and D.R. Hardy, *"Role of Sulfur Compounds in Fuel Instability: A Model Study of the Formation of Sulphonic Acids from Hexyl Sulfide and Hexyl Disulfide"*, ***Energy Fuels*** **5,** 258-262 (1991a).

Oelderik, J.M., S.T. Sie and D. Bode, *"Progress in the Catalysis of the Upgrading of Petroleum Residue - A Review of 25 Years of R&D on Shell's Residue Hydroconversion Technology"*, ***Appl. Catal.*** **47,** 1-24 (1989).

Ouwerkerk, C., P.B. Kwant, P.W.H.L. Tjan and F.M. Dautzenberg, *"Shell's Residue HDM/HCON Process"*, ***32nd Can. Chem. Eng. Conf.***, Vancouver, Canada, Oct 3-6, 664-684, (1982).

Palmer, L.D. and B.V. Copson, *"Hydrotreatment of Light Cycle Oil for Stabilization of Automotive Diesel Fuel"*, in ***Proc. 2nd Int. Conf. on Long-term Storage Stabilities of Liquid Fuels,*** (ed. L.L. Stavinoha), San Antonio, Texas. 902-914 (1986).

Pedley, J.F., L.A. Baranek, M.G. O'Connell and R.K. Solly, *"The Chemistry of Sediment Formation in Australian Middle Distillate Fuels"*, ***ACS Prepr., Div Fuel Chem.*** **35 No 4,** 1100-1116 (1990).

Pedley, J.F., R.W. Hiley and R.A. Hancock, *"Storage Stability of Petroleum-Derived Diesel Fuel. 3. Identification of Compounds Involved in sediment Formation"*, ***Fuel*** **67,** 1124-1130 (1988).

Pedley, J.F., R.W. Hiley and R.A.Hancock, *"Storage Stability of Petroleum-Derived Diesel Fuel. 4. Synthesis of Sediment Precursor Compounds and Simulation of Sediment Formation using Model Systems"* , ***Fuel*** **68,** 27-31 (1989).

Pereira, C.J., R.C. Donnelly and L.L. Hegedus, *"Design of Hydrodemetallation Catalysts"*, in ***Catalyst Deactivation,*** . E.E. Peterson and A.T. Bell, Eds, Marcel Dekker, New york, 315-351 (1987).

Perry, R.H., D.W. Green and J.O. Maloney, *"Perry's Chemical Engineering Handbook"*, 6th Ed.,(1984).

Prins, R., V.H.J. De Beer and G.A. Somorjai, G.A., *"Structure and Function of the Catalyst and the Promoter in C0-Mo Hydrodesulfurization Catalyst"*, ***Catal. Rev. - Sci. Eng.*** **32(1&2),** 1-41 (1989).

Quann, R.J., R.A. Ware, C.W. Hung and J. Wei, *"Catalytic Hydrodemetallization of Petroleum"*, ***Adv. Chem. Eng.*** **14,** 95-259 (1988).

Rakowski-Dubois, M., M.C. VanDerveer, D.L. DuBois, R.C. Haltiwanger and W.K. Miller, *"Characterization of Reactions of Hydrogen with Coordinated Sulfido Ligands"*, ***J. Am. Chem. Soc.,*** **102,** 7456-7461 (1980).

Ruthven, D.M., *"Principles of Adsorption"*, Wiley, N.Y. (1984).

Satterfield, C.N. and S.H. Yang, *"Catalytic Hydrodenitrogenation of Quinoline in a Trickle-Bed Reactor. Comparison with Vapour Phase Reaction"*, ***Ind. Eng. Chem. Proc. Des. Dev.*** **23,** 11-19 (1984).

Shreve, R.N. and J.A. Jr Brink, *"Petroleum Refining"*, in ***Chemical Process Industries,*** 4th ed., McGraw-Hill, New York, 652-686 (1977).

Smith, R.J. and L.D. Palmer, *"Automotive Diesel Fuel Stability- An Australian Viewpoint"*, in ***Proc. 2nd Int. Conf, on Long-term Storage Stabilities of Liquid Fuels,*** (ed. L.L. Stavincha), San Antonio, Texas. 875-886 (1986).

Suzuki. M., K. Tsutsumi and H. Takahashi, *"Characterization and Catalytic Activity of Nickel-Zeolite Catalysts. II. Effects of Hydroxyl Groups on Reduction of Nickel Ions in Mordenites"*, ***Zeolites*** **Vol 2,** 87-93 (1982).

Stirling, K.Q., J.B. Green and D.L. Ripley, *"Synergistic Effects in Middle Distillate Storage Stability"*, in ***Proc. 4th Int. Conf. on Stability and Handling of Liquid Fuels,*** (ed. L.L. Stavinoha), Orlando, Florida. 474-488 (1991).

Søgaard-Andersen, P., B.H. Cooper and P.N. Hannerup, *"Reducing Aromatics in Diesel Fuels"*, in ***Proc. 1992 NPRA Ann. Meet.*** **AM-92-50**, March 22-24 (1992).

Takatsuka, T., Y. Wada, H. Suzuki and S. Komatsu, *"Colour Degradation of Diesel Fuel in Deep Desulfurization"*, in ***Proc. 1991 NPRA Annual Meeting,*** **AM-91-39,** (1991).

Taylor, W.F. and J.W. Frankenfeld, *"Chemistry and Mechanism of Distillate Fuel Stability"*, in ***Proc. 2nd Int. Conf, on Long-term Storage Stabilities of Liquid Fuels,*** (ed. L.L. Stavinoha), San Antonio, Texas. 496-511 (1986).

Taylor, W.F. and T.J. Wallace, *"Kinetics of Deposit Formation from Hydrocarbon Fuels at High Temperatures"*, ***Ind. Eng. Chem. Prod. R&D,*** **6,** 258-262 (1967).

Ternan, M., *"Catalysis, Molecular Weight Change and Fossil Fuels"*, ***Can J. Chem. Eng.,*** **61,** 133-147 (1983).

Topsøe, H., B.S. Clausen, R. Candia. C. Wivel and S. Mørup *"In Situ Mössbauer Emission Spectroscopy Studies of Unsupported and Supported Sulfided Co-Mo Hydrodesulfurization Catalysts: Evidence for and Nature of a Co-Mo-S Phase"*, ***J. Catal.*** **68,** 433-452 (1981).

Topsøe, N.Y. and H. Topsøe, *"Characterization of the Structures and active sites in sulfided Co-Mo/Al_2O_3 and Ni-Mo/Al_2O_3 Catalysts by Chemisorption"*, ***J. Catal.*** **84,** 386-401 (1983).

Tort, F., B. Waegell, C. Bernasconi and L. Germanaud, *"Mechanistic Aspects of Oxidation Processes Involved in Colour and Sediment Formation during Ageing of LCO Containing Fuels"*, in ***Proc. 4th Int. Conf. on Stability and Handling***

of Liquid Fuels, (ed. L.L. Stavinoha), Orlando, Florida. 552-566 (1991).

Vázquez, M.I., A. Escardino and A. Corma, *"Activity and Selectivity of Ni-Mo/HY Ultrastable Zeolites for Hydroisomerization and Hydrocracking of Alkanes"*, **Ind. Eng. Chem. Res. 26,** 1495-1500 (1987).

Voorhoeve, R.J.H. , *"Electron Spin Resonance Study of Active Centres in Nickel-Tungsten Sulfide Hydrogenation Catalysts"*, **J. Catal. 23,** 236-242 (1971).

Voorhoeve, R.J.H. and J.C.M. Stuiver, *"Kinetics of Hydrogenation on Supported and Bulk Nickel-Tungsten Sulfide Catalysts"*, **J. Catal. 23,** 228-235 (1971).

Voorhoeve, R.J.H. and J.C.M. Stuiver, *"The Mechanism of the Hydrogenation of Cyclohexene and Benzene on Nickel-Tungsten Sulfide Catalysts"*, **J. Catal. 23,** 243-252 (1971b).

Ware, R.A. and J. Wei, *"Catalytic Hydrodemetallation of Nickel Porphyrins, I. Porphyrin Structure and Reactivity"*, **J. Catal. 93,** 100-121 (1985a).

Ware, R.A. and J. Wei, *"Catalytic Hydrodemetallation of Nickel Porphyrins, II. Effects of Pyridine and of Sulfiding"*, **J. Catal. 93,** 122-134 (1985b).

Ware, R.A. and J. Wei, *"Catalytic Hydrodemetallation of Nickel Porphyrins, III. Acid-Base Modification of Selectivity"*, **J. Catal. 93,** 135-151 (1985c).

Ware. R.A. and J. Wei, *"Hydrodemetallation Reaction Selectivity on Modified Co-Mo Catalysts"*, **Prepr. Am. Chem. Soc., Div. Petr. Chem. 30,** 62-69 (1985d) .

Weast, R.C., D.R. Lide, M.J. Astle and W.H. Beyer (Eds), *"CRC Handbook of Chemistry and Physics"*, CRC Press inc, **70th ed.** (1989).

Wentrcek, P.R. and H. Wise, *"Defect Control of Hydrogenation Activity of Molybdenum Sulfide Catalyst"*, **J. Catal. 45,** 349-355 (1976).

Wilson, M.F., and J. Kriz, *"Upgrading of Middle Distillate Fractions of a Syncrude from Athabasca Oil Sands"*, **Fuel 63,** 190-196 (1984).

Wilson, M.F., P.R. Mainwaring, J.R.K. Brown and J. F. Kriz, *"Large Pore Nickel/Silica-Alumina Catalysts for Hydrogenation of Synthetic Distillates. Effects of Composition and Structure"*, **Appl. Catal. 41,** 177-198 (1988).

Wivel, C., R. Candia, B.S. Clausen, S. Mørup and H. Topsøe, *"On the Catalytic Significance of a Co-Mo-S Phase in Co-Mo/Al_2O_3 Hydrodesulfurization Catalysts: Combined in Situ Mössbauer Emission Spectroscopy and Activity Studies"*, **J.**

Catal. **68,** 453-463 (1981).

Zhang, Z., W.M.H. Sachtler and S.L. Suib, *"Proximity Requirement for Pd Enhanced Reducibility of Co^{2+} in NaY"*, ***Catal. Let.*** **2,** 395-402 (1989).

Zhang, Z., Y.G. Yin and W.M.H. Sachtler, *"A Novel Preparation Method for Zeolite Encaged Co Clusters"*, ***Catal. Let.*** **18,** 73-79 (1993).

Zoltai T. and J.H. Stout, ***"MINERALOGY Concepts and Principles"***, Burgess Publishing Company, Minneapolis, Min. (1984).

APPENDIX A

SAMPLE CALCULATIONS

CONVERSION

The conversion is the percentage by weight of one species eliminated from the original feedstock. For sulphur, we have

$$HDS\ Conversion\ (\%) = \left(\frac{S_f - (S_p * liquid\ yield)}{S_f}\right) * 100\%$$

where S_f and S_p are the amount of sulphur present in the feed and in the product respectively. For example, using the sulphur content for the catalyst containing 0% Ni in sodalite and 10% sodalite in the Co-Mo catalyst on the first time-on-stream period θ = 3.5h - 4.25h, we obtain

$$HDS\ Conversion = \frac{\frac{3.74\ g\ of\ S}{100\ g\ feed} - \left(\frac{1.05\ g\ of\ S}{100\ g\ product} * \frac{0.91\ g\ liq\ product}{g\ feed}\right)}{\frac{3.74\ g\ of\ S}{100\ g\ feed}} * 100\%$$

$$= 74.45\ \%$$

Conversion data can be found in Appendix B, Tables B-12 to B-14

AREA TURNOVER FREQUENCY

The Area Turnover Frequency of a catalyst is a measure of the number of atoms of a certain species removed per unit of surface area.

$$ATOF\ (atoms\ \frac{converted}{nm^2.s}) = \frac{(\%\ Conversion)_{cat} * atoms\ fed\ /\ s}{Reactor\ load * SA}$$

ATOF calculation requires the conversion from the catalyst only which is obtained from the substraction the thermal conversion (reaction without catalyst) from the total conversion.

$$(\%\ Conversion)_{cat} = (\%\ Conversion)_{cat\ +\ therm} - (\%\ Conversion)_{therm}$$

Following the same example, we have

$$(\%\ Conversion)_{cat} = 74.45\ \% - 13.62\ \% = 60.83\ \%$$

and

$$ATOF\ (\frac{atoms\ converted}{nm^2.\ s}) = \frac{60.83\ g\ of\ S}{100 g\ of\ S_f} * \frac{3.74\ g\ S_f}{100\ g\ feed} * 160\ \frac{mL\ feed}{h}$$

$$* 0.998\ \frac{g\ feed}{mL\ feed} * \frac{1\ g\ cat}{281.6\ m^2\ *\ 50.4\ g\ cat} * \frac{1\ gmol\ S}{32\ g\ S}$$

$$* 6.023 * 10^{23}\ \frac{atoms}{gmol} * \frac{1\ m^2}{10^{18}\ nm^2} * \frac{1\ h}{3600\ s}$$

$$= 1.338\ * 10^{-3}\ \frac{atom\ removed}{nm^2\ .\ s}$$

ATOF data can be found in Appendix B, Tables B-15 to B-17

SURFACE AREA -- t-CURVE METHOD

The t-curve method to calculate the surface area was introduced by Shull who

developed an empirical formula to determine the statistical number of adsorbed nitrogen layers. The number of monolayers n is defined as

$$n = [\frac{5}{\ln(p^o / p)}]^{0.333}$$

where p^o is the saturated vapour pressure of N_2 and p is the partial pressure of N_2. The surface area calculated by the BET method can be verified by comparing the amounts adsorbed between 1.6 and 1.2 statistical monolayers

$$n = 1.6 \; ; \; p / p^o = 0.295$$
$$n = 1.2 \; ; \; p / p^o = 0.055$$

The t-curve surface area $(SA)_t$ is determined by

$$(SA)_t = \frac{(X_m)_t * N * SA_{N_2} * 10^{-20}}{MW}$$

where N = Avogadro's number, SA_{N2} is the surface area of a N_2 molecule, M is the molecular weight and

$$(X_m)_t = \frac{(amount\ adsorbed\ at\ n = 1.6) - (amount\ adsorbed\ at\ n = 1.2)}{0.4}$$

Using the isotherm for the same catalyst,

$$amount\ adsorbed\ at\ n = 1.6 = 89.754\ \frac{mL\ N_2}{g\ cat}$$

$$amount\ adsorbed\ at\ n = 1.2 = 58.406\ \frac{mL\ N_2}{g\ cat}$$

$(X_m)_t$ becomes

$$(X_m)_t = \frac{89.754\ \frac{mL\ N_2}{g\ cat} - 58.406\ \frac{mL\ N_2}{g\ cat}}{0.4} = 78.370\ \frac{mL\ N_2}{g\ cat}$$

and the t-curve surface area $(SA)_t$ is

$$(SA)_t = 78.370\ \frac{mL\ N_2}{g\ cat} * 6.023*10^{23}\ \frac{N_2}{gmol\ N_2} * 16.2*10^{-20}\ \frac{m^2}{N_2} * \frac{gmol}{22414\ mL}$$

$$= 341.16\ \frac{m^2}{g\ cat}$$

APPENDIX B

EXPERIMENTAL DATA

Table B-1 : **Ni Ion Exchange Experimental Data**

	sodalite sol'n		exchange sol'n			
exchange #	sodalite g	H_2O g	$Ni(NO_3)_2$ g	H_2O g	Ni wt %	H_2O : $Ni(NO_3)_2$
1	40.1	80.2	2.52	859.6	2.02%	341
2	41	80.4	2.485	800.1	1.95%	322
3	40	80.1	2.488	883.4	2.00%	355
4	40.1	80.5	2.46	838	1.97%	341
5	40	80.8	2.523	800.3	2.02%	317

Table B-2 : **Ni Impregnation**

Impregnation sol'n		total weight g	total volume mL	sol'n density g/mL	dry sodalite g	sol'n added g	Total % Ni in sodalite
$Ni(NO)_3$ g	H_2O g						
7.33	15	22.33	19.33	1.16	20	21.1	13.12
24.57	20	44.57	32.88	1.36	20	26.6	25.54
40.72	20	60.72	41.68	1.46	20	29.8	34.09
72.91	20	92.91	60.07	1.55	20	30.4	38.51
182	50	232	150.00	1.55	45	64.5	38.51
182	50	232	150.00	1.55	45	64.5	38.51
121.5	20	141.5	85.94	1.65	15	23.3	44.84

Table B-3 : **Potassium Ion Exchange**

		sodalite sol'n		exchange sol'n			
exchange #	% Ni in sodalite	sodalite g	H_2O g	KNO_3 g	H_2O g	K wt%	H_2O : KNO_3
1	13.12	20.8	42.7	2.1	700	3.90	333
2	25.54	23.1	52	2.4	723.5	4.01	301
3	34.09	23.6	39.4	2.4	773.1	3.93	322
4	38.51	25.4	50.6	2.6	798.8	3.95	307
5	38.51	35	70.3	3.5	950.8	3.86	272
6	38.51	35	70.1	3.5	950.2	3.86	271
7	38.51	34.9	70.2	3.5	966.6	3.87	276
8	44.84	18.7	37.4	1.9	951	3.92	501

Table B-4 : **Catalysts Preparation**

Ni	Sodalite	APM solution			CN solution		Al_2O_3	HNO_3	Diluted HNO_3	Oil Paste	
		APM	H_2O	NH_4OH	CN	H_2O		70%	25:1	Sodalite	Zerice
wt %	wt %	g	g	g	g	g	g	g	g	g	g
0	10.18	33.2	74	18.9	20.7	24.7	180	66	74.7	20	20
13.12	10.18	33.2	74	18.7	20.7	24.7	180	66.1	75	20	20
25.54	9.63	33.2	74	18.8	20.7	24.7	180	66	75	18.8	20
34.09	10.18	33.2	74	18.7	20.7	24.8	180	66.2	75.1	20	20
38.51	10.18	33.2	74	18.6	20.7	24.7	180	66.1	75.4	20	20
0	0	24.9	55.5	15	15.5	18.7	150	53.5	56.4	0	0
38.51	5.14	24.9	55.5	13.9	15.5	18.6	142.5	49.6	57.3	7.5	7.5
38.51	19.96	24.9	55.5	14	15.5	18.6	120	53.8	52.3	30	30.5
38.51	25.94	27.6	62.3	15.7	17.3	20.7	109.8	55	21.1	40.2	40.3
44.85	10	27.6	61.7	15.6	17.3	20.8	135	55.3	51.4	15	15

Table B-5 : **ASTM Colour of the Middle Distillate Fraction**

Days	0% Ni 10%	13% Ni 10%	26% Ni 10%	34% Ni 10%	39% Ni 10%	45% Ni 10%
0	1.0	1.0	2.0	1.5	L1.5	L1.0
1	1.5	L2.0	L3.0	2.0	L2.0	L2.0
2	2.5	L2.5	3.0		2.0	
3			3.0		L2.5	
4			L3.5	L3.0		L2.5
5		L3.0		3.0		2.5
6	L3.0	3.0		3.0	2.5	L3.0
7	3.0				2.5	L3.0
8				L3.5		
9		L3.5				
10					3.0	
11			44.0			
12	L3.5					
13						3.0
15				3.5		
16	L3.5	L3.5				
17					L3.5	
18			L4.5			
20						L3.5
22				L4.0		
23	3.5	3.5				
25			L4.5			
27					L3.5	L3.5
30	L4.0	4.0				
32				L4.5		

Days	0% Ni 10%	13% Ni 10%	26% Ni 10%	34% Ni 10%	39% Ni 10%	45% Ni 10%
34						L3.5
35			5.0		3.5	
37	4.0					
40		L4.5		4.5		
41						3.5
42					L4.0	
43			5.0			
44	4.0					
47				4.5		
48		L4.5				L4.0
50			5.0		4.0	
54	L4.5					
55		L4.5		5.0		L4.0
57					4.0	
58			L5.5			
62	L4.5			5.0		L4.0
63		L4.5				
64					4.0	
65			L5.5			
69	L4.5			5.0		
70		4.5				
71					L4.5	
72			L5.5			
76				5.0		
77	L4.5	4.5				

Days	0% Ni 10%	13% Ni 10%	26% Ni 10%	34% Ni 10%	39% Ni 10%	45% Ni 10%
78					L4.5	
79			L5.5			
83				L5.5		
84	L4.5	L5.0				
85					L4.5	
86			L5.5			
90				L5.5		
91	L4.5					
92		L5.0			L4.5	
93			L5.5			
97				L5.5		
98	L4.5					
99		L5.0				
100			L5.5			
105	L4.5					
106		L5.0				
112	L4.5					

* when an exact match is not possible, the next darker colour is used preceeded by the letter L.

Table B-5 : **ASTM Colour of the Middle Distillate Fraction** (cont'd)

Day	0% Ni 0%	39% 5%	39% Ni 10%	39% Ni 20%	39% Ni 26%	AC-1442B	No Catalyst
0	L1.5	L1.0	L1.5			1.0	L2.0 GY
1	L2.0	L1.5	L2.0	L1.0	L1.0	L1.5	5.5 DGY
2			2.0	L2.5 PO	L2.5	1.5	5.5 DGY
3			L2.5	L3.0 PO	2.5 PO		L7.0
4	L2.5	2.0			L3.5		
5	L2.5	L2.5				L2.0	
6	L2.5	L2.5	2.5	L3.5 PO		L2.0	7.5G
7		L2.5	2.5	L3.5 PO	L4.0 O		7.5G
8	2.5			L3.5 PO	L4.0	2.0	7.5G
9					L4.0		
10			3.0				
13		L3.0		L3.5		2.0	
14						L2.5	
15	L3.0						L8.0 DG
16				L3.5			
17			L3.5		L4.0		
19						2.5	
20		3.0					
22				3.5			8.0 DG
23					L4.5	2.5	
26	L3.5						
27		L3.5	L3.5				
29				3.5			
30					L4.5	L3.0	

Day	0% Ni 0%	39% 5%	39% Ni 10%	39% Ni 20%	39% Ni 26%	AC-1442B	No Catalyst
33	L3.5						
34		L3.5					
35			3.5				
37				3.5	L4.5	L3.0	
41	L4.0	L3.5					
42			L4.0				
43				3.5			
44					L4.5	3.0	
48	4.0 GY	3.5					
50			4.0	L4.0			
51					L4.5	3.0	
55	4.0	L4.0					
57			4.0	L4.0			
58					L4.5		
61						3.0	
62		L4.0					
63	L4.5						
64			4.0	L4.0	L4.5		
65							
69	L4.5	L4.0				L3.5	
71			L4.5				
72				L4.0			
76	L4.5	L4.0				L3.5	
78			L4.5				
83	L4.5						
84						L3.5	

Day	0% Ni 0%	39% 5%	39% Ni 10%	39% Ni 20%	39% Ni 26%	AC-1442B	No Catalyst
85			L4.5				
90	L4.5						
91						L3.5	
92			L4.5				
97	L5.0						
98						L3.5	
105						L3.5	
112						L3.5	
119						3.5	

PO : Pale Orange, GY : Grey Yellow, DG : Dark Grey, G : Grey, DGY : Dark Grey Yellow

* when an exact match is not possible, the next darker colour is used preceeded by the letter L.

Table B-6 : **Values of constants for colour formation equation** (120 days)

Ni/SOD	A1	A2	B1	B2
0/10	2.077	2.173	0.04141	0.5125
13/10	2.226	2.524	0.03143	1.024
26/10	2.545	2.705	0.05075	3.545
34/10	2.774	2.476	0.0363	1.47
39/10	2.197	2.053	0.03823	1.536
45/10	1.57	2.18	0.0594	1.434
0/0	2.819	1.931	0.0242	2.053
39/5	1.999	1.751	0.0475	1.07
39/10	2.197	2.053	0.03823	1.536
39/20	0.5502	3.2	0.031	0.4708
39/26	0.6345	3.615	0.07566	0.34
AC 1442B	1.921	1.579	0.02683	1.324
no Catalyst	7.752	0.2477	0.4481	0.02871

Table B-7 : **Values of constants for colour formation equation** (30 days)

Ni/SOD	A1	A2	B1	B2
0/10	1.411	2.339	0.05461	0.4535
13/10	1.605	2.395	0.06469	1.099
26/10	1.733	2.517	0.1343	12.96
34/10	1.893	2.357	0.07105	1.573
39/10	1.734	1.516	0.1563	262.1
45/10	1.821	1.429	0.1796	2518
0/0	1.542	1.708	0.08805	2.969
39/5	1.856	1.394	0.1036	1.452
39/10	1.734	1.516	0.1563	262.1
39/20	0.1641	3.336	0.0307	1.452
39/26	0.555	3.695	0.06533	0.3349
AC 1442B	1.53	1.22	0.08192	2.687

Table B-8 : **Analytical Results for Hydrocracking Experiments,** Whole product, θ = 3.5h - 4.25h, LHSV = 1.07

Nickel wt % in sodalite	Sodalite wt % in catalyst	Density kg/m^3	Carbon content wt%	Hydrogen content wt%	Nitrogen content wt%	Sulphur content wt%	Vanadium content ppm	Nickel content ppm	MCR wt%	H/C Ratio
0	10	946.4	86.8	11.5	0.41	1.05	38	21	7.39	1.59
13	10	945.4	87.2	11.7	0.29	1	32	20	7.61	1.61
26	10	948.5	86.9	11.7	0.34	1.26	42	24	8.17	1.62
34	10	942.6	87	11.6	0.29	1.16	38	23	7.55	1.60
39	10	941	87	11.9	0.27	0.9	24	16	6.95	1.64
45	10	948.6	86.7	11.6	0.31	1.26	40	22	7.99	1.61
0	0	945.1	86.4	11.8	0.27	1.47	72	36	9.64	1.64
39	5	948.6	86.7	11.8	0.34	1.35	58	37	9.22	1.63
39	10	941	87	11.9	0.27	0.9	24	16	6.95	1.64
39	20	948.2	86.9	11.9	0.31	1.28	37	26	8.11	1.64
39	26	952.9	86.7	11.6	0.35	1.33	34	24	8.69	1.61
No catalyst		989.4	85.1	10.6	0.37	3.55	138	63	14.4	1.49

Table B-9 : **Analytical Results for Hydrocracking Experiments,** Whole Product, θ = 5.8h - 9.8h, LHSV = 0.59

Nickel wt % in sodalite	Sodalite wt % in catalyst	Density kg/m^3	Carbon content wt%	Hydrogen content wt%	Nitrogen content wt%	Sulphur content wt%	Vanadium content ppm	Nickel content ppm	MCR wt%	H/C Atomic Ratio	IBP to 288°C wt%
0	10	933.2	86.9	12.1	0.21	0.82	14	11	5.93	1.67	10.8
13	10	933.3	86.8	12	0.21	0.66	19	16	5.8	1.66	9.6
26	10	936.6	86.7	11.8	0.23	0.9	27	18	6.54	1.63	10.6
34	10	932.7	86.8	12	0.2	0.74	23	16	6.16	1.66	10.1
39	10	929.3	86.9	12.1	0.2	0.5	13	10	5.17	1.67	9.9
45	10	932.4	86.9	12.1	0.21	0.82	11	8	6.45	1.67	8.9
0	0	928.2	86.2	12.3	0.19	1.19	58	29	8.53	1.71	15.2
39	5	934.4	86.6	12	0.21	1.14	42	23	7.1	1.66	10.4
39	10	929.3	86.9	12.1	0.2	0.5	13	10	5.17	1.67	9.9
39	20	929.7	86.9	11.8	0.26	1.02	29	22	7.58	1.63	6
39	26	939.1	87	11.9	0.26	1	16	13	7.35	1.64	7.2
AC 1442B		918.4	87.4	12.6	0.15	0.2	12	4	3.19	1.73	9.2
No catalyst		983.4	85.1	10.6	0.37	3.39	131	57	14.4	1.49	9.4
Feedstock		998.1	84.4	11.4	0.45	3.74	123	57	13.4	1.62	1

Table B-10 : **Analytical Results for Hydrocracking Experiments,** Product Fractions, θ = 5.8h - 9.8h. LHSV = 0.59

Catalyst		Diesel fraction (288°C - 343°C)				Residue (+343°C)					
Nickel wt % in sodalite	Sodalite wt % in catalyst	Weight fraction %	Density kg/m^3	Nitrogen content ppm	Sulphur content wt%	Weight fraction %	Density kg/m^3	Sulphur content wt%	Vanadium content ppm	Nickel content ppm	MCR wt%
0	10	6.63	886	673	0.1	82	954.5	0.84	19	15	7.67
13	10	7.12	887	672	0.094	82.9	952.5	0.8	23	34	7.52
26	10	6.75	887.9	597	0.16	82.5	958.6	1.08	33	20	8.44
34	10	7.77	888.7	529	0.14	81.8	940.4	0.9	28	35	7.65
39	10	7.64	888.1	544	0.076	82.2	949.1	0.66	15	12	7.07
45	10	8.68	879.9	602	0.1	81.9	955	0.89	26	16	8.09
0	0	8	884.4	226	0.113	76.4	960.1	1.41	76	72	10.4
39	5	10.12	881.5	379	0.12	79	960.7	1.28	55	31	9.41
39	10	7.64	888.1	544	0.076	82.2	949.1	0.66	15	12	7.07
39	20	8.32	881	667	0.14	84	965.2	1.15	34	25	10.1
39	26	8.21	881.4	834	0.18	84.1	962	1.08	19	21	9.18
AC 1442B		10.33	884.8	468	0.051	80.2	934.6	0.22	15	17	3.75
No catalyst		7.1	900.6	509	2.55	83	1013.8	3.48	158	69	18.1
Feedstock		2.7	898.6	156	1.89	96.6	1002.6	3.9	133	59	14.2

Table B-11: **Analytical Results for Hydrocracking Experiments,** Whole product, θ = 11.8h - 12.5h, LHSV = 1.07

Nickel wt % in sodalite	Sodalite wt % in catalyst	Density kg/m^3	Carbon content wt%	Hydrogen content wt%	Nitrogen content wt%	Sulphur content wt%	Vanadium content ppm	Nickel content ppm	MCR wt%	H/C Ratio
0	10	950.9	86.7	11.7	0.34	1.35	38	23	8.88	1.62
13	10	948.4	86.8	11.8	0.36	1.25	39	24	8.41	1.63
26	10	950.7	86.8	11.6	0.34	1.41	45	25	8.54	1.60
34	10	947.4	86.7	11.7	0.3	1.32	43	31	8	1.62
45	10	949.1	86.7	11.7	0.31	1.37	41	24	8.46	1.62
0	0	949.6	86.2	11.8	0.29	1.71	79	39	10.2	1.64
39	5	950.7	86.3	11.6	0.28	1.64	62	32	9.1	1.61
39	20	954.9	86.5	11.7	0.35	1.5	43	27	8.98	1.62
39	26	956.4	86.3	11.6	0.43	1.65	38	26	9.35	1.61

Table B-12 : **Conversion of Feedstock Components,** Whole product, θ = 3.5h - 4.25h, LHSV = 1.07

Nickel wt % in sodalite	Sodalite wt % in catalyst	Nitrogen conversion %	Sulphur conversion %	Vanadium conversion %	Nickel conversion %	MCR conversion %
0	10	17.09	74.45	71.89	66.47	49.81
13	10	41.36	75.67	76.33	68.07	48.32
26	10	31.24	69.34	68.93	61.68	44.52
34	10	41.36	71.78	71.89	63.28	48.73
39	10	45.40	78.10	82.24	74.46	52.80
45	10	37.31	69.34	70.41	64.88	45.74
0	0	45.40	64.23	46.73	42.53	34.53
39	5	31.24	67.15	57.09	40.93	37.39
39	10	45.40	78.10	82.24	74.46	52.80
39	20	37.31	68.86	72.63	58.49	44.92
39	26	29.22	67.64	74.85	61.68	40.99
No catalyst		25.18	13.62	-2.10	-0.58	2.21

Table B-13: **Conversion of Feedstock Components,** Whole Product, time-on-stream θ = 5.8h - 9.8h, LHSV = 0.59

Nickel wt % in sodalite	Sodalite wt % in catalyst	Nitrogen conversion %	Sulphur conversion %	Vanadium conversion %	Nickel conversion %	MCR conversion %
0	10	57.53	80.05	89.64	82.44	59.73
13	10	57.53	83.94	85.94	74.46	60.61
26	10	53.49	78.10	80.02	71.26	55.59
34	10	59.56	81.99	82.98	74.46	58.17
39	10	59.56	87.83	90.38	84.04	64.89
45	10	57.53	80.05	91.86	87.23	56.20
0	0	61.58	71.05	57.09	53.70	42.07
39	5	57.53	72.26	68.93	63.28	51.78
39	10	59.56	87.83	90.38	84.04	64.89
39	20	47.42	75.18	78.54	64.88	48.52
39	26	47.42	75.67	88.16	79.25	50.09
AC 1442B		69.67	95.13	91.12	93.61	78.34
No catalyst		25.18	17.52	3.08	9.00	2.21

Table B-14 : **Conversion of Feedstock Components,** Whole product, θ = 11.8h - 12.5h, LHSV = 1.07

Nickel wt % in sodalite	Sodalite wt % in catalyst	Nitrogen conversion %	Sulphur conversion %	Vanadium conversion %	Nickel conversion %	MCR conversion %
0	10	31.24	67.15	71.89	63.28	39.70
13	10	27.20	69.59	71.15	61.68	42.89
26	10	31.24	65.69	66.71	60.09	42.00
34	10	39.33	67.88	68.19	50.51	45.67
45	10	37.31	66.67	69.67	61.68	42.55
0	0	41.36	58.39	41.55	37.74	30.73
39	5	43.38	60.10	54.13	48.91	38.20
39	20	29.22	63.50	68.19	56.89	39.02
39	26	13.04	59.85	71.89	58.49	36.50

Table B-15 : **Area Turnover Frequency,** Whole product, θ = 3.5h - 4.25h, LHSV = 1.07

Nickel wt % in sodalite	Sodalite wt % in catalyst	N atoms removed/ nm^2*s	S atoms removed/ nm^2*s	V atoms removed/ nm^2*s	Ni atoms removed/ nm^2*s	MCR removed/ nm^2*s
0	10	-2.45e-05	1.34e-03	2.65e-06	1.23e-06	1.00e-02
13	10	4.04e-05	1.13e-03	2.94e-06	1.04e-06	8.00e-03
26	10	1.80e-05	1.20e-03	3.16e-06	1.11e-06	8.70e-03
34	10	4.92e-05	1.29e-03	3.38e-06	1.17e-06	9.82e-03
39	10	4.71e-05	1.09e-03	2.95e-06	1.06e-06	8.19e-03
45	10	3.10e-05	1.04e-03	2.79e-06	1.01e-06	7.73e-03
0	0	5.09e-05	9.26e-04	1.85e-06	6.55e-07	5.65e-03
39	5	1.67e-05	1.07e-03	2.45e-06	6.92e-07	6.74e-03
39	10	4.71e-05	1.09e-03	2.95e-06	1.06e-06	8.19e-03
39	20	2.98e-05	9.88e-04	2.76e-06	8.77e-07	7.30e-03
39	26	1.10e-05	1.07e-03	3.15e-06	1.02e-06	7.33e-03

Table B-16 : **Area Turnover Frequency,** Whole product, θ = 5.8h - 9.8h, LHSV = 0.59

Nickel wt % in sodalite	Sodalite wt % in catalyst	N atoms removed/ nm^2*s	S atoms removed/ nm^2*s	V atoms removed/ nm^2*s	Ni atoms removed/ nm^2*s	MCR removed/ nm^2*s
0	10	5.38e-05	7.57e-04	2.16e-06	7.38e-07	6.65e-03
13	10	4.45e-05	6.64e-04	1.71e-06	5.43e-07	5.58e-03
26	10	4.61e-05	7.17e-04	1.88e-06	6.12e-07	6.04e-03
34	10	5.74e-05	7.84e-04	2.01e-06	6.61e-07	6.50e-03
39	10	4.40e-05	6.55e-04	1.68e-06	5.81e-07	5.58e-03
45	10	4.55e-05	6.39e-04	1.88e-06	6.65e-07	5.28e-03
0	0	5.04e-05	5.39e-04	1.12e-06	3.74e-07	3.83e-03
39	5	4.91e-05	6.04e-04	1.50e-06	4.98e-07	5.23e-03
39	10	4.40e-05	6.55e-04	1.68e-06	5.81e-07	5.58e-03
39	20	3.01e-05	5.67e-04	1.53e-06	4.56e-07	4.35e-03
39	26	3.33e-05	6.33e-04	1.91e-06	6.35e-07	4.98e-03
AC 1442B		4.47e-05	5.67e-04	1.33e-06	5.14e-07	5.31e-03

Table B-17 : **Area Turnover Frequency,** Whole product, θ = 11.8h - 12.5h, LHSV = 1.07

Nickel wt % in sodalite	Sodalite wt % in catalyst	N atoms removed/ nm^2*s	S atoms removed/ nm^2*s	V atoms removed/ nm^2*s	Ni atoms removed/ nm^2*s	MCR removed/ nm^2*s
0	10	1.84e-05	1.18e-03	3.36e-06	1.17e-06	7.88e-03
13	10	5.05e-06	1.02e-03	2.75e-06	9.40e-07	7.06e-03
26	10	1.80e-05	1.12e-03	3.06e-06	1.08e-06	8.18e-03
34	10	4.30e-05	1.20e-03	3.21e-06	9.38e-07	9.18e-03
45	10	2.83e-05	8.99e-04	2.51e-06	8.76e-07	6.53e-03
0	0	4.14e-05	8.33e-04	1.68e-06	5.92e-07	5.07e-03
39	5	4.58e-05	8.50e-04	2.12e-06	7.52e-07	6.29e-03
39	20	1.12e-05	1.00e-03	2.91e-06	9.58e-07	7.06e-03
39	26	-2.83e-05	7.83e-04	2.59e-06	8.31e-07	5.55e-03

Table B-18 : **Chemisorbtion on laboratory prepared catalysts**

Ni content in Ni-SOD (wt%)	Ni-SOD in catalyst (wt%)	% Chemisorbed
39	5	0.175
39	10	0.29
39	20	0.177
39	26	0.24

Table B-19 : **Content Ratio for Hydrocracking Product Fractions,** θ = 5.8h - 9.8h, LHSV = 0.59

Catalyst		Diesel fraction (288°C-343°C)		Residue (+343°C)			
Nickel wt % in sodalite	Sodalite wt % in catalyst	Nitrogen content ratio	Sulphur content ratio	Sulphur content ratio	Vanadium content ratio	Nickel content ratio	MCR content ratio
0	10	4.31	0.05	0.22	0.14	0.25	0.54
13	10	4.31	0.05	0.21	0.17	0.58	0.53
26	10	3.83	0.08	0.28	0.25	0.34	0.59
34	10	3.39	0.07	0.23	0.21	0.59	0.54
39	10	3.49	0.04	0.17	0.11	0.20	0.50
45	10	3.86	0.05	0.23	0.20	0.27	0.57
0	0	1.45	0.06	0.36	0.57	1.22	0.73
39	5	2.43	0.06	0.33	0.41	0.53	0.66
39	10	3.49	0.04	0.17	0.11	0.20	0.50
39	20	4.28	0.07	0.29	0.26	0.42	0.71
39	26	5.35	0.10	0.28	0.14	0.36	0.65
AC 1442B		3.00	0.03	0.06	0.11	0.29	0.26
No catalyst		3.26	1.35	0.89	1.19	1.17	1.27

Table B-20 : **Physical Properties of Used Catalysts**

Chemical Composition						
Ni-SOD (wt%)	10.2	10.2	9.6	10.2	10.2	10.2
Nickel in Ni-SOD (wt%)	0	13.1	25.5	34.1	38.5	44.8
Deposits						
Vanadium (ppm)	2880	2506	2990	2686	2044	3267
Nickel (ppm)	1411	754	1407	1679	1817	4345
Carbon (wt%)	13.2	12.9	13.1	13.3	10.6	11.7
Physical Properties						
BET Specific Surface Area SA_{BET} (m^2/g)	182.2	170.1	165.7	163.6	171.7	187.2
t-curve Surface Area $(SA)_t$ (m^2/g)	201.2	204.3	193.8	191.6	200.9	210.2
Total Pore Area SA_{Hg} (m^2/g)	126.6	129.9	132.0	124.6	152.1	147.9
Total Pore Volume V_p (mL/g)	0.2674	0.4113	0.2690	0.3759	0.4233	0.2978
Average Pore Diameter (nm)	8.4	12.7	8.4	12.1	11.1	8.1
Bulk Density (g/mL)	1.0164	1.1678	1.1876	1.2075	1.2193	1.38
Skeletal Density (g/mL)	1.3958	2.2469	1.7451	2.2109	2.5196	2.343
Porosity (%)	27.18	48.03	31.94	45.38	51.61	41.1

Table B-21 : **Physical Properties of Used Catalysts** (cont'd)

Chemical Composition						AC-1442B
Ni-SOD (wt%)	0	5.1	10.2	20.0	25.9	0
Nickel in Ni-SOD (wt%)	0	38.5	38.5	38.5	38.5	0
Deposits						
Vanadium (ppm)	2636	2792	2044	2343	2549	945
Nickel (ppm)	933	1352	1817	1506	2267	761
Carbon (wt%)	4.6	8.2	10.6	11.2	8.9	19.4
Physical Properties						
BET Specific Surface Area SA_{BET} (m^2/g)	171.9	200.4	171.7	154.5	141	181.9
t-curve Surface Area $(SA)_t$ (m^2/g)	183.0	219.2	200.9	164.0	153.9	214.7
Total Pore Area SA_{Hg} (m^2/g)	101.7	154.9	152.1	118.3	107.5	127.2
Total Pore Volume V_p (mL/g)	0.3439	0.3207	0.4233	0.3505	0.4014	0.3890
Average Pore Diameter (nm)	13.5	8.3	11.1	11.8	14.9	12.2
Bulk Density (g/mL)	1.2959	1.3360	1.2193	1.3057	1.1984	1.1736
Skeletal Density (g/mL)	2.3376	2.3373	2.5196	2.4072	2.3096	2.1594
Porosity (%)	44.56	42.84	51.61	45.76	48.11	45.65

APPENDIX C

LANGMUÏR ISOTHERMS

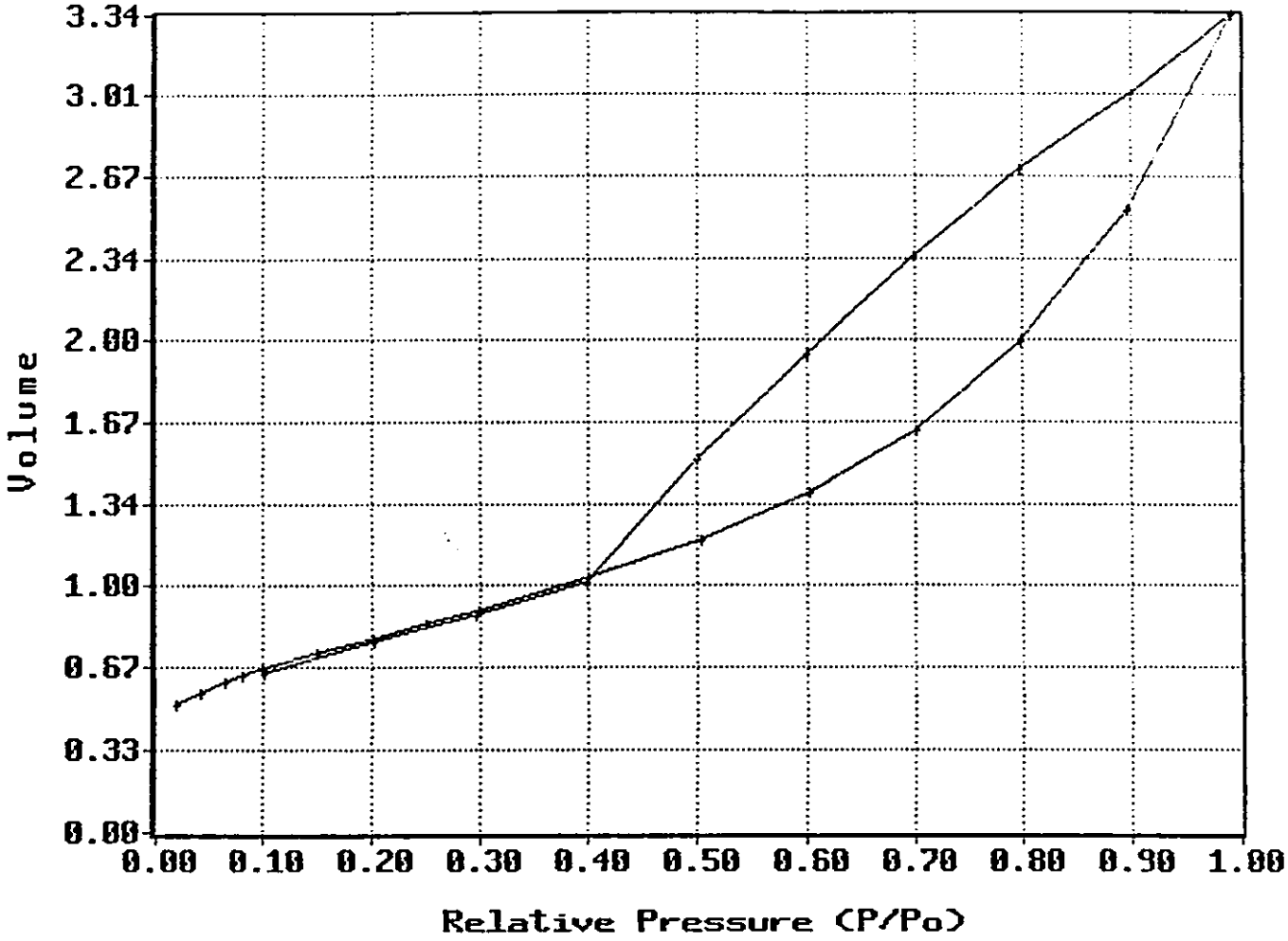

Figure C-1 : **Langmuïr Isotherm. Nitrogen adsorption volume (X 10^2 cm^3/g cat) versus relative pressure (P/P^o)** Co-Mo catalyst containing 10% sodalite and 0% impregnated Ni in the sodalite.

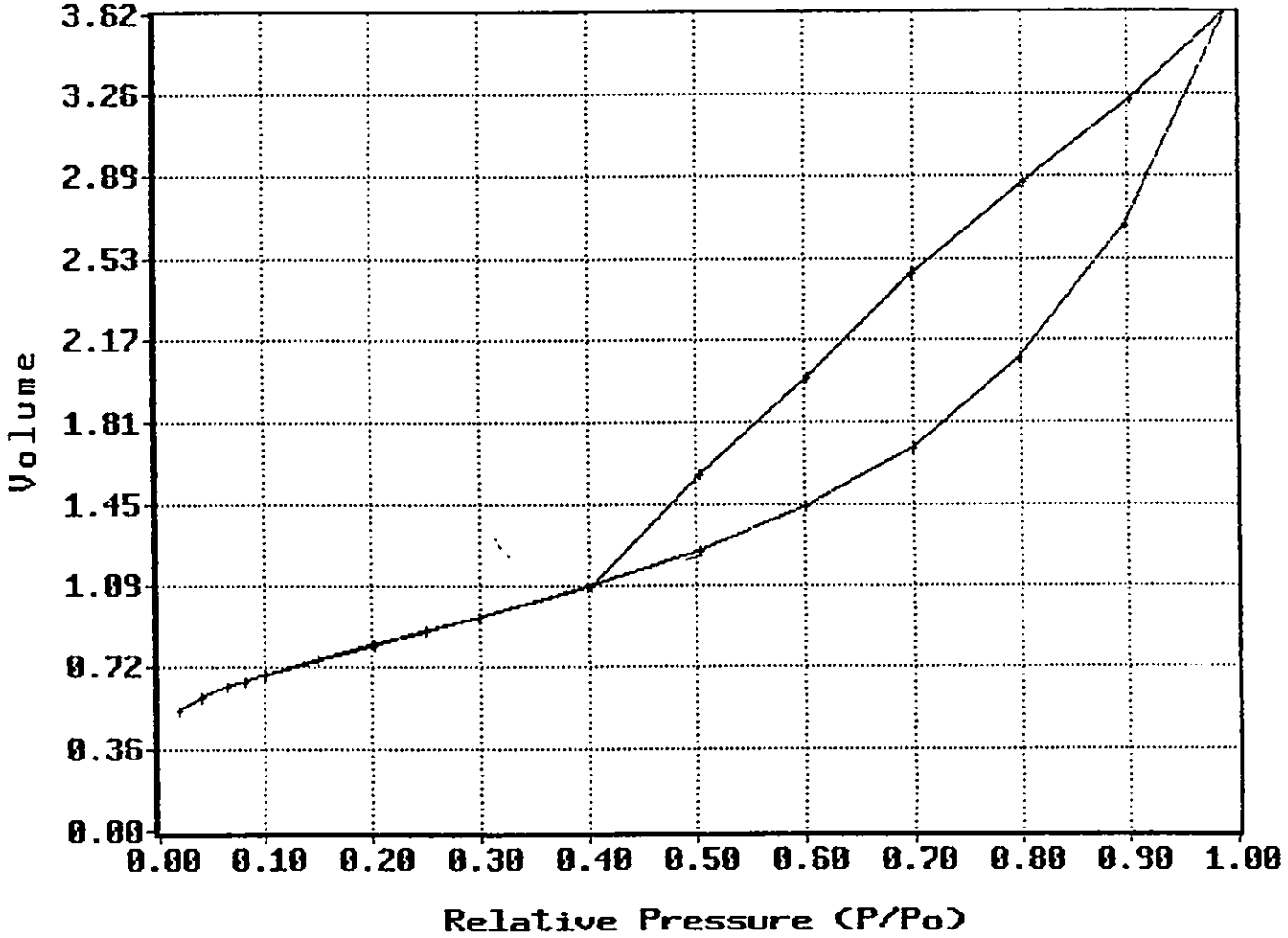

Figure C-2 : **Langmuïr Isotherm. Nitrogen adsorption volume (X 10^2 cm^3/g cat) versus relative pressure (P/P^o)** Co-Mo catalyst containing 10% sodalite and 13% impregnated Ni in the sodalite.

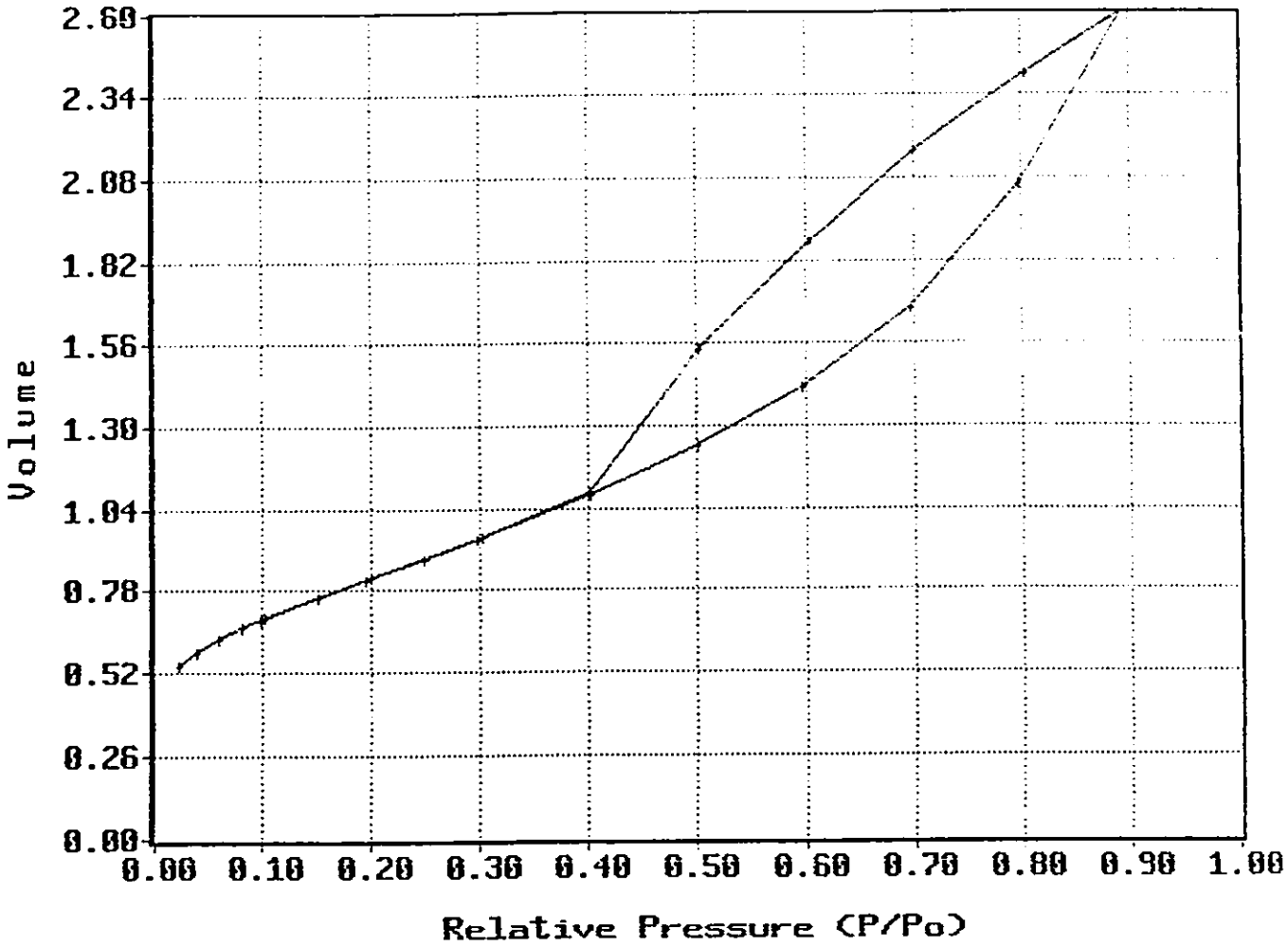

Figure C-3 : **Langmuïr Isotherm. Nitrogen adsorption volume (X 10^2 cm^3/g cat) versus relative pressure (P/P^o)** Co-Mo catalyst containing 10% sodalite and 26% impregnated Ni in the sodalite.

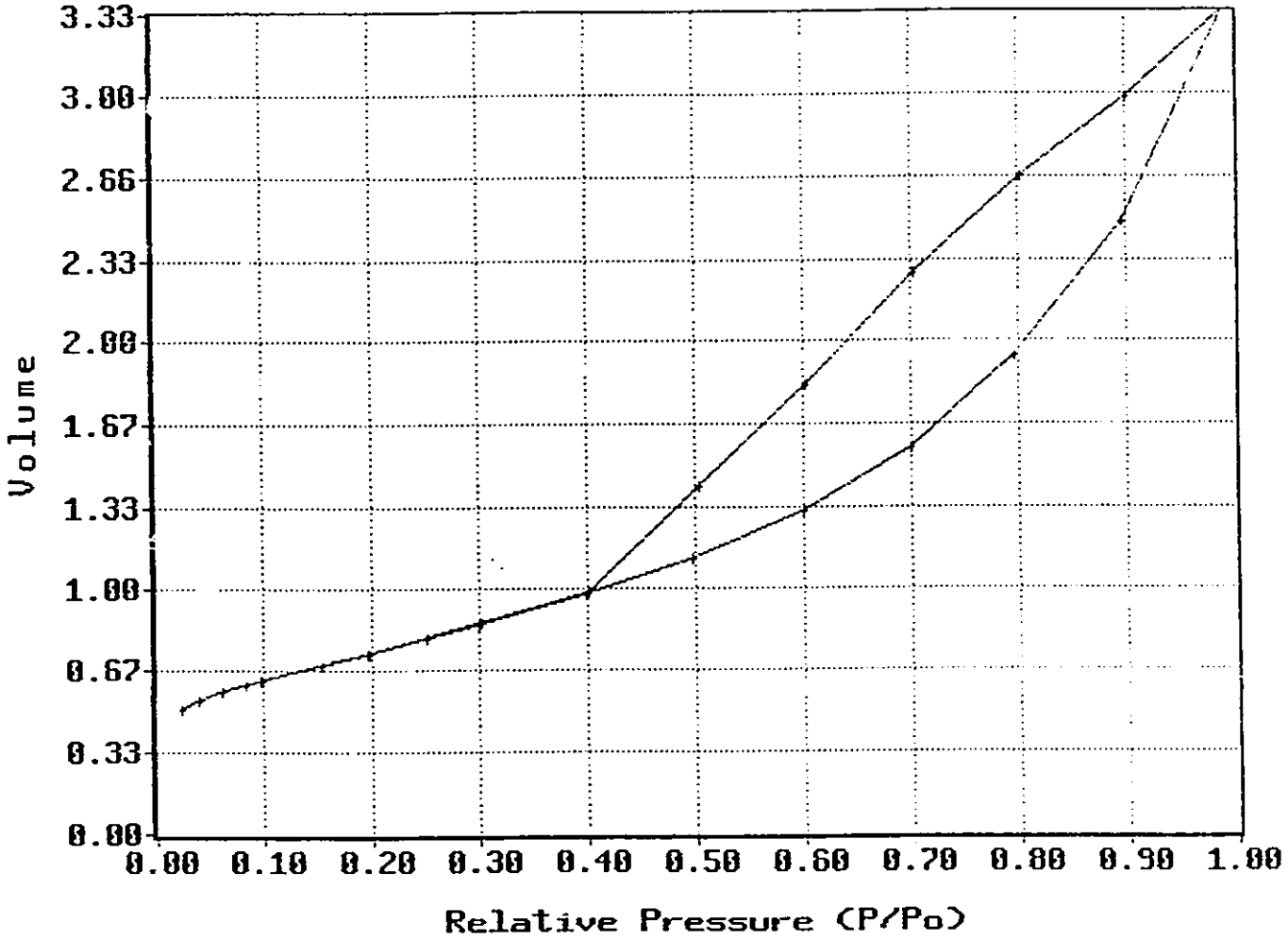

Figure C-4 : **Langmuïr Isotherm. Nitrogen adsorption volume (X 10^2 cm^3/g cat) versus relative pressure (P/P^o)** Co-Mo catalyst containing 10% sodalite and 34% impregnated Ni in the sodalite.

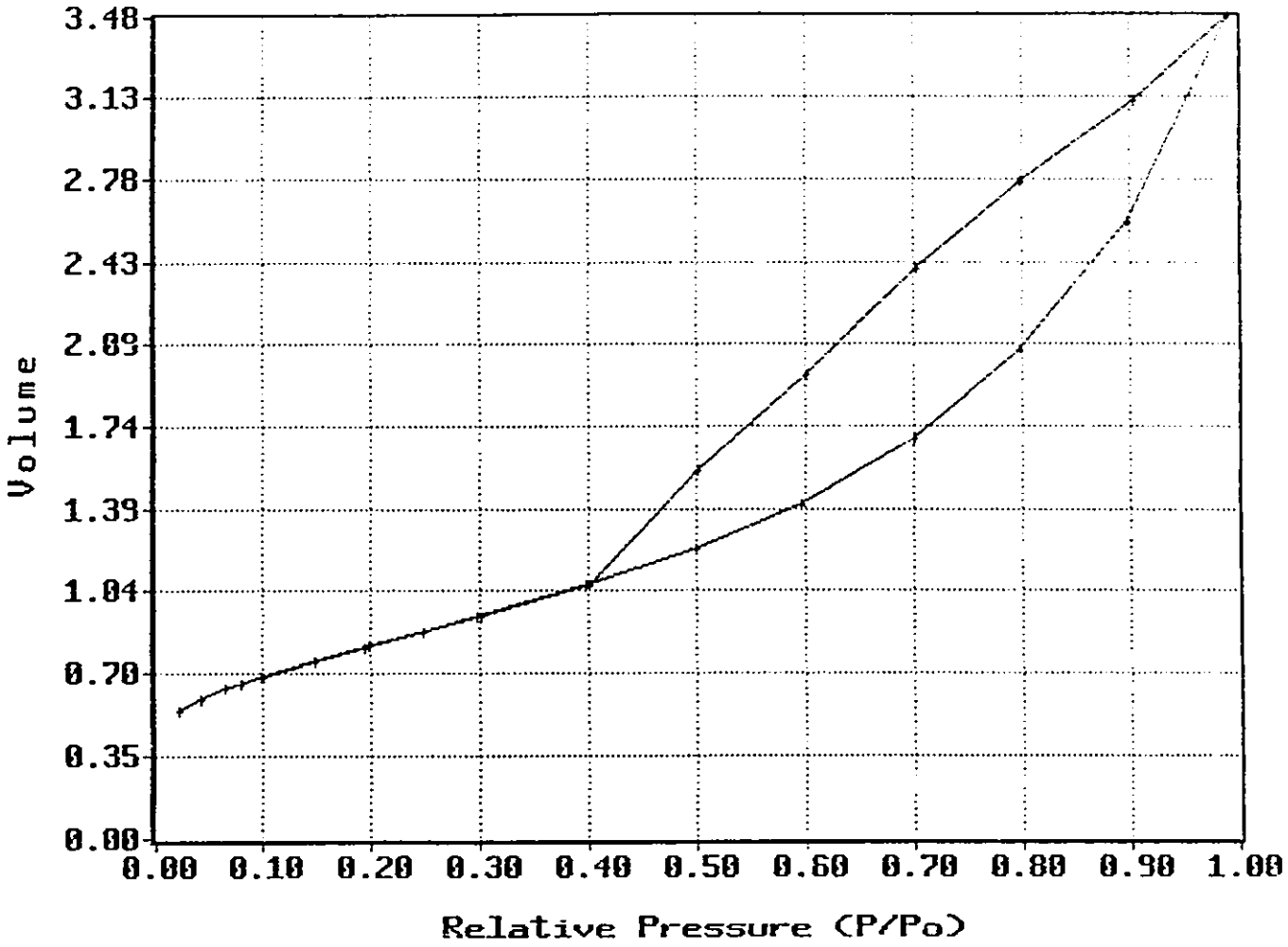

Figure C-5 : **Langmuïr Isotherm. Nitrogen adsorption volume (X 10^2 cm^3/g cat) versus relative pressure (P/P^o)** Co-Mo catalyst containing 10% sodalite and 39% impregnated Ni in the sodalite.

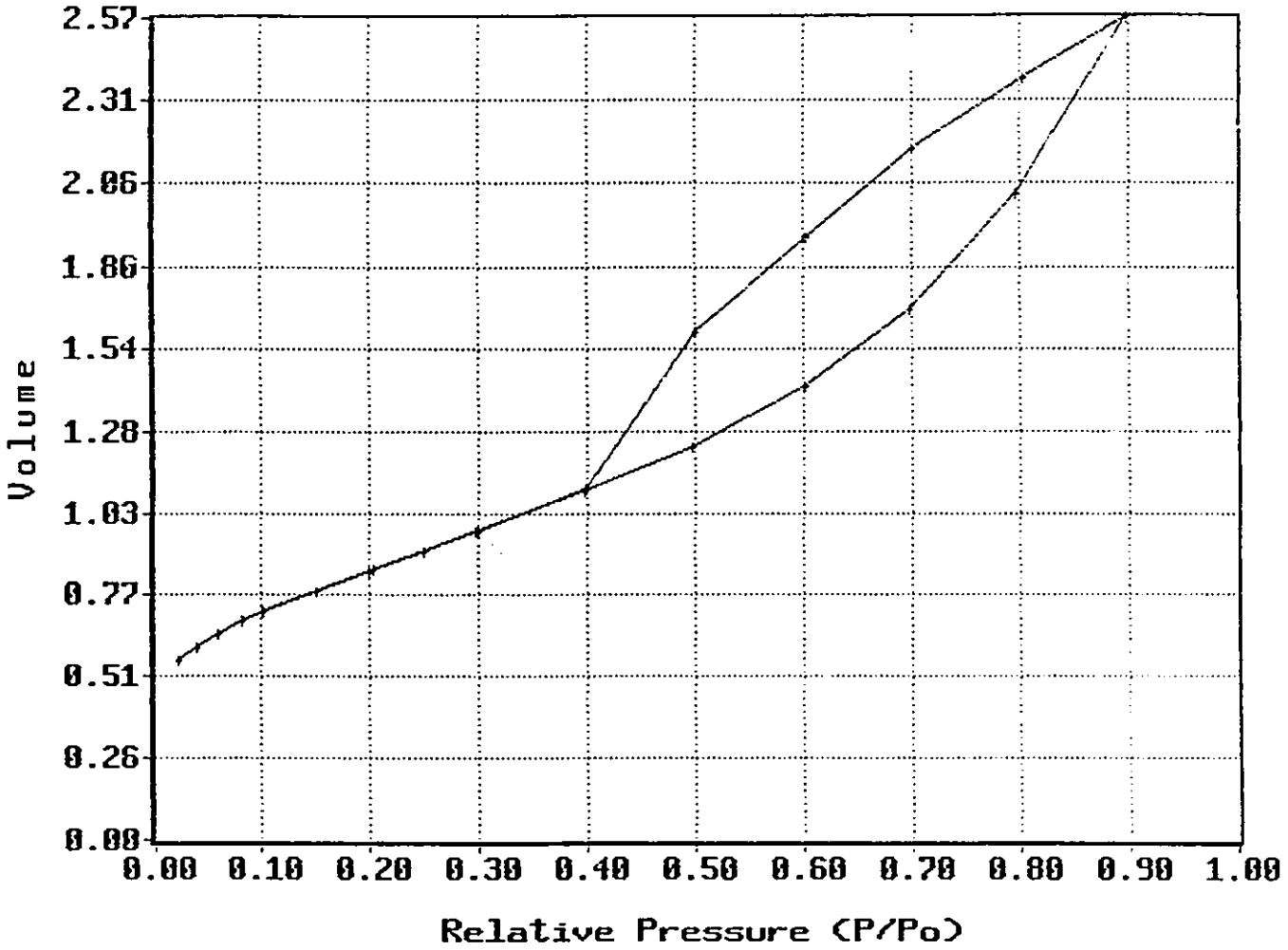

Figure C-6 : **Langmuïr Isotherm. Nitrogen adsorption volume (X 10^2 cm^3/g cat) versus relative pressure (P/P^o)** Co-Mo catalyst containing 10% sodalite and 45% impregnated Ni in the sodalite.

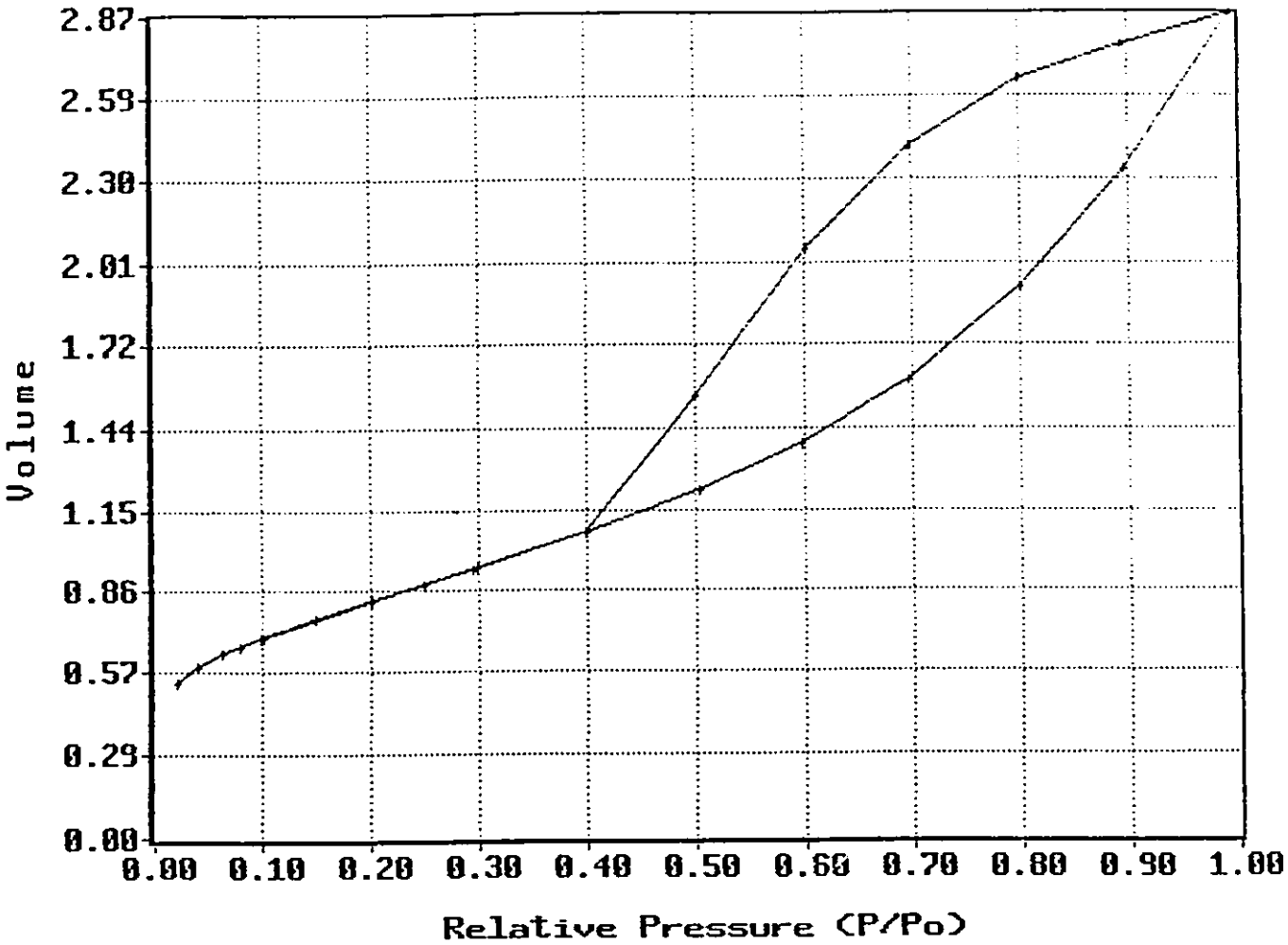

Figure C-7 : **Langmuïr Isotherm. Nitrogen adsorption volume (X 10^2 cm^3/g cat) versus relative pressure (P/P^o)** Co-Mo catalyst containing 0% sodalite and 0% impregnated Ni in the sodalite.

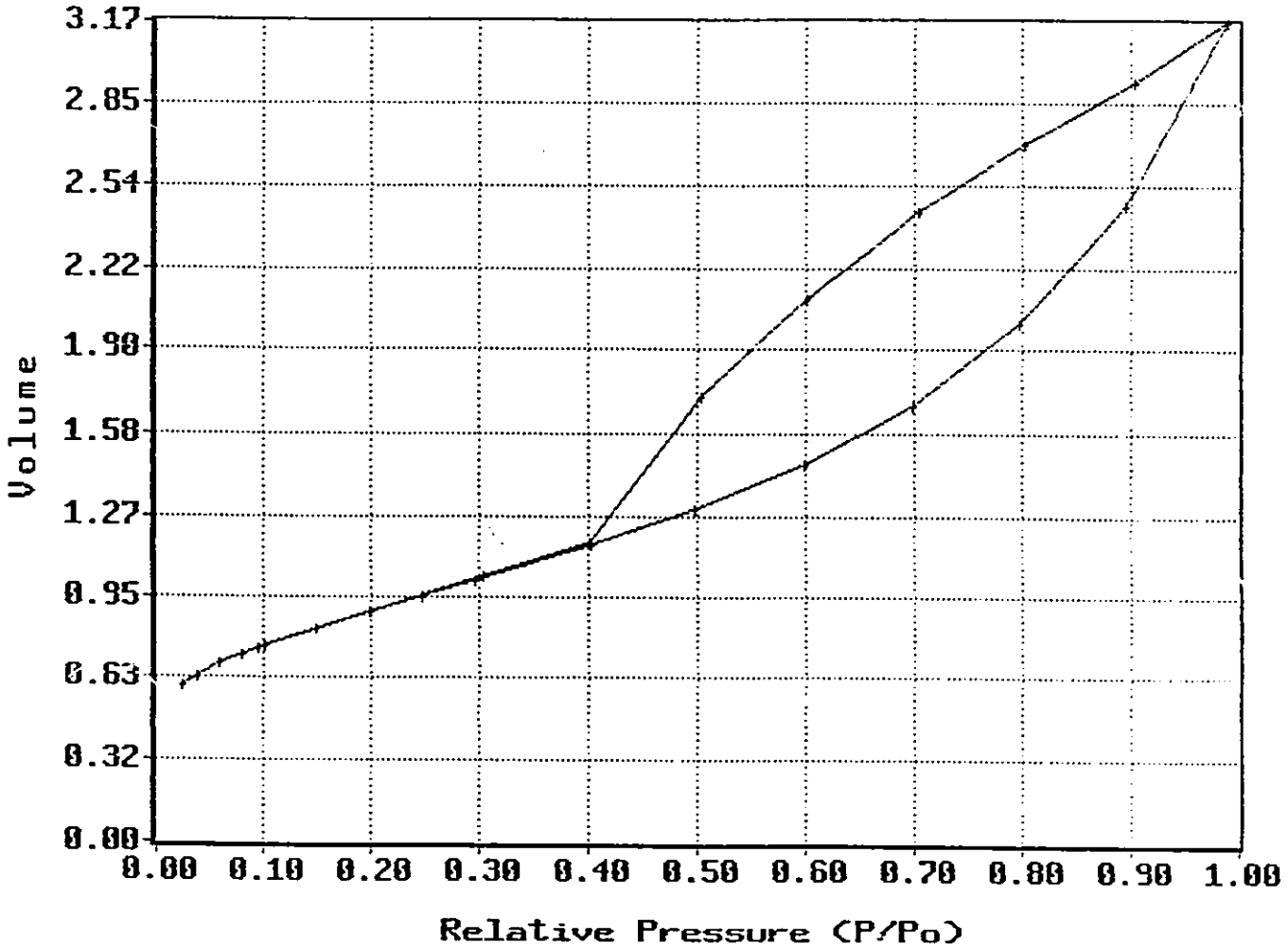

Figure C-8 : **Langmuïr Isotherm. Nitrogen adsorption volume (X 10^2 cm^3/g cat) versus relative pressure (P/P^o)** Co-Mo catalyst containing 5% sodalite and 39% impregnated Ni in the sodalite.

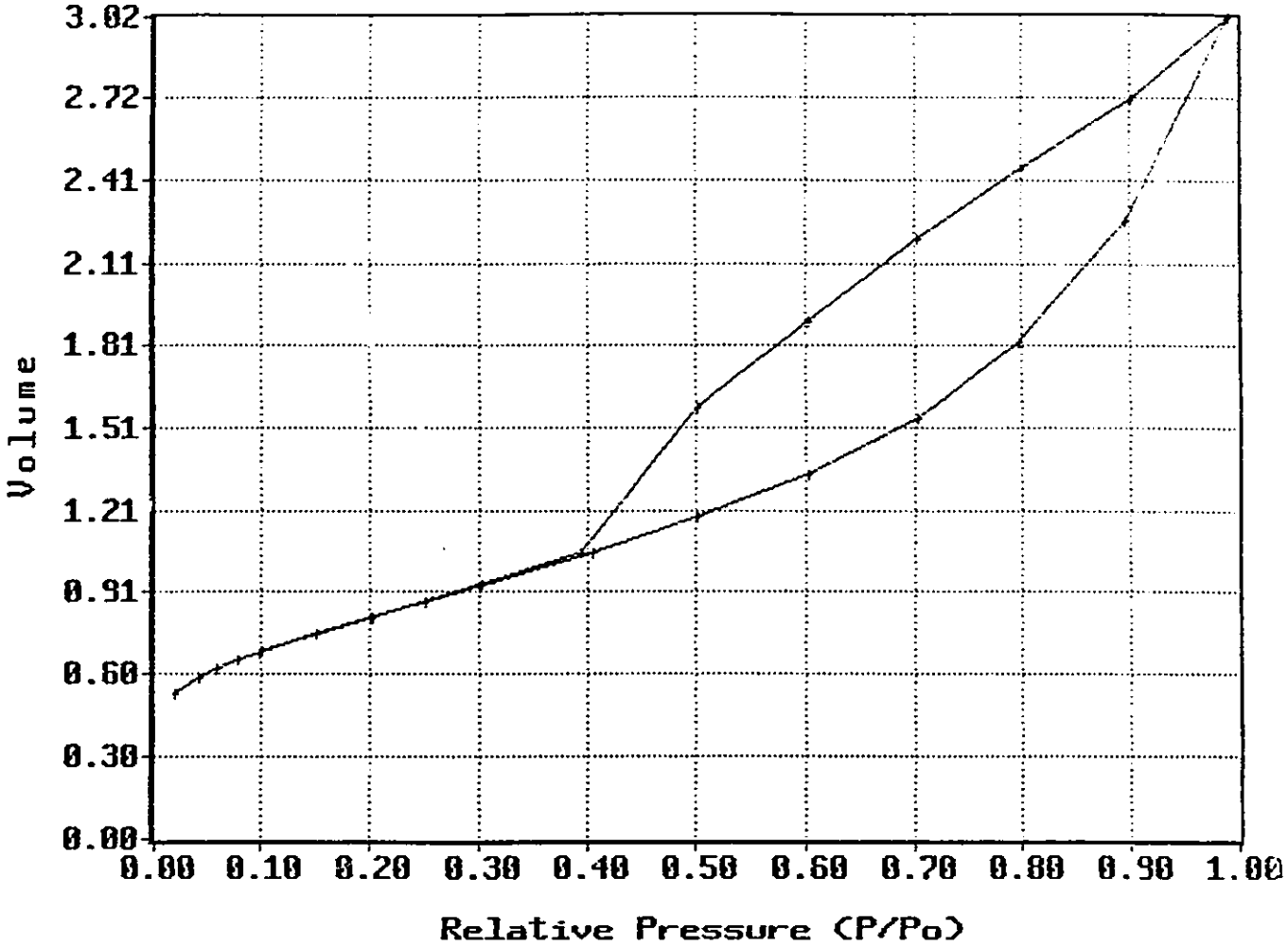

Figure C-9 : **Langmuïr Isotherm. Nitrogen adsorption volume (X 10^2 cm^3/g cat) versus relative pressure (P/P^o)** Co-Mo catalyst containing 20% sodalite and 39% impregnated Ni in the sodalite.

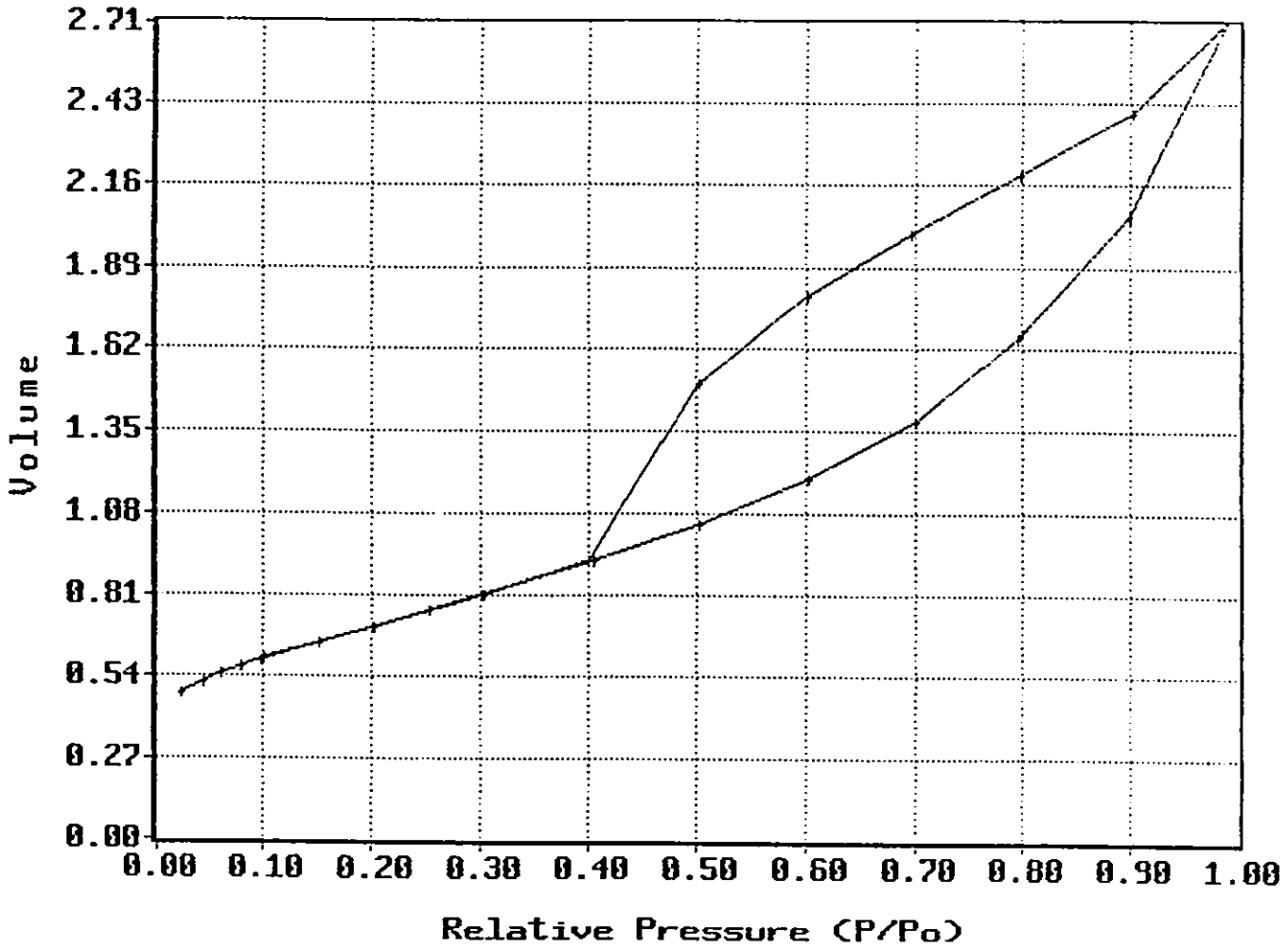

Figure C-10 : **Langmuïr Isotherm. Nitrogen adsorption volume (X 10^2 cm^3/g cat) versus relative pressure (P/P^o)** Co-Mo catalyst containing 26% sodalite and 39% impregnated Ni in the sodalite.

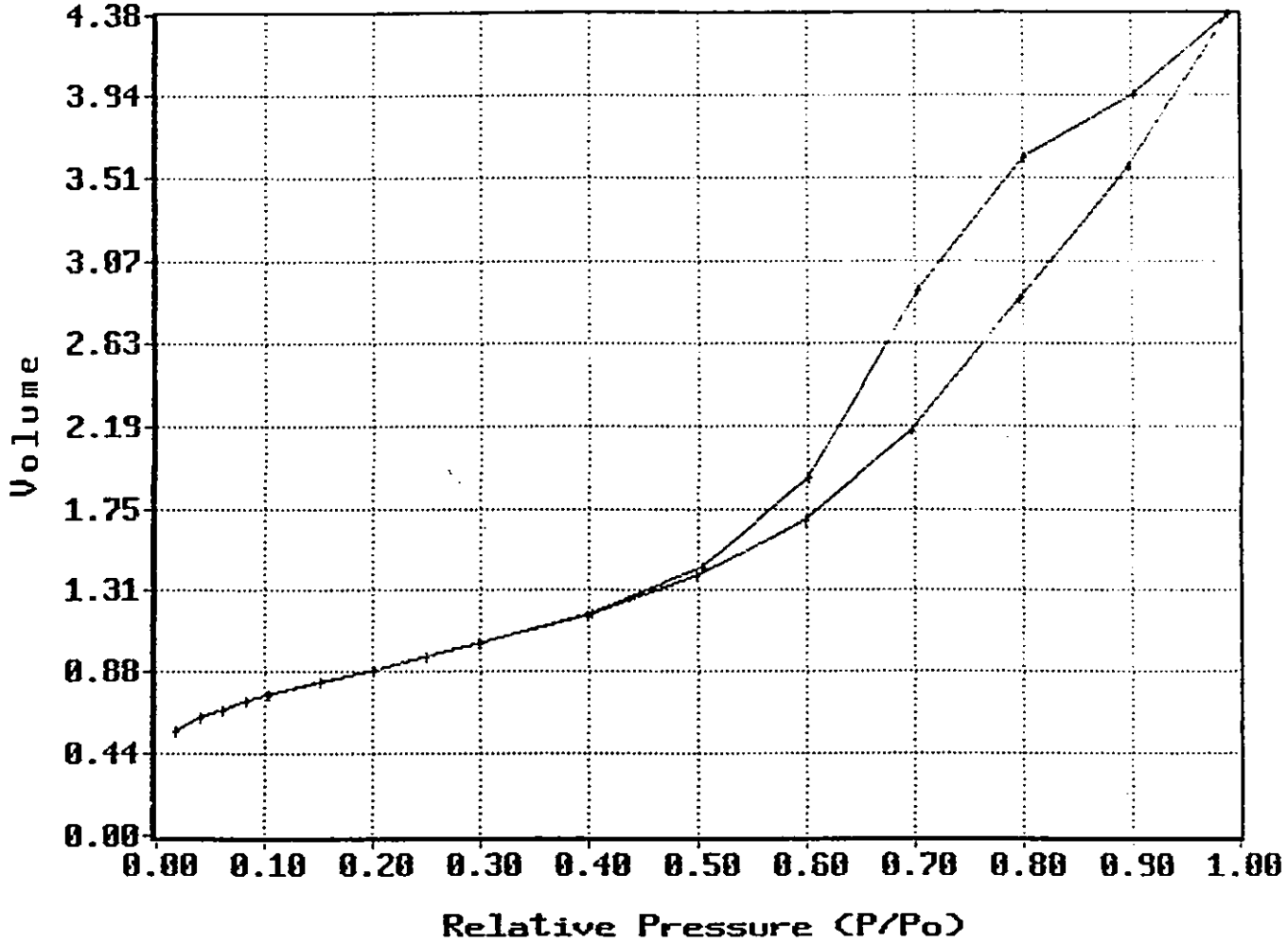

Figure C-11 : **Langmuïr Isotherm. Nitrogen adsorption volume (X 10^2 cm^3/g cat) versus relative pressure (P/P^o)** Reference AC-1442B catalyst.

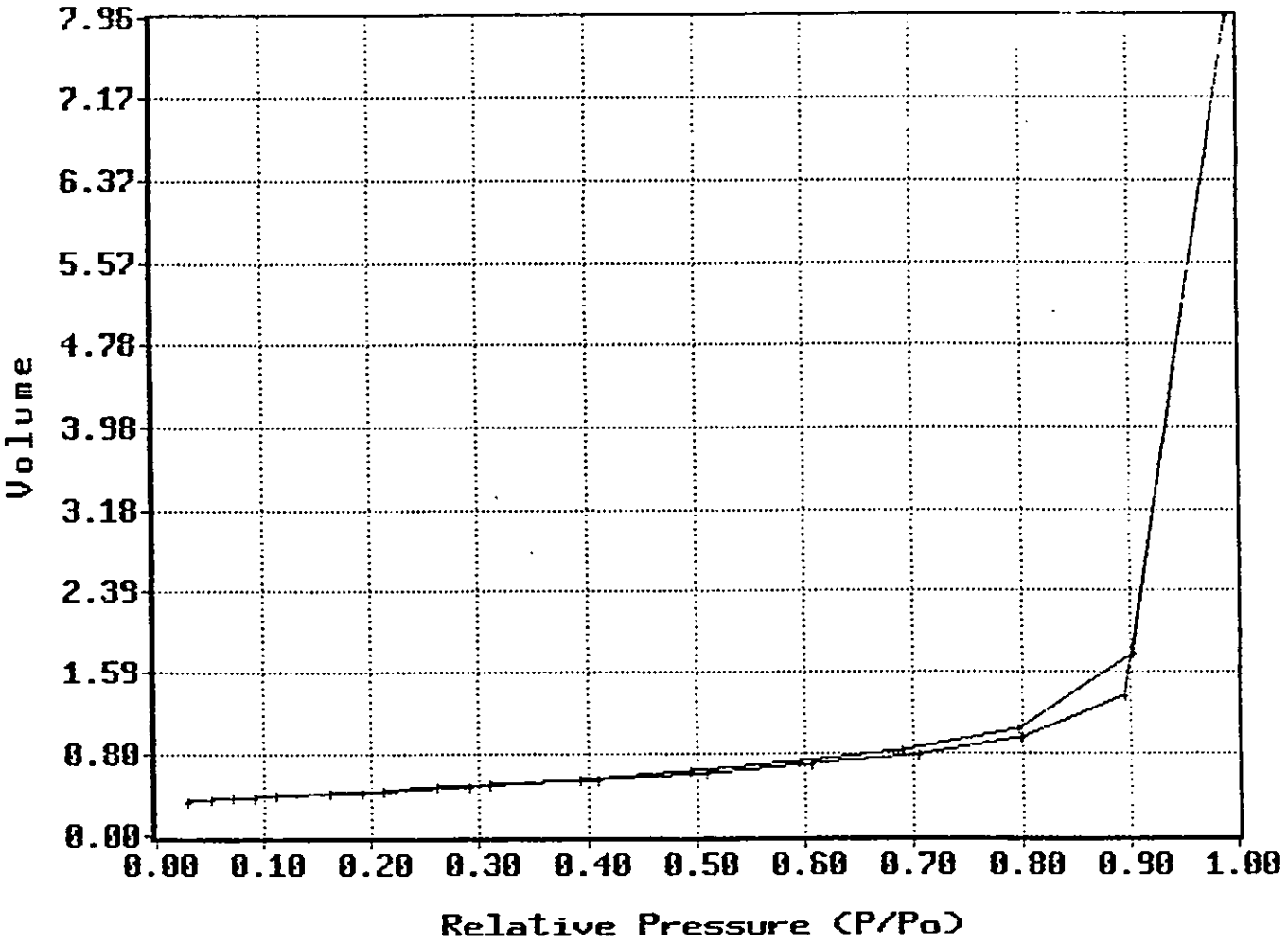

Figure C-12 : **Langmuïr Isotherm. Nitrogen adsorption volume (X 10^2 cm^3/g cat) versus relative pressure (P/P^o)** 100% sodalite.

APPENDIX D

MERCURY POROSIMETRY

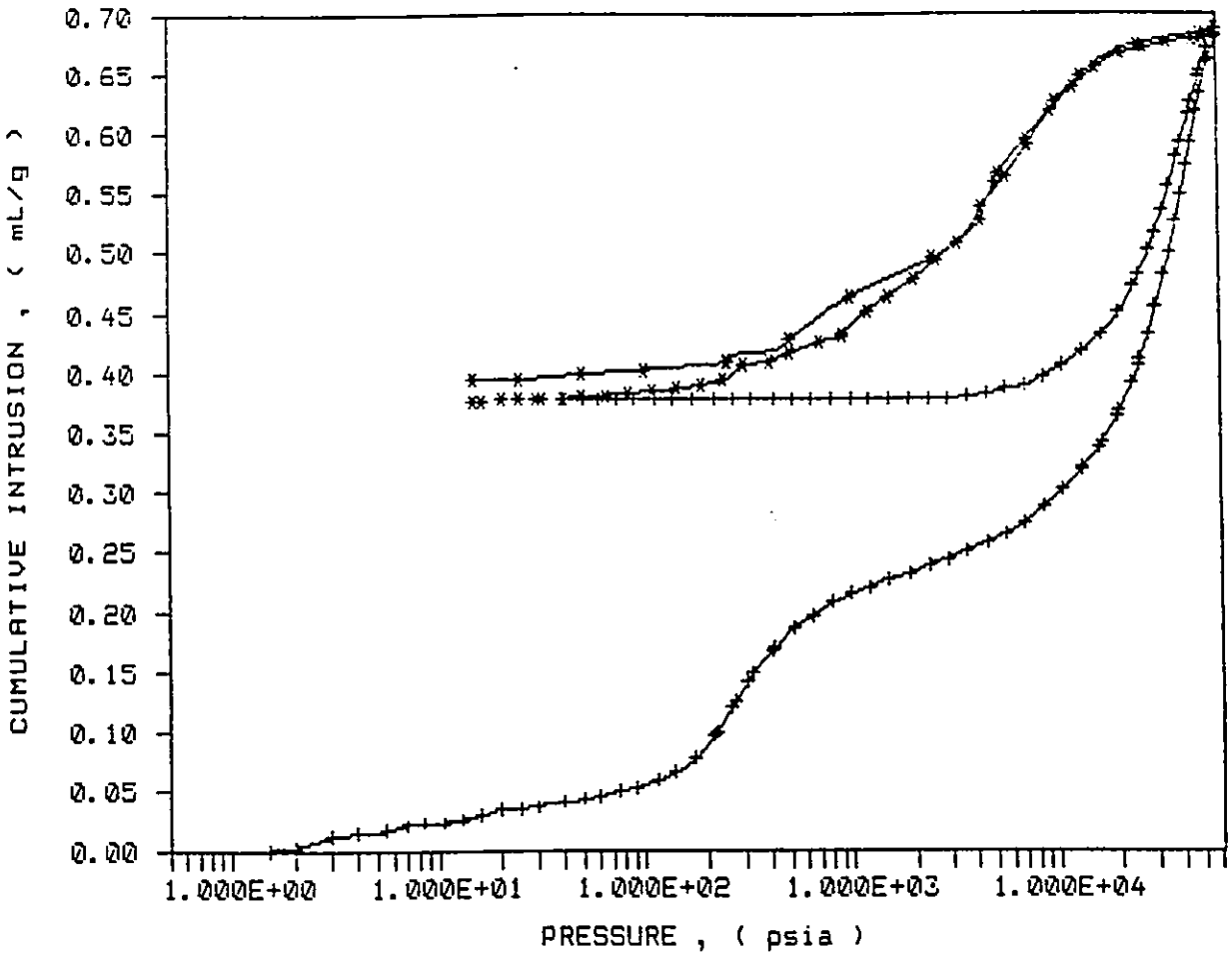

Figure D-1 : **Cumulative mercury intrusion volume (mL/g) versus pressure (psia).** Fresh catalyst containing 0% impregnated Ni in SOD and 10% SOD in the Co-Mo catalyst.

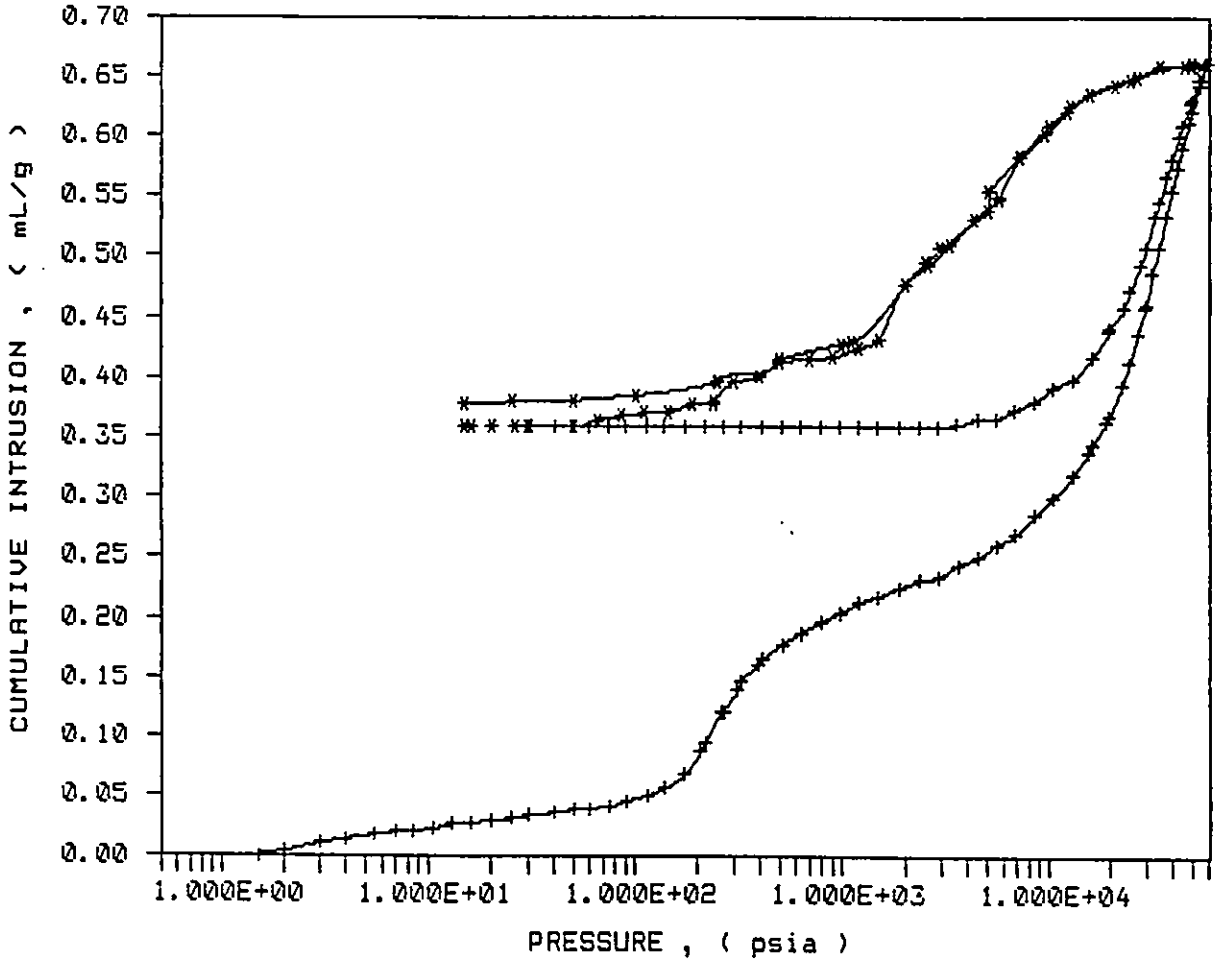

Figure D-2 : **Cumulative mercury intrusion volume (mL/g) versus pressure (psia).** Fresh catalyst containing 13% impregnated Ni in SOD and 10% SOD in the Co-Mo catalyst.

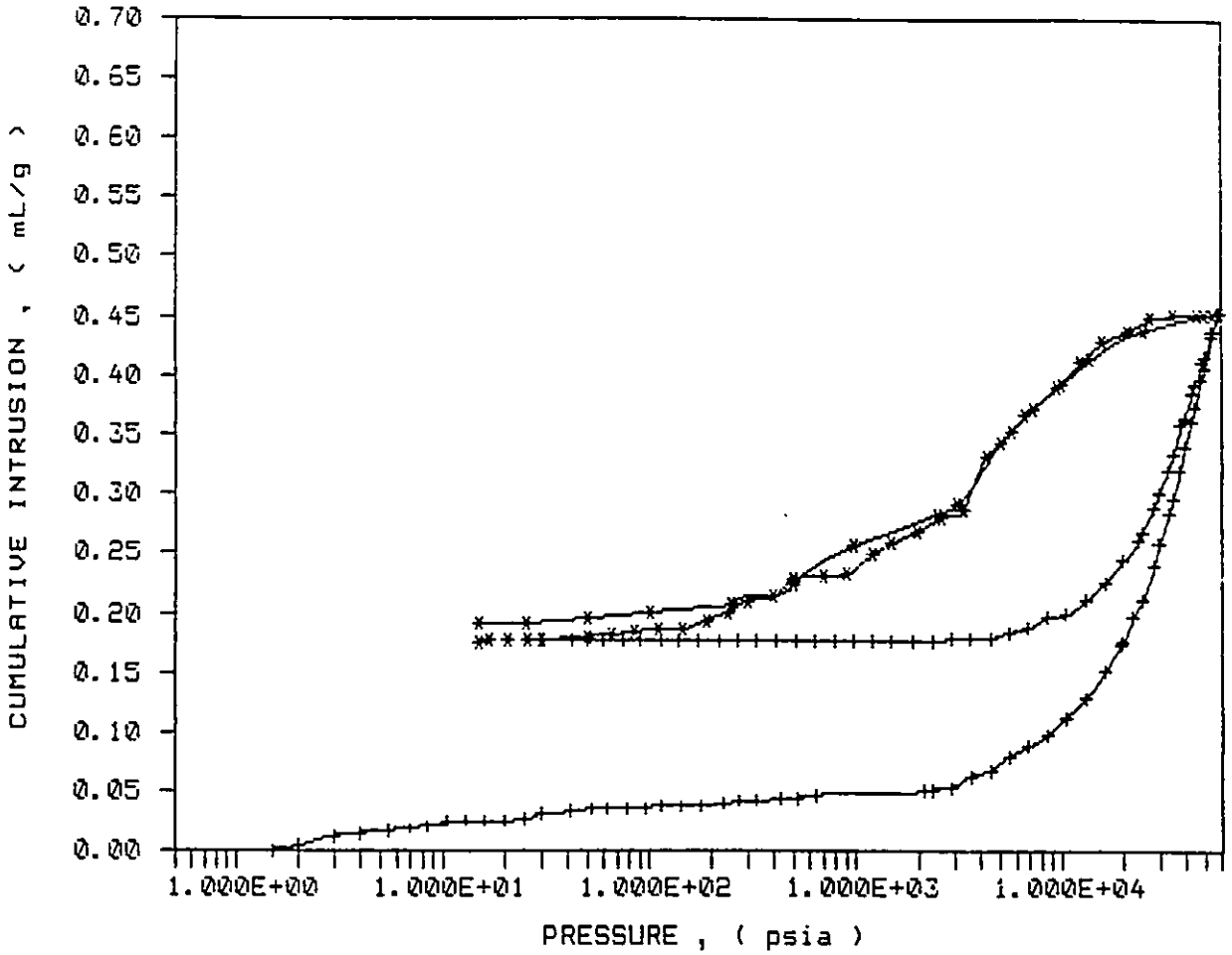

Figure D-3 : **Cumulative mercury intrusion volume (mL/g) versus pressure (psia).** Fresh catalyst containing 26% impregnated Ni in SOD and 10% SOD in the Co-Mo catalyst.

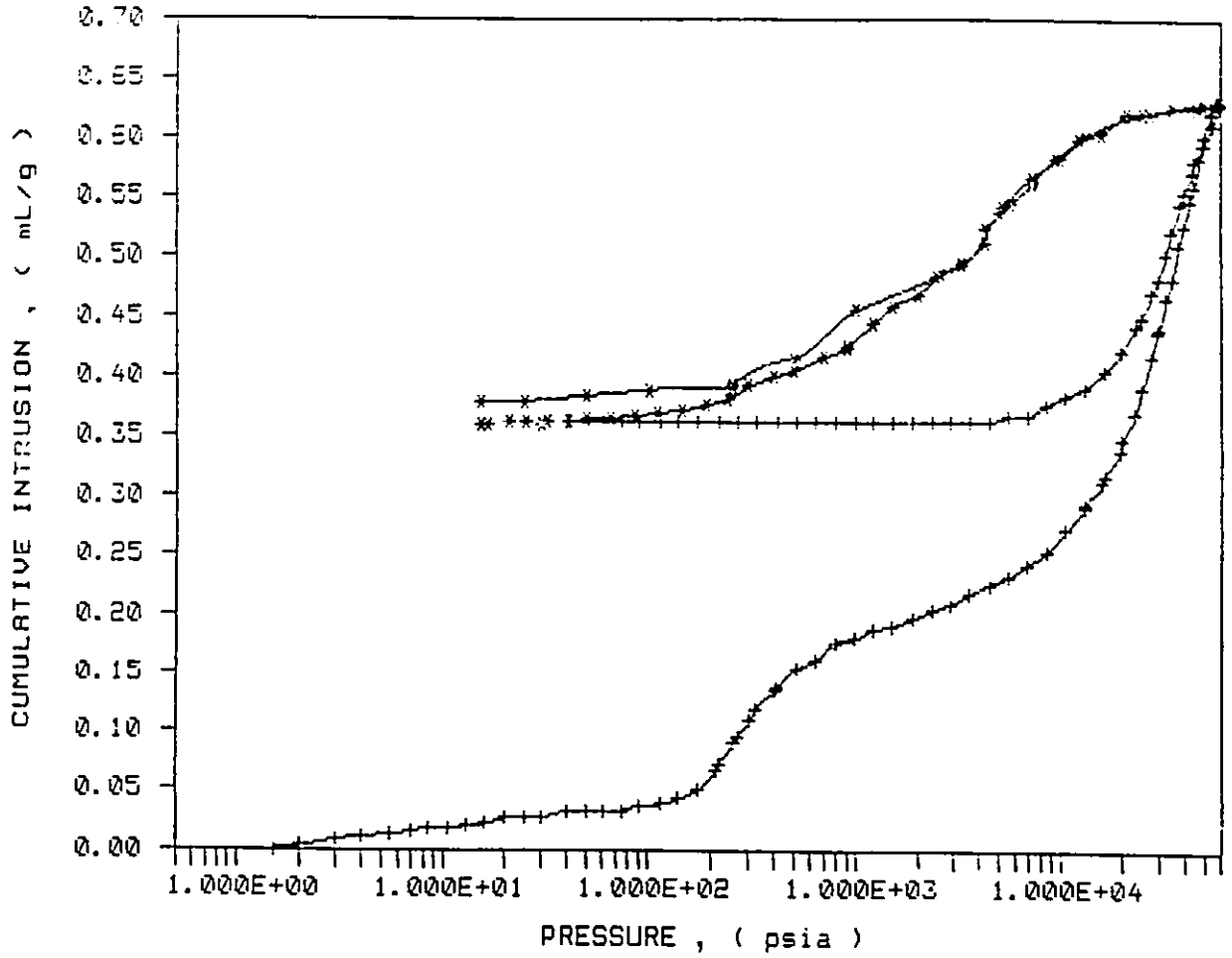

Figure D-4 : **Cumulative mercury intrusion volume (mL/g) versus pressure (psia).** Fresh catalyst containing 34% impregnated Ni in SOD and 10% SOD in the Co-Mo catalyst.

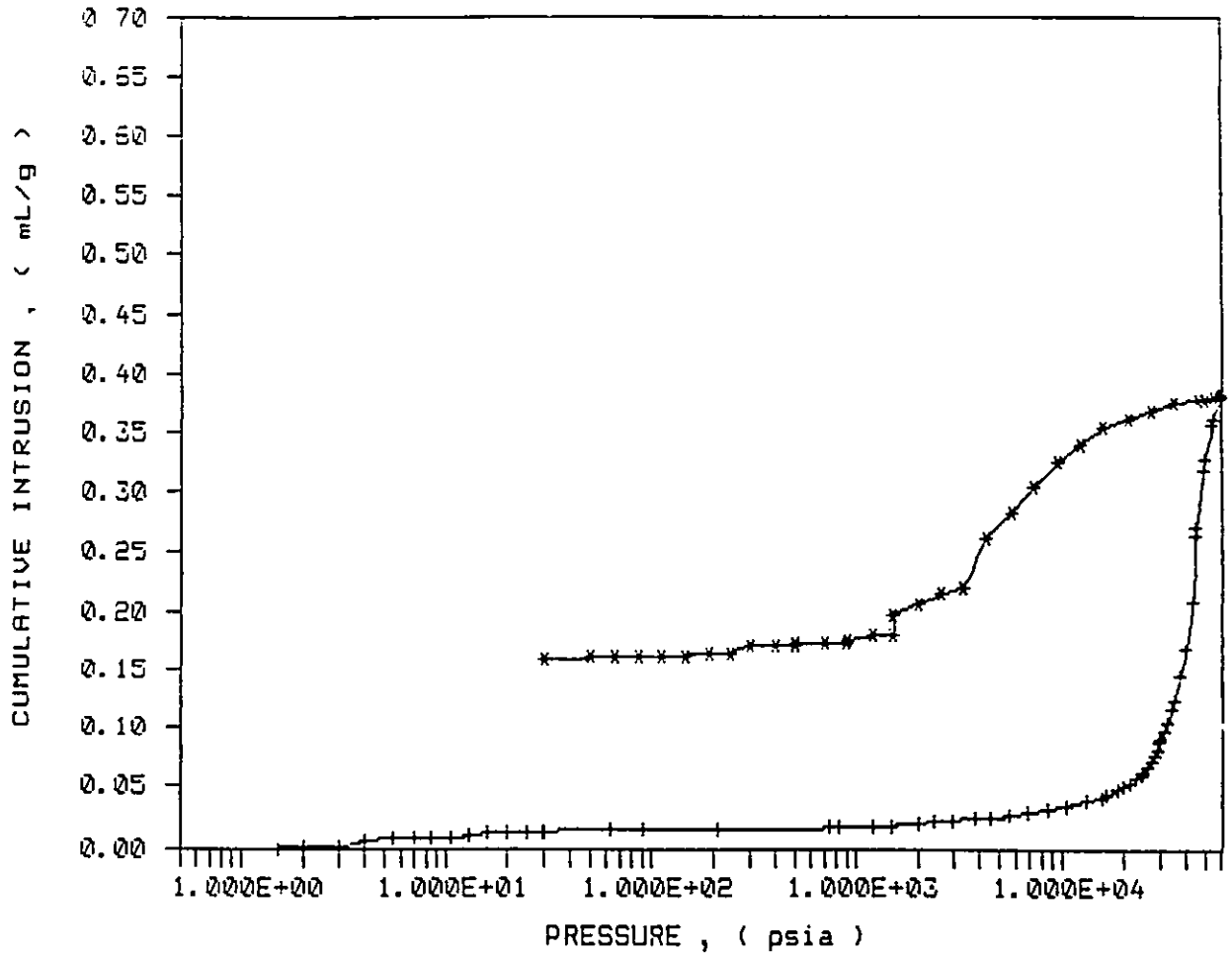

Figure D-5 : **Cumulative mercury intrusion volume (mL/g) versus pressure (psia).** Fresh catalyst containing 0% impregnated Ni in SOD and 0% SOD in the Co-Mo catalyst.

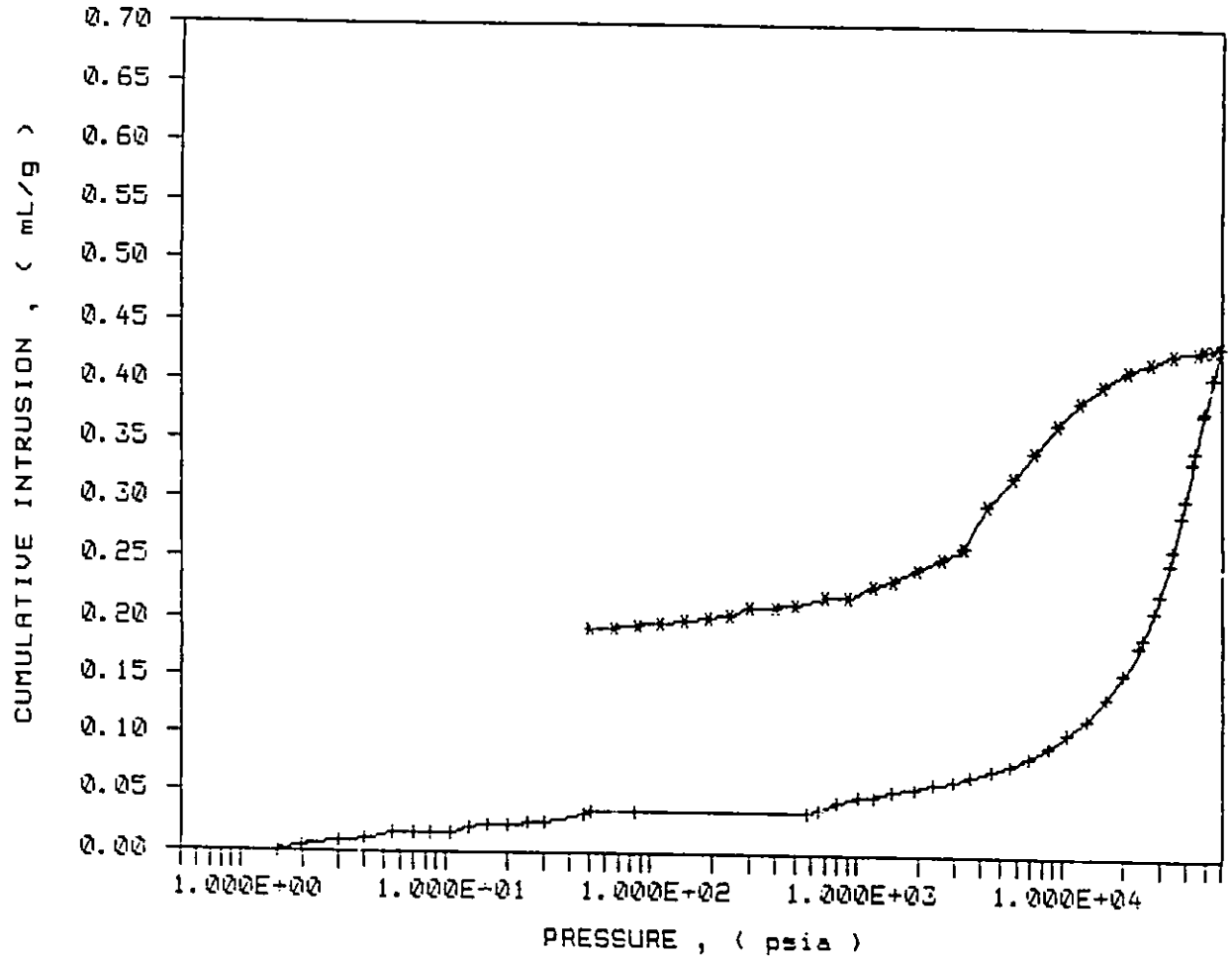

Figure D-6 : **Cumulative mercury intrusion volume (mL/g) versus pressure (psia).** Fresh catalyst containing 39% impregnated Ni in SOD and 5% SOD in the Co-Mo catalyst.

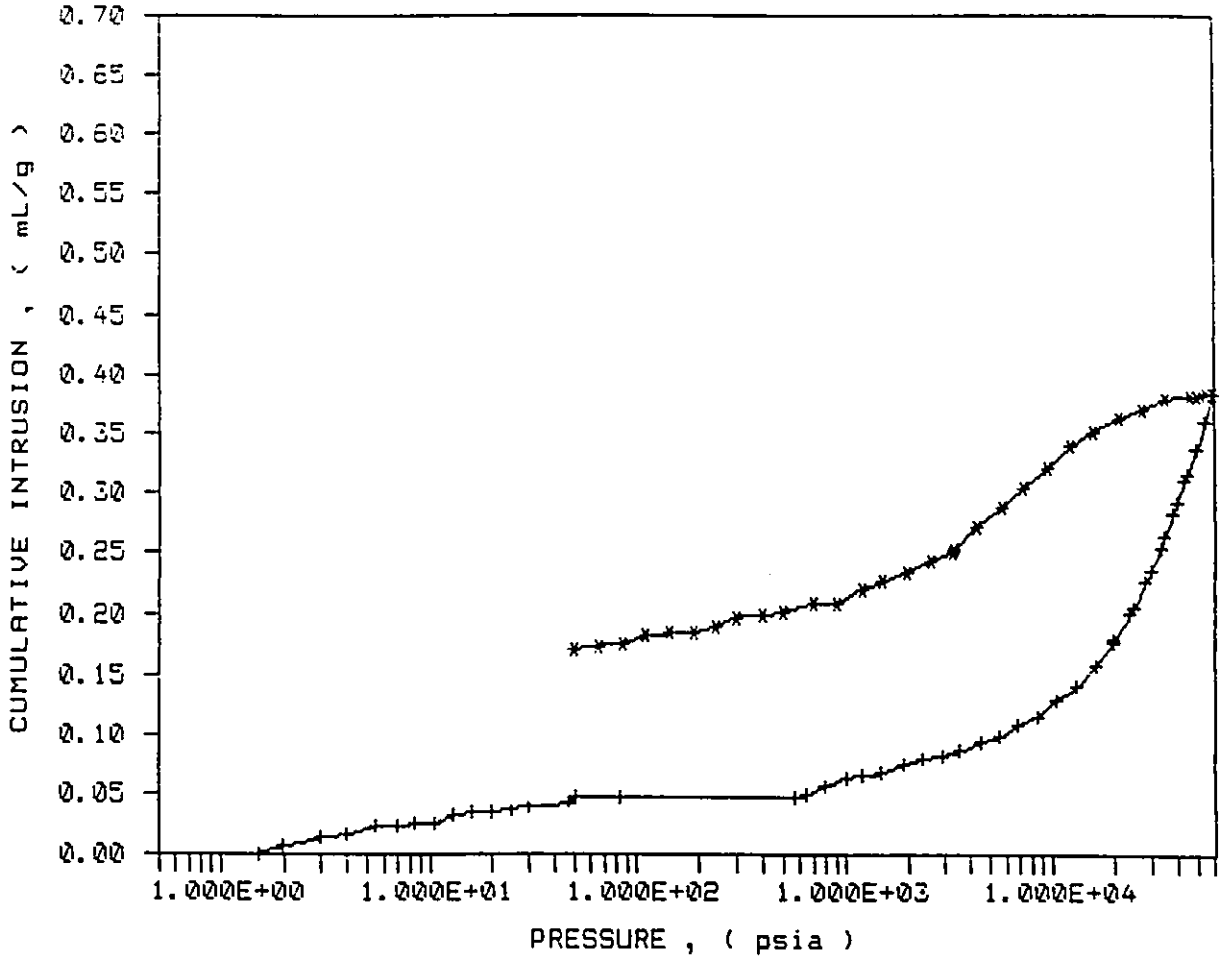

Figure D-7 : **Cumulative mercury intrusion volume (mL/g) versus pressure (psia).** Fresh catalyst containing 39% impregnated Ni in SOD and 20% SOD in the Co-Mo catalyst.

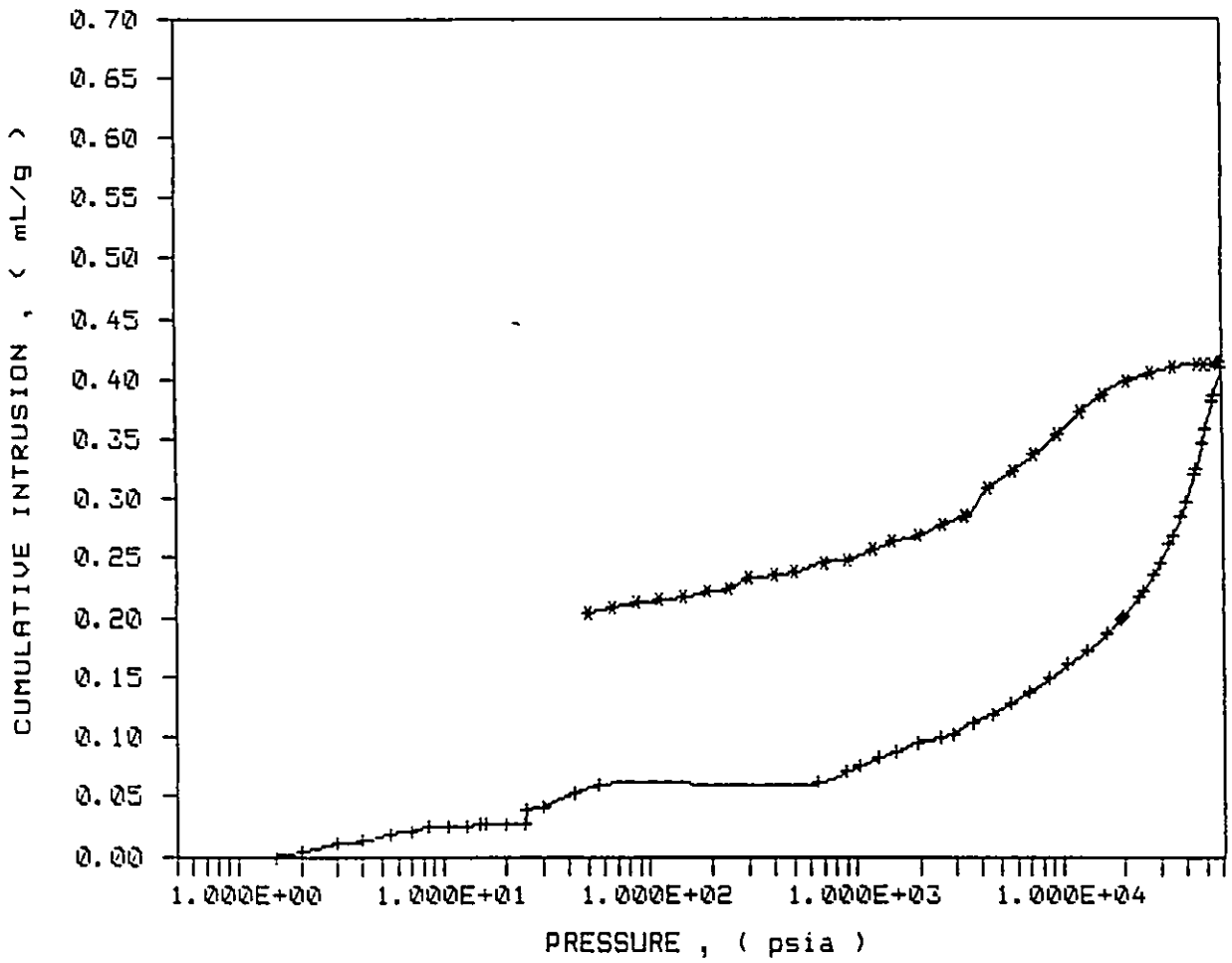

Figure D-8 : **Cumulative mercury intrusion volume (mL/g) versus pressure (psia).** Fresh catalyst containing 39% impregnated Ni in SOD and 26% SOD in the Co-Mo catalyst.

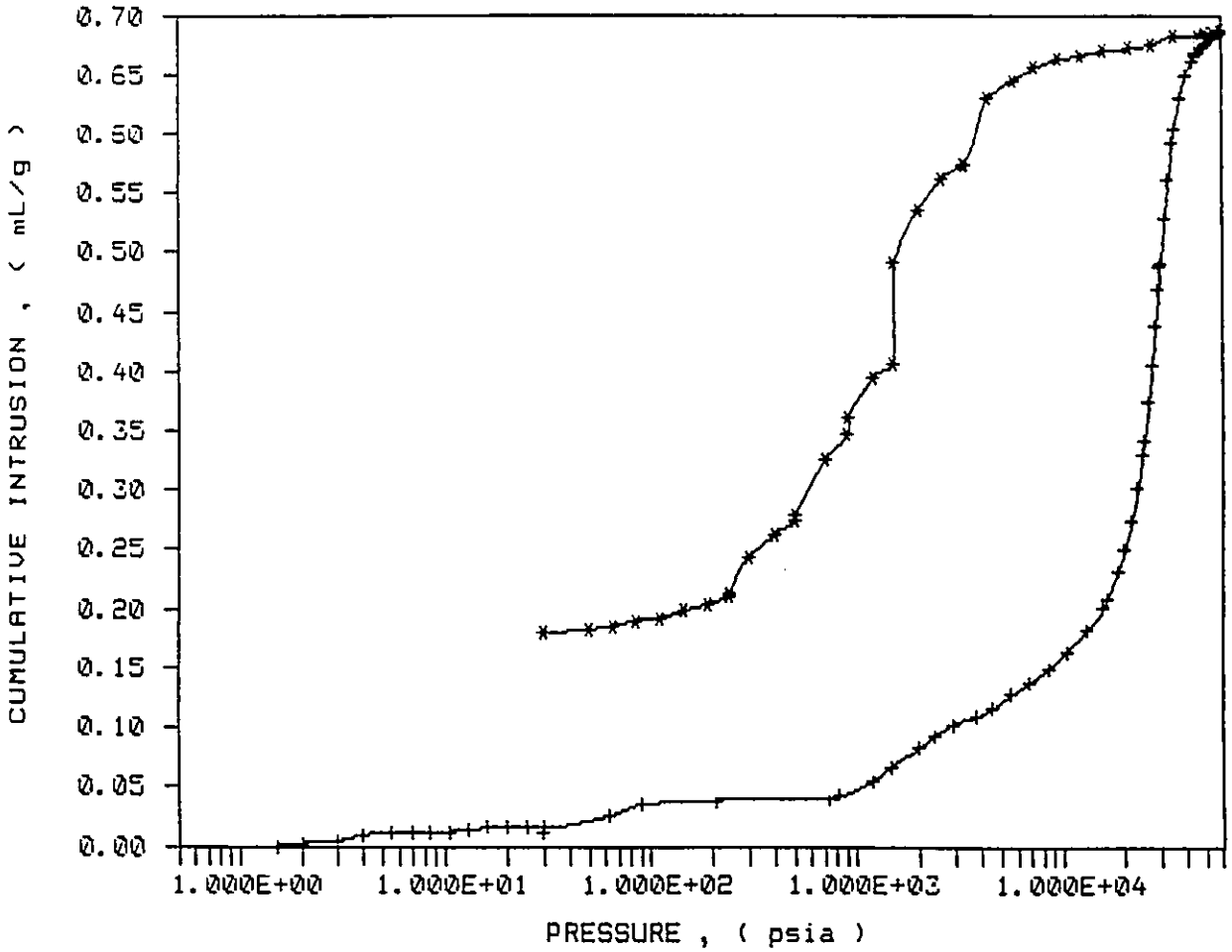

Figure D-9 : **Cumulative mercury intrusion volume (mL/g) versus pressure (psia).** Fresh AC-1442B reference catalyst.

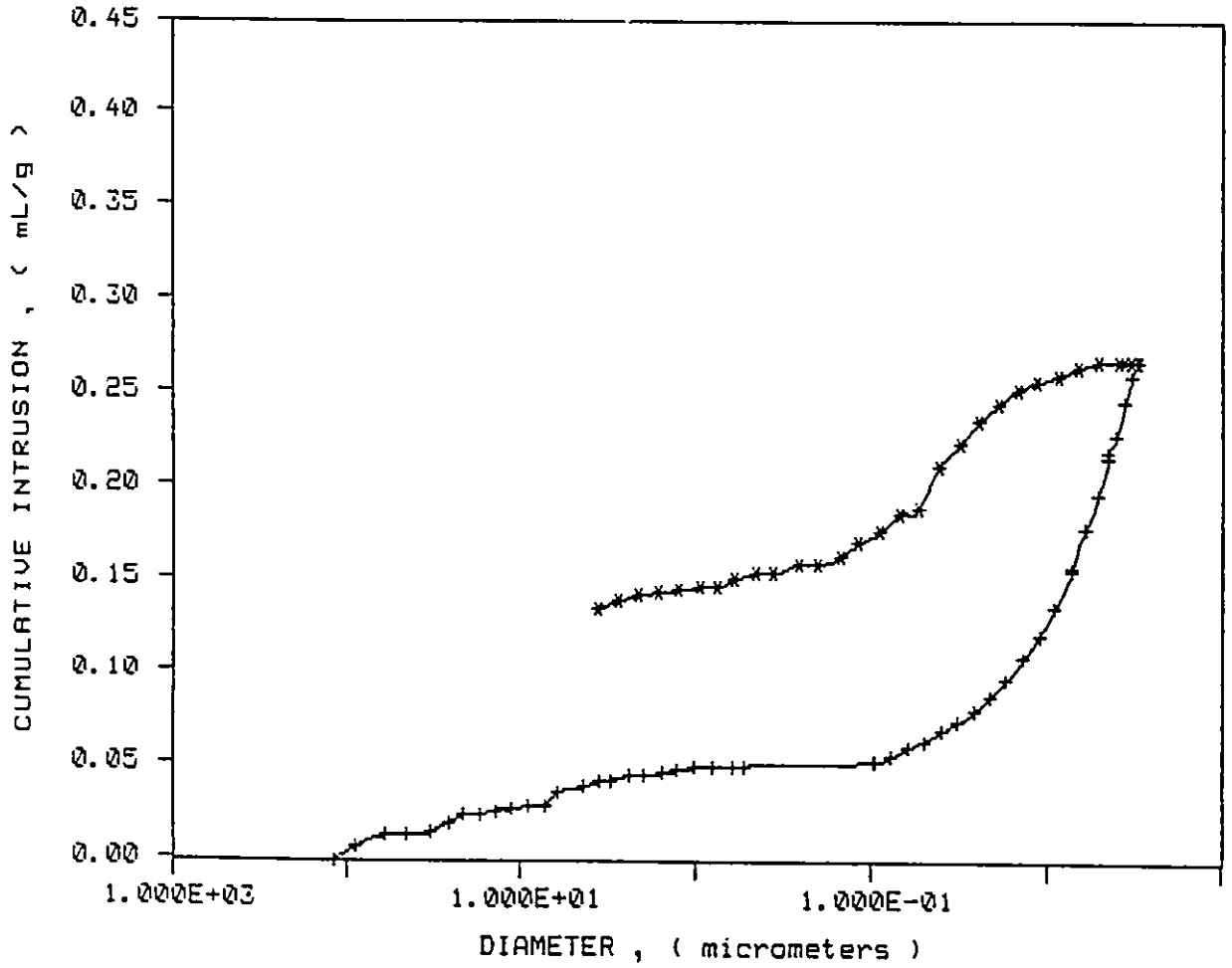

Figure D-10 : **Cumulative mercury intrusion volume (mL/g) versus catalyst pore diameter (μm).** Used catalyst containing 0% impregnated Ni in SOD and 10% SOD in the Co-Mo catalyst.

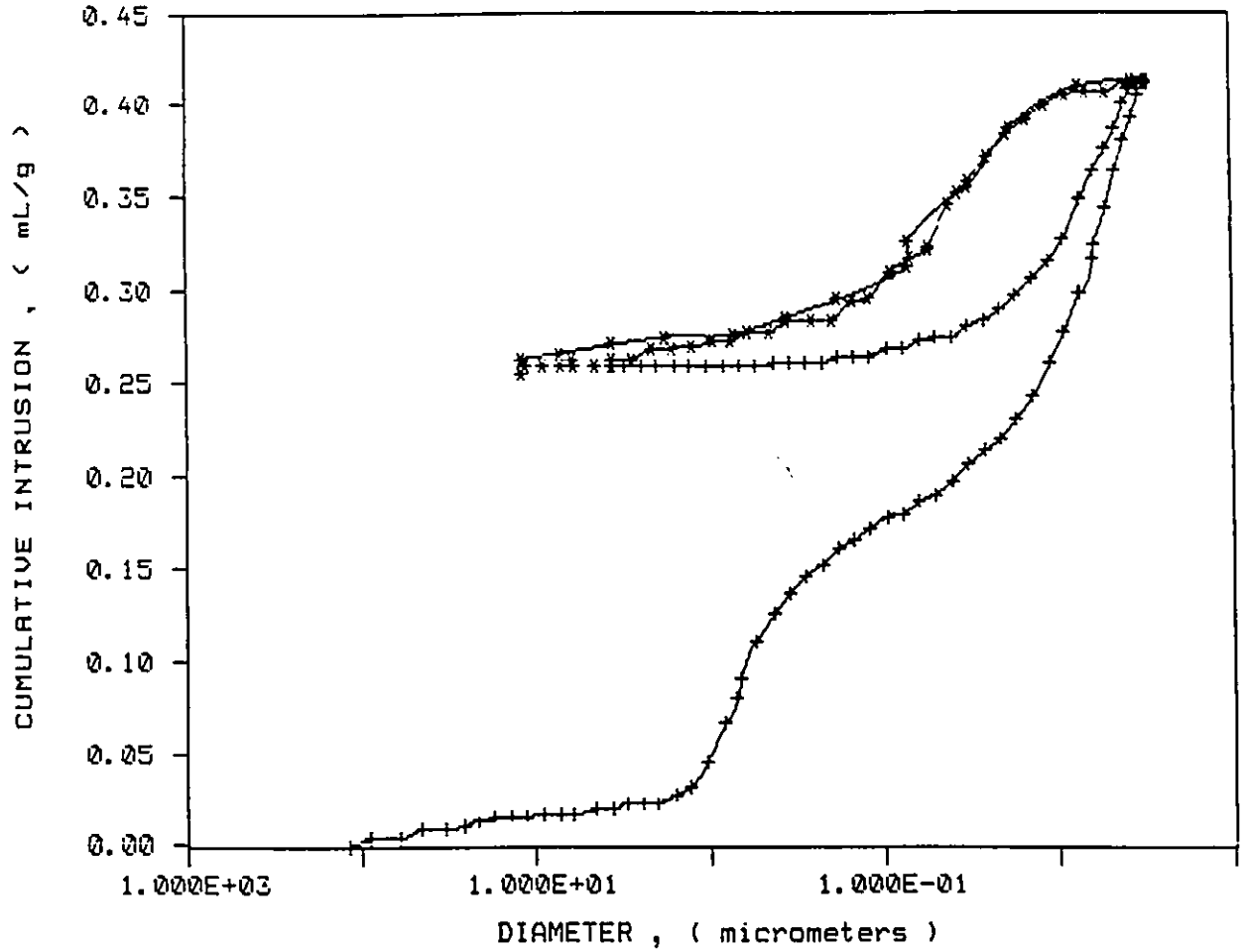

Figure D-11 : **Cumulative mercury intrusion volume (mL/g) versus catalyst pore diameter (μm).** Used catalyst containing 13% impregnated Ni in SOD and 10% SOD in the Co-Mo catalyst.

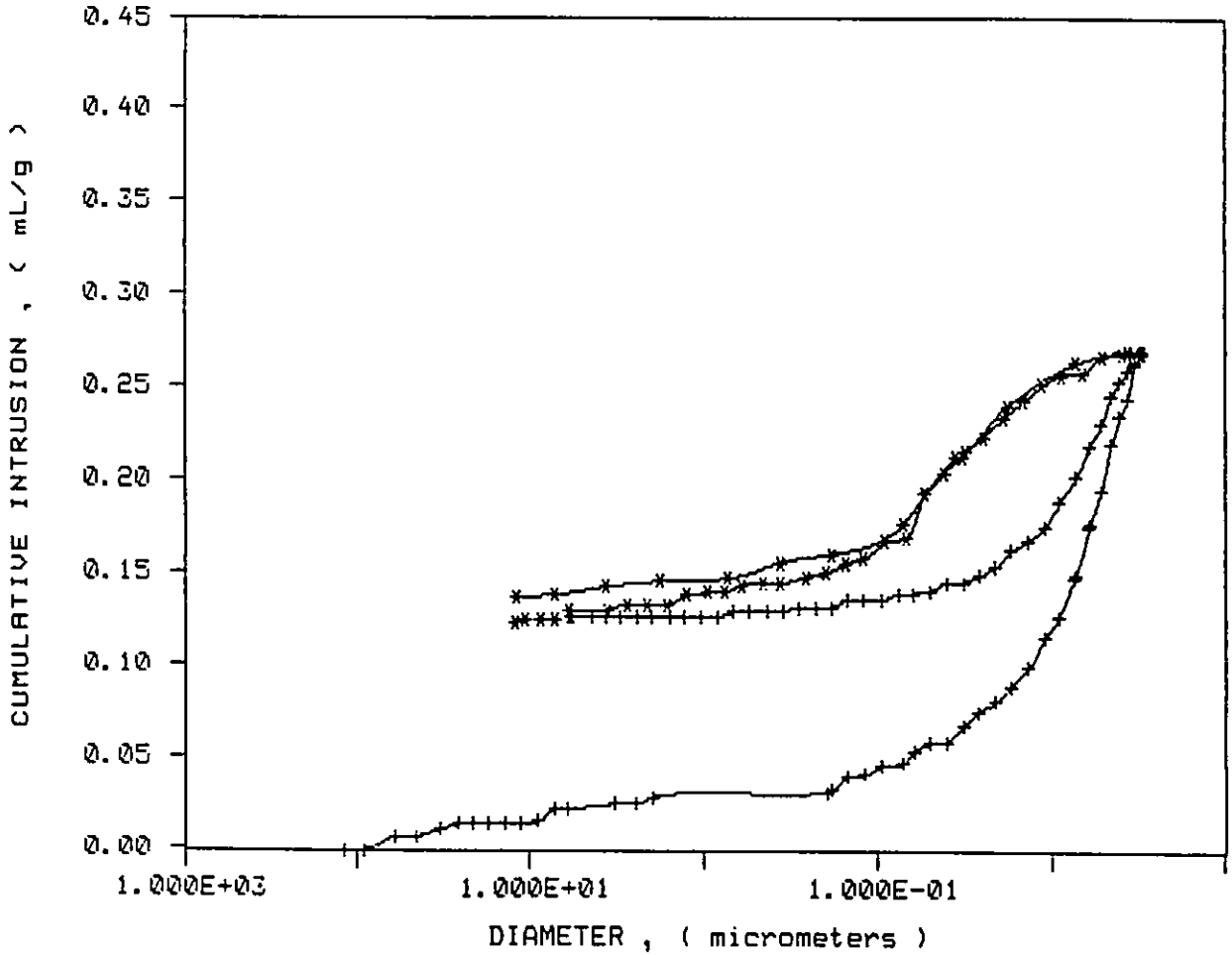

Figure D-12 : **Cumulative mercury intrusion volume (mL/g) versus catalyst pore diameter (μm).** Used catalyst containing 26% impregnated Ni in SOD and 10% SOD in the Co-Mo catalyst.

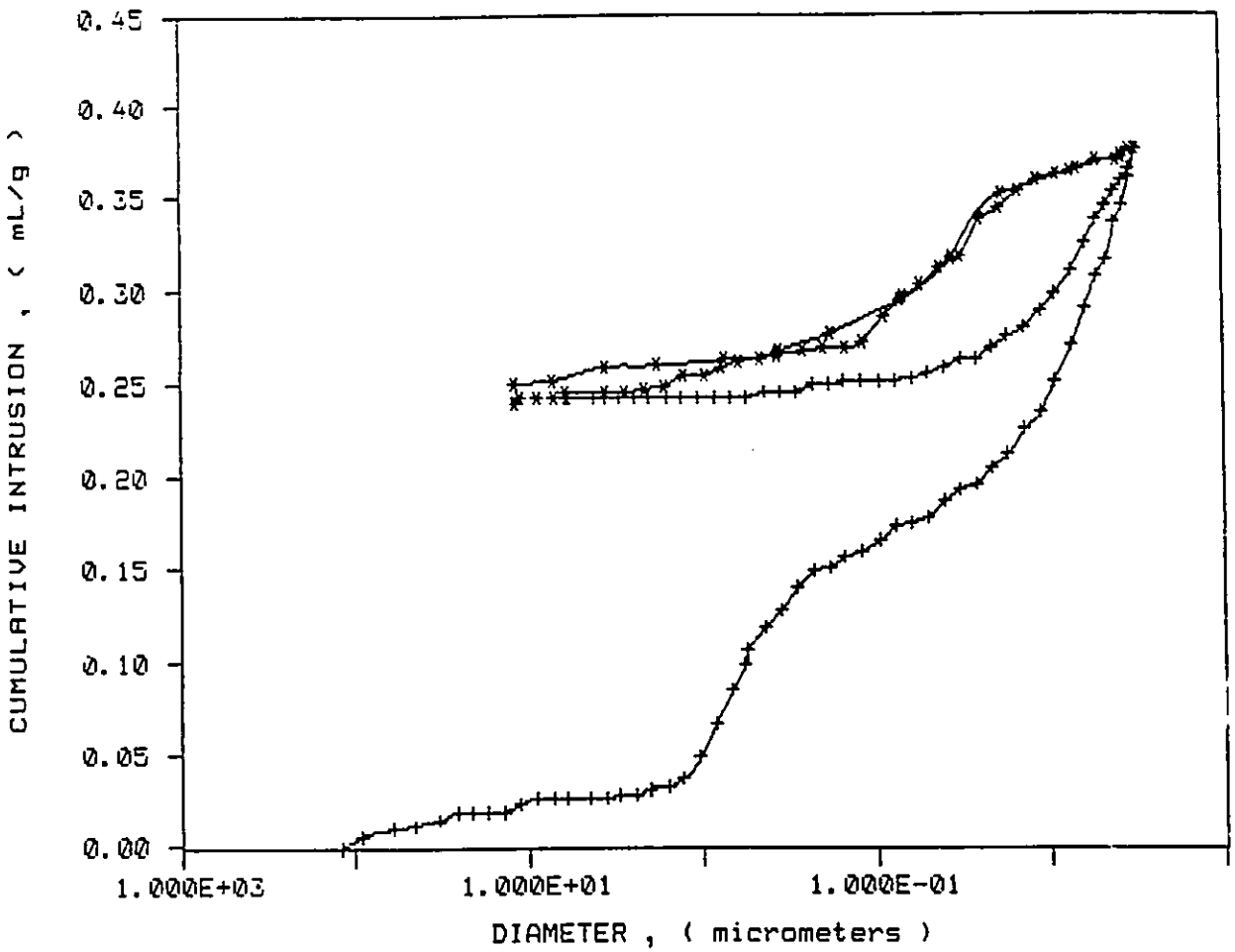

Figure D-13 : **Cumulative mercury intrusion volume (mL/g) versus catalyst pore diameter (μm).** Used catalyst containing 34% impregnated Ni in SOD and 10% SOD in the Co-Mo catalyst.

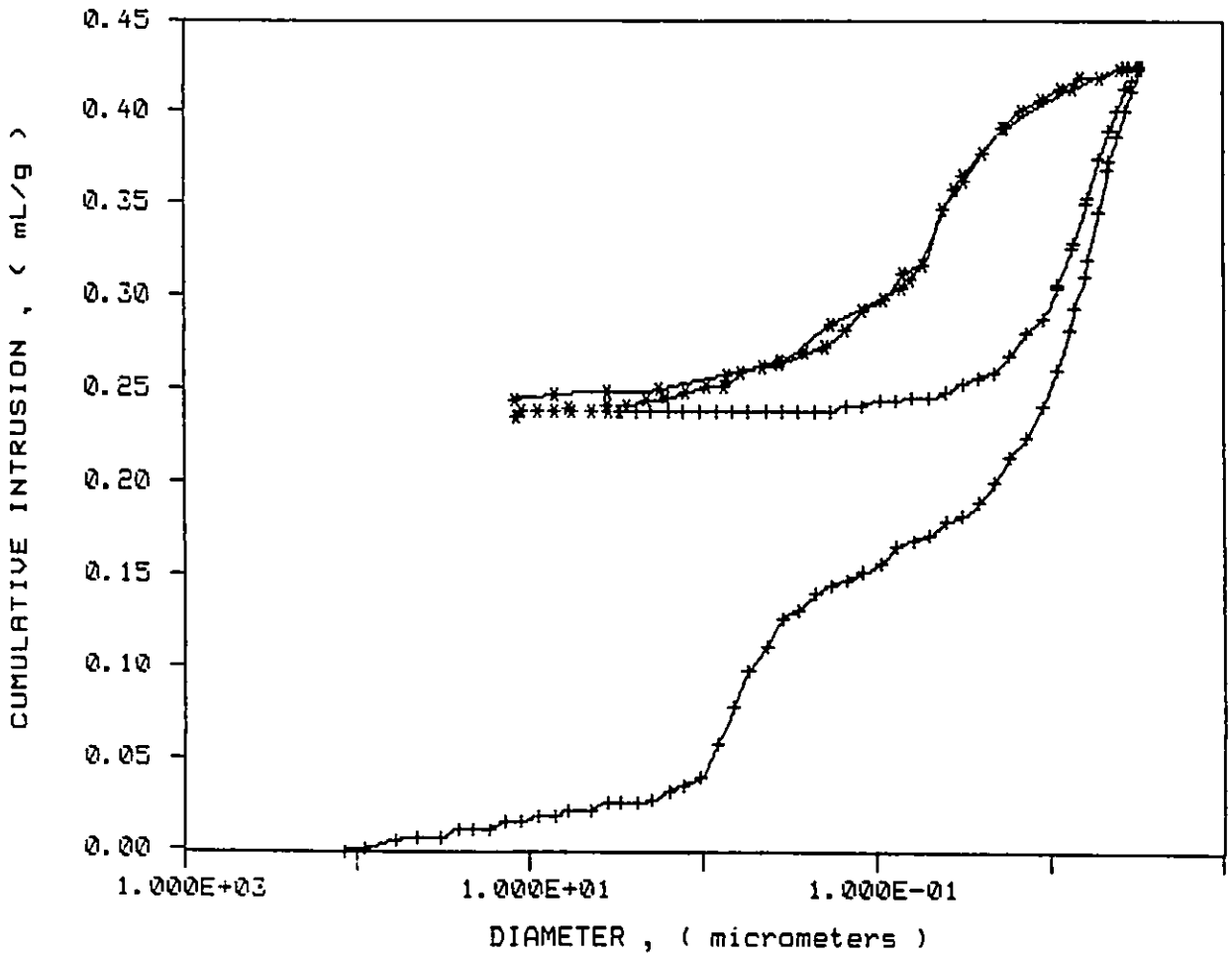

Figure D-14 : **Cumulative mercury intrusion volume (mL/g) versus catalyst pore diameter (μm).** Used catalyst containing 39% impregnated Ni in SOD and 10% SOD in the Co-Mo catalyst.

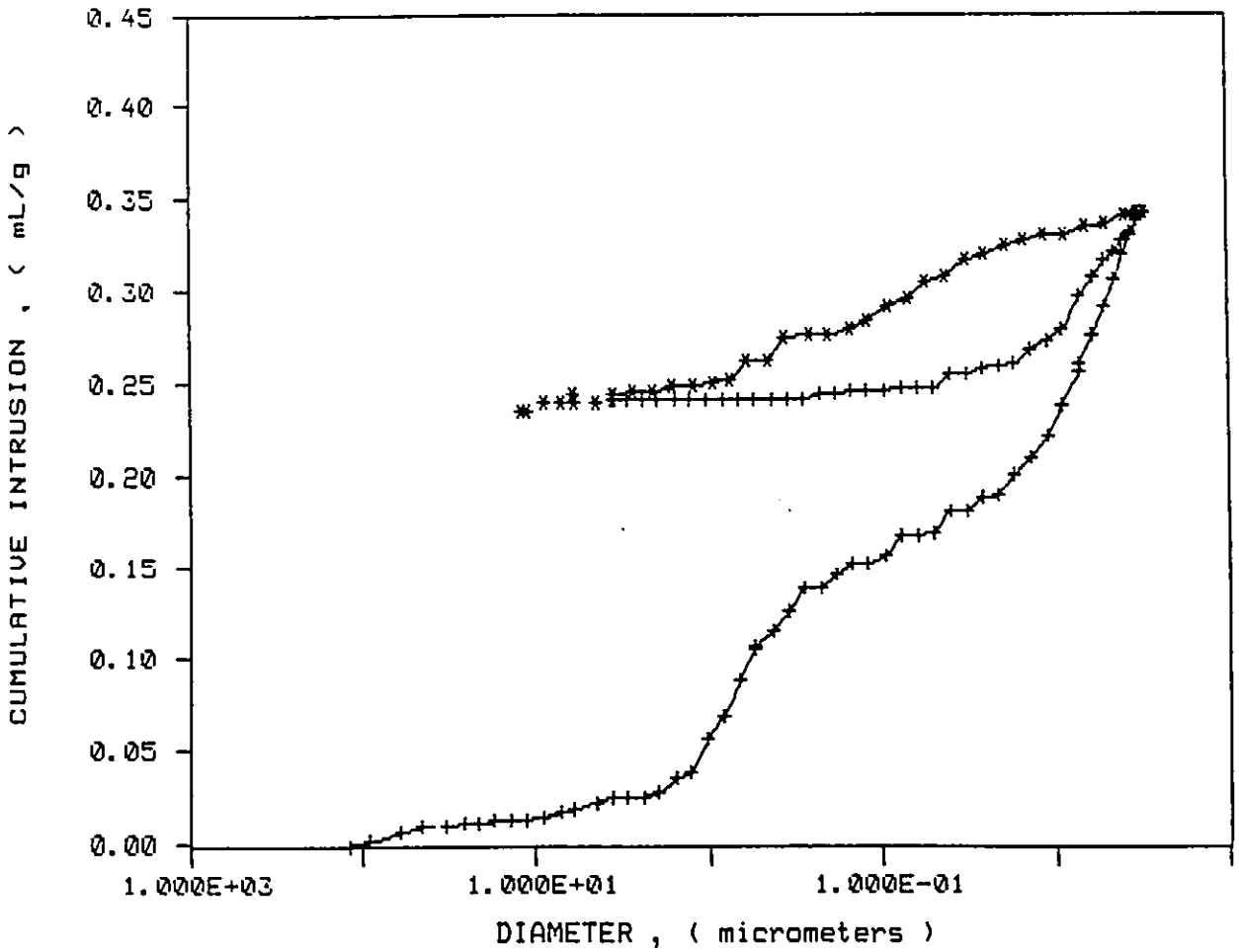

Figure D-15 : **Cumulative mercury intrusion volume (mL/g) versus catalyst pore diameter (μm).** Used catalyst containing 45% impregnated Ni in SOD and 10% SOD in the Co-Mo catalyst.

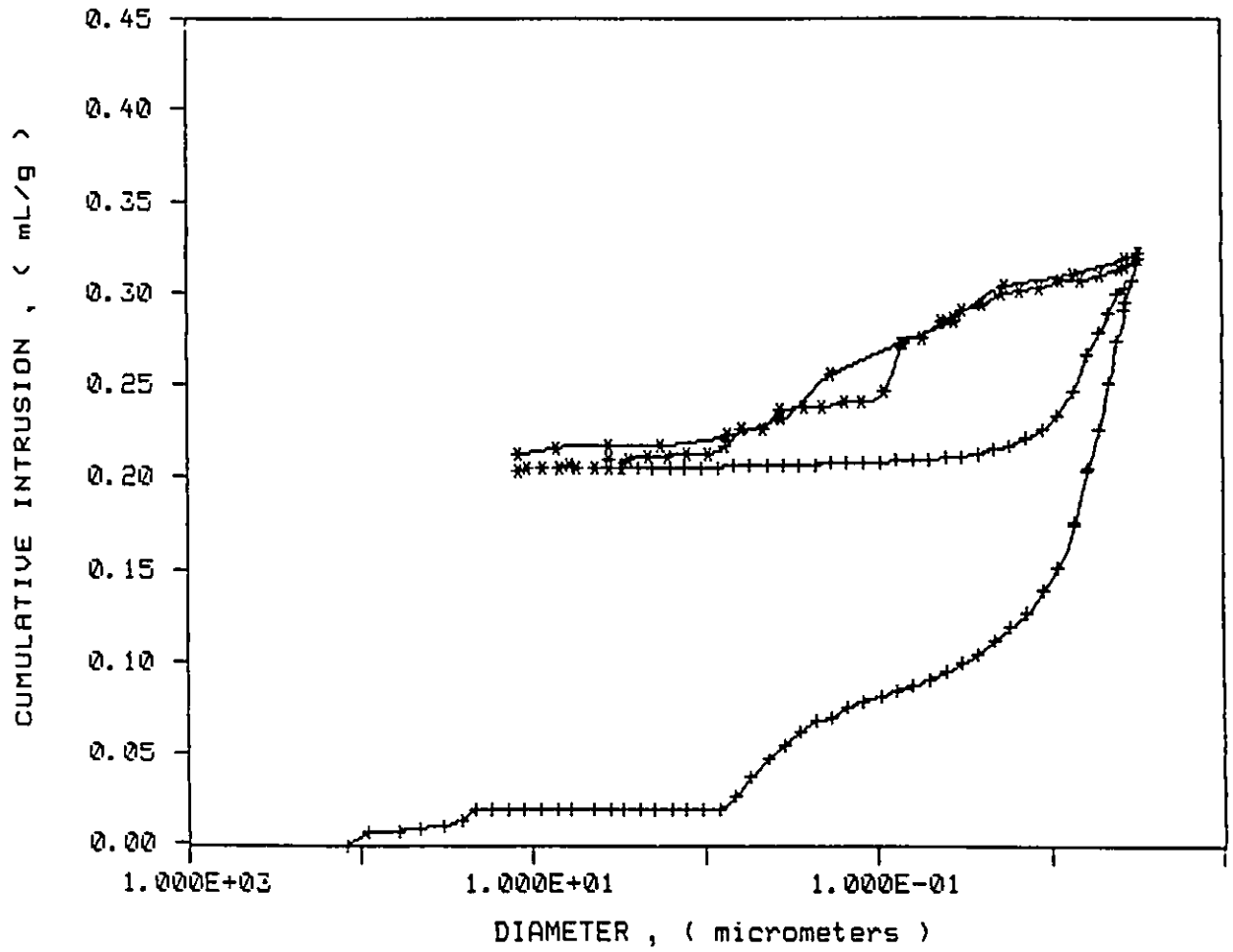

Figure D-16 : **Cumulative mercury intrusion volume (mL/g) versus catalyst pore diameter (μm).** Used catalyst containing 0% impregnated Ni in SOD and 0% SOD in the Co-Mo catalyst.

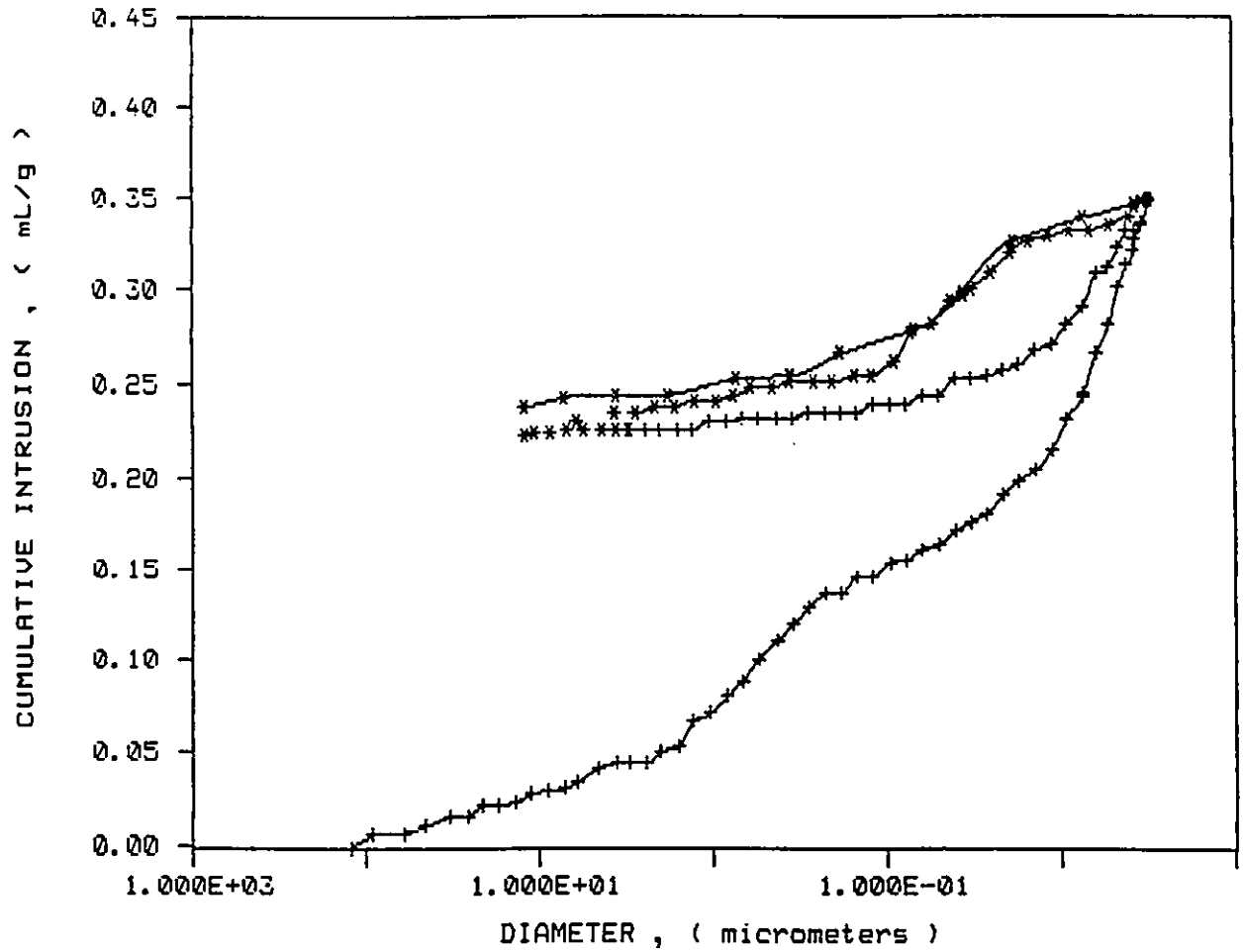

Figure D-17 : **Cumulative mercury intrusion volume (mL/g) versus catalyst pore diameter (μm).** Used catalyst containing 39% impregnated Ni in SOD and 5% SOD in the Co-Mo catalyst.

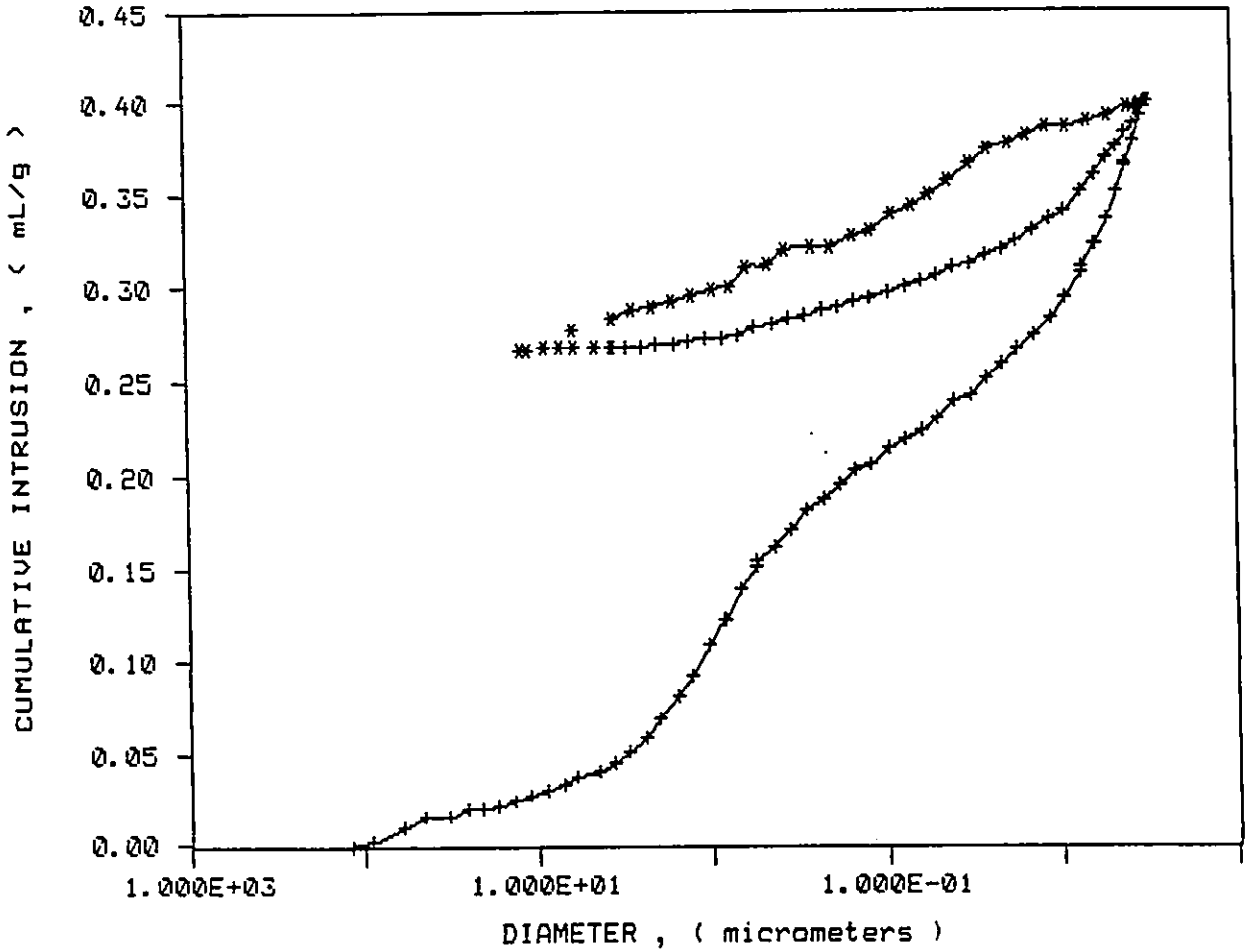

Figure D-18 : **Cumulative mercury intrusion volume (mL/g) versus catalyst pore diameter (μm).** Used catalyst containing 39% impregnated Ni in SOD and 20% SOD in the Co-Mo catalyst.

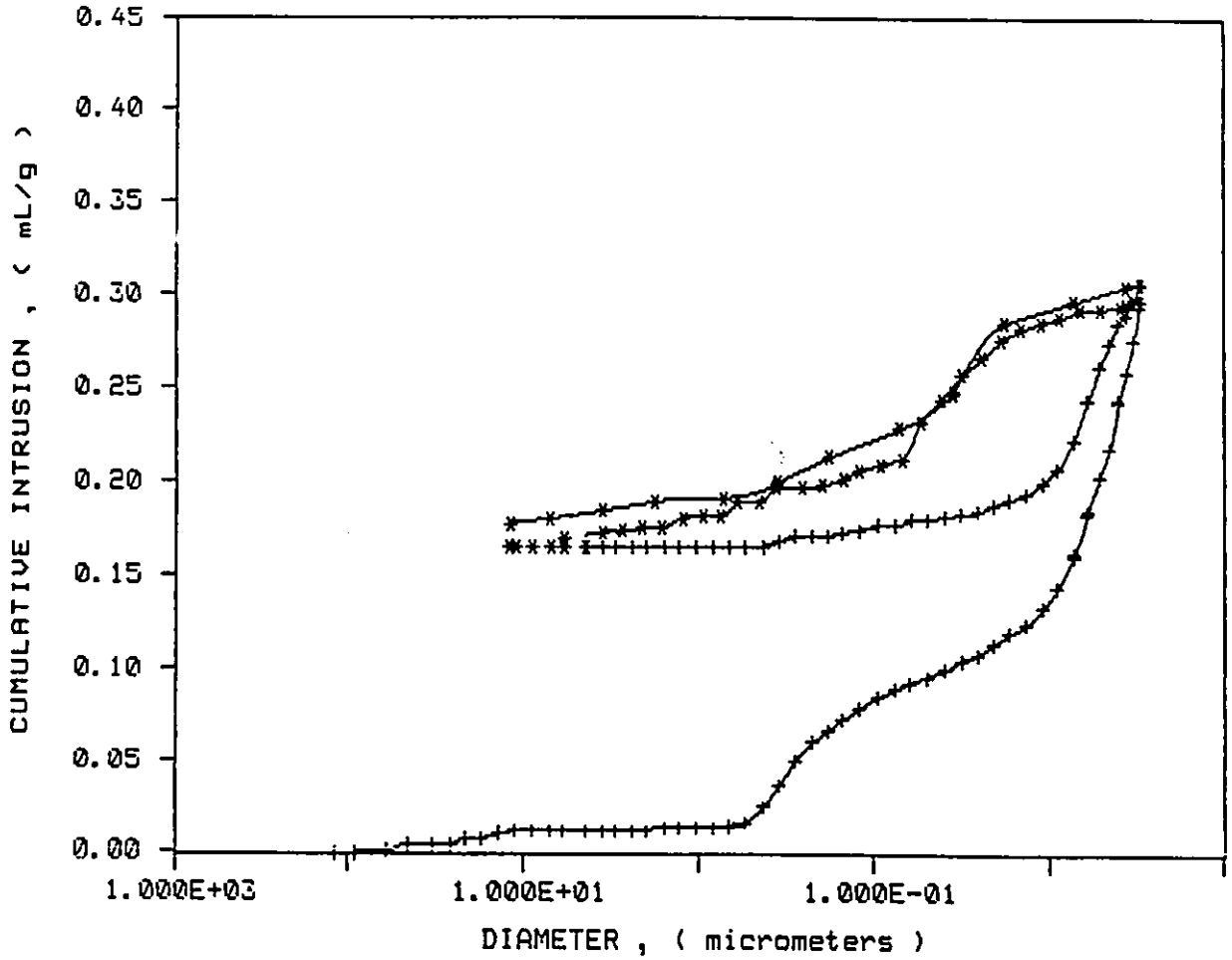

Figure D-19 : **Cumulative mercury intrusion volume (mL/g) versus catalyst pore diameter (μm).** Used catalyst containing 39% impregnated Ni in SOD and 26% SOD in the Co-Mo catalyst.

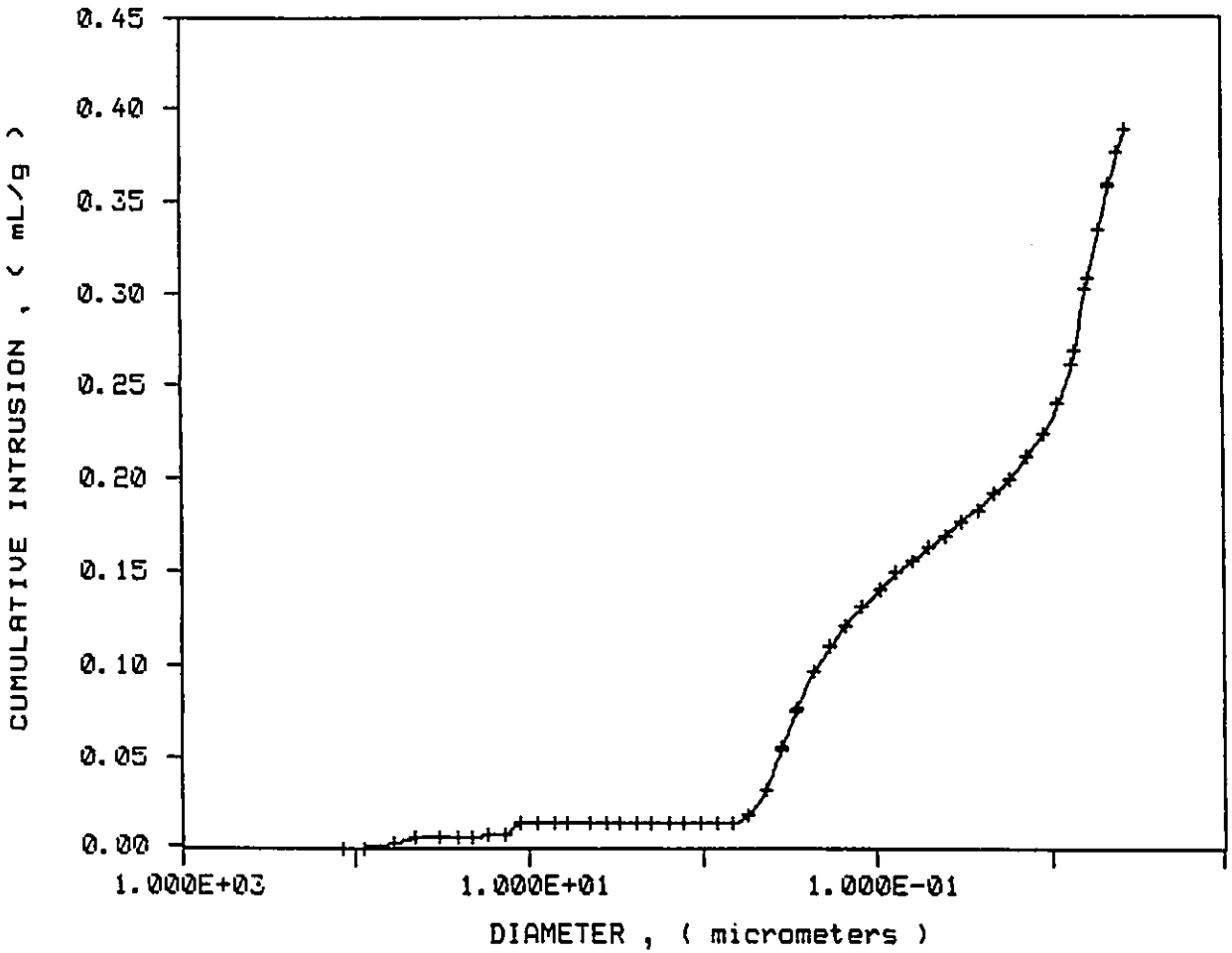

Figure D-20 : **Cumulative mercury intrusion volume (mL/g) versus catalyst pore diameter (μm).** Used AC-1442B reference catalyst.

APPENDIX E

THERMOGRAVIMETRIC ANALYSIS

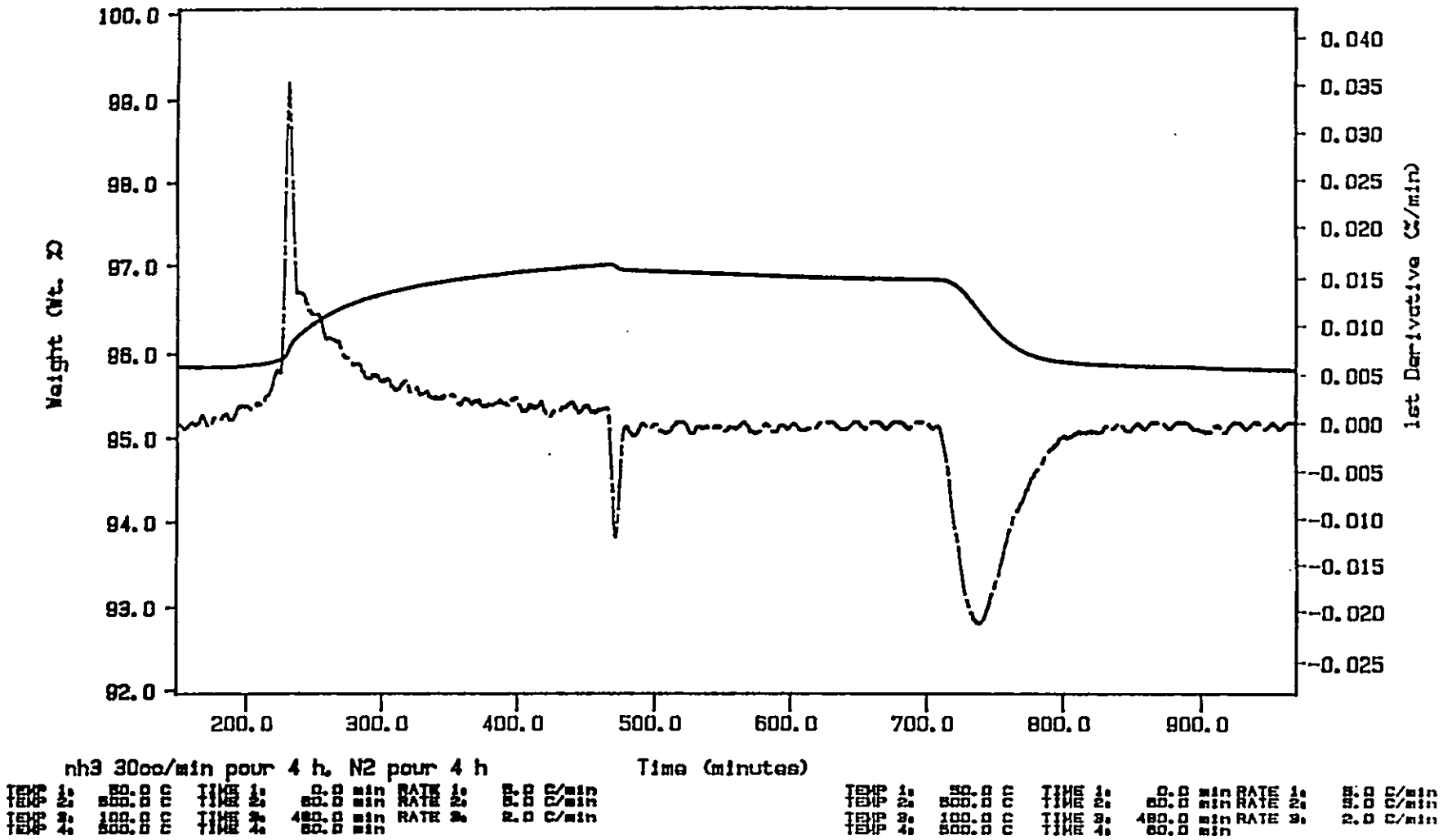

Figure E-1 : Thermogravimetric analysis -- Ammonia adsorption and desorption 100% sodalite.

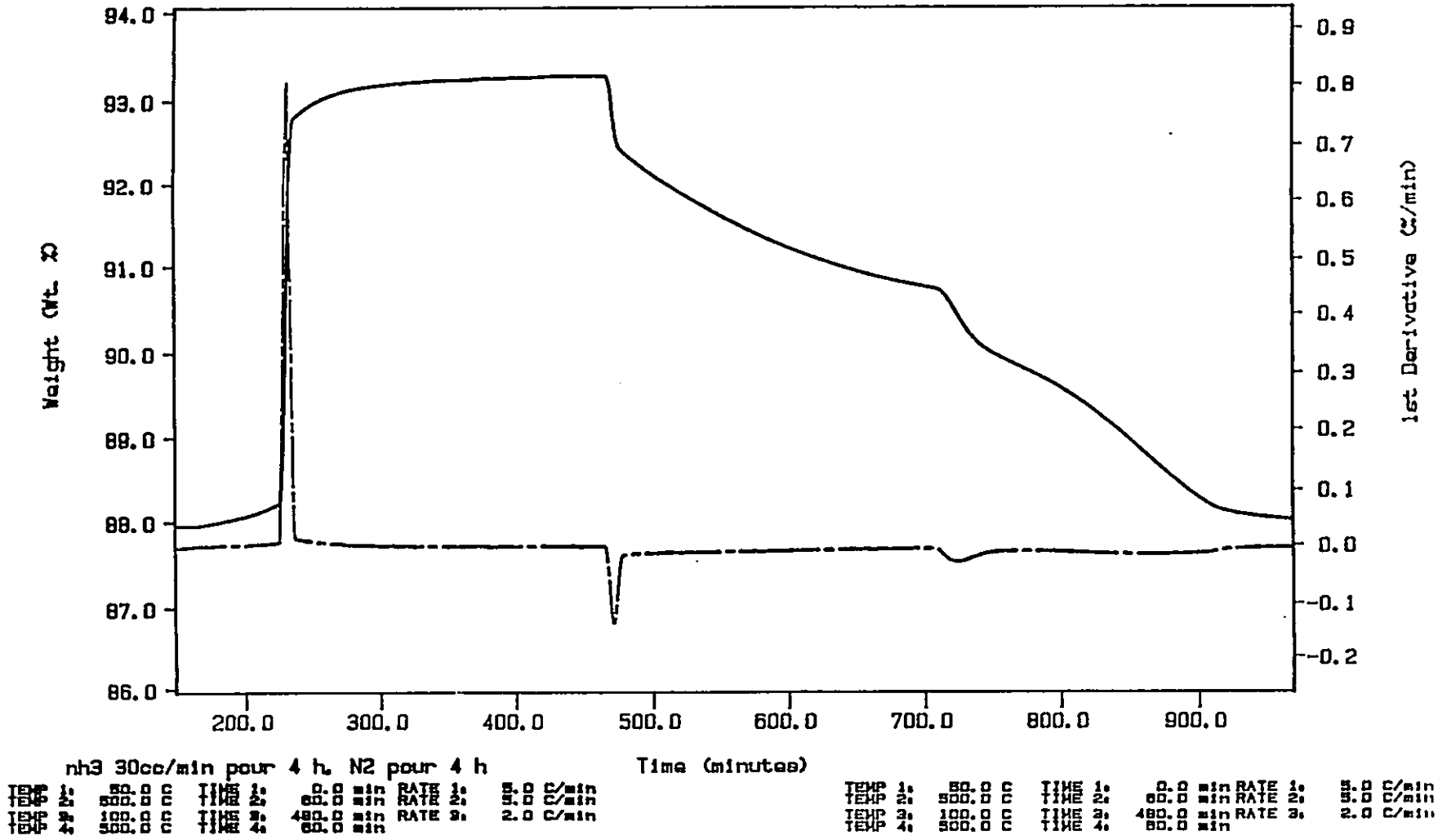

Figure E-2 : **Thermogravimetric analysis -- Ammonia adsorption and desorption** 100% H-mordenite.

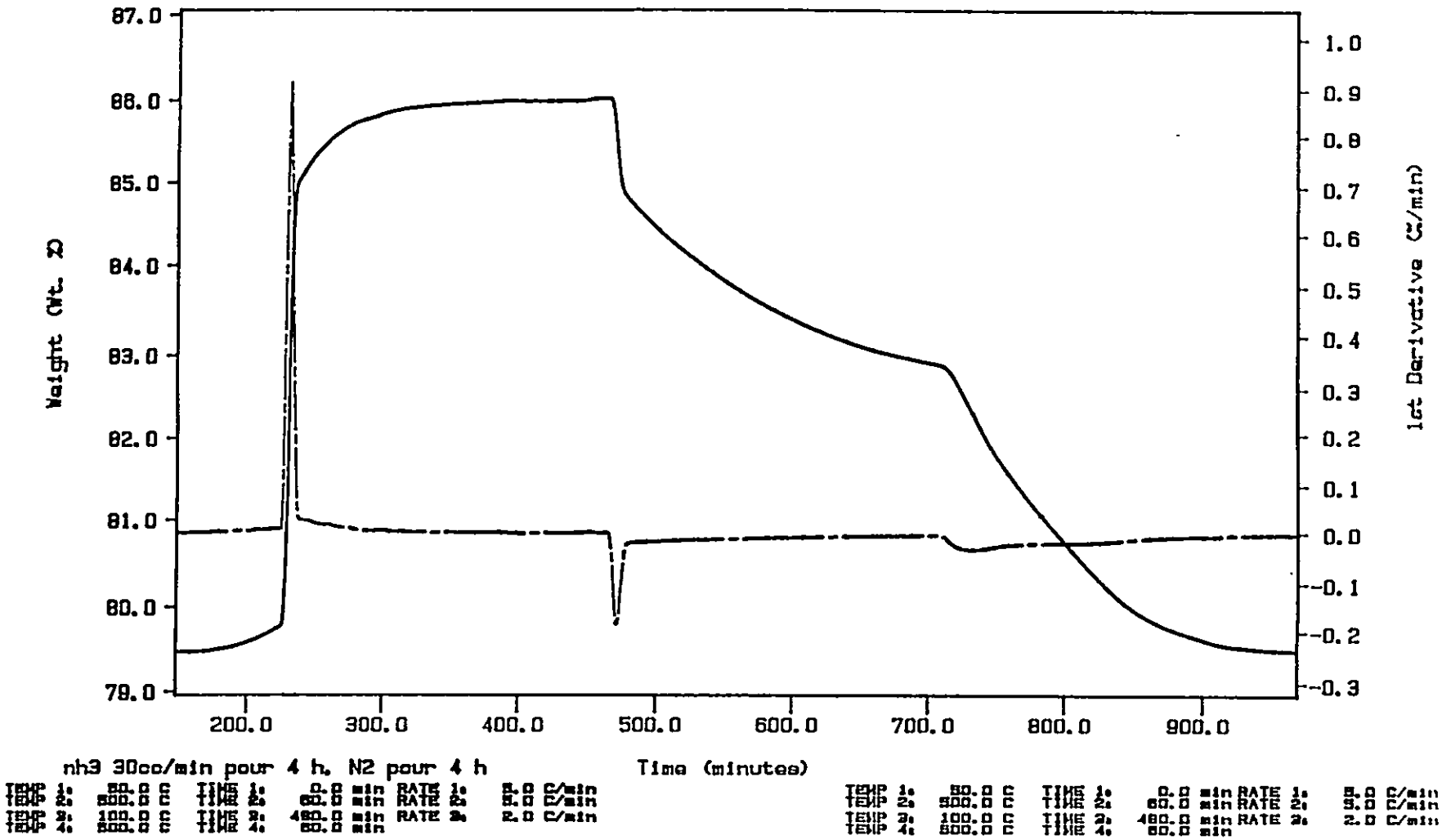

Figure E-3 : Thermogravimetric analysis -- Ammonia adsorption and desorption 100% HY zeolite.

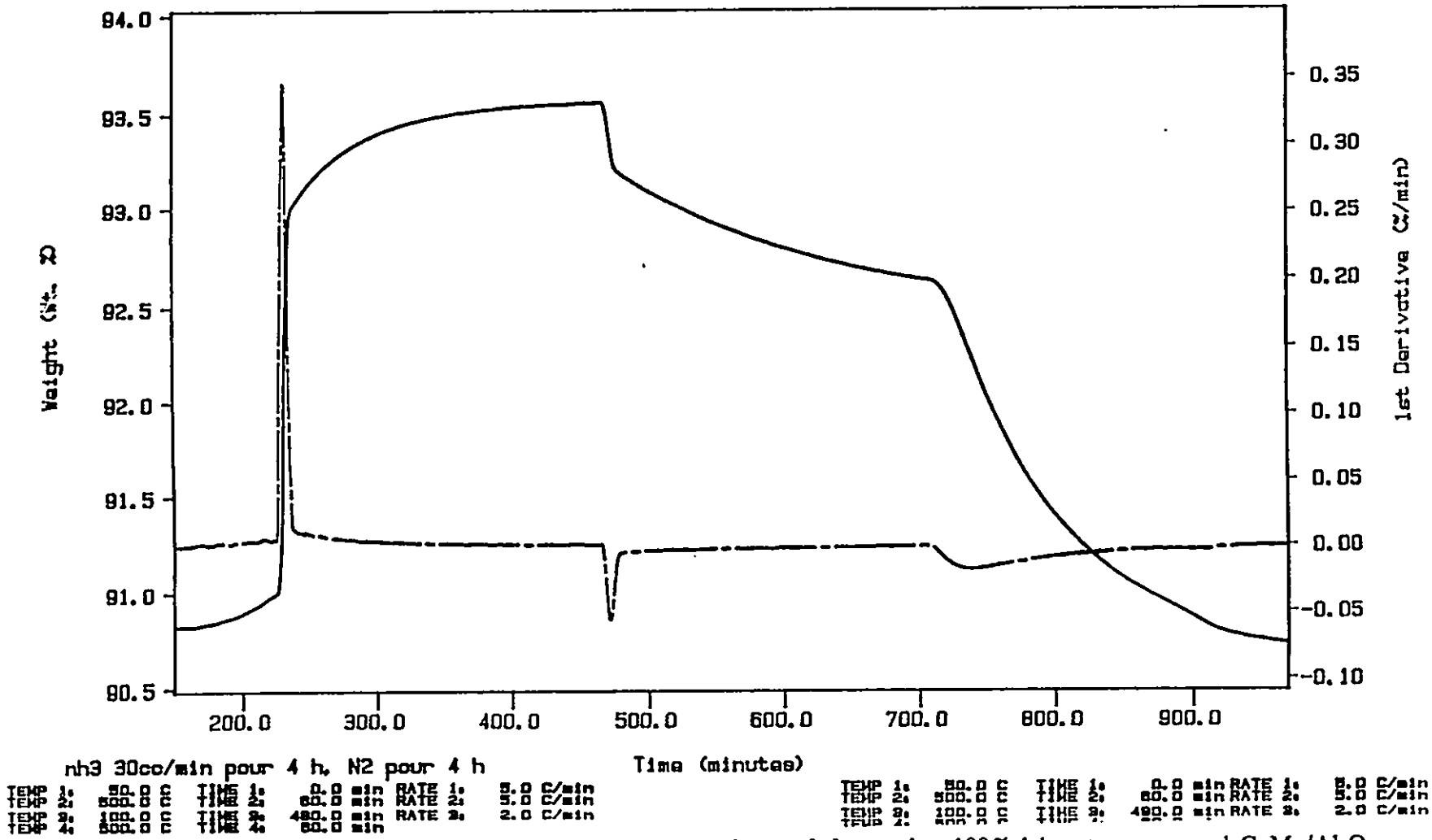

Figure E-4 : **Thermogravimetric analysis -- Ammonia adsorption and desorption** 100% laboratory prepared $CoMo/Al_2O_3$ catalyst.

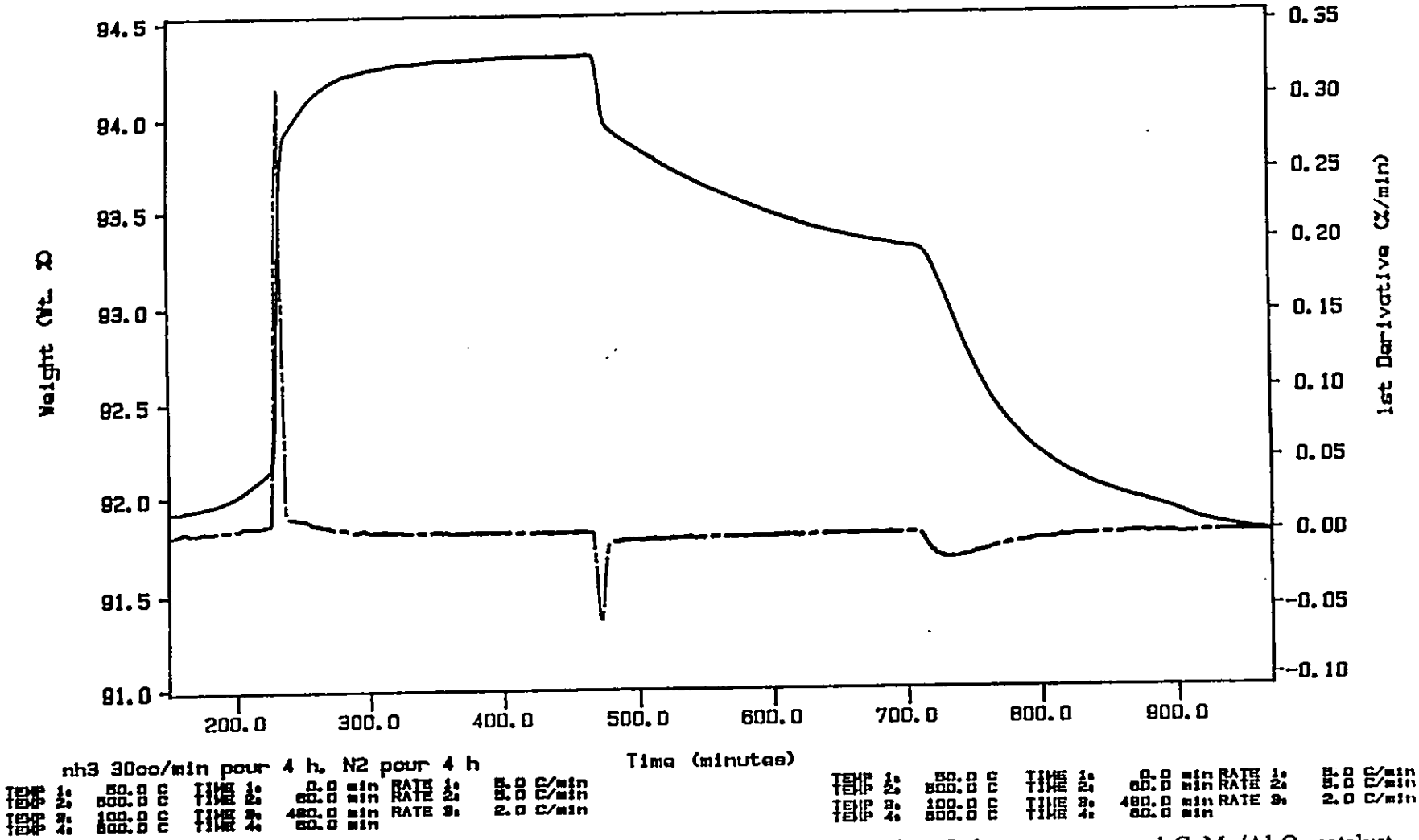

Figure E-5 : **Thermogravimetric analysis -- Ammonia adsorption and desorption.** Laboratory prepared $CoMo/Al_2O_3$ catalyst containing 10% Ni-SOD impregnated with 39% nickel.

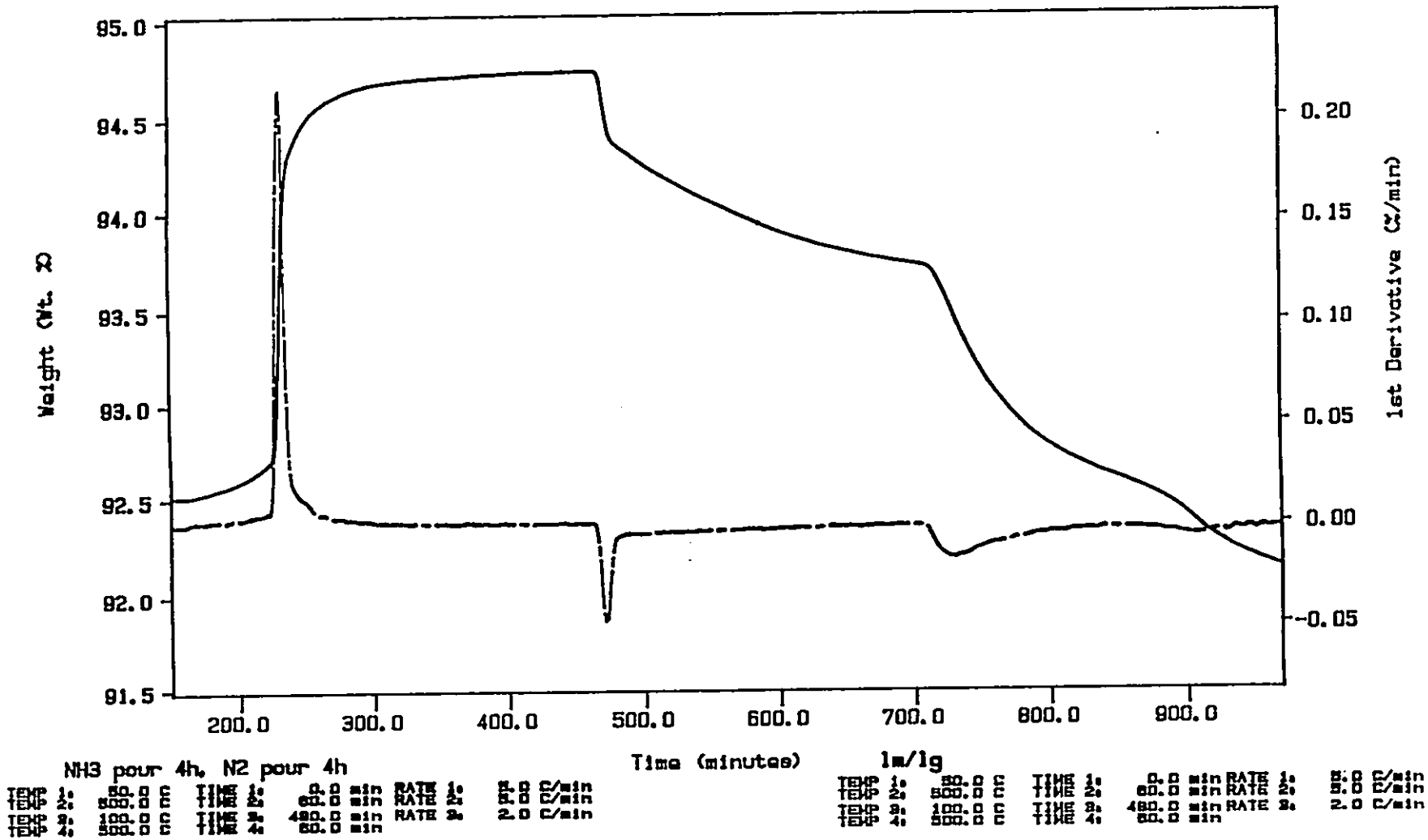

Figure E-6 : **Thermogravimetric analysis -- Ammonia adsorption and desorption.** Laboratory prepared $CoMo/Al_2O_3$ catalyst containing 26% Ni-SOD impregnated with 39% nickel.

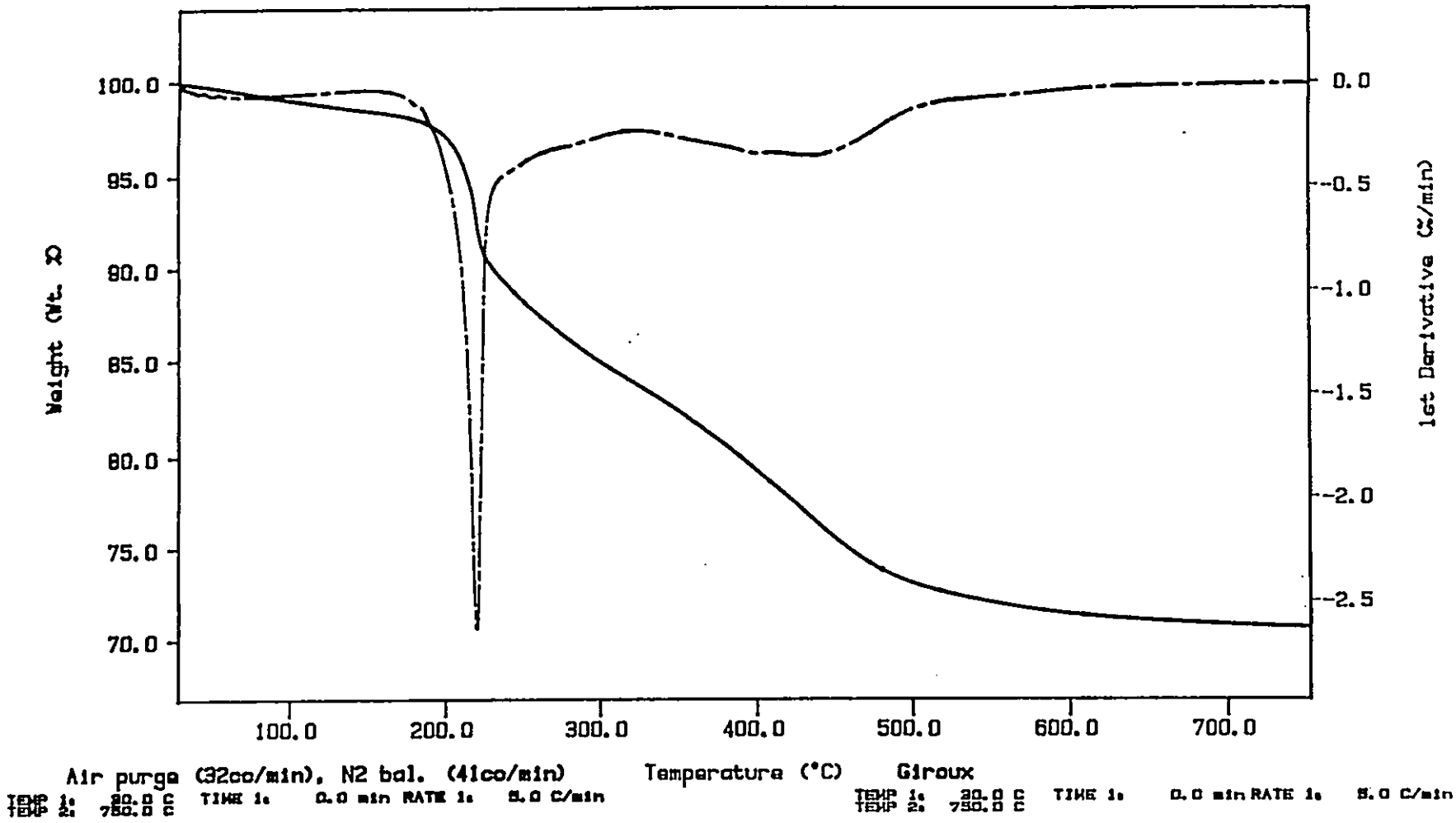

Figure E-7 : **Thermogravimetric analysis in presence of air.** Laboratory prepared $CoMo/Al_2O_3$ catalyst containing 5% Ni-SOD impregnated with 39% nickel.

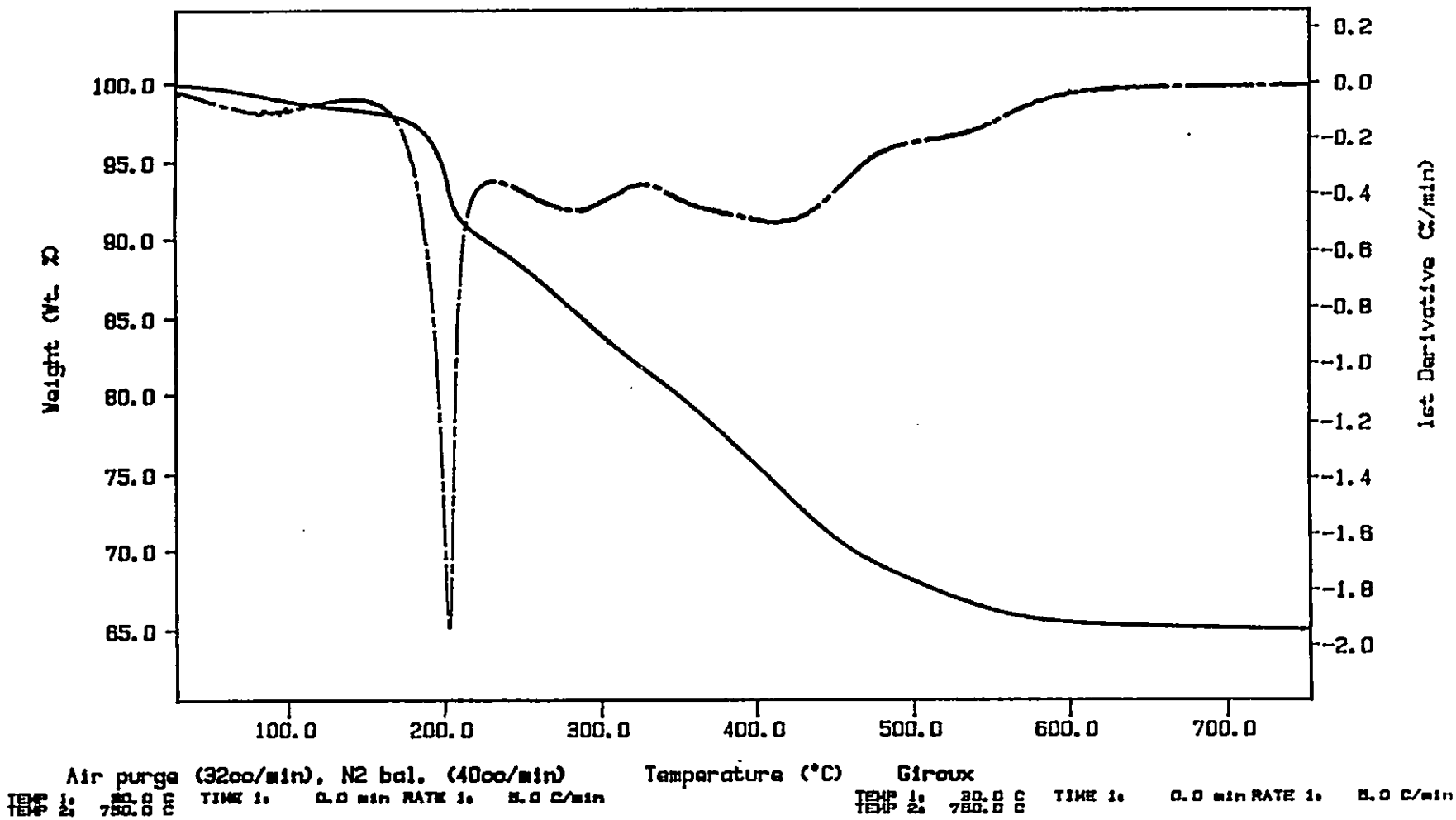

Figure E-8 : **Thermogravimetric analysis in presence of air.** Laboratory prepared $CoMo/Al_2O_3$ catalyst containing 20% Ni-SOD impregnated with 39% nickel.